



BINDING SERVICES
Tel +44 (0)29 2087 4949
Fax +44 (0)29 20371921
e-mail bindery@cardiff.ac.uk

**Understanding the mechanism of action of
endosomolytic polyamidoamines by studying
their physico-chemical properties**



**A thesis submitted to Cardiff University in
candidature for the degree of Doctor of Philosophy**

Zeena Khayat

UMI Number: U584075

All rights reserved

INFORMATION TO ALL USERS

The quality of this reproduction is dependent upon the quality of the copy submitted.

In the unlikely event that the author did not send a complete manuscript and there are missing pages, these will be noted. Also, if material had to be removed, a note will indicate the deletion.



UMI U584075

Published by ProQuest LLC 2013. Copyright in the Dissertation held by the Author.
Microform Edition © ProQuest LLC.

All rights reserved. This work is protected against
unauthorized copying under Title 17, United States Code.



ProQuest LLC
789 East Eisenhower Parkway
P.O. Box 1346
Ann Arbor, MI 48106-1346

Acknowledgments

First I would like to thank Professor Ruth Duncan and Dr. Peter Griffiths for their guidance, support and total patience during my PhD studies leading to the completion of my thesis. Thanks to Professor Ringsdorf (University of Mainz), Professor Ferruti (University of Milan), Professor Veronese (University of Padua), Dr. Jones and Dr. Schmaljohann for their helpful scientific discussions. Also I would like to thank Cardiff University for supporting my PhD studies.

I would like to thank my colleagues, from both Pharmacy and Chemistry who helped me with the techniques I used during this study, Jacopo (PAA synthesis), Kawai (RBC lysis and general help) and Nathalie (liposomes preparation), from chemistry Alison (SANS), James, Sarah and Dr. Damien Murphy (EPR studies). The knowledge obtained was great but the experience working with them was priceless.

I would like to thank Michelle and Dr. Jannette Davidge for their help in the lab and continued support. A special thanks to Wendy Meeson for proof reading my thesis, and for being a great friend.

During my study I have met the most amazing people, all had to listen to me moan, so a huge THANK YOU to Alison, Champa, Elaine, Helena, Kerrie, Lucile, Maria², Marie, Neal, Nilmini, Vivian, Sam, Sarah and Tuss, and my housemates. Finally a very special thanks to Fran, Kaz, Kawai, and Tom. We all have been through so much together and shared many experiences both good and bad, my life would not have been the same if I have chosen another path, I wish them all the best in the future.

And finally, a BIG thank you to my family (especially my mum) for their great support during this study.

**Dedicated to my mother
and the rest of my family**

Abstract

Polyamidoamines (PAAs) are a family of synthetic, water-soluble, linear polymers that are synthesised by hydrogen-transfer polyaddition of aliphatic amines or *bis*-secondary amines to *bis*acrylamides (reviewed by Ferruti et al 2002). Over the last 15 years, PAAs have been developed as drug carriers and as pH-responsive polymers for protein and gene delivery (Richardson et al, 2001). The latter, called endosomolytic PAAs, can disrupt membranes at low pH, but the delivery of genes and proteins is still poorly efficient. The precise mode of action is still poorly understood, therefore the main aim of this work was to examine the physico-chemical properties of PAAs in order to better define their mechanism of membrane permeabilisation to allow design of more efficient chemical structures.

First PAA ISA1 (23 k g/mol) and ISA23 (52 - 67 k g/mol) were synthesised and were characterised using ¹H-NMR, GPC and acid-base titration. In agreement with past studies, ISA23.HCl demonstrated a pH-dependant haemolytic activity.

The solution conformation of ISA23.HCl was then investigated using small-angle neutron scattering (SANS). ISA23.HCl possessed a Gaussian coil like-shape in solution at all pHs (pH 2 to 14) and polymer concentrations examined (10 mg/ml to 50 mg/ml). However as the pH decreased the radius of gyration increased to a maximum ($R_g \sim 8$ nm) at \sim pH = 3.

Surface tension, electron paramagnetic resonance (EPR) and SANS were then used to investigate the interaction of ISA23.HCl with simple micelles as model surfaces. Both pH and micelle composition played an important role in the strength of interaction seen. For SDS micelles, three different responses were observed, strong interaction at pH < 4.5, weak interaction at pH 4.5 – 6.5, and no interaction at pH > 7. However, ISA23.HCl did not appear to interact with more biologically relevant lyso-PC surfactants at pHs 7.4 - 5.5. EPR experiments showed that micelle fluidity was effected when a PAA-micelle interaction occurred, and SANS reinforced this conclusion.

Finally, liposomes were used as a more complex model membrane. Liposomes were prepared to mimic three phospholipids composition of plasma, endosomal and lysosomal membranes. The liposomes were stable over 2 days at pH 7.4, 5.5 and 4, but not at pH 3. SANS was used to study polymer-liposomes interaction, and the Schultz polydisperse 3 shell sphere model was used to fit the liposomal (alone) SANS scattering data. The radius of the plasma, endosome and lysosome liposomes was \sim 50 nm. When liposomes were incubated in the presence of ISA23.HCl, it was difficult to interpret the scattering data. However, it was clear that at pH 4 and 5.5 scattering of model liposomes alters in the presence of PAA indicating possible interaction. Using a contrast approach the scattering data for ISA23.HCl in the presence of model liposomes could be extracted. This was again fitted using Gaussian coil model. Generally, the polymer increased in size in the presence of liposomes, at pHs where there was an interaction. However, these are only preliminary experiments, and there is a need for further mathematical modelling.

In conclusion, this project emphasises the importance of combining the different disciplines to fully understand a system that can be the first step in finding a way to cure devastating genetic diseases.

Content

	Page
Abbreviations	i
List of Figures	v
List of Tables	x
1 General Introduction	1
1.1 Background	1
1.2 Use of water-soluble polymers to promote targeting and cytosolic delivery	3
1.3 The complexity and the implications of intracellular trafficking for design of non-viral vector for cytosolic delivery	4
1.3.1 Physical and biochemical barriers that therapeutic agent faces during the endocytic pathways	7
1.3.1.1 Pinocytosis	7
1.3.1.2 Mechanisms of Internalisation	10
1.3.1.3 Intracellular Trafficking	11
1.3.2 Endosomotropic Delivery	13
1.3.3 Mechanisms of endosomal membrane breakage	15
1.4 Non-viral vectors for intracytoplasmic delivery	19
1.4.1 Cationic lipids/liposomes	19
1.4.2 Polymers as non-viral vectors for cytosolic delivery	21
1.4.2.1 Anionic polymers	21
1.4.2.2 Cationic polymers	25
1.5 PAAs	27
1.5.1 Historical background and the evolution of PAAs	27
1.5.2 Development of PAAs for drug delivery applications	28
1.5.3 Physico-chemical properties of PAAs	33
1.5.4 Mechanism of PAA endosomolytic activity	34
1.6 Aims of the studies in this thesis	35

	Page
Chapter 2 Materials and Methods	
2.1 Apparatus	37
2.1.1 Analytical Instruments	37
2.1.2 PAA purification and the freeze drying	37
2.1.3 General equipment	38
2.2 Materials	38
2.2.1 General chemicals	38
2.2.2 Material used for the synthesis of ISA 1 and 23	39
2.2.3 Materials for the analytical experiments	39
2.2.4 Materials used in liposomes preparation and characterisation	39
2.3 Methods	40
2.3.1 Characterisation of PAAs using GPC	40
2.3.2 Evaluation of the haemolytic activity of PAAs	43
2.3.3 Liposome preparation and stability testing	43
2.3.4 Evaluation of ISA23.HCl interaction with micelles and liposomes as model membranes	47
2.3.5 Lyophilisation and storage of polymers	49
Chapter 3 Synthesis and characterisation of poly(amidoamine)s	
3.1 Introduction	50
3.2 Methods	53
3.2.1 General methods	53
3.2.2 Synthesis of ISA1	55
3.2.3 Synthesis of ISA23	57
3.3 Results	59
3.3.1 Characterisation of ISA1 and ISA23	59
3.3.2 The effect of time and temperature on ISA1 and ISA23 polymerisation	64
3.3.3 Studies on the degradation of PAAs at room temperature and 37°C (pH 7.4 and 5.5)	71
3.3.4 Evaluation of the haemolytic activity	71

	Page
3.4 Discussion	71
3.5 Conclusions	79
Chapter 4 The investigation of the solution behavior of ISA23.HCl using SANS	
4.1 Introduction	80
4.1.1 Small-angle neutron scattering	80
4.2 Methods	89
4.2.1 Sample preparation	89
4.2.2 SANS measurements of ISA23.HCl in solution	91
4.3 Results	92
4.3.1 Data fitting of neutron scattering data using rod, sphere and Gaussian coil model	92
4.3.2 The effect of pH on ISA23.HCl conformation	94
4.3.3 The effect of concentration, molecular weight and temperature on the polymer conformation	99
4.4 Discussion	107
4.5 Conclusions	111
Chapter 5 Studies on the interaction between ISA23 and model micelles	
5.1 Introduction	112
5.1.1 Surfactants and Model surfaces	113
5.1.2 Methods used to characterise polymer-micelles interaction	117
5.2 Methods	121
5.2.1 Measurement of the surface tension of surfactants in the present of ISA23.HCl	121
5.2.2 EPR spectroscopy of micelle-ISA23.HCl interaction	122
5.2.3 SANS of ISA23.HCl-micelle interaction	123
5.3 Results	123
5.3.1 Interaction of ISA23.HCl with SDS surfactants	123

	Page
5.3.2 Interaction of ISA23.HCl with SDS/C ₁₂ E ₄ as heterogeneous system	133
5.3.3 Interaction of ISA23.HCl with SDS/C ₁₂ BNMG and CTAB/C ₁₂ BNMG as heterogeneous system	133
5.3.4 Interaction of ISA23.HCl with Lyso-PC micelles	140
5.4 Discussion	147
5.5 Conclusions	155
Chapter 6 Studies on the interaction between ISA23 and liposomes	
6.1 Introduction	160
6.1.1 Biomembranes and their organisation	160
6.1.2 Selection of lipids compositions for these studies	163
6.2 Methods	166
6.2.1 Preparation of liposomes and stability testing	166
6.2.2 SANS measurements	168
6.3 Results	168
6.3.1 Liposomes characterisation	168
6.3.2 Stability of liposomes	171
6.3.3 Preparation of calcein entrapped liposomes	171
6.3.4 SANS analysis of protonated and deuterated liposomes mimicking biological membranes	171
6.3.5 The effect of ISA23.HCl on the morphology of biological membranes model liposomes	178
6.4 Discussion	191
6.5 Conclusions	201
Chapter 7 General Discussion	
7.1 Recent development in the non-viral vectors	202
7.2 Mechanism of action of ISA23.HCl as an endosomolytic polymer	204
7.3 Conclusions and future studies	208

	Page
Bibliography	211
Appendix I	
List of abstract and publication	230
Appendix II	
Papers	231
Appendix III	
EPR figure	249

Abbreviations

AIDS	Acquired immune deficiency syndrome
BAC	2,2- <i>Bis</i> -(acrylamido)acetic acid
BHE	<i>Bis</i> -hydroxyethylethylenediamine
BIS-PIP	<i>Bis</i> -acryloylpiperazine
CAC	Critical aggregation concentration
CAD	Coronary artery disease
C ₁₂ E ₄	Tetra(ethylene glycol)dodecylether
C ₁₂ BNMG	Dodecylmalono- <i>bis</i> (<i>N</i> -methylglucamide)
CMC	Critical micelle concentration
¹³ C-NMR	Carbon (13) nuclear magnetic resonance
CTAB	Cetyltrimethylthylammonium bromide
D-DPPC	1,2-Dipalmitoyl-D62- <i>sn</i> -glycero-3-phosphocholine
D-DPPE	1,2-Dipalmitoyl-D62- <i>sn</i> -glycero-3-phosphoethanolamine
D-DPPS	1,2-Dipalmitoyl-D62- <i>sn</i> -glycero-3-[phospho-L-serine] (sodium salt)
DEAE-dextran	Diethylaminoethyl-dextran
DOPE	1,2-Dioleoyl- <i>sn</i> -glycerol-3-phosphoethanolamine
DOTAP	1,2-Dioleoyl-3-trimethylammonium-propane
DPPC	1,2-Dipalmitoyl- <i>sn</i> -glycero-3-phosphocholine
DPPE	1,2-Dipalmitoyl- <i>sn</i> -glycero-3-phosphoethanolamine
DPPS	1,2-Dipalmitoyl- <i>sn</i> -glycero-3-[phospho-L-serine] (sodium salt)
d-SDS	Deuterated SDS
16-DSE	16-Doxyl stearic acid methyl ester

EPR	Electron paramagnetic resonance
k_f	Scattered wavevectors
k_i	Incident wavevectors
HCl	Hydrochloric acid
HIV	Human immunodeficiency virus
$^1\text{H-NMR}$	Proton nuclear magnetic resonance
HPLC	High performance liquid chromatography
GPC	Gel permeation chromatography
ILL	Institute Max von Laue-Paul Langevin
LCST	Lower critical solution temperature
LS	Light scattering
Lyso-PC	1-Palmitoyl-2-hydroxy- <i>sn</i> -glycero-3-phosphocholine
MBI	N,N' - <i>bis</i> (2-hydroxyethyl) ethylenediamine
2-MePip	2-Methyl piperazine
M_n	Average number molecular mass
M_w	Average-weight molecular mass
N_{agg}	Aggregation number
NIPAM	N-isopropylacrylamide
NMR	Nuclear magnetic resonance
NPC	Nuclear pore complexes
P	Packing parameter
PA	Phospholipids phosphatidic acid
PAAs	Polyamidoamines
PAMAM dendrimers	Poly(amidoamine) dendrimers

PC	Phosphatidylcholine
PCS	Photon correlation spectroscopy
pDAMA	Poly(2-methyl-acrylic acid 2-[(2-(dimethylamino)-ethyl)-methyl-amino]-ethyl ester
p(DMAEDMA)	Poly [2-(dimethylamino)ethyl methacrylate]
PE	Phosphatidylethanolamine
PEG	Poly(ethylene glycol)
PEI	Poly(ethylene imine)
PG	Phosphatidylglycerol
PI	Phosphatidylinositol
PLL	Poly(L-lysine)
P(Q)	Form factor
PS	Phosphatidylserine
PVC	Poly(vinyl chloride)
PVP	Poly(vinylpyrrolidone)
Q	Wavevector
R	Radius
RAC	Ricin A chain
RBC	Red blood cells
RES	Reticular endothelial system
R_g	Radius of gyration
RI	Refractive index
rpm	Round per minutes
SANS	Small-angle neutron scattering
SDS	Sodium dodecyl sulphate
SAXS	Small-angle X-ray scattering
S(Q)	Structure factor

TB	Tuberculosis
T _m	Transition temperature
TOF	Time-of-flight
TX-100	Triton X-100

List of Figures

Chapter 1 General Introduction

- Figure 1.1** Schematic diagram of polymer therapeutics now in, or progressing towards, clinical development (adapted from Duncan, 2003a)
- Figure 1.2** The intracellular trafficking and the barriers that the therapeutic agent faces at the cellular level
- Figure 1.3** Mechanisms by which cells uptake large macromolecules
- Figure 1.4** The mechanisms of cellular uptake of cationic, anionic, non-ionic, amphoteric polymers and polyplexes
- Figure 1.5** The overall scheme of endosomotropic delivery (adapted from Duncan, 2003a)
- Figure 1.6** The proton sponge hypothesis
- Figure 1.7** Pore formation mechanism
- Figure 1.8** The membrane bending mechanism
- Figure 1.9** Structures of widely studied endosomolytic polymers
- Figure 1.10** Typical structures of number of PAAs
- Figure 1.11** The chemical structures of ISA1, ISA4, ISA22 and ISA23

Chapter 2 Materials and methods

- Figure 2.1** A schematic showing the principle of GPC
- Figure 2.2** The schematic representation of the red blood cell lysis assay
- Figure 2.3** Schematic diagram summarising the preparation of liposomes using freeze-thaw/extrusion method
- Figure 2.4** The schematic illustration of the changing pressure inside the bubble with bubble life-time (adapted from Dukhin et al, 1996)

Chapter 3 Synthesis and characterisation of poly(amidoamine)s

- Figure 3.1** The overall mechanism of Michael addition
- Figure 3.2** Synthesis of ISA1

- Figure 3.3** Synthesis of ISA23
- Figure 3.4** $^1\text{H-NMR}$ spectra of ISA1 and ISA23
- Figure 3.5** Titration curves of ISA1 and ISA23
- Figure 3.6** GPC of PEG and pullulan standards
- Figure 3.7** The GPC traces of PAAs
- Figure 3.8** The effect of time and temperature on PAA polymerisation
- Figure 3.9** Evaluation of the degradation of ISA23 using GPC
- Figure 3.10** The heamoglobin release (1h) by PAA polymers (1 mg/ml) at different pH values
- Figure 3.11** Concentration dependent haemolysis of ISA23
- Figure 3.12** The relationship between PAA induced haemolysis and solution pH

Chapter 4 The investigation of the solution behaviour of ISA23.HCl using SANS

- Figure 4.1** Schematic diagram of SANS instrumentation and neutron production at ILL
- Figure 4.2** Schematic diagram of SANS instrumentation and the neutron production at ISIS
- Figure 4.3** Schematic diagram summarising application of different scattering methods, according to their size
- Figure 4.4** Schematic diagram showing the mechanism for studying a multicomponent system by varying the contrast
- Figure 4.5** The theory behind and the mathematical derivation of the scattering wavevector (Q)
- Figure 4.6** The theoretical shapes that ISA23.HCl might adopt
- Figure 4.7** SANS data obtained for ISA23.HCl (50 mg/ml) in D_2O (pH 3.15) at 37°C
- Figure 4.8** The effect of pH on the data form of ISA23.HCl
- Figure 4.9** The effect of pH on PAA conformation
- Figure 4.10** The scattering data of ISA23.HCl samples at pH 7.4 and 5.5 with the same ionic strength, with the fitting using the Gaussian coil model (solid line)

- Figure 4.11** Effect of concentration and pH on the solution conformation of ISA23.HCl in D₂O (37 °C) evaluated by SANS
- Figure 4.12** The effect of temperature on the scattering raw data obtained for ISA23.HCl at different pHs
- Figure 4.13** The effect of ISA23.HCl molecular weight on SANS
- Figure 4.14** Correlation between ISA23.HCl haemolytic activity and its R_g and degree of protonation

Chapter 5 Studies on the interaction between ISA23 and model micelles

- Figure 5.1a** The chemical structure of non-ionic and anionic surfactants
- Figure 5.1b** The chemical structure of zwitterionic and cationic surfactants, and the spin-probe
- Figure 5.2** The distribution of surfactant molecules at the surface and the bulk of the solution, and the maximum bubble pressure technique used to measure the surface tension
- Figure 5.3** Schematic diagram showing the possible location where polymer interacts with surfactants, and the techniques used to investigate polymer-surfactant interaction
- Figure 5.4** Electron spin levels in a magnetic field
- Figure 5.5** Effect of ISA23.HCl on the surface tension of SDS surfactant solution
- Figure 5.6** The effect of ISA23.HCl on the SANS data of the SDS micelles
- Figure 5.7** The SANS data of d-SDS micelles in the presence of ISA23.HCl
- Figure 5.8** EPR spectra of SDS micelles as a function of pH
- Figure 5.9** The polarity of SDS + HCl (open diamond) as a function of pH and the polarity (open circle) of SDS plus NaCl with concentration that is equivalent to that of HCl
- Figure 5.10** The EPR of SDS in the presence of ISA23.HCl as a function of pH
- Figure 5.11** The effect of ISA23.HCl on the fluidity of SDS micelles, as a function pH
- Figure 5.12** The polarity of SDS micelles in the presence (open circles) and absence of ISA23.HCl (open diamond) as a function of pH

- Figure 5.13** The surface tension of C₁₂BNMG in the presence (black circles) and absence (blue squares) of ISA23.HCl
- Figure 5.14** The surface tension curve of SDS/C₁₂BNMG in the presence (blue triangles) and absence (black circles) of ISA23.HCl at pH 5.5 (panel a) and pH 7.4 (panel b)
- Figure 5.15** The surface tension curve of CTAB/C₁₂BNMG in the presence (blue squares) and absence (black circles) of ISA23.HCl at pH 5.5
- Figure 5.16** The effect of ISA23.HCl on the surface tension of lyso-PC
- Figure 5.17** The effect of ISA23.HCl on the morphology of lyso-PC micelles
- Figure 5.18** The EPR spectra of lyso-PC micelles as a function of pH
- Figure 5.19** The polarity of lyso-PC micelles in the presence (open red circles) and absence of ISA23.HCl (open black diamonds) as a function of pH
- Figure 5.20** The EPR spectra of lyso-PC in the presence (red line) and absence (blue line) of ISA23.HCl at pH 5.5 (panel a) and pH 7.4 (panel b)
- Figure 5.21** Summary of the ISA23.HCl interaction with SDS/C₁₂E₄ micelles using surface tension
- Figure 5.22** The schematic diagram which represent the hypothetical interaction of ISA23.HCl with SDS molecules as a function of surfactant concentration (adapted from Goddard, 2002)
- Figure 5.23** The possible structures that represent the three different possible responses observed in SANS and EPR study
- Figure 5.24** The effect of the control polymers used in the haemolysis assay on the morphology of lyso-PC micelles

Chapter 6 Studies on the interaction between ISA23 and liposomes

- Figure 6.1** The major phospholipids found in biological membranes
- Figure 6.2** Schematic representation the packing parameter of amphiphiles
- Figure 6.3** The effect of extrusion on liposome size distribution
- Figure 6.4** The stability of plasma-model liposomes at 4 °C
- Figure 6.5** The stability of endosomal-model liposomes
- Figure 6.6** The stability of lysosomal-model liposomes

- Figure 6.7** Schematic representation of the changing scattering length densities of the different layers of liposomes in solution (the Schultz polydisperse 3 shell sphere model)
- Figure 6.8** SANS data obtained using the plasma membrane-model liposomes
- Figure 6.9** SANS data obtained using the endosomal membrane-model liposomes
- Figure 6.10** SANS data obtained for the lysosomal membrane-model liposomes
- Figure 6.11** The effect of ISA23.HCl on the scattering of plasma membrane-model liposomes
- Figure 6.12** The effect of ISA23.HCl on the scattering of endosomal membrane-model liposomes
- Figure 6.13** The effect of ISA23.HCl on the scattering of endosomal membrane-model liposomes
- Figure 6.14** The effect of ISA23.HCl on the scattering obtained from lysosomal membrane-model liposomes
- Figure 6.15** The effect of ISA23.HCl on the scattering of lysosomal membrane-model liposomes
- Figure 6.16** The size distribution of liposomes measured by PCS in the presence (panel b) of and absence (panel a) of TX-100
- Figure 6.17** The schematic diagram representing parts of the liposomes/polymer system responsible for scattering in the protonated (panel a and b) and the deuterated liposomes (panel c and d)
- Figure 6.18** The hypothetical representation of the different possible interaction between ISA23.HCl and model-liposomes
- Figure 6.19** The effect of control polymers on the scattering of endosome membrane-model liposomes

Chapter 7 General Discussion

- Figure 7.1** The comparison between what the polymer encountered during intracellular trafficking and its comparison to the experiments conducted in this study

List of Tables

Chapter 1 General Introduction

- Table 1.1** List of endosomolytic polymers, their pKa, type of structure, molecular weight and current status
- Table 1.2** Summary of the different applications of PAAs

Chapter 2 Materials and methods

- Table 2.1** Polymer standards used for GPC calibration

Chapter 3 Synthesis and characterisation of poly(amidoamine)s

- Table 3.1** The lipid composition of the plasma membrane of human erythrocyte
- Table 3.2** Characteristics of the PAAs batches synthesised, and their code numbers
- Table 3.3a** The molecular weight characteristics of PAAs calculated using PVP standard
- Table 3.3b** The molecular weight characteristic of PAAs calculated using PEG and pullulan standards
- Table 3.4** The final molecular weight (M_w) of ISA1 and ISA23 after polymerisation, at different temperatures

Chapter 4 The investigation of the solution behaviour of ISA23.HCl using SANS

- Table 4.1** The coherent scattering lengths of some common nuclei
- Table 4.2** The effect of concentration on the size of ISA23.HCl, at pH 7.4 and 5.5
- Table 4.3** Summary of the fitting parameters for ISA23.HCl calculated using Gaussian coil model

Chapter 5 Studies on the interaction between ISA23 and model micelles

- Table 5.1** The summary of the parameters calculated from the model fittings to the SDS in the presence and absence of ISA23.HCl at pH 4, 5.5 and 7.4
- Table 5.2** The summary of the parameters calculated from the model fittings to the d-SDS micelles in the presence of ISA23.HCl at pH 4, 5.5 and 7.4

Table 5.3 Summary of the parameters calculated from model fittings to lyso-PC in the presence and absence of ISA23.HCl at pH 5.5 and 7.4

Table 5.4 Summary of the parameters calculated from the model fittings to the lyso-PC in the presence of TX-100, dextran and PEI

Chapter 6 Studies on the interaction between ISA23 and liposomes

Table 6.1 Transition temperature of the phospholipids used to prepare the model liposomes in this study

Table 6.2 Summary of the major components of the three biological membranes, plasma, endosome and lysosome

Table 6.3 The molar of the three phospholipids used to prepare the liposomes

Table 6.4 Experiments undertaken to study liposomes ISA23 interaction

Table 6.5 Summary of the fixed parameters used to fit the SANS data obtained using liposomes

Table 6.6 Summary of liposome characteristics, calculated from the Schultz polydisperse 3 shell sphere mathematical model

Table 6.7 The summary of the R_g of ISA23.HCl, in the presence and the absence of the different model liposomes at pH 7.4, 5.5 and 4

Chapter 1
General Introduction

1 General Introduction

1.1 Background

Currently, the four main causes of mortality worldwide are cancer, cardiovascular, cerebrovascular and infectious diseases (Mathers et al, 2001). Cancer was responsible for 7 million deaths in 2000 (Felay et al, 2000). Cardiovascular and cerebrovascular diseases were responsible for more than 15 million i.e. 30% of total global mortality (Opari, 1999). Approximately 50% of these deaths were due to coronary artery disease (CAD), and nearly 33% were associated with stroke (Opari, 1999). Acquired immune deficiency syndrome (AIDS) caused by human immunodeficiency virus (HIV), tuberculosis (TB) and lower respiratory diseases are the main infectious diseases that cause mortality. Almost 38 million people are living with HIV, and there have been 20 million deaths since the first AIDS diagnosis in 1981 (UNAIDS/WHO 2004). One-third of the world's population is currently infected with the TB bacillus, and it caused two million deaths in 2002.

These facts, coupled with the emergence of multi-drug resistance diseases highlight the importance of developing new and improved medicines. In this context, there has been growing interest in the use of macromolecular drugs such as peptides, proteins, genes and polymer therapeutics as treatments for such life-threatening diseases.

Many of these macromolecular agents work at the intracellular level. So their ability to access the cell cytoplasm is crucial for therapeutic efficacy. Design and development of effective delivery vehicles that are both safe and efficient has proved a major challenge. For example, for gene therapy, thus far viral vectors have been the most widely used, but viruses have limitations such as toxicity and immunogenicity (reviewed in Aneed, 2004). Therefore, there is an urgent need to find safe and effective alternatives. In this context, many have been developing endosomolytic polymers as non-viral vectors for cytosolic delivery (Duncan et al, 1994; reviewed in Smith et al, 1998; reviewed in Christie and Grainger, 2003).

Non-viral delivery systems include physical and chemical delivery methods. For the physical approach, naked DNA is delivered directly to the cytoplasm by-passing the intracellular vesicles such as endosome and the lysosome, thus degradation by the

lysosomal enzymes can be avoided (reviewed in Wolf and Wolf, 2003). Physical techniques for gene delivery include direct injection (Capecchi, 1980; reviewed in Auerbach, 2004), electroporation (reviewed in Gehl, 2003), the gene gun (Klein et al, 1987; Williams et al, 1991; Trimble et al, 2003), laser irradiation (Kurata et al, 1986; Terakawa et al, 2004), sonoporation and magnetofection.

The chemical approach for non-viral delivery usually involves cationic vehicles such as lipids / liposomes and polymers. To be useful a non-viral delivery vehicle must be (Schatzlein, 2003; Roth and Sundaram, 2004; Mastrobattista et al, 2005)

- Biocompatible, non-toxic, non-immunogenic and non-pathogenic
- Able to carry and protect the payload from degradation
- It must be stable
- It must be able to:
 - target the appropriate cell type
 - avoid the accumulation in the liver
 - ideally introduce the payload into the cytosol via interaction with endosomal membrane or the plasma membrane
 - release the therapeutic agent at the target site
 - direct the payload to the intracellular target (e.g. nucleus)

In addition it must be:

- Easy to administer
- Inexpensive to synthesise and purify

Increase in interest in the use of polymers as non-viral vectors has occurred due to advances in polymer chemistry which are allowing the synthesis of polymers with specific chemical structure. These structures vary from simple linear polymers to highly branched dendrimers (reviewed Duncan, 2004), and they can be designed to have precisely defined physical and chemical properties, as well as three-dimensional structure in the case of dendrimers.

Over the last 15 years, Duncan and Ferruti et al (Ranucci et al, 1991) have started to design amphoteric polyaminoamines (PAAs) as endosomolytic polymers for gene and toxin delivery. Although much less toxic than polycations (Ranucci et al, 1991; Richardson et al, 1999), and able to avoid liver capture after intravenous injection

(Richardson et al, 1999) (leading to tumor targeting by the enhanced permeability and retention effect (Richardson et al, 2001)), their ability to deliver genes (Richardson et al, 1999) and non-permeant toxins (e.g. ricin A chain and gelonin) (Patrick et al, 2001a) was still poorly efficient (Richardson et al, 1999; Patrick et al, 2001a).

Thus the overall aim of this project was to better understand the mechanism of action of PAAs by defining their physico-chemical and bio-physical properties. It was hoped that this information would help to improve PAAs design to improve efficiency of transfer when used as endosomolytic polymers for intracellular delivery of genes and proteins. Here small-angle neutron scattering (SANS) was chosen to investigate PAA conformation in physiological solutions. The mechanism at which PAAs cause pH-dependent membrane breakage was also investigated by studying the interaction between PAAs and model membranes, including red blood cells, surfactant micelles and liposomes, with a phospholipid composition similar to that of biological membranes (plasma, endosomal and lysosomal membranes). Techniques used in this context included: surface tension measurements, to study the onset of an interaction, SANS to study the effect of PAA on the morphology of model membranes, and electron paramagnetic resonance (EPR) to investigate the effect of PAA on the fluidity of model membranes.

To understand the rationale for this interdisciplinary project it is important to have a background understanding of polymer therapeutics, the design and current status of non-viral vectors for intracytoplasmic delivery, the mechanism by cellular uptake of macromolecules (i.e. endocytosis) and intracellular trafficking. These topics are briefly reviewed in the next section. Also, it is important to introduce the physico-chemical techniques that have been used to characterise polymer properties. As PAAs were used for these studies, their evolution as biomedical polymers, and the current understanding of their physico-chemical properties are reviewed in detail.

1.2 Use of water-soluble polymers to promote targeting and cytosolic delivery

Over recent years the development of polymer therapeutics (reviewed in Duncan, 2003a) has been leading to the design of sophisticated nanosized medicines. Polymer therapeutics is a term used to describe **polymeric drugs**, **polymer-drug conjugates** (Kopecek et al, 2000; Duncan, 2003b) and **polymer-protein conjugates**

(reviewed in Harris and Chess, 2003), **drug entrapment in polymer micelles** by covalent linkage and those **polymeric multicomponents polyplexes** used as non-viral vectors (Ogris and Wagner, 2002; Niidome and Huang, 2002) (Figure 1.1). Thanks to the successful clinical application of polymer-protein conjugates, and promising clinical results arising from trials with polymer-anticancer-drug conjugates (reviewed in Duncan, 2003a), there has been growing interest in the field of polymer therapeutics, and particularly the bioresponsive polymer designed to deliver proteins and genes to the cytosol (Boussif et al, 1995; Li et al, 2004; Griffiths et al, 2004).

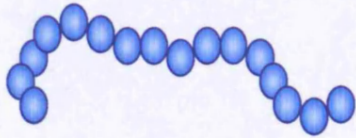
All macromolecular therapeutics and nanosized delivery systems enter the cell by mechanism known as endocytosis (reviewed in Jones et al, 2003). To optimise their design, it is therefore very important to understand the processes of endocytosis and intracellular trafficking. Both play a key role in determining the therapeutic efficiency, and they are briefly explained in the next section.

1.3 The complexity and the implications of intracellular trafficking for design of non-viral vector for cytosolic delivery

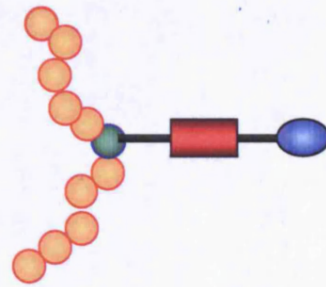
Macromolecular therapeutics such as, genes, peptides and proteins, normally require access to intracellular components to exert a therapeutic effect. At the cellular level there are number of barriers that such macromolecular therapeutics will encounter before they can reach their site of action. These include:-

- The plasma membrane, which is a physical barrier (Hawiger, 1999),
- The mechanism of cellular uptake and trafficking (Wiethoff and Middaugh, 2003)
- The effect of the change in pH in the endosome and lysosome
- The effect of the lysosomal enzymes, which can degrade proteins and nucleotide (Alberts et al, 1994)
- The endosomal or lysosomal membranes, which are also physical barriers

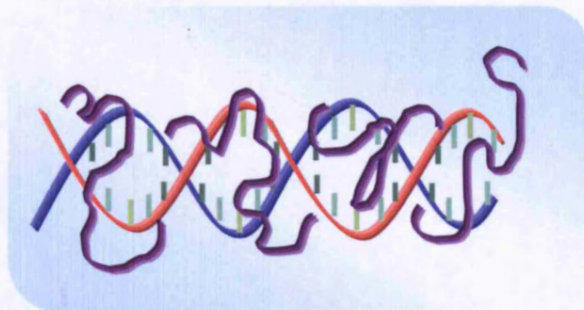
These biochemical and physical barriers will be discussed in more detail in the next section (Figure 1.2).



Polymeric drugs



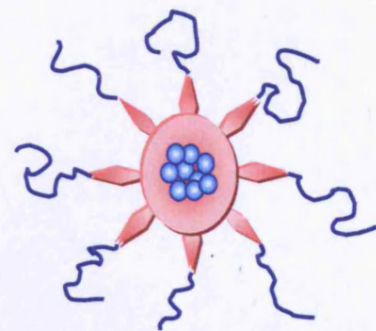
Polymer-drug conjugates



**Non-viral vector
For gene delivery**



Polymer-protein conjugates



**Drug entrapment in a
polymer micelle**

Figure 1.1 Schematic diagram of polymer therapeutics now in, or progressing towards, clinical development (adapted from Duncan, 2003a).

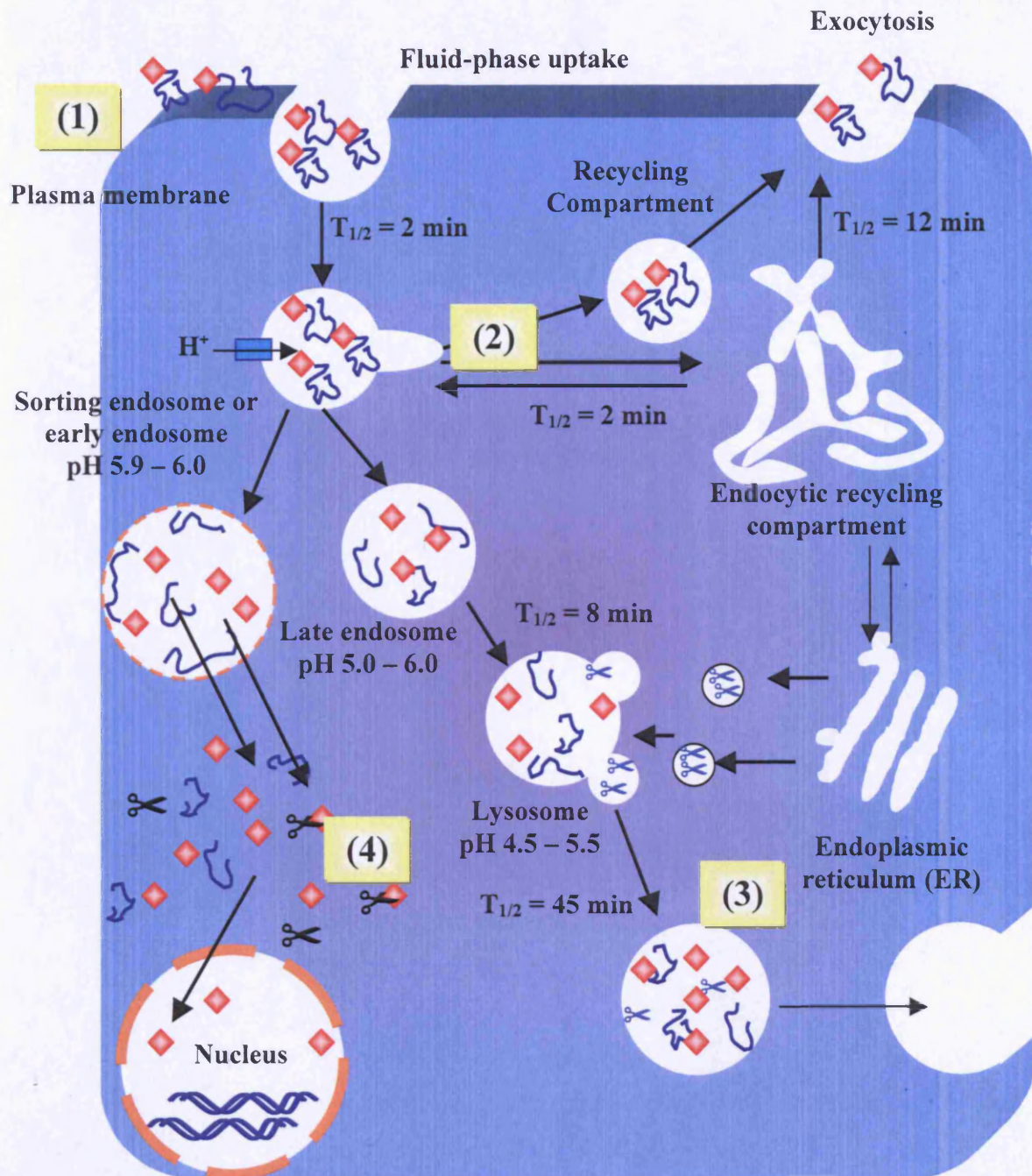


Figure 1.2 The intracellular trafficking and the barriers that the therapeutic agent faces at the cellular level. The first barrier that it will encounter is the plasma membrane (1). Following endocytosis, the therapeutic drug can either be recycled back to the cell surface (2) or it is carried to the late endosome. If the therapeutic agent does not escape to the cytosol it will get degraded by lysosomal enzymes (∞) (3). Once the protein / DNA is successfully delivered into cytoplasm, here it must spend very little time to avoid the degradation by the enzymes found there (nucleases, ∞) (adapted from Ogris and Wagner, 2002; Maxfield and McGraw, 2004)

1.3.1 Physical and biochemical barriers that therapeutic agents face during the endocytic pathways

The first barrier that the macromolecular drugs encounter is plasma membrane (Parkes and Hart, 2000). This has a complex structure, being composed of lipids and proteins. Cellular entry is via endocytosis (Asokan and Cho, 2002). It involves the invagination (folding inward) of small portion of the plasma membrane enclosing a droplet of the external medium containing macromolecules, and this “buds off” to form intracellular vesicles (Slepnev and Camilli, 1998). This mechanism of endocytosis has been divided into two main groups, pinocytosis (cell drinking) and phagocytosis (cell eating) (Aderem and Underhill, 1999; Maxfield and McGraw, 2004). The latter describes the uptake of large particulate (e.g. bacteria by macrophages) so it will not be discussed further.

1.3.1.1 Pinocytosis

The term pinocytosis is used to describe the non-specific uptake of small droplets of extracellular medium (Slepnev and Camilli, 1998) (see Figure 1.3 for an overview of endocytosis). There are three main mechanisms of internalisation; receptor-mediated pinocytosis, non-specific adsorptive pinocytosis and fluid-phase pinocytosis. The chemical properties of macromolecules play a crucial role in determining their mechanism of cellular uptake. Negatively charged macromolecules (e.g. the polyanion DNA) and neutral macromolecules (e.g. poly(ethylene glycol) (PEG)) do not associate with the membrane, and cellular uptake may be by non-specific fluid-phase endocytosis (Figure 1.4) (Godbey et al, 1999a; Kristensen et al, 2001). In contrast, positively charged macromolecules, poly(ethylene imine) (PEI) and cationic polyplexes, DNA associated with positively charged vectors (with excess positive charge) binds by ionic interaction to the negatively charged membrane. Thus, they are taken up by a non-specific adsorption process (Godbey et al, 1999a; Kristensen et al, 2001). Binding of the positively charged macromolecule to the membrane can induce membrane depolarization, which causes the formation of membrane invagination, which is then followed by budding and vacuole formation

This study largely investigates PAA polymers, so it is important to consider their possible mechanism of endocytic uptake. The previously described cationic PAAs (e.g. ISA1 and ISA4) (reviewed in Ferruti et al, 2002), are probably endocytosed by a non-specific adsorptive process. However, the amphoteric PAAs (e.g. ISA22 and ISA23)

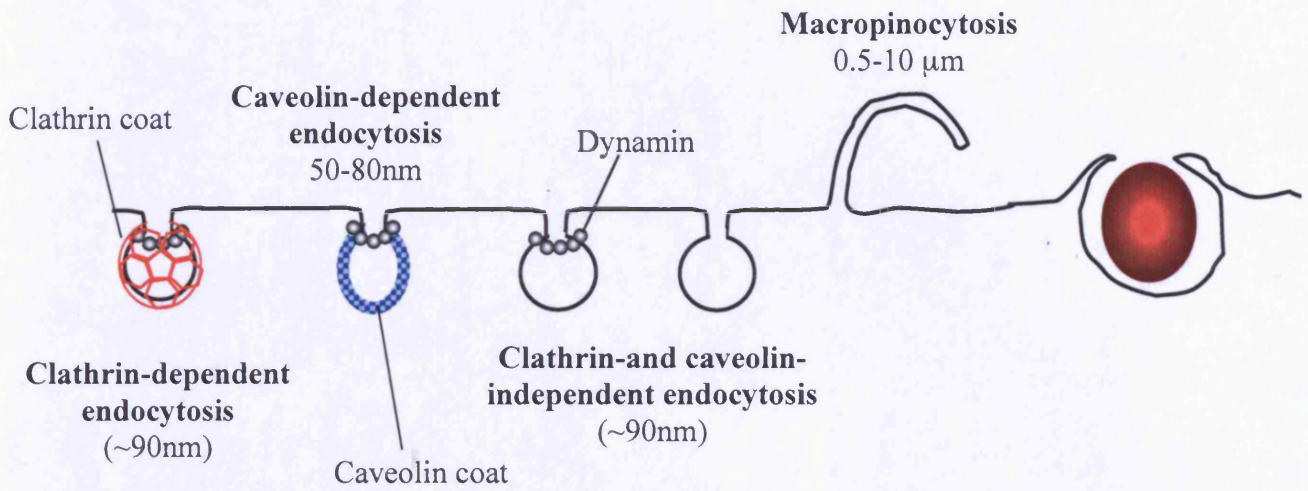


Figure 1.3 Mechanisms by which cells uptake large macromolecules. Summary of the different types of endocytosis (diagram adapted from Conner and Schmid, 2003)

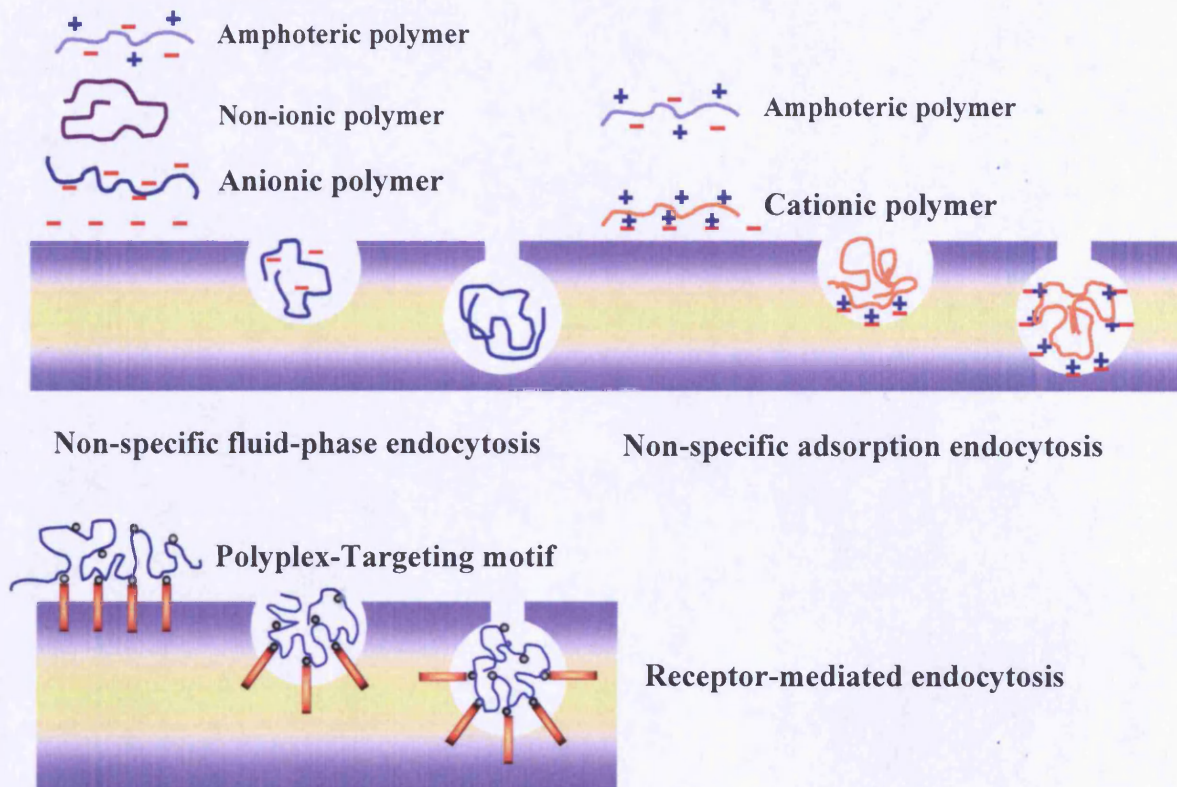


Figure 1.4 The mechanisms of cellular uptake of cationic, anionic, non-ionic, amphoteric polymers and polyplexes. The non-ionic and anionic polymers will not interact with the plasma membrane and the internalisation is relied on non-specific fluid-phase endocytosis. On the other hand cationic polymers are able to interact with the plasma membrane and it enters the cell by adsorption mechanism. For amphoteric polymer (e.g. ISA23) both mechanisms can be responsible for their cellular uptake. Finally to achieve selectivity, polyplexes are conjugated to targeting motifs (for transferrin receptors as an example), this is an example of active targeting

would predominantly be negatively charged at pH 7.4 (although they would carry some positive charge), so their mechanism of uptake might not be that straightforward. Attraction of the positive charges on the PAA and the negatively charged membrane could lead to an interaction but repulsion would also result from the negative charge on the PAA and the negatively charged membrane. PAA could theoretically be endocytosed by either fluid-phase endocytosis or by adsorptive process (or a combination of both, which is most likely). Although cationic PAAs and the polyplexes they form, would show enhanced binding to the cell membrane, they suffer from disadvantages of increased toxicity, non-specific interaction with RBC and plasma proteins leading to activation of the complement system (Plank et al, 1996), and also increased uptake by the reticular endothelial system (RES) (Richardson et al, 1999). Hence, the move towards the amphoteric PAAs, ISA22 and ISA23, that tend to be less toxic than cationic PAA (ISA1 and ISA 4).

1.3.1.2 Mechanisms of Internalisation

Many different gateways have been described for endocytic uptake. The main mechanisms of internalisation are described below:-

➤ Invaginations can occur at a specific region of the plasma membrane called coated pits with either clathrin or caveolae (reviewed in Watson et al, 2005). Alternatively, internalisation occurs in a region of the plasma membrane where there is no “coating”, known as macropinocytosis, and clathrin- and caveolin-independent endocytosis. The best-studied route of cellular uptake is clathrin-mediated endocytosis (Schnatwinkel et al, 2004), and in all mammalian cells where it accounts for receptor-mediated endocytosis (Slepnev and Camilli, 1998). Clathrin-coated vesicles have a morphologically characteristic bristle coat made up of a complex protein called clathrin (Marsh, 2001). This protein is a triskelion (a three-legged structure consisting of three heavy and three light chains) (reviewed in Mousavi et al, 2004) and it forms a polygonal lattice, pentagons and hexagons (Heuser, 1980), which helps to deform the overlying plasma membrane into coated pit (reviewed in Conner and Schmid, 2003). Clathrin-mediated endocytosis is responsible for uptake of many physiological ligands such as transferrin, immunoglobulins and growth factors (reviewed in Trowbridge, et al 1993). It also modulates signal transduction, and is involved in cell and serum homeostasis (reviewed in Conner and Schmid, 2003).

- The caveolae-dependent uptake mechanism uses caveolae (flask-shaped invaginations) that are present in many cell types (reviewed in Nichols and Schwartz, 2001). These structures were first observed 50 years ago on the surface of endothelial cells, where they are abundant and play a role in transcytosis and endocytosis of blood components (reviewed in Conner and Schmid, 2003). Caveolae have a single major, cholesterol-binding coat protein, caveolin (reviewed in Okamoto, 1998), which is implicated in the formation and maintenance of caveolae structures (reviewed in Nichols and Schwartz, 2001).
- Macropinocytosis occurs primarily at sites of membrane ruffling (reviewed in Swanson and Watts, 1995) and it involves the formation of large, irregular primary endocytic vesicles, called macropinosomes (reviewed in Nichols and Schwartz, 2001). Macropinosomes are dynamic vesicular structures (reviewed in Johannes and Lamaze, 2002) and are heterogeneous in size (reviewed in Swanson and Watts, 1995).

1.3.1.3 Intracellular Trafficking

Following endocytic internalisation, the vesicle contents are delivered to a number of different intracellular compartments by a series of vesicle fusion events. These include early and late endosomes, and lysosomes.

Early Endosome

The early endosome is the first endocytic compartment entered following internalisation (Gruenberg et al, 1989; Slepnev and Camilli, 1998). Early endosomes are usually located in the periphery of the cell. It has been shown that Oregon green-labelled PAAs enter this compartment (Patrick et al, 2001b). A decrease in pH occurs (acidification) in the lumen of the early endosome (pH 6.5), due to the proton pump located in the vesicle membrane. This change in pH is the trigger used to deliver drugs from pH-responsive linkers (cis-aconityl and hydrazone), and causes a change in conformation of pH-responsive polymers such as PAAs (reviewed in Ferruti et al, 2002). Physiologically, the acidic environment is also important for the dissociation of the ligand from the receptor (e.g. transferrin and iron). Subsequently the vesicle contents are either recycled back into the cell or carried forward into the late endosome. The recycling stage can be a disadvantage for therapeutic agents such as polyplexes that are required to access the cytosol for their activity. Inclusion of transferrin into a non-

viral vectors is often used to enhance cellular uptake, as transferrin receptors are over expressed in rapidly dividing tumour cells (reviewed in Merdan et al, 2002a), and, in theory this could enhance cancer targeting.

Late Endosome

If the polyplex is not recycled, it will experience a further decrease in pH in the late endosome (pH 6-5). For the pH-responsive polymer, this effect may enhance its ability to cause membrane permeabilisation. However, in many cases the endosomal membrane remains an obstacle to cytosolic delivery. For example a polyplex must act quickly to cause the endosomal disruption before it is transferred to the lysosome where the nuclease would rapidly degrade the DNA.

Lysosome

The endosomal contents can either escape to the cytosol or be further trafficked to either the golgi apparatus or the lysosome. The lysosome contains more than sixty hydrolytic enzymes (pH 5.5-4.5) (reviewed in Blott and Griffiths, 2002), and this compartment is able to degrade proteins that were not recycled, DNA, RNA, glycosides and lipids. In fact many naturally occurring macromolecules are degraded here. Due to the hydrolytic capacity of the lysosomes, it is essential that the entry of degradable therapeutic agents such as DNA and protein is avoided.

Even if a polyplex can escape from the endosome, its journey does not end in the cytosol. For gene therapy, the DNA must yet reach its final destination, i.e the nucleus. Diffusion of the macromolecule through the cytoplasm is usually slow due to its high viscosity, and the presence of a cytoskeleton, which forms a mesh (Lukacs et al, 2000; reviewed in Merdan et al, 2001a). These factors greatly slow down the diffusion of high molecular weight macromolecules and in turn this also increases the chances of the DNA degradation by cytoplasmic nucleases (Lechardeur et al, 1999). This itself can cause a dramatic decrease in DNA half-life.

For successful gene therapy the DNA must also enter the nucleus via a nuclear pore or during cell division. Thus it is important that the system is stable until the next cycle of the cell division (reviewed in Merdan et al, 2001a). Nuclear pore complexes (NPC) (reviewed in Pouten, 1998), present in the nuclear membrane allow small molecules to passively diffuse through them. However, macromolecules require a motif

that can be recognised by the receptors found in the nuclear membrane. Only in this case will the pore allow their translocation of the cargo into the nucleus (reviewed in Merdan et al, 2001a).

The complexity of the barriers to transfection have led many to focus on cytosolic delivery of protein toxins e.g. PAA delivery of ricin and gelonin (Patrick et al, 2001a).

Endosomal escape into cytoplasm remains the main factor limiting transfection efficiency of non-viral vectors, and the ability of the endosomolytic polymers to deliver proteins. Endosomotropic delivery can be defined as delivery via the endosomal compartment and this concept is described in more detail here.

1.3.2 Endosomotropic Delivery

Efficient cytosolic access of macromolecules such as genes and proteins (e.g. toxins) is crucial for many therapeutic strategies (reviewed in Plank et al, 1998). There is therefore a need for efficient delivery vectors to mediate rapid and efficient endosomal membrane translocation, before progress into lysosome (Murthy et al, 1999). Endosomolytic delivery systems are usually designed to use the decrease in endosomal pH to trigger the release of the therapeutic agents. The process begins with the endocytic uptake of the polymer/ therapeutic conjugate/complex. In the early endosome, hydrogen ions will be pumped into the endosome by a proton pump decreasing the pH (Richardson et al, 1999). This will cause the polymer to protonate, and a change in conformation results. Ideally, an endosomolytic polymer will display a charge that changes significantly as the pH decreases from pH 7.4 (extracellular) to pH 6.5 (endosomal). The polymer should be able to diffuse to, and rapidly interact with the endosomal membrane. There should be enough time to allow the escape of the molecular therapeutic agent, before it reaches the lysosome (Figure 1.5). It is hypothesised that the polymer binds to the endosomal membrane, causing its disruption (loss of membrane function) (Richardson et al, 1999).

The mechanism by which the endosomolytical polymer causes endosomal breakage is very important for the activity of the polymer, and this will be discussed in the next section.

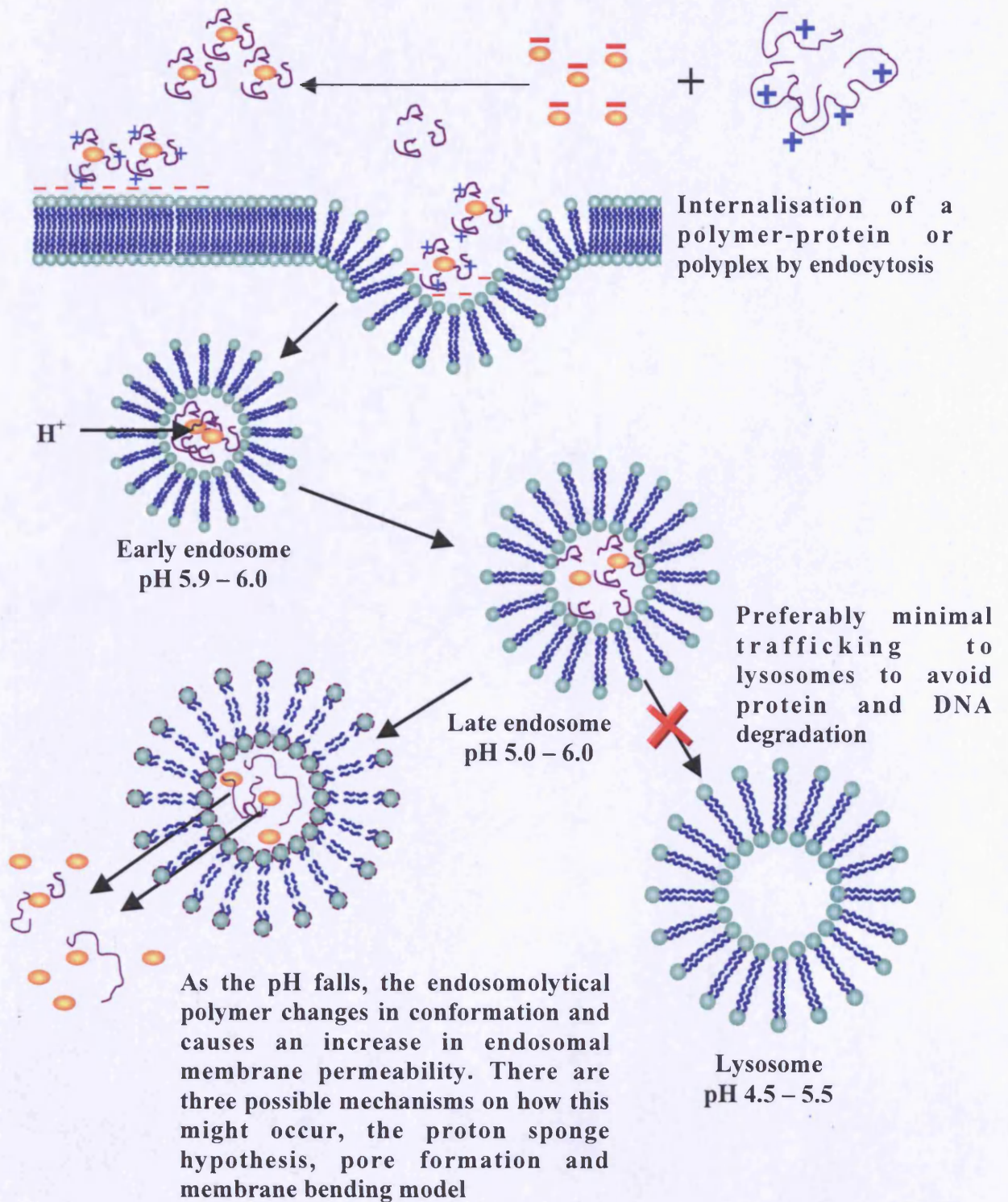


Figure 1.5 The overall scheme of endosomotropic delivery (adapted from Duncan, 2003a). For successful delivery it is crucial that the therapeutic agent escapes from the endosomal compartment thus it avoids the degradation by the lysosomal enzymes

1.3.3 Mechanisms of endosomal membrane breakage

An accurate understanding of the mechanisms by which non-viral vectors cause endosomal membrane breakage is crucial to help the development of more efficient genes and proteins delivery systems. A number of mechanisms have been proposed to explain the ability of polymers to permeabilise endosomal membrane. These include:

Proton sponge hypothesis

It has been suggested that cationic polymers such as PEI produce a proton sponge effect that is responsible for the permeabilisation of endosomal membrane. As the pH falls, PEI in the early endosome becomes more protonated. In turn this causes a depletion in H^+ that drives an increase influx of H^+ followed by Cl^- and water, leading to an increase osmotic pressure inside the endosome. And this causes a membrane destruction (Figure 1.6). For the proton sponge mechanism to operate, it is important that the polymer possesses functional groups that will protonate between pH 7.4 and 5 (reviewed in Merdan et al, 2002a). In this case membrane breakage will be independent of membrane composition.

The proton sponge hypothesis was first proposed by Behr (1997) and is based on the perceived mechanism of action of chloroquine which is known to enhance the transfection activity of polyelectrolytes such as poly(L-lysine) (PLL) (reviewed in Pouton and Seymour, 1998). Chloroquine is a weak base. It is neutral at pH 7.4 and becomes positively charged at pH 5.5. Thus in the acidic environment of the intracellular vesicle it is present (and trapped) in the protonated form. Chloroquine increases the residence time of a polyplex in the endosome by preventing or slowing down the acidification process. Which leads to a decrease in vesicle-vesicle fusion. Consequently this increases transfection efficiency.

A growing number of studies support this theory. It has been demonstrated that the transfection activity of PEI (Kichler et al, 2001) and imidazole-containing polymers (Benns et al, 2001) can be dramatically decreased by the inclusion of bafilomycin A1, which is a specific inhibitor of vacuolar-type H^+ -ATPase (Yoshimori et al, 1991), that prevents the acidification of endosome and lysosome. Merdan et al (2002b) used confocal laser scanning microscopy of live cells to show that the release of PEI polyplex occurs as a sudden event. They suggested that this could be due to the bursting of the vesicles (reviewed in Merdan et al, 2002a; 2002b). Similar results have been obtained

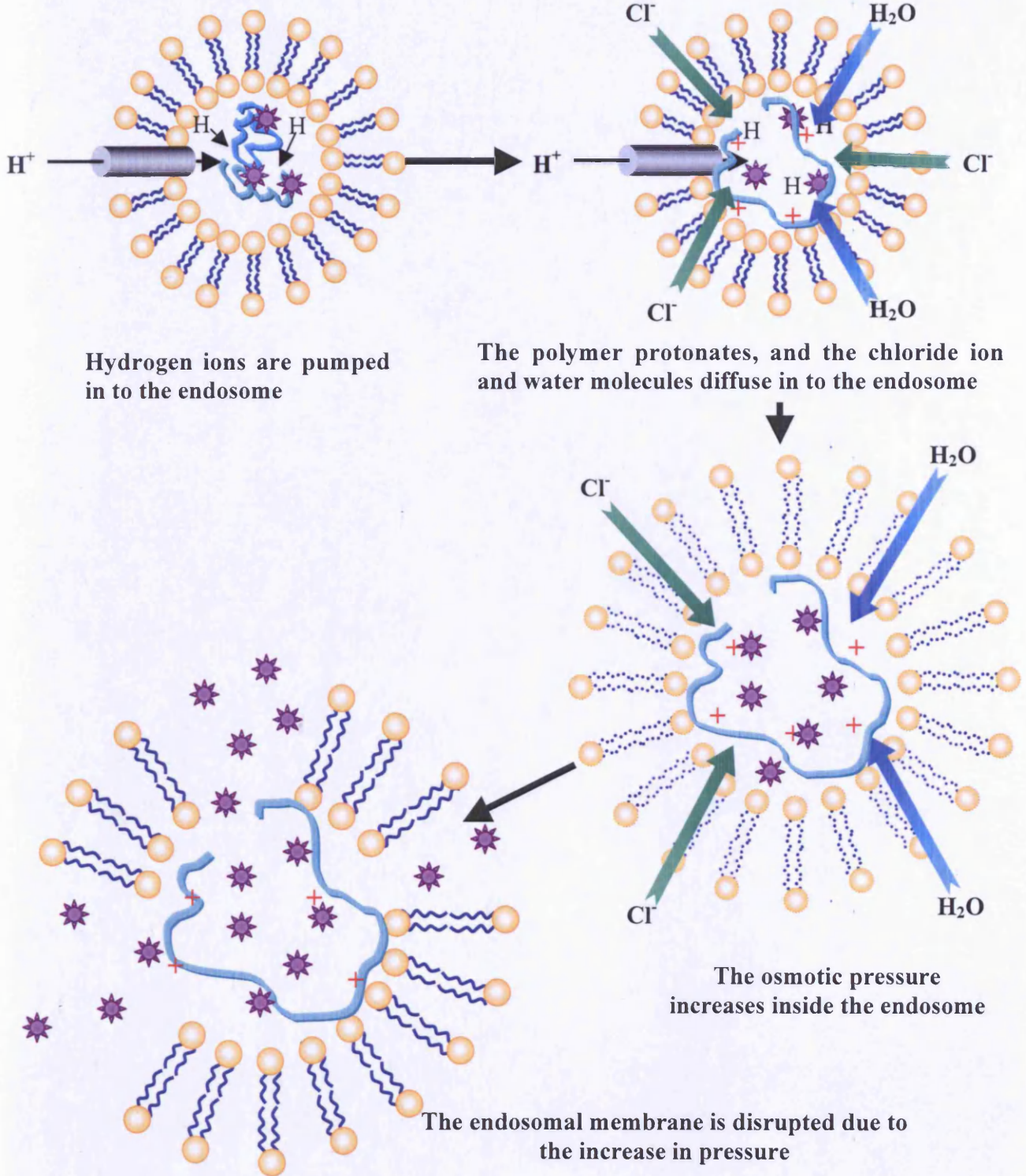


Figure 1.6 The proton sponge hypothesis. Here the protonation of polymer causes influx of chloride ions and water, this causes the endosome to swell resulting in the increase of osmotic pressure and the breakage of the endosomal membrane, thus allowing the therapeutic agent to escape to the cytosol (adapted from Cho et al, 2003)

by Sonawane et al, (2003) using hamster cells incubated with buffering polymers (polyamines) who found that the polymer caused an increased chloride ion concentration leading to an increase in the volume of the endosome (Sonawane et al, 2003).

Many debate the validity of the proton sponge hypothesis. Studies have demonstrated that another weak base, ammonium sulphate, with similar buffering capacity to chloroquine at endosomal pH, does not improve transfection (reviewed in Pouton and Seymour, 2001). Studies conducted by Godbey et al (2001) showed that the lysosomal pH 5 was not altered in cells that were transfected with PEI/DNA polyplex. More recently Funhoff et al (2004) have demonstrated that with the newly synthesised polymer [poly(2-methyl-acrylic acid 2-[(2-(dimethylamino)-ethyl)-methyl-amino]-ethyl ester (pDAMA), which has two tertiary amine groups (pKa 5 and 9) was not able to promote transfection. However, the addition of peptide (INF-7, a fusogenic peptide derived from the influenza virus (Funhoff et al, 2004)) caused an increase in the transfection efficiency. These findings strongly suggest that the proton sponge effect is not a universal mechanism, although it may be able to explain endosomal destabilisation caused by polymers with pKa values between 7 and 5.

Pore formation

It has also been suggested that endosomolytic polymers might permeabilise the endosomal membrane by forming pores in the membrane. However, the polymer must be an amphiphilic in nature, i.e. must carry both hydrophilic and hydrophobic groups. The hydrophilic (charged) part is attracted to, and interacts with the headgroups of the phospholipids. Thus it will be located outside the membrane. The hydrophobic section is then inserted in the alkyl part of the lipid bilayer forming the pore (Figure 1.7). Natural macromolecules known to cause pore formation include membrane-active peptides toxins (melittin) (Benachir and Lafleur 1995), viral fusogenic peptides (Epanand et al, 1992) and bacterial toxins (Gazit et al, 1995; Wagner, 1999). Such agents have been explored as a way to develop new synthetic membrane active-polymer conjugates or they have been added (none covalently) to existing non-viral vectors to enhance their membrane disruption activity.

The N-terminal domain of hemagglutinin (reviewed in Cheung et al, 2001) from influenza virus has also been used to prepare the fusogenic peptide, INF (Wagner, 1999) and GALA-based peptides (Plank et al, 1994). These peptides contain aspartic acid and

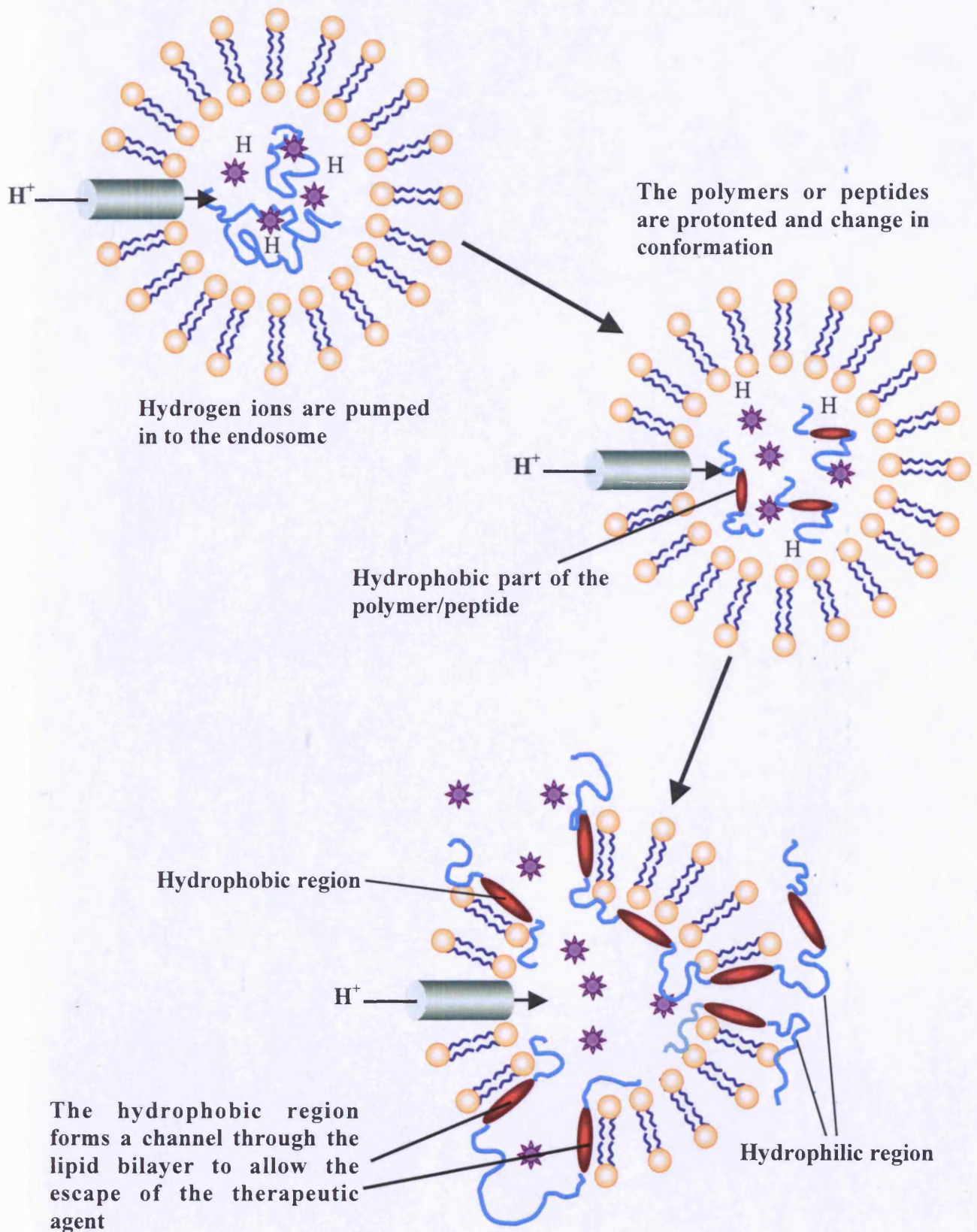


Figure 1.7 Pore formation mechanism. The polymer or peptide protonates and change in conformation, they become more hydrophobic, and due to this region, a channel is formed through the bilayer.

glutamic acid. At neutral pH they are negatively charged, and upon acidification a change in peptide conformation occurs, which promotes membrane interaction and then pore formation. Bacterial toxins such as Listeriolysin O toxin also form membrane pores following activation in the acidic endosomal environment. This is the mechanism that allows the escape of bacterium *Listeria monocytogenes*.

Membrane disruption by bending

Another mechanism that has been proposed to explain membrane disruption is the concept of “membrane bending” (Figure 1.8). It has been proposed that poly(amidoamine) (PAMAM) dendrimers destabilise anionic liposomes by this mechanism (Zhang and Smith, 2000). The rigid spherical polycationic dendrimers bind to the membrane by electrostatic interaction causing the membrane to bend, this induces stress in the bilayer packing and disruption of the membrane results (Zhang and Smith, 2000).

In the following section the different macromolecules that are used as non-viral vectors will be discussed.

1.4 Non-viral vectors for intracytoplasmic delivery

The use of non-viral vectors (such as cationic lipids, liposomes and polymers) for gene delivery have been developed by many groups, but the pioneers were Felgner, Behr and Huang (reviewed in Kabanov, 1999). Cationic lipids, liposomes and polymers form complexes with DNA by electrostatic interaction between the positive charges on the non-viral vectors and the negative charges on the DNA to form lipoplexes (lipids-DNA complex) or polyplexes (polymer-DNA complex). The major advantage of using polyplexes and lipoplexes systems as an alternative to viral vectors is they are a lot safer (Loup et al, 1999). However, there is one major disadvantage. Non-viral vectors have transfection efficiencies that are much lower compared to viral vectors. Thus it is very important to investigate further the mechanisms that will help to design and develop vectors that are safe, can be used in patients and that will routinely give efficient gene and protein delivery.

1.4.1 Cationic lipids/liposomes

Cationic lipids were first introduced as gene carriers in 1987 (Felgner et al,

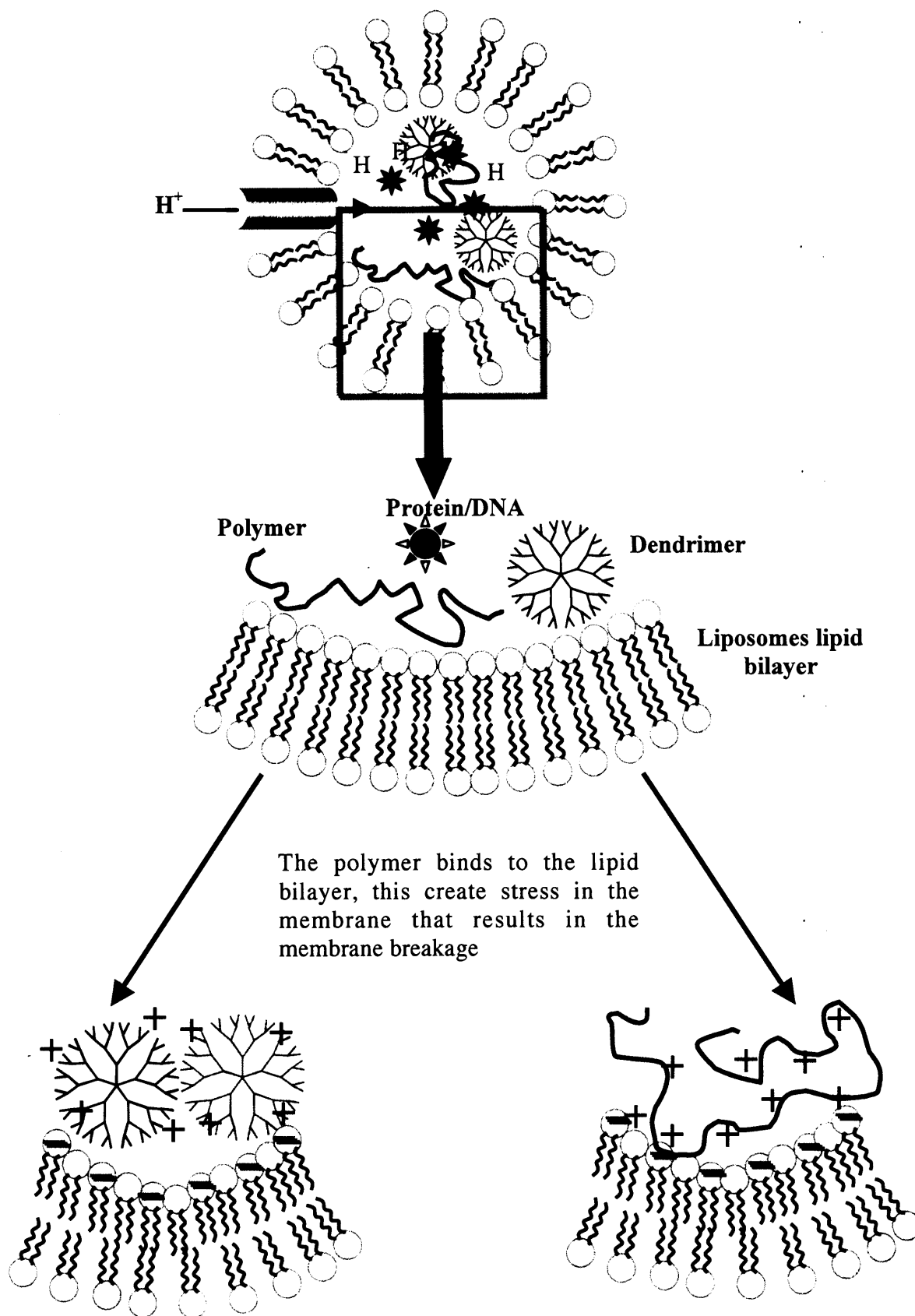


Figure 1.8 The membrane bending mechanism. It has been reported that dendrimer PAMAM can cause membrane breakage by this mechanism. The rigid structure of the dendrimer causes stress and bending of the lipids bilayer resulting in their destruction

1987). Gene transfer using cationic lipid-pDNA complexes (lipoplexes) has also been tested in clinical trials (reviewed in Wolf and Wolf, 2003). Cationic liposomes are usually small unilamellar vesicles that are composed of cationic and other helper lipids (Fang et al, 2003). Initially most were composed of a single lipid, (e.g. 1,2-dioleoyl-3-trimethylammonium-propane (DOTAP), using 1,2-dioleoyl-*sn*-glycerol-3-phosphoethanolamine (DOPE), as a helper lipid (reviewed in Ciani et al, 2004). DOPE was chosen because of its ability to reduce the cytotoxicity of cationic liposomes and it has been shown that in the presence of DOPE, DNA translocation and transfection efficiency are improved (Ciani et al, 2004; Zhdanov et al, 2002).

The second important example of non-viral vectors is polymers and this will be described in the next section.

1.4.2 Polymers as non-viral vectors for cytosolic delivery

The polymers here can be divided into two main groups that are separated according to their nature e.g. cationic and anionic polymers, there are also amphoteric polymers but this is very small group and will not be discussed here (Table 1.1 and Figure 1.9).

The anionic polymers are the smaller group of the two, and will be discussed first in the next section

1.4.2.1 Anionic polymers

Stayton and Hoffman have systematically developed a series of synthetic, pH-sensitive homo- and co-polymers of anionic carboxylated groups such as acrylic and methacrylic acid groups. They can interact with and disrupt biological membranes in a pH-dependent manner, and the interaction is governed by hydrophobic forces. It has been shown that changing pH, causes a change in the polymer conformation from a hydrophilic coil at neutral pH 7.4 to a hydrophobic globule at acidic pH 5.5 (Yessine et al, 2003). Such polymers display a pH-dependant red blood cell (RBC) lysis with increasing haemolysis at < pH 6.5 (Murthy et al, 1999; Yessine et al, 2003). It appeared that the haemolytic activity of these polymers increased with an increase in hydrophobic nature. Polymers with a high degree of hydrophobicity also showed a high degree of toxicity (Yessine et al, 2003).

Table 1.1 List of endosomolytic polymers, their pKa, type of structure, molecular weight and current status.

	Mw	pKa	Structure	Status	Reference
Cationic polymers					
Poly-L-lysine (PLL)	4 kDa - 224 kDa	9 to 10	Branched	<i>in vivo</i>	Dash et al, 1999 Reviewed in Smedt et al, 2000 Kawano et al, 2004
Poly(ethyleneimine) (PEI)	22 kDa - 220 kDa	8.18 to 9.94	Linear	<i>in vivo/ clinical</i>	Boussif et al, 1995 Fischer et al, 1999 Harpe et al, 2000 Reviewed in Brown et al, 2001
	0.6 kDa - 800 kDa	pKa of primary amine is 5.5	Branched		Brownlie et al, 2004 Ohana et al, 2004
Poly(amidoamine) (PAMAM) dendrimer	1.4 kDa - 853 kDa	3.9 and 6.9	Hyperbranched	<i>in vivo</i>	Malik et al, 2000 Reviewed in Smedt et al, 2000
Cationic PAAs, ISA1 and ISA4	5 kDa - 13 kDa	2.1 to 9	Linear	<i>in vivo</i>	Ferruti et al, 2002 Wan et al, 2004
Poly[2(dimethylamino)-ethylmethacrylate] P(DMAEDMA)	22 kDa - 300 kDa	7.5	Branched	<i>in vivo</i>	Wetering et al, 1999 and 2000

Chitosan	108 kDa - 540 kDa	6.5	Linear	<i>in vivo</i> / clinical	Smedt et al, 2000 Kean et al, 2005
Diethylaminoethyl-dextran (DEAE dextran)	500 Da		Linear	<i>in vivo</i>	Takai and Ohmori, 1990 Gregory et al, 2003
Poly-2-[N-(2-hydroxyethyl)- D,L-aspartamide] (PHEA)	48.3 kDa - 56.9 kDa		Branched	<i>in vivo</i> / clinical	Pitarresi et al, 2003 Martins et al, 2003
Amphoteric polymers					
PAA, ISA22 and ISA23	11 kDa - 48 kDa	2.1 to 7.5	Linear	<i>in vivo</i>	Ferruti et al, 2000 Wan et al, 2004
Polyanions					
N-isopropylacrylamide (NIPAM)	7 to 10kDa		Branched		Miura et al, 1993 Meyer et al, 2001
Poly(ethyl acrylic acid) (PEAAc) Poly(propyl acrylic acid) (PPAAc)	22-24 kDa		Branched		Murthy et al, 1999

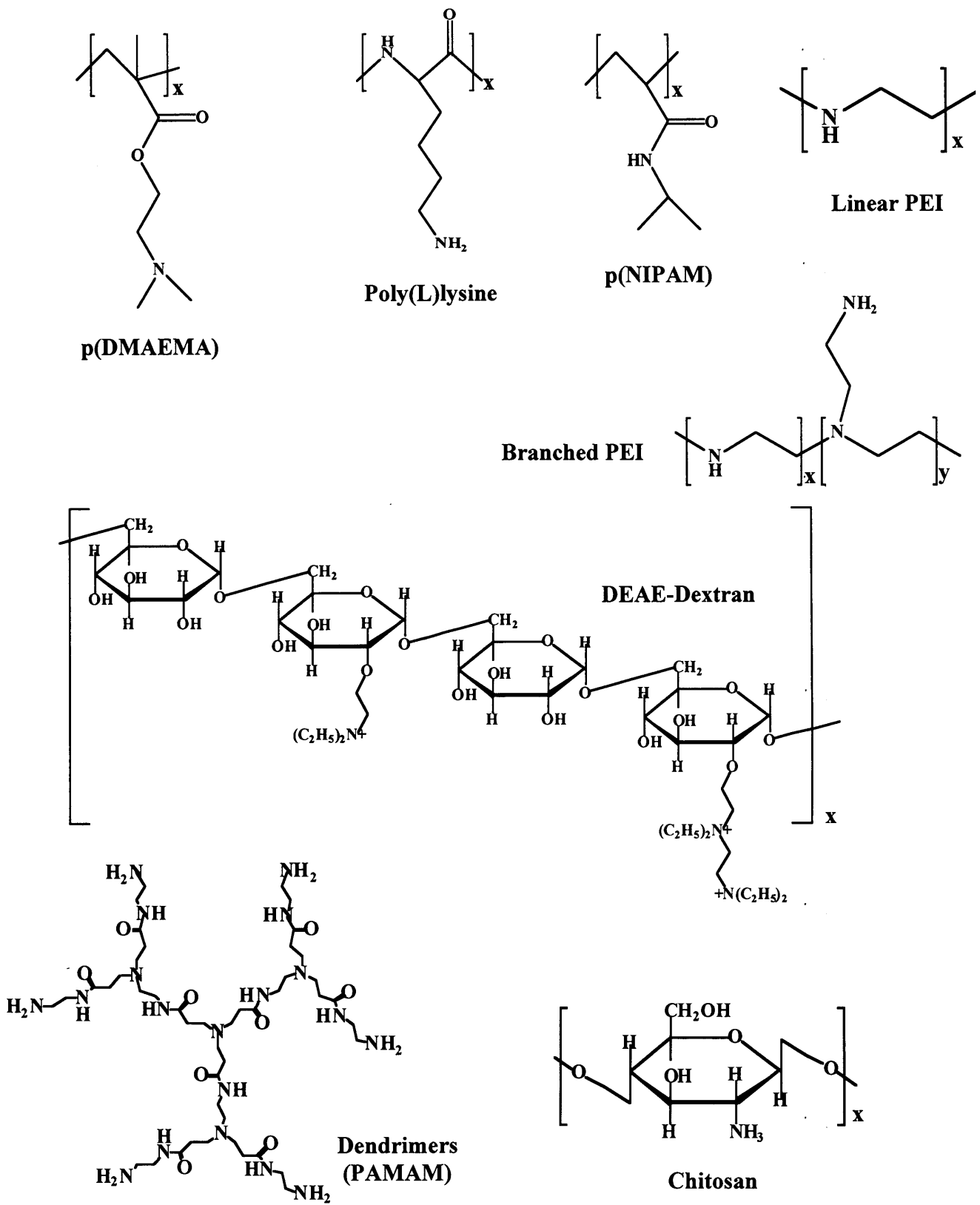


Figure 1.9 Structures of widely studied endosomolytic polymers.

1.4.2.2 Cationic polymers

A diverse range of polymer structures have been used for gene or protein delivery, for example linear, branched, and hyperbranched polymers, dendritic architectures, and random- and block copolymers.

All possess different chemical, physical and biological properties, as they contain amine groups, which are primary, secondary, tertiary or quaternary amines. These amines can be part of an aliphatic chain, or as cyclic or aromatic systems. Therefore the pKa values vary widely. The amine groups are not only required for the interaction with DNA, but they are crucial for the polymer's ability to cause endosomal membrane disruption. In addition, amine functionality can be used as a site for conjugation with other polymers, lipids, drug, targeting moieties and proteins such as toxins.

PLL

PLL (linear polypeptide) was the first polycation used to promote gene transfer. Although it has been reported that Wu and Wu (1987) were the first to use PLL in gene delivery, this is not true, since in 1974 Schell investigated the effect of PLL on the cellular uptake of polynucleotides (reviewed in Chirila et al, 2002). Many studies have since used PLL as a vector for gene delivery. It is clear that PLL molecular weight plays an important role in the DNA complex formation, their ability to transfect cells and the cellular toxicity (Wolfert and Seymour, 1996). Unmodified PLL is poorly efficient, but the addition of the lysosomotropic agent chloroquine dramatically improved the transfection efficiency. Other methods have been employed to improve the activity of PLL. These include the conjugation with poly-L-histidine, and the substitution of some of the L-lysine monomers with tryptophan or cysteine (McKenzie et al, 2000). The resultant copolymers showed better transfection efficiency compared to PLL.

PLL has a number of advantages. It is widely available, and the side-substituents are suitable for attachment of other molecules. It can protect an oligonucleotide or DNA from enzymatic attack and it possesses a high solubilising power (Ferruti et al, 1998). However, PLL does have two major drawbacks. It is highly toxic, and the fact that PLL-derived polyplexes usually interact with plasma proteins after i.v. injection leads to liver and lung uptake. In order to reduce its toxicity, PLL has been chemically modified by the addition of N,N-dimethylacrylamide to the primary amine groups (Ferruti et al, 1998). This kind of modification reduces toxicity, but also leads to a reduction in transfection efficiency too.

PEI

PEI has been the most widely investigated as a non-viral vector. It was first developed by Jean-Paul Behr and colleagues and has been used to promote gene delivery in cell culture and *in vivo* (Boussif et al, 1995). PEI is made up of ethylamine repeating units, and it possesses a very high positive charge density when fully protonated in aqueous solution (Ham, 1980). This property is required for polyplex formation which depends on the ratio of PEI nitrogen to the phosphate of DNA. PEI are very effective at protecting DNA from the degradation by nucleases (Campeau et al, 2001). Branched and linear PEIs of different molecular weight have been synthesised and their transfection activity evaluated *in vitro* and *in vivo*. As mentioned earlier, it was suggested that PEIs exert their endosomolytic activity by proton-sponge mechanism (see section 1.3.3) (Behr, 1997).

To minimise interaction of the PEI-polyplex with plasma proteins, the complex was coated with a hydrophilic polymer (e.g. hydroxypropyl methacrylic acid) (reviewed in Brown et al, 2001). While this prolonged the plasma circulation it also led to a decrease in transfection efficiency (reviewed in Oupicky et al, 2002a).

Other polycations

In the search for better polycations Hennink and colleagues have developed a series of methacrylate/methacrylamide homo- and copolymers (Wetering et al, 1999). Poly[2-(dimethylamino)ethyl methacrylate], p(DMAEDMA) contains a tertiary amine and an ester group. The amine can be ionised with a pKa value of 7.5. Wetering et al (2000) showed that the transfection efficacy of p(DMAEMA) is higher than that of PLL-polyplex, with a similar transfection efficacy to Lipofectin-plasmid complexes (Wetering et al, 2000). Although it was openly proposed that these polymers exert their membrane activity by proton-sponge mechanism (Pang et al, 2002), recent work by Jones et al (2004) has brought this theory into question. It was found that p(DMAEMA) was able to change the morphology of the late endosomes and lysosomes, but the polymer did not physically break them. Thus another mechanism must be responsible for their ability to transfect cells and their high cytotoxicity.

Cationic polysaccharides have also been investigated. Chitosan and diethylaminoethyl-dextran (DEAE-dextran) have been widely used. Chitosan possesses primary amine groups, which can be used to form complexes with DNA. Studies using

different molecular weights of chitosan showed that low molecular weight chitosan forms excellent polyplexes that protect DNA against nuclease degradation (Richardson et al, 1999), but chitosan shows a molecular weight and counter ion dependent toxicity (Gomez and Duncan, 1997). A number of studies have shown that chitosan can form a complex nanoparticle with recombinant DNA plasmids, that provide an effective mean for delivering genes into cells (Leong et al, 1998). Numerous studies conducted by Sato et al (2001), have demonstrated the effect of molecular weight, pH and serum concentration on the transfection efficiencies of chitosan.

DEAE-dextran was shown to transfect mammalian cells in very early studies (Vaheri and Pagano, 1965), and experiments with this vector continued (Mack et al, 1998). However, the transfection efficiency of DEAE-dextran is still low. The polymer is non-biodegradable, and it displayed high toxicity so interest in these polymers for drug delivery is decreasing.

The polycations described so far are either linear or branched. Cationic dendrimers are another important group of polymers being explored for gene delivery. Dendrimers are hyperbranched structures that contain many terminal functional groups. There are several advantages of dendrimers compared to linear polymer. For example, low polydispersity, which allows predictable chemical, physical, and biological behaviour. PAMAM dendrimers have been most extensively studied, and are commercially available under the trade name 'Starburst Dendrimers' (reviewed in Aulenta et al, 2003). PAMAM dendrimers are capable of disrupting endosomal membrane and are able to promote gene transfer and this depends on its generation number. There are other dendrimers with different chemical composition that have been investigated as drug vehicles, e.g. PLL dendrimers (Niidome et al, 2000), phosphorous containing dendrimers (Loup et al, 1999) and low generation polypropyleneimine dendrimers (Zinselmeyer et al, 2002).

As this project has focused on amphoteric PAA polymers they are described in more detail in the next section.

1.5 PAAs

1.5.1 Historical background and the evolution of PAAs

PAAs are a unique family of synthetic, water-soluble, linear polymers that are synthesised by hydrogen-transfer polyaddition of aliphatic amines or *bis*-secondary amines to *bis*acrylamides (Ferutti et al, 2000). They are characterised by the presence of

amido and tertiary amino groups that are arranged in a regular manner along the main backbone (reviewed in Ferruti et al, 2002), that act as a weak base in solution. A vast number of PAAs have been synthesised, each one has a unique chemical structure and properties (Table 1.2, Figure 1.10).

PAAs were first synthesised by (Ferruti et al, 1967) in the late 1960's and early 1970's. Initially they were developed as new heparin complexing agents (Marchisio, 1973). During the 1970's, PAAs were developed further as non-thrombogenic polymers for material coating. New linear PAAs, graft and block polymers were prepared and their chemical, structural and mechanical properties were investigated. Also during this decade PAAs were investigated for a possible inherent antitumour activity (Ferruti et al, 1973).

In the 1980's, the development of PAAs as heparin-complexing agents continued. Graft polymers composed of poly(vinyl chloride) (PVC) and PAA chains (Ferruti et al, 1982a), and PAA-surface-grafted glass microspheres (Ferruti et al, 1983) were prepared. Their heparin absorbing capacity was investigated. Several studies also found that soluble PAAs and cross-linked resins of PAAs were able to form complexes with heavy-metal ions such as Co^{2+} , Cu^{2+} and Ni^{2+} (Barbucci et al, 1981b). Those PAAs able to form such complexes must have aliphatic amines with no more than three methylene groups separating the two aminic groups (reviewed in Ferruti et al, 2002). Such PAAs were proposed for use in water purification (Barbucci et al, 1981b; Ferruti et al, 1982b). Finally in the 1980's new PAAs were synthesised and evaluated as an antimicrobial agents (Ranucci et al, 1989).

1.5.2 Development of PAAs for drug delivery applications

Studies on the development of PAAs as drug carriers began in the early 1980's (Ferruti et al, 1982c). First, experiments examined the cytotoxicity and degradation and cellular toxicity of PAAs derived from *N,N'*-bis(2-hydroxyethyl)ethylenediamine (MBI) (Figure 1.10) (Duncan et al, 1994). These PAAs were less toxic than other cationic polymers such as PLL (Ranucci et al, 1991). This research initiated a new potential application of PAAs in the field of polymer therapeutics. To explore the possibility of 'hiding' a molecule inside the pH-responsive MBI, this PAA (MBI) was later conjugated with triton X-100 (TX-100). The RBC lysis model was used to investigate the pH-dependent haemolytical activity of MBI and its TX-100 conjugate.

Table 1.2 Summary of the different applications of PAAs.

Biomedical application	References
De-heparinizer filter	Marchisio et al, 1973
Cross-linked PAA resin as de-heparinizer	Ferruti et al, 1983 Barbucci et al, 1983
Heparinizable materials	Tanzi et al, 1985 Barbucci et al, 1985 Barbucci et al, 1987 Barbucci et al, 1990
Anticancer agents with inherent activity	Ferruti et al, 1973
Antibacterial agents with inherent activity	Ranucci et al, 1989
Drug carriers	Ferruti et al, 1994 Ferruti et al, 1999
As endosomolytic polymers and non-viral vectors for gene and protein delivery	Duncan et al, 1994 Richardson et al, 1999; 2001 Ferruti et al, 2000 Pattrick et al, 2001 Wan et al, 2004 Lavignac et al, 2004
Non-biomedical application	
Complexing with heavy metal ions (for water treatment)	Barbucci et al, 1981 Ferruti et al, 1982b

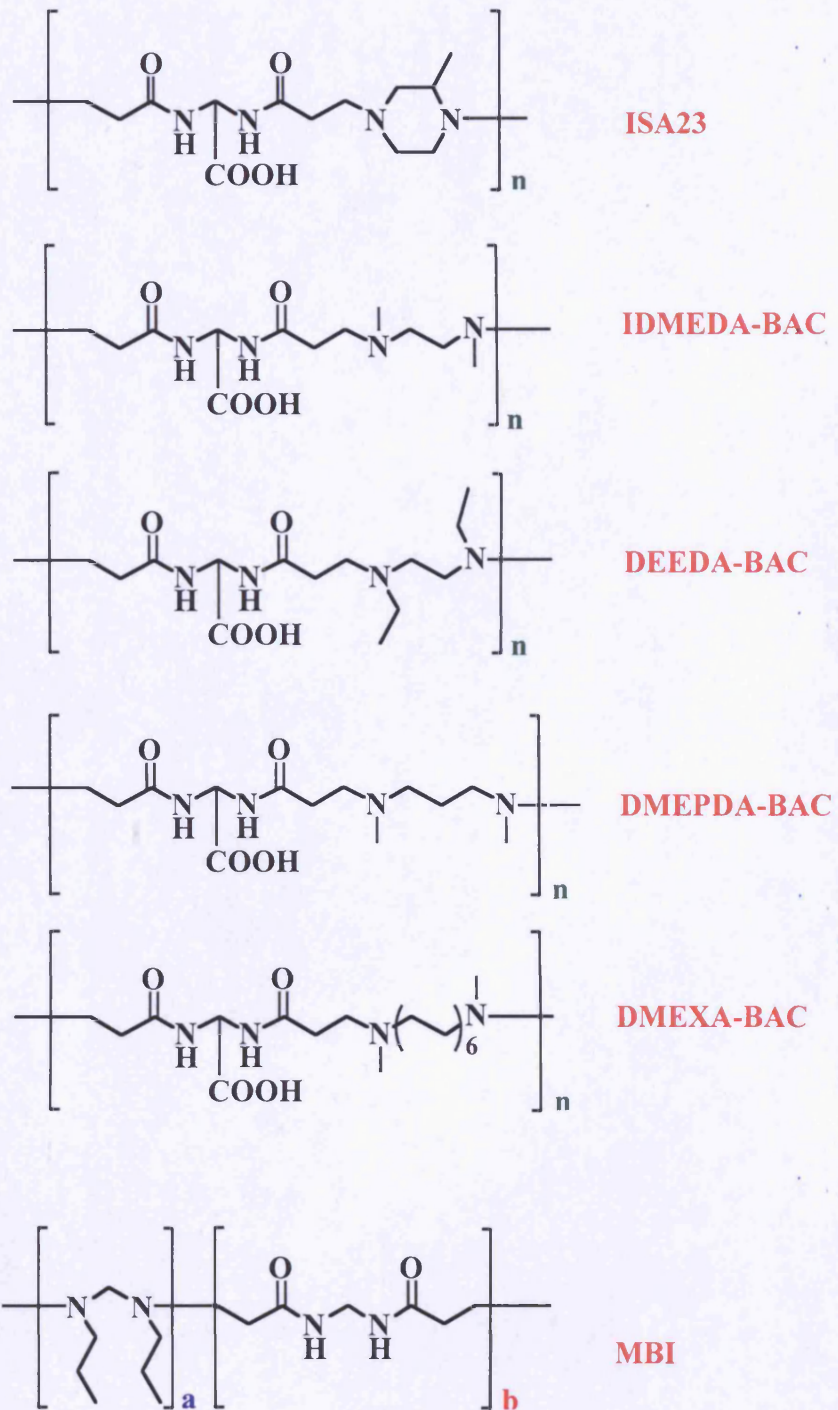


Figure 1.10 Typical structures of number of PAAs.

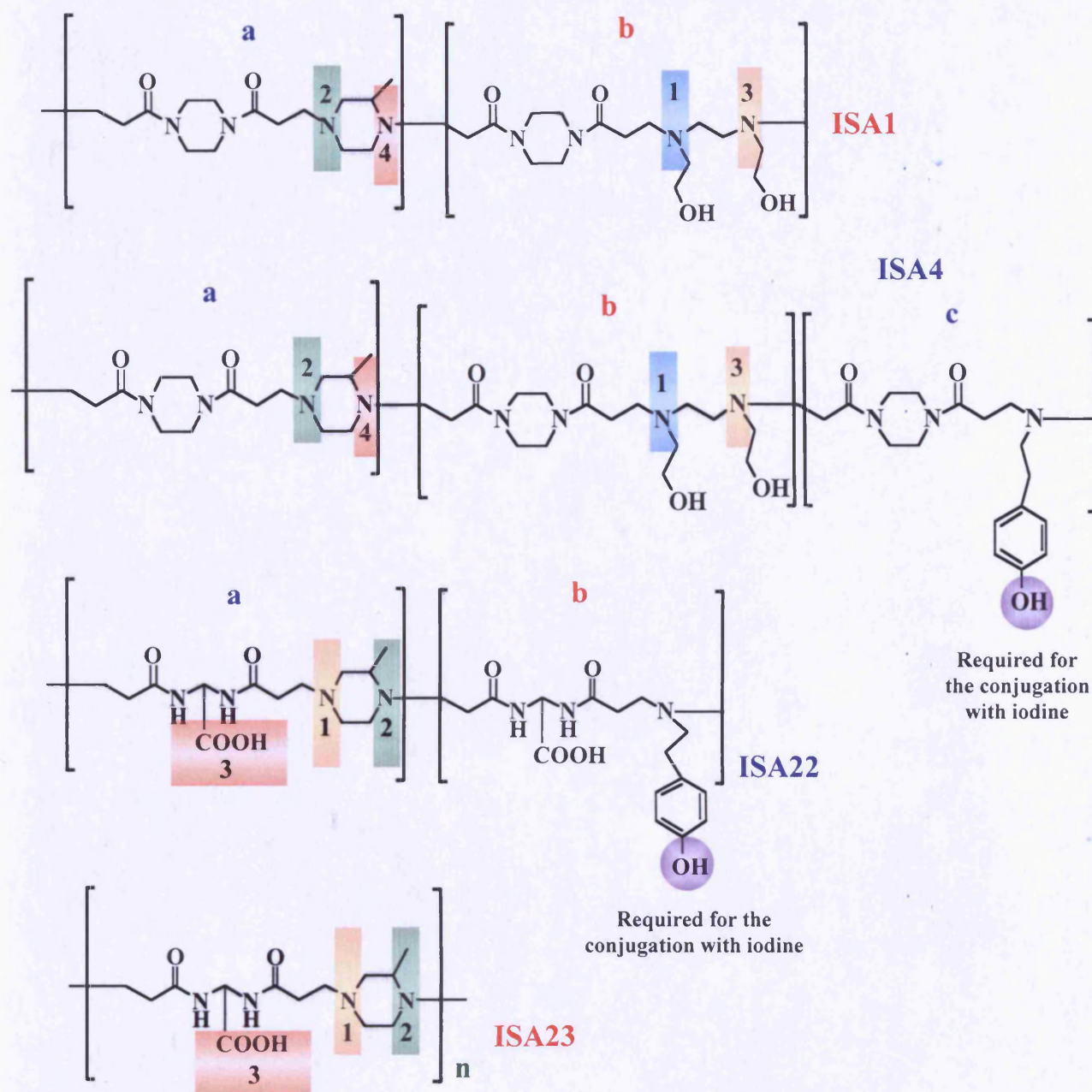
Whereas free TX-100 displayed considerable haemolysis at all pHs (5.5, 7.4 and 8), MBI did not cause any RBC lysis at any concentration or pH examined. The PAA-TX-100 conjugate only caused concentration-dependent haemolysis at pH 5.5 (Duncan et al, 1994). Although MBI-TX-100 was less toxic than TX-100, it was more toxic than MBI against human leukaemic cells (Duncan et al, 1994). These results were very interesting, as they demonstrated for the first time the potential to use PAAs as bioresponsive polymers that would change conformation and potentially deliver drugs within acidic intracellular compartments such as the endosome and lysosome (Duncan et al, 1994).

In 1999, a number of PAAs-cisplatin were prepared (Ferruti et al, 1999). The chemical properties, and preliminary antitumour behaviour, both *in vitro* and *in vivo*, of the PAA-platinates were investigated (Ferruti et al, 1999). It was found that the PAA-platinates were less toxic than cisplatin toward lung tumour cell lines (Ferruti et al, 1999).

The search for improved endosomolytic polymers led to the birth of a very important series of PAAs, ISA1, ISA4, ISA22 and ISA23 (Figure 1.11). These polymers were optimised to display low cellular toxicity and pH-dependant membrane activity. Since, further investigation has mainly conducted on these PAAs and their derivatives (copolymers and block copolymers), Richardson et al (1999) synthesised ISA1 and ISA23, and their analogues, ISA4 and ISA22, these were prepared for radiolabelling with ^{125}I iodine (^{125}I). It was demonstrated by Richardson et al, (1999) that the toxicity of ISA1 and ISA23 was low, with IC_{50} values of >2 mg/ml (72h incubation). They were lower less toxic than PLL. ^{125}I -labelled ISA4, was taken by the liver following i.v. injection, where as ISA22 was not captured and was successfully taken by the tumour tissue.

PAAs used for gene and toxin deliveries

For parenteral administration it is crucial that the polymer picked must be biocompatible (Williams, 1987), i.e. non-toxin and non-immunogenic. It was shown by Richardson et al (1999) that all PAAs (ISA1, ISA4, ISA22 and ISA23) displayed little cytotoxicity against B16F10 and Mewo cell lines. Both ISA22 and ISA23 caused greater haemolysis at pH 5.5 and were more effective as transfection agents compared to ISA1 and ISA4 (Richardson et al, 1999; 2001). However ISA1 and ISA4 were able to deliver non-permeant ribosome-inactivating toxins, such as ricin A chain (RAC) and



Polymer	pKa1	pKa2	pKa3	pKa4
ISA1	8.1	6.9	3.8	3
ISA4	8.1	6.9	3.8	3
ISA22	7.5	3.25	2.1	
ISA23	7.5	3.25	2.1	

Figure 1.11 The chemical structures of ISA1, ISA4, ISA22 and ISA23.

gelonin (both can potentially be used as anticancer drugs). In contrast ISA22 and ISA23 were not successful (Patrick et al, 2001a). It is unclear to why this occurs. These experiments were carried in B16F10 cells and the PAA and protein were added to the cells as a noncovalent mixture. It was mentioned that the results might be explained by the difference in the polymers trafficking inside the cell (Patrick et al, 2001a).

Effect of counterion on the properties of PAAs

While investigating mild reaction conditions suitable for PAA-protein conjugation (to deliver protein, like toxin, that can be used as anti-tumour agents), different PAA salt forms were used. In all the earlier experiments, PAAs were in the hydrochloride salt form were used. Therefore, Wan et al (2004) systematically studied the effect of ISA23 counterion (acetate, citrate, hydrochloride, lactate, phosphate and sulphate) on the pH-dependent haemolysis and cytotoxicity. They demonstrated that the counter ion plays a very important role. Whereas ISA1, ISA4, ISA22 and ISA23 chloride, phosphate and sulphate salt forms (the strong acids) caused significant haemolysis at pH 5.5, citrate and lactate salt forms (weak acids), were non-haemolytic at pH 5.5.

1.5.3 Physico-chemical properties of PAAs

Over the years there has been relatively little investigation of the physico-chemical properties of PAAs. All PAA polymers may be classified as polyelectrolytes due to the presence of *tert*-amino group in the main chain backbone. The combination of high molecular weight and charge density leads to unique physicochemical properties that set PAAs apart from uncharged polymers and simple electrolytes (Breuer and Jenkins, 1972).

Techniques such as ^{13}C NMR, potentiometric and calorimetric have been used to obtain the protonation constants for several PAAs (Barbucci et al, 1980). PAAs have both sharp thermodynamic and basicity constants. Generally, for polyelectrolytes, the protonation constants depend on the degree of protonation of the whole of the macromolecule, and an "apparent" constant is determined. However, for some cationic PAA (for chemical structures of these polymers see Ferruti et al, 2002), a "real" basicity constant can be determined (Ferruti et al, 1981). For these PAAs, the protonation of the amine groups is independent of the protonation of the whole polymer, i.e. groups are said to behave as if belonging to a small molecule (Ferruti, 1980; reviewed in Ferruti et al, 2002). This unusual behaviour of PAAs, can be explained by the relatively long

distance between the amino groups of the different repeating units, coupled with the high charge-sheltering effect of the amido groups (Ferruti et al, 2000; reviewed in Ferruti et al, 2002). For amphoteric PAAs such as ISA23, polymer carries both carboxyl and amino groups on each monomer. In this case, the PAA exhibits a typical polyelectrolyte behaviour, although it is less pronounced when the amino and the carboxyl groups are attached to different monomers (Ferruti et al, 2000; reviewed in Ferruti et al, 2002).

Potentiometric titration (Emf measurements), ^{13}C NMR, viscosity measurements and conformational analysis have been used to examine the structure of PAAs (Barbucci et al, 1980; 1981a; Ferruti et al, 2000). These studies demonstrated that the PAA stiffness and the flexibility depend on both polymer protonation, and the aliphatic chain length between the aminic nitrogens of each monomer unit (Barrucci et al, 1981). The rigidity of PAAs increases with the increasing degree of protonation, and the length of aliphatic chain in the monomer. Protonation of the first amino group nitrogen causes a decrease in the conformational freedom due to the formation of strong hydrogen bonding between "onium" ion and the carbonyl group belonging to the same monomeric unit (Barrucci et al, 1981). Protonation of the second amino group nitrogen causes a further increase in rigidity due to the repulsion between the positively charged onium ions. As the aliphatic chain between the two aminic nitrogen increases in length repulsion will decrease, thus causing a decrease in rigidity (Barrucci et al, 1981).

Ferruti et al, (2000) used SEC and light scattering techniques to investigate the solution properties of PAAs. They found that PAAs (e.g. ISA23) can form small aggregates in solution (Ferruti et al, 2000).

1.5.4 Mechanism of PAA endosomolytic activity

The mechanisms by which PAAs causes endosomal membrane breakage are still unknown. Both cationic and amphoteric PAAs (i.e. ISA1 and ISA23) have shown endosomolytic behaviour, but to improve the efficiency of PAA-mediated gene/toxin delivery it is essential to better understand their mechanism of action (Patrick et al, 2001a; Richardson et al, 2001). It is possible that ISA1 and ISA23 have different mechanisms, but they might act in the same way.

PAAs might theoretically cause membrane breakage by one (or a combination

of) the following mechanisms (as described in section 1.3.3) :-

- (i) Proton-sponge effect. The decrease in pH in the endosome will cause PAA protonation. If the proton sponge hypothesis applies, influx of hydrogen ions into the endosome would be accompanied by the influx of chloride ions and water. As discussed earlier this would cause osmotic effects leading to the permeabilisation of the endosomal membrane.
- (ii) By causing pore formation in the membrane. PAAs could theoretically form membrane pores. If polymer binds to the membrane by electrostatic interaction, and then the less hydrophilic part (more hydrophobic region) inserts it could form a 'channel' through the lipid bilayer.
- (iii) By causing membrane stress or bending. The more simple membrane bending model would apply if the protonation of PAAs promotes membrane interaction, this in turn would cause membrane stress and this would lead to membrane breakage.

All three mechanisms seem plausible. However, two of these mechanisms have arguments against them. If the proton-sponge hypothesis is the right mechanism then theoretically the polymer molecular weight should not affect PAAs activity, but this is not true. In addition the proton sponge hypothesis does not explain why the different salt forms of the same PAAs (with quite similar molecular weight) showed different membrane activity.

All the PAAs are not naturally amphiphilic, and this is not affected by decrease in pH that occurs in the endosome. Thus it is unlikely that PAAs would be able to penetrate pores through the lipid bilayer. It appears likely that the mechanism of PAA-induced membrane permeabilisation is by direct interaction with the membrane, but this still remains unproven.

1.6 Aims of the studies in this thesis

First it was necessary to synthesise and characterise the PAAs, ISA1 and ISA23 to be used in these studies (Chapter 3). The effect of the reaction conditions on the molecular weight distribution of ISA1 and ISA23 was investigated. PAAs were characterised using common methods used for synthetic polymers such as gel permeation chromatography (GPC), titration and NMR. To ensure that the biological behaviours of these polymers was consistent with previous observations (Richardson et

al, 1999; Patrick et al, 2001a) the pH-dependence of RBC lysis was studied, and also the stability was examined in physiological solution using GPC (Chapter 3).

Having verified the biological properties of the new batch of ISA23 prepared here, this sample was used to study the physico-chemical behaviour of the polymer. First, SANS was used to examine the solution properties of ISA23.HCl at the pHs it would encounter in the endosomal/lysosomal systems (pH 7.4-5.5) (Chapter 4). First it was necessary to find an appropriate mathematical model that would fit the neutron scattering data obtained. Rod, sphere, polyelectrolytes and Gaussian coil models were explored. Having established the Gaussian coil model as the best fit, the effect of pH, polymer concentration, temperature and polymer molecular weight on the R_g of the polymer coil could be determined (Chapter 4).

The next step was to investigate ISA23.HCl-model membrane interaction (Chapter 5). Micelles were used as simple models to study interaction as a function of pH and also micelle composition. Initially, changes in surface tension were measured to study the onset of interaction. Then EPR was used to examine the effect of ISA23.HCl on the micelle fluidity. In addition, the effect of ISA23.HCl on the conformation of the micelle was also studied using SANS.

Finally, liposomal models were prepared using phospholipid compositions chosen to mimic the plasma, endosomal and lysosomal membranes. Their stability at various pHs was assessed using photon correlation spectroscopy. This was considered a more realistic and more complex model to study ISA23 interaction (Chapter 6). SANS was again used to study ISA23.HCl-liposomal interaction at different pHs. In this case, Schultz polydisperse 3 shell sphere model was used to fit the scattering data obtained from the protonated- and the deuterated-liposomes (alone). However, it was not possible to fit the SANS data of the liposomes in the presence of ISA23.HCl, a more complex model will be required to fit the data of this system.

Chapter 2
Materials and Methods

2.1 Apparatus

2.1.1 Analytical Instruments

The GPC system used to determine the PAA molecular weight consisted of two ultrahydrogel columns (250 and 1000) (Waters Corporation, USA) in a series which provide a polymer molecular weight separation up to $\sim 70,000$ g/mol. A Jasco PU-980 high performance liquid chromatography (HPLC) (Jasco UK Ltd, UK) pump, and a UV detector 486 (Waters Corporation, USA) together with a model 133 refractive index (RI) detector (Gilson, UK) were used. Polymer Laboratories (Shropshire, UK) Caliber GPC/SEC software version 7.04 was used to interpret all the GPC data. Fluorescence was detected with an Aminco-Bowman Series 2 luminescence spectrophotometer (Spectronic Instruments, USA) and Fluostar Optima fluorescence plate reader (BMG Labtechnologies, Germany). The size distribution of liposomes was measured using photon correlation spectroscopy (PCS), a N4 Plus submicron particle sizer (Beckman Coulter Ltd, UK). The $^1\text{H-NMR}$ of ISA1 and ISA23 was carried out on Bruker 400 MHz spectrometer.

The surface tension of surfactants was measured using the tensiometer SITA-online t60 (SITA, Messtechnik GmbH, Germany) with a bubble lifetime of 10 s. EPR spectra were measured using cw-Bruker EMX spectrometer (Bruker BioSpin, UK), operating at 100 kHz field modulation in a Bruker ER4102ST standard cavity (sweep width was 60G).

The SANS measurements were performed using the D11 and D22 diffractometers at the Institute Laue-Langevin (ILL), Grenoble (France), or the LOQ diffractometer at the ISIS Spallation Neutron Source, Oxfordshire (UK). The neutron scattering data were analysed and fitted using SigmaPlot 2002 and FISH2.

2.1.2 PAA purification and freeze drying

PAAs were purified using a stirred ultrafiltration cell, model 8200 (Amicon, Bioseparation, Millipore) UK, used ultrafiltration membranes (10,000 and 50,000 g/mol Mw cut-off). The polymer left on the membrane was collected. The apparatus and the membranes used were purchased from Fisher Scientific UK Ltd (UK). The purified polymer was dried using Flexi-dry lyophiliser from FTS systems, USA.

2.1.3 General equipment

The mixing and vortexing was carried using WhirlrliMixer TM from Fisher Scientific UK Ltd. (UK), and a Sartorius BP221S analytical balance (from Fisher Scientific UK Ltd., UK) was used for general weighing. Filtration of the mobile phase was carried out using nylon membrane filters (0.2 μm pore size, 47 mm in diameter, Whatman International Ltd, England). The polymer samples were filtered through 0.2 μm Sartorius single use filter units (Minisart, Germany). A sonicator from Decon Laboratories Ltd (UK) was used to sonicate the samples and GPC mobile phase.

Centrifugation was carried out with a Varifuge 3.0 RS with swing out rotor buckets (type 8080, r_{max} 21.1 cm) from Heraeus Instruments (Hanau, Germany). For the ultracentrifugation studies, Optima LE-80K centrifuge (Beckman, USA) and a Ti 50.4 fixed angle rotor (r_{max} 9.64 cm, r_{min} 6.57 cm) (Beckham, USA) were used to centrifuge the liposome samples that were contained in thick-walled 6.5 ml polycarbonate centrifugation tubes (Beckham, USA).

Eppendorfs, centrifuge tubes and non-sterile 96-well microtitre plates for general used were obtained from Fisher Scientific UK Ltd., (UK). The water bath was from Grant Instruments Ltd. (Hertfordshire, UK). Lithium/heparin tubes were purchased from L.I.P. Services and Equipments Ltd. (West Yorkshire, UK). A Mettler Toledo 320 pH meter (Mettler-Toledo Ltd. Leicester, England) was used to measure the pH of the samples and to conduct basic acid-base titration of the polymers to obtain their pKa values.

The liposome samples were extruded using an extruder supplied by Lipex Biomembranes Inc., Canada, and the liposome samples were put through nuclepore track-etch membranes (100 and 200 nm) supplied from Fisher Scientific, UK.

2.2 Materials

2.2.1 General chemicals

TX-100, dextran of M_w 74,000 g/mol (clinical grade) [code number D4751] and PEI of M_w 750,000 g/mol [code number P3143], sodium chloride (NaCl), sodium dihydrogen orthophosphate (NaH_2PO_4), disodium hydrogen orthophosphate. dodecahydrate ($\text{Na}_2\text{HPO}_4 \cdot 12\text{H}_2\text{O}$), methanol and chloroform were all from Sigma (Sigma-Aldrich, UK). Phosphate buffered saline Dulbecco A BR14 tablets were from Oxoid, U.K. Hydrochloric acid (HCl), acetic acid and sodium hydroxide (NaOH) were

from Fisher Scientific UK Ltd., UK. GPC standards including the polysaccharides pullulan (PS), and PEG were from Polymer Laboratories Inc., UK.

2.2.2 Materials used for the synthesis of ISA1 and ISA23

Lithium hydroxide monohydrate ($\text{LiOH}\cdot\text{H}_2\text{O}$) and *bis*-(hydroxyethyl)ethylenediamine (BHE) and were from Fluka, UK. 2-Methyl piperazine (2-MePip) was from Fluka, UK, and was recrystallised from *n*-heptane. Its purity was determined titrimetrically before use. 2,2-*bis*-(acrylamido)acetic acid (BAC) and *bis*-acryloylpiperazine (BIS-PIP) were kindly donated by Professor Paolo Ferruti, Milan, Italy (Ferruti et al, 1985 for details of synthesis).

2.2.3 Materials for the analytical experiments

Deuterium oxide solution (D_2O) was purchased from Fluorochem Ltd., UK. Cetyl Trimethyl Ammonium Bromide (CTAB), sodium dodecyl sulphate (SDS), deuterated SDS (d-SDS), spin probe 16-doxy stearic acid methyl ester (16-DSE) and tetraethyleneglycol dodecylether (Brij35, C_{12}E_4) were from Sigma-Aldrich, UK, and were used without further purification. Sugar surfactant dodecylmalono-*bis*(*N*-methylglucamide) (C_{12}BNMG) was prepared by Dr.J. Roe (2000), School of Chemistry, Cardiff.

The lyso-phospholipids, 1-palmitoyl-2-hydroxy-*sn*-glycero-3-phosphocholine (lyso-PC) was obtained from Avanti Polar Lipids, Inc. (Alabaster, Alabama, USA). The lysophospholipid contained one fatty acid chain with 16 carbons, and was used without further purification.

2.2.4 Materials used in liposome preparation and characterisation

Calcein fluorescence dye was from Sigma, UK. The following phospholipids, 1,2-dipalmitoyl-*sn*-glycero-3-phosphocholine (DPPC), 1,2-dipalmitoyl-*sn*-glycero-3-[phospho-L-serine] (sodium salt) (DPPS) and 1,2-dipalmitoyl-*sn*-glycero-3-phosphoethanolamine (DPPE), and the deuterated form of these phospholipids (the fatty chain was deuterated only) 1,2-dipalmitoyl-D62-*sn*-glycero-3-phosphocholine (D-DPPC), 1,2-dipalmitoyl-D62-*sn*-glycero-3-phosphoethanolamine (D-DPPE) and 1,2-dipalmitoyl-D62-*sn*-glycero-3-[phospho-L-serine] (sodium salt) (D-DPPS) all were from Avanti Polar Lipids, Inc., (USA). All the phospholipids contained saturated fatty acid chains with 16 carbons in each chain, they were supplied in powder form, and were

used without further purification.

2.3 Methods

2.3.1 Characterisation of PAAs using GPC

GPC also known as size exclusion chromatography (SEC) was used to characterise PAA molecular weight characteristics. This technique was developed in the mid 1960's by Moore (1964), for the determination of the molar mass distribution of a polymer (Feng and Fan, 1990). GPC separates polymers according to their size (Nishikida et al, 1990). The most important information obtained from GPC is the average number molecular mass (M_n), average-weight molecular mass (M_w) and polydispersity (Zhu et al, 1990). These are calculated as follows:

$$M_n = \frac{\sum N_i M_i}{\sum N_i} \quad 2.1$$

$$M_w = \frac{\sum N_i M_i^2}{\sum N_i M_i} \quad 2.2$$

$$\text{Polydispersity} = M_w / M_n \quad 2.3$$

Briefly the theoretical basis of GPC is as follows. The GPC column is packed with a porous gel composed of beads. The pore size depends on the packing material used. When the polymer solution is passed through the column, small polymer molecules pass through the pores of the gel, travelling a longer path than bigger polymer molecules that are excluded by most of the pores. Thus larger polymer molecules are eluted first (Figure 2.1).

A precolumn and two ultrahydrogels SEC columns (pore sizes of 250 and 1000 Å) were used here, with PBS buffer as eluent. The buffer was filtered through 0.2 µm membrane, and sonicated for 30 min before use. To analyse the polymer molecular weight the PAA (ISA23.HCl batch 1 and 2, ISA23.cit, ISA23, ISA1.HCl and ISA1) solutions were prepared in PBS buffer (pH 7.4) to a concentration of 3 mg/ml. The sample solution was injected (60 µl loop) onto the column, with an eluent flow rate of 1 ml/min using refractive index detection.

The GPC system was calibrated using both pullulan and PEG standards (Table 2.1), that were also prepared in PBS (pH 7.4) at a concentration of 3 mg/ml.

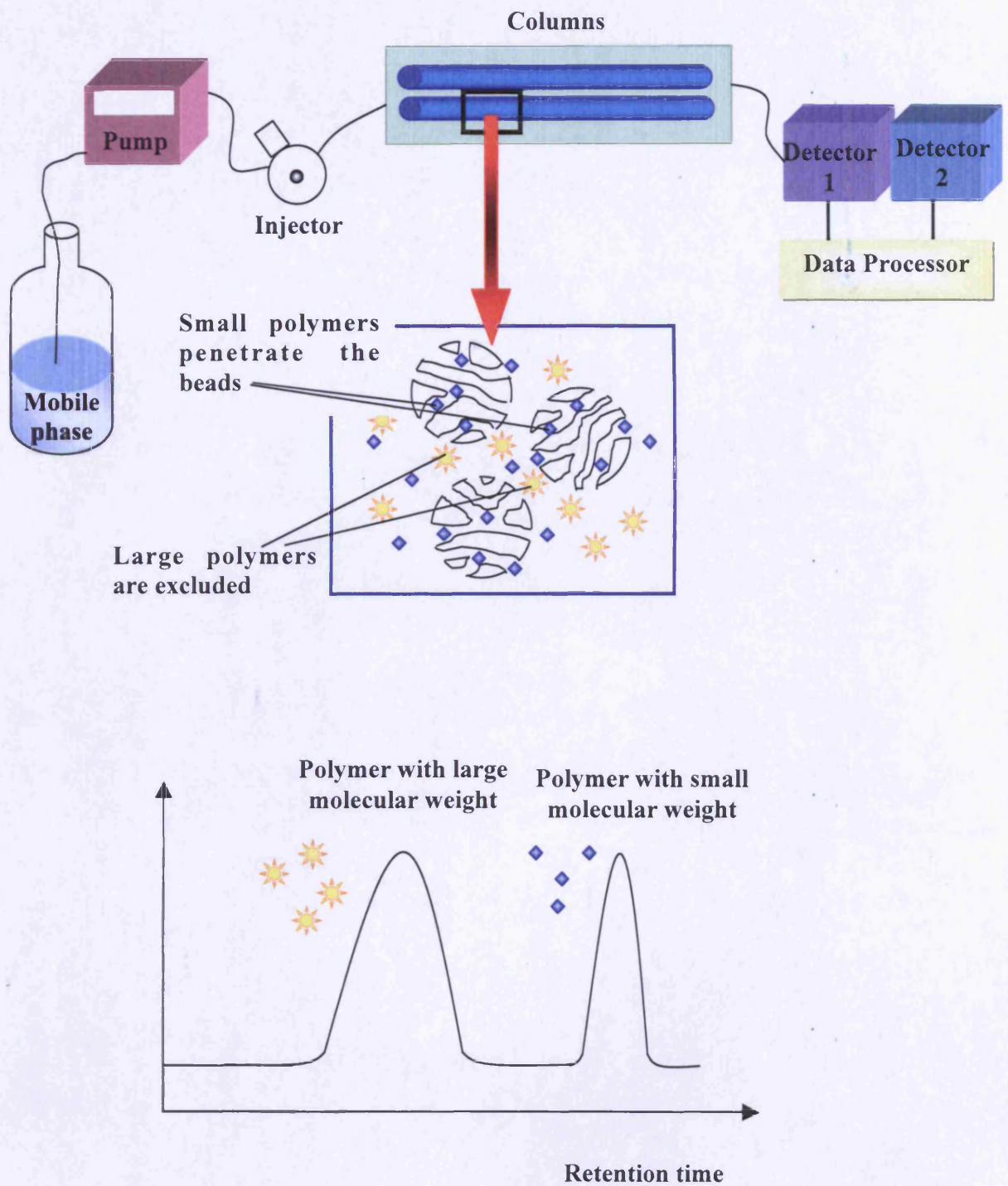


Figure 2.1 A schematic showing the principle of GPC. Polymer molecules are separated according to their size using the GPC. The smaller molecular weight polymer molecules travel longer distance compared to that of a polymer with high molecular weight. Thus the smaller polymer molecules appear later

Table 2.1 Polymer standards used for GPC calibration.*†

Polymer	M_w (g/mol)	M_n (g/mol)	M_w/M_n
PS	212,000	187,610	1.13
	112,000	100,000	1.12
	47,300	44,622	1.06
	22,800	21,308	1.07
	11,800	10,727	1.10
	5,900	5,412	1.09
PEO	278,300	271,000	1.03
	222,800	217,800	1.03
	128,100	125,900	1.02
	78,000	75,500	1.04
	42,870	41,920	1.03
	20,400	20,000	1.02

* M_w , M_n and M_w/M_n supplied by the manufacturer

† The GPC profiles obtained are shown in Chapter 3

2.3.2 Evaluation of the haemolytic activity of PAAs

RBC were used as a model to study membrane activity of PAAs under different conditions. Freshly prepared PAAs (ISA23.HCl batch 1 and 2, ISA23.cit, ISA23, ISA1.HCl and ISA1) (1 mg/ml) in PBS (pH 7.4, 6.5 or 5.5) were plated (100 μ l) into non-sterile 96-well microtitre plates.

To prepare RBC, a male Wistar rat (~ 250g) was killed by 4% CO₂ asphyxiation and blood obtained by cardiac puncture (Gomez and Duncan, 1997). RBCs were isolated by centrifugation at 1500 x g for 10 min at 4°C (repeated 3 times). Using the final pellet, a 2 % w/v RBC solution was prepared with pre-chilled PBS and it was added (100 μ l) to the previously prepared microtitre plates containing the test compounds (Wan et al, 2004). The plate was then incubated for 1 h at 37 °C before centrifugation at 1500 x g for 10 min at room temperature. The supernatant was then pipetted into another 96-well microtitre plate and the absorbance of the haemoglobin was measured at 550 nm (Figure 2.2) (Richardson et al, 1999). Dextran was used as a negative reference control, and PEI was used as the positive controls. TX-100 (2 mg/ml) was used to cause 100% haemolysis. The results were expressed as a percentage of the haemolysis caused by TX-100.

To study the concentration-dependent haemolysis of ISA23.HCl (batch 1 and 2) and ISA23.cit (Table 3.2, Chapter 3), at pH 5.5, the concentrations examined varied from 0 to 2 mg/ml, and the method described above was used. In certain experiments (see Chapter 3) pH was also varied.

2.3.3 Liposome preparation and stability testing

The widely used freeze/ thaw extrusion method (Hope et al, 1985; Mayer et al, 1986) was used to prepare large unilamellar liposomes (Figure 2.3). Prior to the liposomes preparation, stock phospholipid solutions were prepared with protonated or deuterated DPPC in chloroform (10 mg/ml), protonated or deuterated DPPE in chloroform (4 mg/ml), and protonated or deuterated DPPS in 3:1 ratio of chloroform:methanol (2 mg/ml). These stock solutions were then used to prepare the model liposomes (described below). It should be noted that the compositions chosen were to reflect plasma, endosomal, or lysosomal membranes (see Chapter 6 for more details).

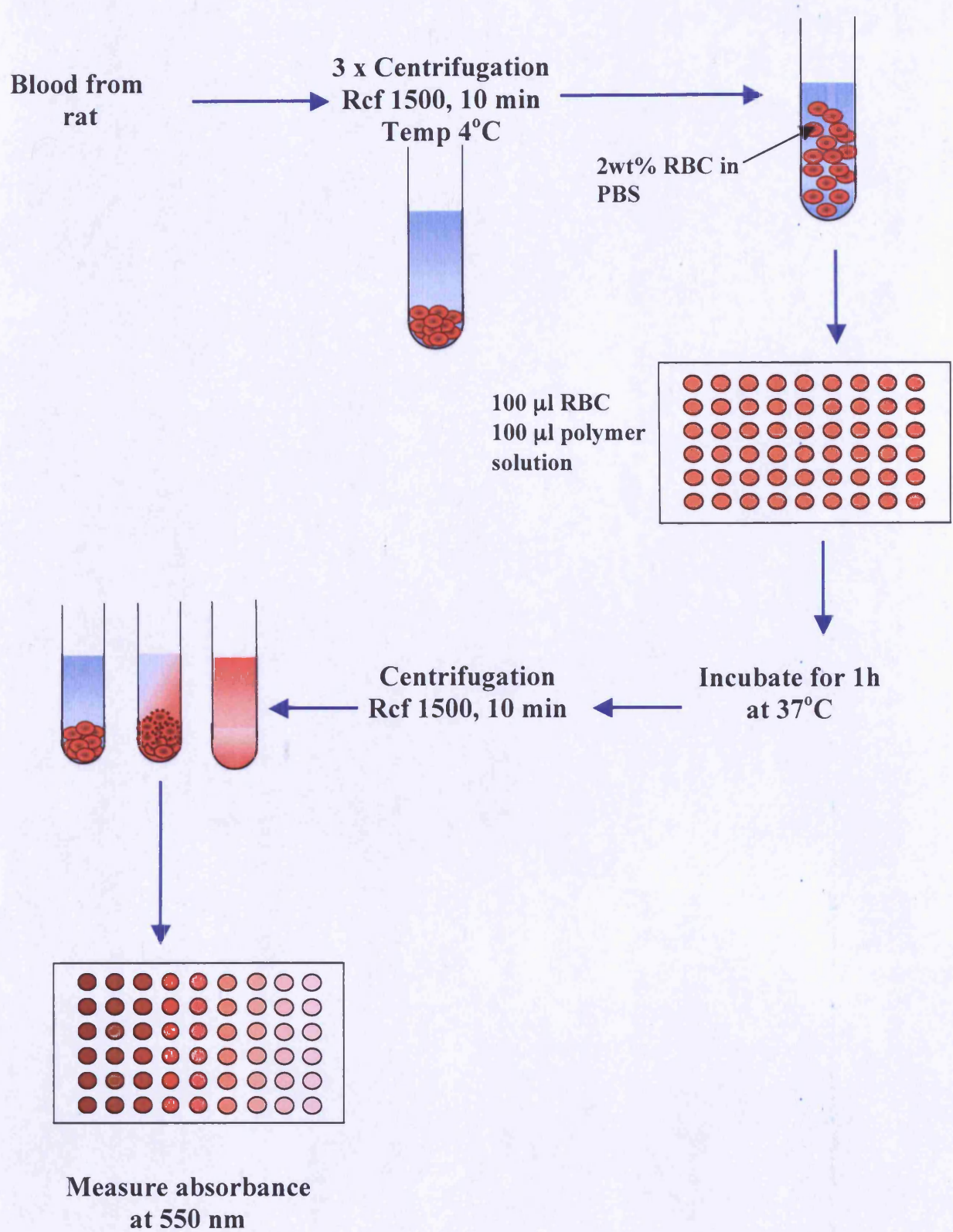


Figure 2.2 The schematic representation of the red blood cell lysis assay.

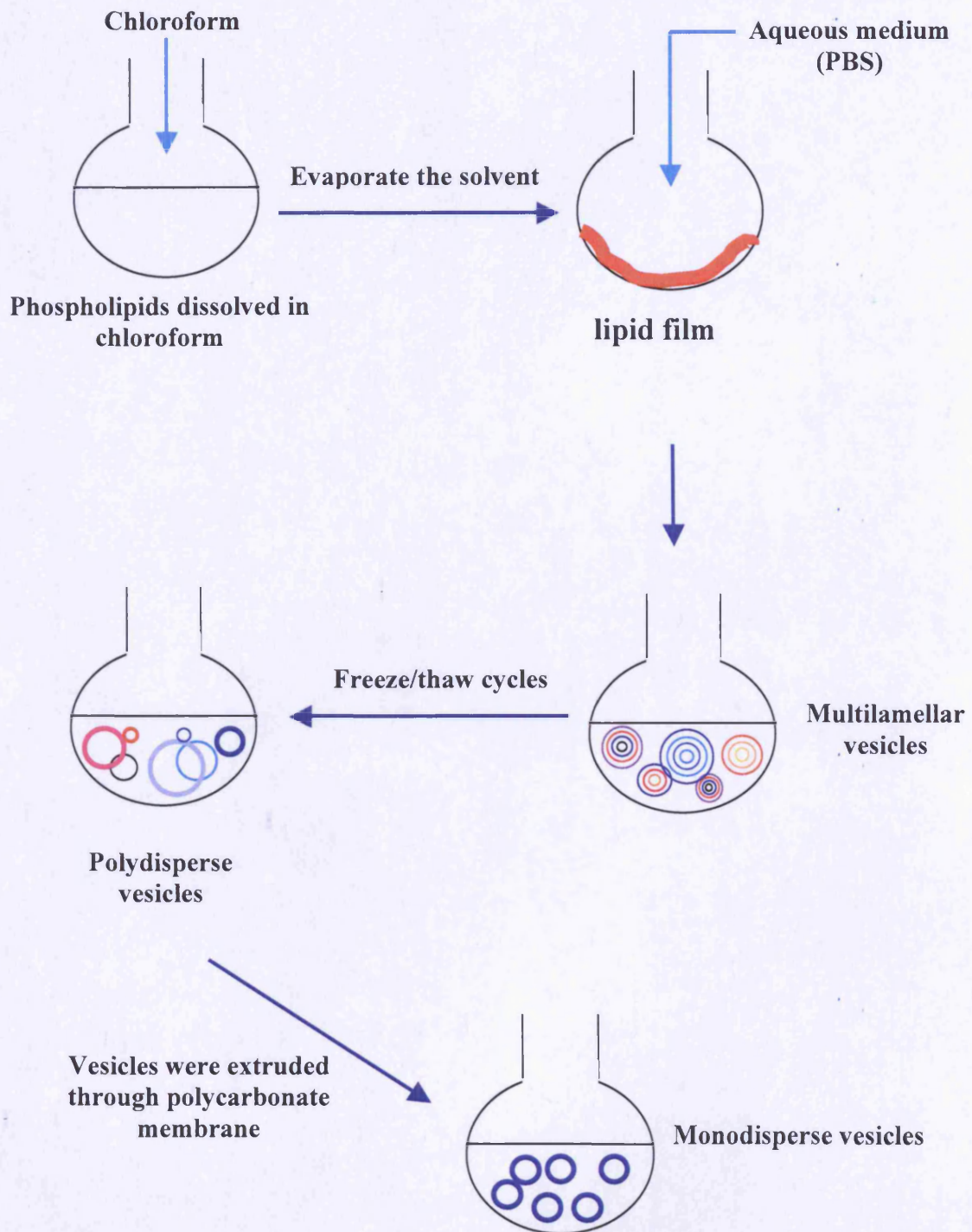


Figure 2.3 Schematic diagram summarising the preparation of liposomes using freeze-thaw/extrusion method.

Protonated plasma membrane model-liposomes

0.861 ml of DPPC stock solution	8.6 mg, 5.9 mM,
0.985 ml of DPPE stock solution	3.9 mg, 2.8 mM
0.97 ml of the DPPS stock solution	1.9 mg, 1.3 mM

Deuterated plasma membrane model-liposomes

0.934 ml of deuterated -DPPC (D-DPPC) stock solution	9.3 mg, 5.9 mM
1.075 ml of D-DPPE stock solution	4.3 mg, 2.8 mM,
1.053 ml of D-DPPS stock solution	2.1 mg, 1.3 mM

Protonated endosomal membrane model-liposomes

0.986 ml of DPPC stock solution	9.8 mg, 6.7 mM
0.937 ml of DPPE stock solution	3.7 mg, 2.7 mM
0.432 ml of DPPS stock solution	0.9 mg, 0.6 mM

Deuterated endosomal membrane model-liposomes

1.070 ml of D-DPPC stock solution	10.7 mg, 6.7 mM
1.022 ml of D-DPPE stock solution	4.1 mg, 2.7 mM
0.468 ml of D-DPPS stock solution	0.9 mg, 0.6 mM

Protonated lysosomal membrane model-liposomes

0.768 ml of DPPC stock solution	7.7 mg, 5.3 mM
0.980 ml of DPPE stock solution	3.9 mg, 2.8 mM
1.461 ml of the DPPS stock solution	2.9 mg, 1.9 mM

Deuterated lysosomal membrane model-liposomes

0.834 ml of D-DPPC stock solution	8.3 mg, 5.3 mM
1.070 ml of D-DPPE stock solution	4.3 mg, 2.8 mM
1.58 ml of the D-DPPS stock solution	3.2 mg, 1.9 mM

To prepare the liposomes (for each sample), the required amount of each phospholipid was added to a round bottomed flask, 1 ml of chloroform was added, and was thoroughly mixed. The chloroform was evaporated (using a rotary-evaporator), to give a phospholipid film. The film was left to evaporate further for 60 min, at 25 °C. Then 2 ml of PBS, at pH 7.4, was added, and the film left to hydrate in a hot water bath (70 °C) for around 50 min. The hydrated lipid film was then put through 5 freeze/thaw cycles (5 min freezing in liquid nitrogen, 2 min thawing in water at room temperature

and 5 min mixing by a vortex). Subsequently, the liposome mixture was put through 10 cycles of extrusion through 200 nm polycarbonate membrane and 20 cycles through 100 nm polycarbonate membrane.

The liposomes were prepared in this way and were characterised using PCS. The liposomes used for stability testing were prepared in H₂O. The stability studies were conducted over two days, at pH 7.5, 5, 4 and 3. The liposomes used for SANS measurements were prepared in D₂O. PCS was also used to examine the stability of the liposomes, described in Chapter 6.

2.3.4 Evaluation of ISA23.HCl interaction with micelles and liposomes as model membranes

The three techniques used to investigate the interaction of ISA23.HCl with liposomes and micelles were, surface tension measurements (surfactants), EPR (micelles) and SANS (micelles and liposomes). The experimental detail of each study is given in the related experimental chapters (Chapters 5 and 6).

The techniques mentioned above are very important for the understanding of the mechanism of action of PAAs and background information on SANS and EPR are given in Chapter 4 and 5 respectively. Here, a brief introduction will be given on the theory behind the maximum bubble pressure, which was used to measure the surface tension.

Maximum bubble pressure was used to measure the dynamic surface tension (Mysels, 1990). Basically, air is blown through a narrow capillary into the sample solution. At the base of the capillary a bubble is formed, as the bubble grows the pressure increases, and it reaches a maximum pressure when the bubble has a shape of a hemisphere (the radius of the bubble is equal to that of the capillary) (Kjellin et al, 2003). Beyond this point, the size of the bubble increases exponentially with time and the pressure inside the bubble decreases (Buzacchi et al, 2006). Ultimately the bubble is detached from the capillary and it travels to the surface. At the same point, a new bubble begins to form and the whole process is repeated (Buzacchi et al, 2006) (Figure 2.4). The maximum pressure reached is proportional to the surface tension, the pressure is converted into surface tension via the Laplace's relation (Kjellin et al, 2003):

$$\sigma = \frac{\rho_{\max} - \rho_0}{2} R$$

2.4

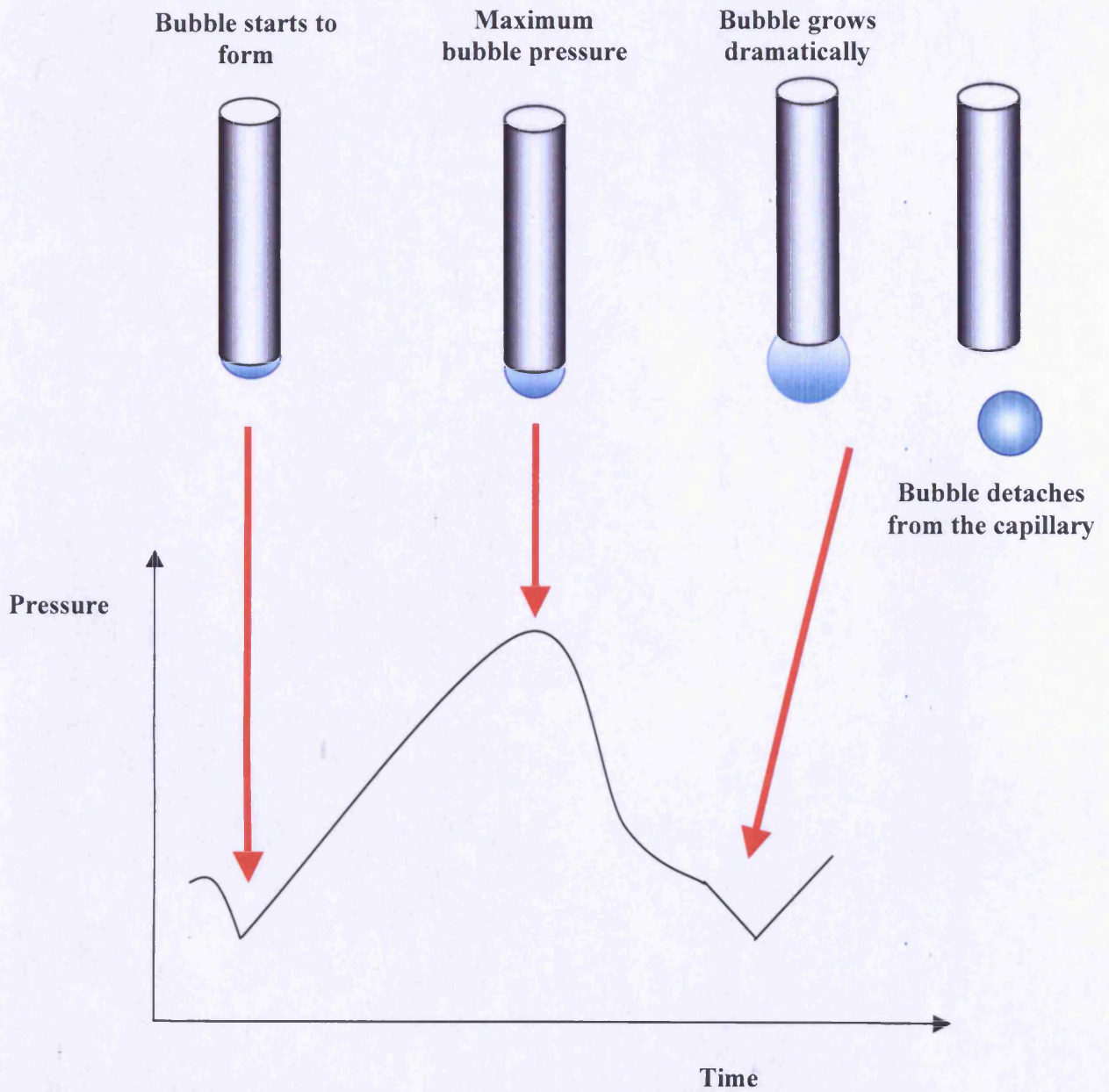


Figure 2.4 The schematic illustration of the changing pressure inside the bubble with bubble life-time (adapted from Dukhin et al, 1996).

where σ is the surface tension, ρ_{\max} is the maximum pressure reached, ρ_0 is the hydrostatic pressure at the tip of the capillary and R is the maximum radius of the bubble (Buzzacchi et al, 2006).

2.3.5 Lyophilisation and storage of polymers

The polymers to be lyophilised were dissolved in the minimal amount of double distilled water, this is followed by the freezing of the polymer solution in liquid nitrogen, they were left in liquid nitrogen for at least 10 min. Once the samples were frozen, then they were put into the lyophiliser for drying until a constant weight of the samples was reached (approximately three days). PAAs were stored in the freezer (-20°C).

Chapter 3
Synthesis and characterisation of PAAs

3.1 Introduction

To begin this study it was first necessary to synthesise the PAAs ISA1 and ISA23 that would be used in all subsequent experiments. The synthetic method is well established (Richardson et al, 1999; reviewed in Franchini and Ferruti, 2004) so the main purpose of this study was to prepare sufficient polymer for the later studies on physico-chemical behaviour and to confirm the reproducibility with the earlier work.

As mentioned in Chapter 1 (section 1.5.1) PAAs are synthetic, water-soluble polymers prepared by stepwise polyaddition of primary or secondary aliphatic amines to bis(acrylamide)s (reviewed in Ferruti et al, 2002). Using different monomers, many diverse polymers (linear, block, cross-linked or grafted polymers) can be produced (Vansteenkiste et al, 1992). Thus the chemistry of polyamidoamine polymers can be easily tailored to suit specific application (reviewed in Ferruti et al, 2002). The preparation of PAAs usually involves five main steps. Polymerisation is generally carried out in a proton carrying solvent, e.g. alcohol or water (Ferruti, 1996), and the reaction mechanism is Michael addition (Ranucci et al, 1991). This involves the reaction of the α - β -unsaturated carbonyl group with nucleophilic group of the primary or secondary aliphatic amine group (Figure 3.1). Polymerisation is followed by acidification, and during this step the polymer salt is produced, where the counterion depends on the particular acid used, e.g. hydrochloric acid for the chloride salt form. Ultrafiltration is used as a final purification step, to remove the un-reacted monomer and low molecular weight polymer, and lyophilisation gives a solid PAA suitable for storage.

Even though the synthetic methods used to prepare both ISA1 and ISA23 are well documented, it was considered important to examine the effect of the reaction conditions (e.g. reaction temperature, the length of the reaction, the choice of solvent, the chemical nature, the concentration and molar ratio of monomers and the presence of chain terminators) to see if it was possible to alter the molecular weight average of the product. During polymerization PAA molecular weight usually increases with time until it reaches a maximum, after which the molecular weight average starts to decrease (reviewed in Ferruti et al, 2002). This could be due to polymer degradation. It is known that generally increasing the reaction temperature decreases the time taken for the reaction to reach completion, but the resulting overall PAA molecular weight decreases slightly (Danusso and Ferruti, 1970). Also the inclusion of chain terminators (e.g. dimethyl acrylic acid), and the use of monomers containing hindered amino groups

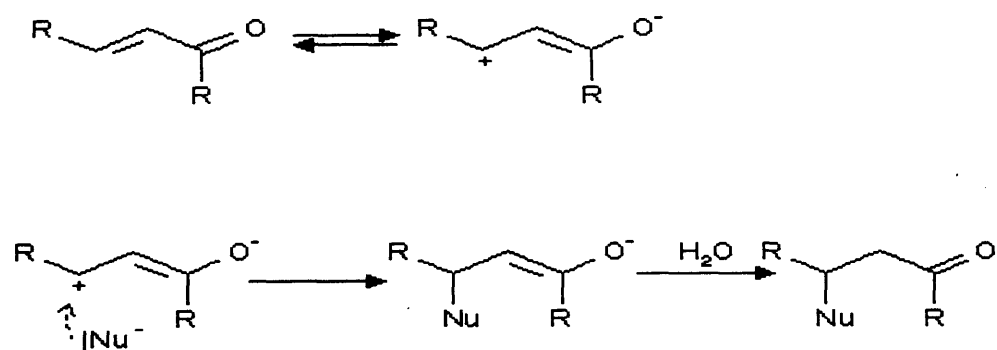


Figure 3.1 The overall mechanism of Michael addition.

can be used to cause a decrease in the molecular weight of the product (Danusso and Ferruti, 1970; reviewed in Franchini and Ferruti, 2004). All these factors can be manipulated to optimise the synthetic conditions of PAAs.

Three main physical and chemical techniques have been used to characterise PAAs, these are nuclear magnetic resonance (NMR spectroscopy), acid-base titration and GPC. NMR is commonly employed to analyse the chemical structure and molecular microstructure of polymers, and was used here to confirm the successful polymerisation of ISA1 and 23 (Ferruti et al, 2000). Acid-base titration is used to deduce the pKa of ISA1 and ISA23 to ensure that these polymers exhibit ionization properties similar to that of the previous batches (Ferruti et al, 2000). The pKa value of a polymer is important as it determines the average charge of the polymer at a particular pH, its reactivity and the pH condition required for a chemical reaction. Acid-base titration is also used to obtain the concentration of acid or base in solution of unknown concentration. GPC can be used to obtain the M_w , the M_n and polydispersity (M_w/M_n) (described in Chapter 2, section 2.3.1) of a polymer (Patrick et al, 2001). GPC does not give an absolute value, as polymer standards of a known molecular weight are used to calibrate the columns. As there are no PAA standards, to calibrate the GPC to analyse ISA1 and ISA23, the standards (poly(vinylpyrrolidone) (PVP), PS and PEG) were used as reference.

In the context of the proposed use of ISA1 and ISA23 as endosomlytic polymers (see Chapter 1, section 1.4.2) their ability to show a pH-dependant membrane permeabilisation is a key property (Richardson et al, 1999; Ferruti et al, 2000) if they are to show effective gene (Richardson et al, 2001) or toxin delivery (Patrick et al, 2001). Here isolated RBC were used as a model to study pH-dependant membrane breakage caused by the PAAs. The RBC model was chosen because it is a well established technique to evaluate the pH-dependant membrane activity of PAAs (Duncan et al, 1994; Richardson et al, 1999; Ferruti et al, 2000; Patrick et al, 2001; Wan et al, 2004) and other polymers (Dubruel et al, 2003; Fisicaro et al, 2005). Before moving on to the physical-chemical studies described later in this thesis, it was considered important to establish the pH-dependent membrane breakage of the ISA1 and ISA23 batches synthesised here. This also ensured that it was possible to correlate the biological and physico-chemical properties of these polymer batches.

An advantage of the RBC lysis model is the simplicity of the experimental

design, and the fact that the results are reproducible. However it does have an important disadvantage for the assessment of endosomolytical polymers. The membrane composition of the RBC (see Table 3.1) is very different from that of a “normal” cell plasma membrane and also the endosomal and lysosomal membranes (see Chapter 6 for the composition of the plasma, endosomal and lysosomal membranes). The RBC membrane is composed of 49% protein, 43% lipid and 8% carbohydrate by weight (Becker et al, 2000). The major proteins of the RBC membrane are actin, α - and β -spectrin, ankyrin and glycophorin A, B and C, these are skeletal proteins, and are not present in the plasma membrane or the intracellular vesicle membranes. These skeletal proteins allow the RBC to withstand the mechanical stress and permit the rapid recovery of their shape after squeezing through the narrow passages of blood capillaries and vessels. Whereas most biological membranes exist in the fluid phase, RBC membrane is an example of a solid membrane (Nelson, 1989).

Thus, in summary the aims of these studies were:

- To synthesise and characterise ISA1 and ISA23, batches that would be used in all subsequent experiments.
- To study the effect of the polymerisation conditions (temperature and time) and the effect of varying the monomer molar ratio on molecular weight and polydispersity of the product.
- As it had been claimed that PAAs are biodegradable in aqueous solution (Ferruti et al, 1994), experiments were conducted to establish the degradation behaviour of the PAAs prepared here, both as a function of pH and temperature.
- It was considered important to define PAA stability, so that future experiments could be carried out with intact polymer and not the degradation products.
- Finally, the effect of the ISA1 and ISA23 samples prepared here on the RBC integrity (1h) was investigated, as a function of pH, polymer concentration and molecular weight. The pH values chosen were 7.4, 6.5 and 5.5 and these values were selected to mimic the pH of the extracellular fluid, the endosome and the lysosome respectively.

3.2 Methods

3.2.1 General methods

NMR. 30 mg of ISA1 or ISA23 was dissolved in 3 ml of D₂O (10 mg/ml), 2 ml of

Table 3.1 The lipid composition of the plasma membrane of human erythrocyte.

Lipid	Human erythrocyte plasma membrane Percent of the total composition*
Phosphatidic acid	1.5
Phosphatidylcholine	19
Phosphatidylethanolamine	18
Phosphatidylglycerol	0
Phosphatidylinositol	1
Phosphatidylserine	8.5
Sphingomyelin	17.5
Glycolipids	10
Cholesterol	26
Cardiolipin	0

* Taken from Smith and Wood, 1996

polymer solution was then added to NMR tube and the ^1H NMR was measured.

Acid-base titrations. The pKa of ISA1.HCl and ISA23.HCl, was determined by titration. Samples were made up in PBS at concentration of 1 %w/v (3 ml). The solution was then titrated with 0.1 M HCl, and following the addition of known amount of acid or base, the pH was measured.

GPC. ISA1 and ISA23 samples were prepared (3 mg/ml in PBS), and 60 μl was injected into the column (see Chapter 2, section 2.3.1 for details), PBS buffer was used as the eluent with a flow rate of 1 ml/min, a RI was the choice of detector (see Chapter 2, section 2.3.1 for details).

RBC haemolysis assay. Isolated rat RBCs (2 w/v%) were incubated with ISA1 and ISA23 (up to 2.5 mg/ml) for 1 h, at pH 7.4, 6.5 and 5.5. The released haemoglobin was measured at this time as described in Chapter 2, section 2.3.2.

PAA Stability studies. GPC was also used to study polymer stability with time. An Ultrahydrogel column was used, with PBS as the mobile phase and polymer detected using a refractive index detector. The stability of ISA23.HCl (batch 1 and 2) and ISA23.citrate during the incubation at room temperature was studied at pH 7.4, 6.5 and 5.5 over 2 weeks. At 37 °C the stability of ISA23.HCl (batch 1 and 2), at pH 7.4, 6.5 and 5.5 was investigated over 7 days. For these experiments, stock polymer solution was made up in PBS at a concentration of 3 mg/ml (total volume 10ml). The polymer samples were kept in a water bath at either 25 or 37 °C, and samples were taken overtime for GPC analysis.

As this chapter mainly deals with the synthesis of ISA1 and ISA23, a detailed description of the synthetic methods used are given below.

3.2.2 Synthesis of ISA1

To synthesise ISA1, 1 g of BIS-PIP (5.15 mmol) and 402 mg of BHE were dissolved in 1.72 ml of double distilled water. To that, 2-MePip (266 mg, 2.58 mmol) was added (Figure 3.2). The amount of water added was calculated in order to have a 3 M solution of BIS-PIP. After ensuring all the reactants have dissolved, the reaction was stirred under nitrogen in a water bath at 25 °C, and stopped after 3 days by adding water. To purify and isolate the product (ISA1 and ISA1.HCl), the reaction mixture was filtered using a stirred, ultrafiltration cell (model 8200, Amicon, Bioseparation, Millipore), with a membrane cut-off 10,000 g/mol. To prepare ISA1.HCl, before the

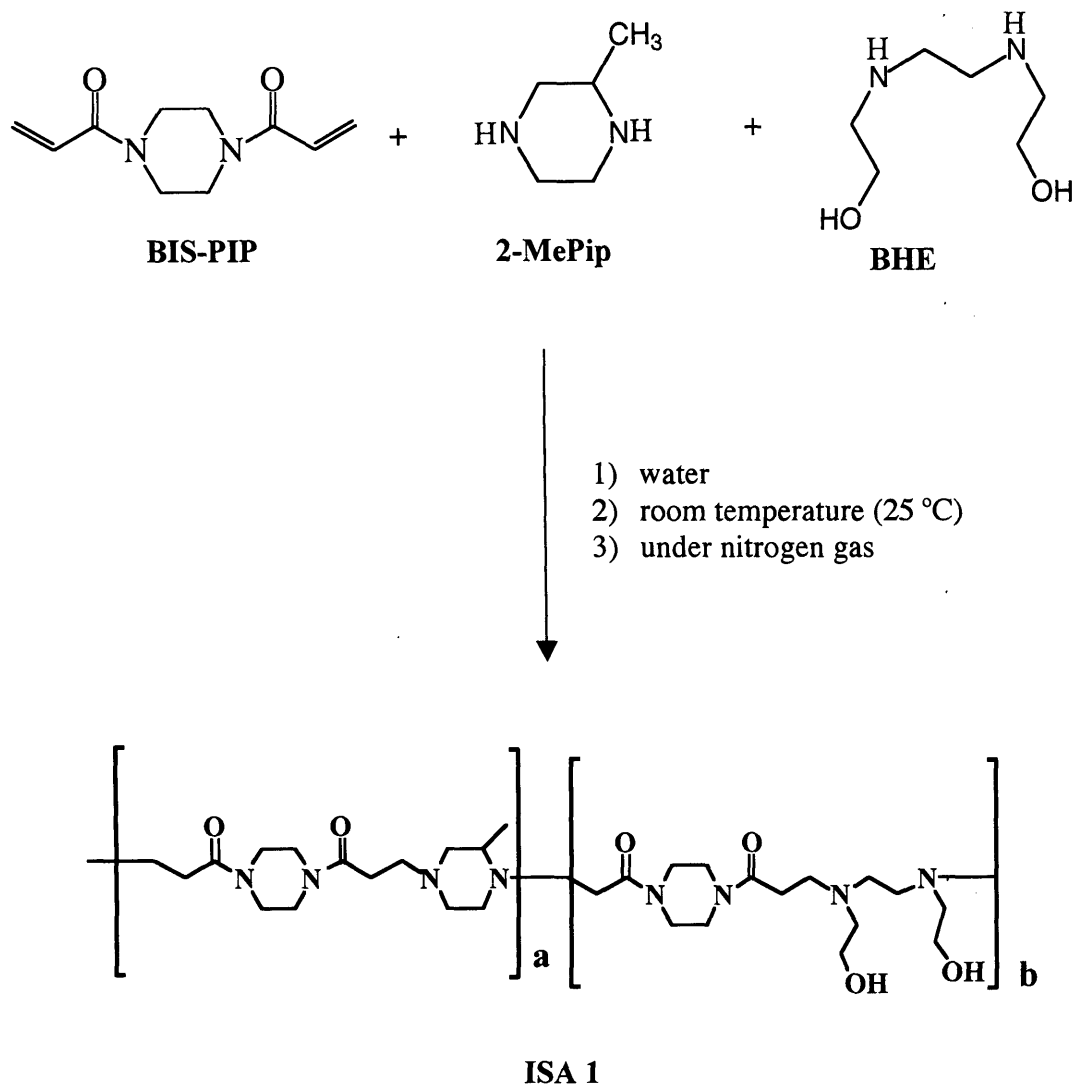


Figure 3.2 Synthesis of ISA1.

filtration step concentrated HCl (10 M) was added dropwise to obtain pH between 3 and 4. In both cases, the product was finally lyophilised (Richardson et al, 1999).

To investigate the effect of time and temperature on the polymerisation, ISA1 polymerisation was carried out using the methods described above, but on a smaller scale. 0.2 g of BIS-PIP (1.03 mmol) and 80.2 mg of BHE (0.52 mmol) were dissolved in 334 μ l of double distilled water, and to that 53.2 mg of 2-MePip (0.52 mmol) was added. Four separate reactions mixtures were prepared, and they were subsequently incubated in water bath at 25, 35, 50 or 70 °C. A sample of each (~ 0.1 ml) was taken after 0, 5, 24, 48 and 72 h, water was added (5 ml), and the molecular weight was then determined using GPC as described above. GPC analysis was undertaken without further purification of the polymer.

3.2.3 Synthesis of ISA23

ISA23 was synthesised as previously described (Richardson et al, 1999; Ferruti et al, 2000). To prepare ISA23.HCl (batch 1), 1 g BAC (5 mmol) and 0.212 g LiOH.H₂O (5 mmol) were dissolved in double distilled water (1.67 ml, amount required to make 3 M of BAC) (Figure 3.3). To this mixture, 0.516 g 2-MePip (1% NH₂ excess) was added. For ISA23.HCl batch 2, briefly BAC (5 g, 25 mmol) and LiOH.H₂O (1.06 g, 25 mmol) were dissolved in double distilled water (8.35 ml, amount required to make 3 M of BAC). This mixture was stirred for 10 min, or until all the chemicals had dissolved. For ISA23.citrate and ISA23, 1 g BAC (5 mmol) and 0.212 g LiOH.H₂O (5 mmol) were dissolved in 1.67 ml double distilled water, and 0.511 g of 2-MePip (5 mmol) was added to the mixture. All the reaction mixtures were then stirred for 3 days at 25 °C under a nitrogen atmosphere in the dark. The reactions were then stopped by adding water. Each reaction product was then filtered using stirred ultrafiltration cell (with membrane cut off 10,000 g/mol) and then the product was recovered by lyophilisation (Richardson et al, 1999). For ISA23.HCl (batches 1 and 2), concentrated HCl (10 M) was added until the pH reached 3 – 4, prior to purification. To prepare ISA23.citrate, before the filtration step citric acid was added until the pH reached 3 – 4 before purification.

To study the effect of time-and temperature on the polymerisation of ISA23, the synthesis was carried out as described above, but on a smaller scale. To a 0.2 g of BAC

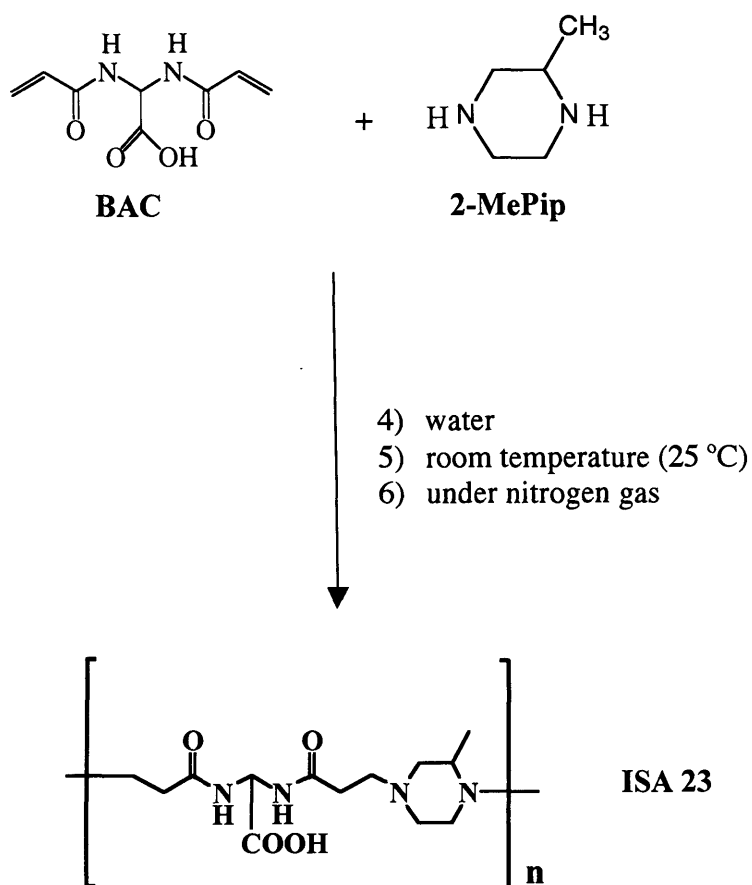


Figure 3.3 Synthesis of ISA23.

(1 mmol) and 42.2 mg of LiOH.H₂O (1 mmol) were dissolved in 334 μ l double distilled water and to that 0.10 g of 2-MePip (1 mmol) was added. Four separate reactions mixtures were prepared, and these were incubated in a water bath at 25, 35, 50 or 70 °C. From each reaction a sample was taken after 0, 5, 24, 48 and 72 h, and as above the molecular weight of the polymer characterised using GPC, without further purification step.

3.3 Results

Table 3.2 gives a summary of all the polymers synthesised and their codes.

3.3.1 Characterisation of ISA1 and ISA23

¹H NMR was used to confirm the identity of ISA1 and ISA23 (Figure 3.4a,b). For ISA1, the peaks are not well separated and this makes it difficult to assign them. The peak at 1.264 ppm corresponds to the three protons of the -CH₃ on the 2-methylpiperazine.

For ISA23, again it is quite difficult to assign the peaks due to the poor separation of the peaks. The peak at 5.390 ppm is the -CH proton on the BAC monomer. The peak at 1.220 ppm corresponds to the three protons of the -CH₃ on the 2-MePip. The theoretical ratio between the two integrals should be 1:3, from the spectra this ratio is 1:3.24 which is consistent with the experimental error of the NMR technique.

In solution the polymers ISA1.HCl, ISA23.HCl (batch 1 and 2), and ISA23.citrate (Figure 3.5a,b), displayed an initial pH of ~ 3, indicating that they act as a weak acid. In contrast, ISA1 and ISA23 act as a weak base, and they have an initial solution pH of ~ 9. Acid-base titration of the ISA1.HCl showed three pK_a values. These were 3.5, 6.4 and 8, and these values correspond to each amino group; present as part of the cyclic ring of the 2-MePip or in the aliphatic chain of the BHE. Previous studies have shown that ISA1 displayed 4 pK_a values (Patrick et al, 2001a), but here only 3 pK_a values were observed, this is due to the fact that the initial pH of the polymer solution was ~ 3.4, which is quite high, this can be solved by conducting a backward titration, which takes the pH of solution down, enough to obtain the final pK_a value. For ISA23.HCl, two pK_a values were seen, 3.3 and 7.5, which corresponds to the amino groups of the cyclic 2-MePip. It was not possible to obtain the third pK_a value of ISA23

Table 3.2 Characteristics of the PAAs batches synthesised, and their code numbers.

PAAs	Salt forms	Method of synthesis	Codes	Yield (%)
ISA 1	Chloride	1 % excess ^a	ISA1.HCl	75
	–	1 % excess	ISA1	73
ISA 23	Chloride	1 % excess	ISA23.HCl (batch 1)	88
	Chloride	1:1 ratio ^b	ISA23.HCl (batch 2)	85
	–	1:1 ratio	ISA23	80
	Citrate	1:1 ratio	ISA23.citrate	83

^a synthesised with 1% excess of NH₂ - containing monomer

^b synthesised with 1:1 ratio of NH₂ - containing monomer (BAC for ISA23 polymer and BIS-PIP for ISA1 polymer)

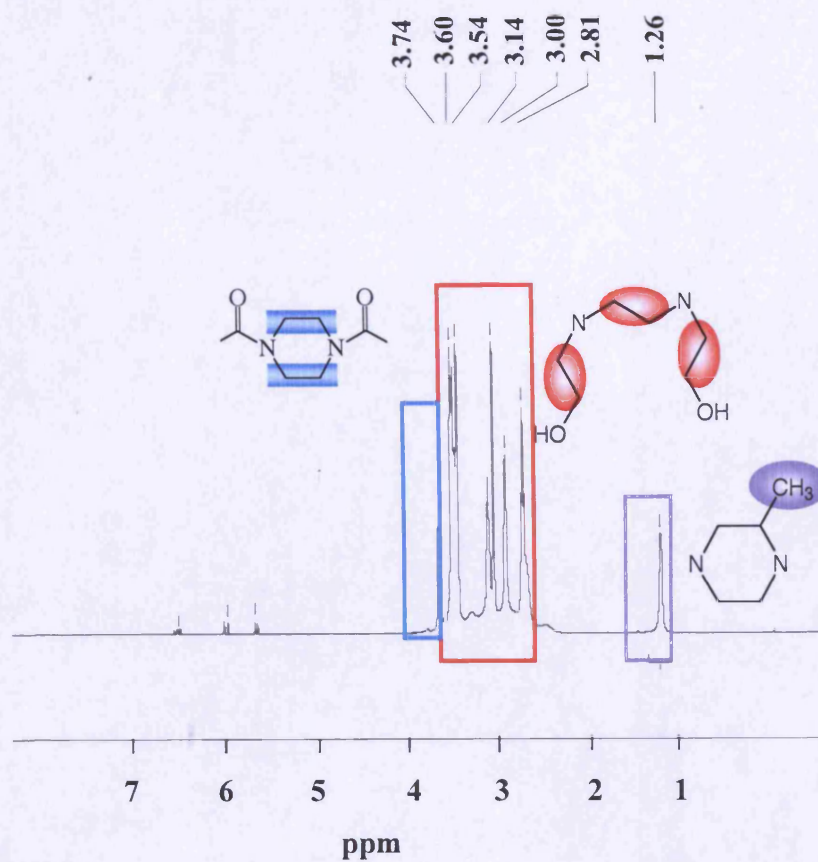


Figure 3.4 ¹H-NMR spectra of ISA1 and ISA23. Panel (a) shows the ¹H-NMR spectra of ISA1

¹H-NMR (D₂O): δ = 1.28 (d, CH₃ group of the 2-MePip), 2.81-3.6 (m, CH₂ of ethylenediamine and BHE, complex system), 3.74 (m, CH₂ of BIS-PIP)

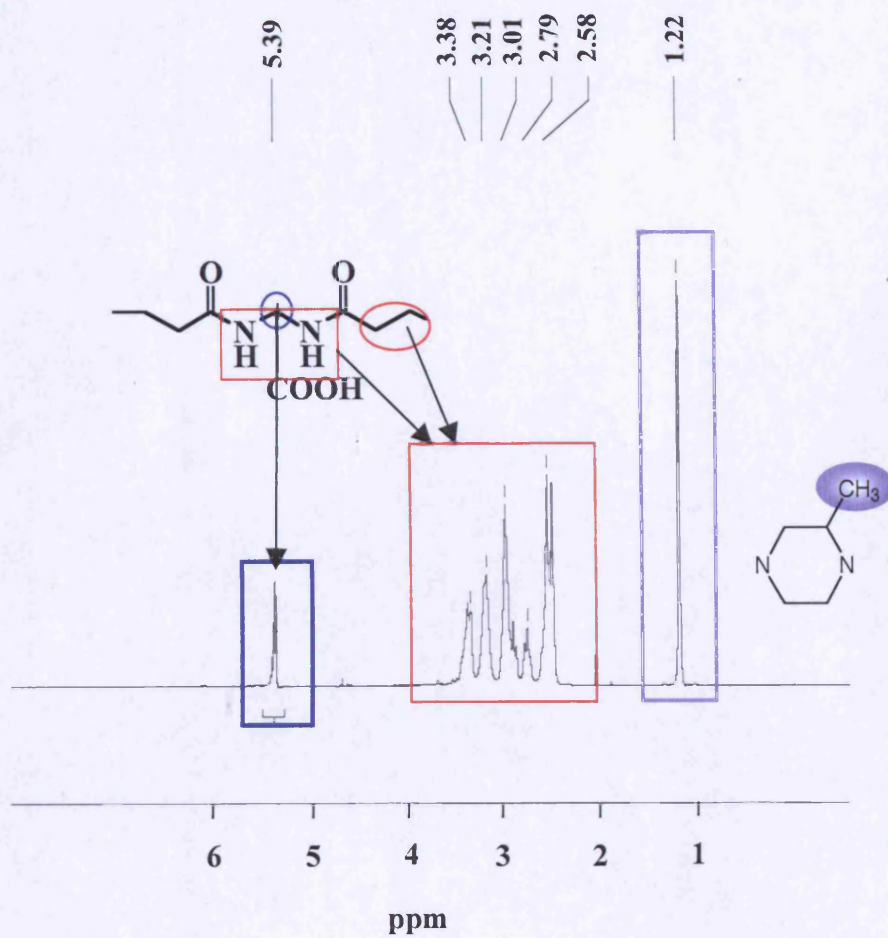


Figure 3.4 (continued). Panel (b) ¹H-NMR spectra of ISA23.

¹H-NMR (D₂O): $\delta = 1.22$ (d, CH₃ group of the 2-MePip), 2.58-3.38 (m, CH₂-CH₂ and N-H, of BAC, complex system), 5.39 (t, CH of BAC)

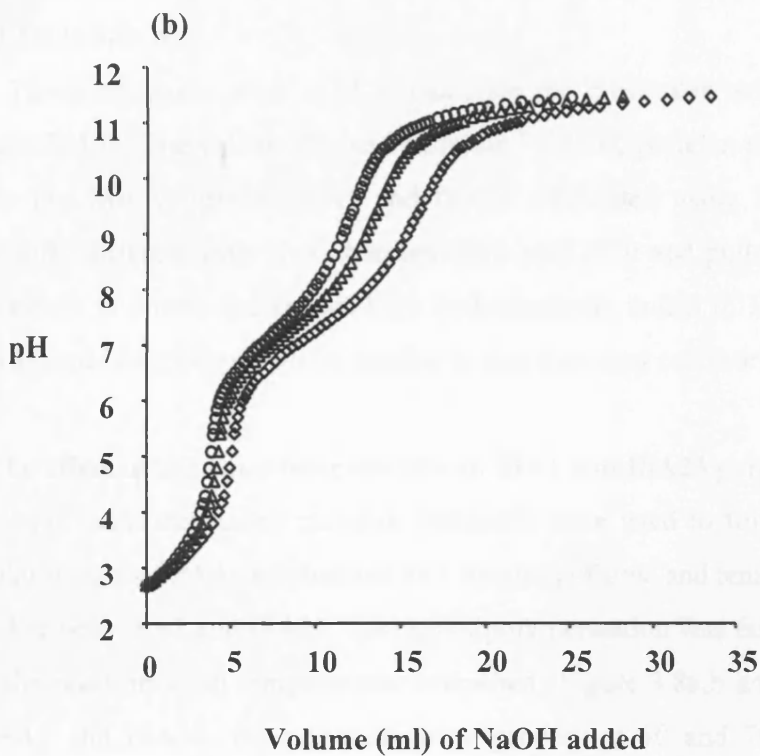
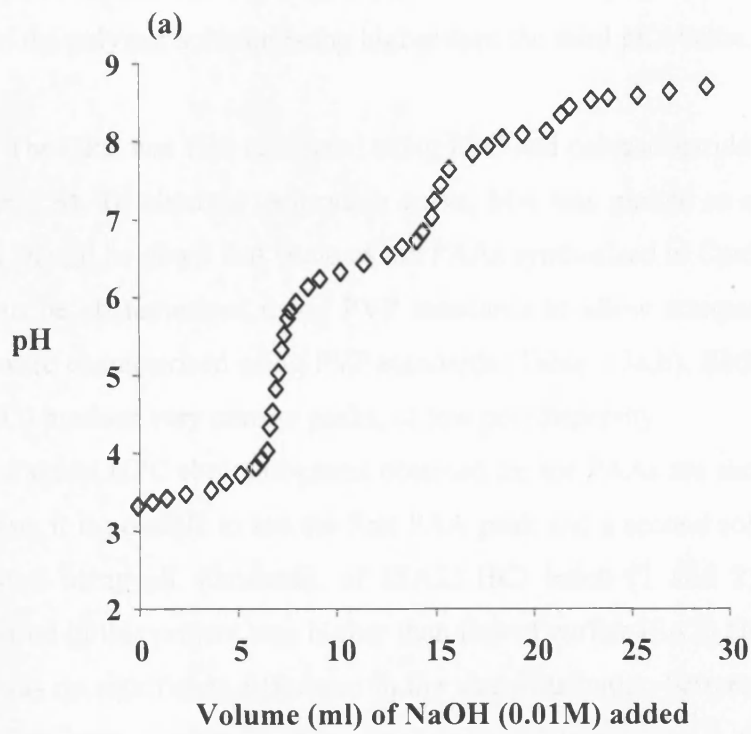


Figure 3.5 Titration curves of ISA1 and ISA23. Panel (a), titration curves of ISA1.HCl, panel (b), titration curves of ISA23.HCl batch 1 (circles) batch 2 (triangles) and ISA23.citrate (diamonds)

(corresponds to the carboxylic group), which is ~ 2.1 , again this is due to the initial value of the polymer solution being higher than the third pKa value.

The GPC was first calibrated using PEG and polysaccharide standards (pullulan) (Figures 3.6). To obtain a calibration curve, Mw was plotted as a function of elution time. It should be noted that some of the PAAs synthesised in Cardiff were also sent to Milan to be characterised using PVP standards to allow comparison as historically PAAs were characterised using PVP standards (Table 3.3a,b). Both standards (pullulan and PEG) produce very narrow peaks, of low polydispersity.

Typical GPC chromatograms obtained for the PAAs are shown in Figure 3.7. In each case, it is possible to see the first PAA peak and a second solvent peak. The Mw, calculated using all standards, of ISA23.HCl batch (1 and 2) and ISA23.citrate synthesised in this project was higher than that of earlier ISA23.HCl (reference batch). There was no significant difference in the size distribution between the ISA23 batches synthesised here. Generally, ISA1 had a lower Mw compared to that of ISA23 (Figure 3.7 and Table 3.3a,b).

Three standards were used to calculate the molecular weight distribution of ISA1 and ISA23. The values obtained from the PVP and pullulan standards, were quite similar. The Mw weight of ISA1 and ISA23 calculated using PEG standards was significantly different from that obtained from both PVP and pullulan standards. This inconsistency is due to the known high hydrodynamic radius of PEG standards, thus both ISA1 and ISA23 appear to be smaller in size than they really are.

3.3.2 The effect of time and temperature on ISA1 and ISA23 polymerisation

GPC calibrated using pullulan standards were used to follow changes in the molecular weight of PAAs synthesised as a function of time and temperature.

For both ISA1 and ISA23, the rate of polymerisation was fastest during the first 5 h of the reaction at all temperatures examined (Figure 3.8a,b and Tables 3.4). For both ISA1 and ISA23, the polymerisation process at 50 and 70 °C slowed down virtually to zero, after this initial 5 h period. This was also true for the polymerisation of ISA1 at 35 °C. Polymerisation of ISA1 and ISA23 at 25 °C, continued for the whole 3 days, but the rate of reaction slowed down over time. For ISA23, the polymerisation at 35 °C continued for an additional 20 h (at a slower rate), before the reaction stopped.

Temperature (between 25 and 35 °C) had an effect on the rate of polymerisation

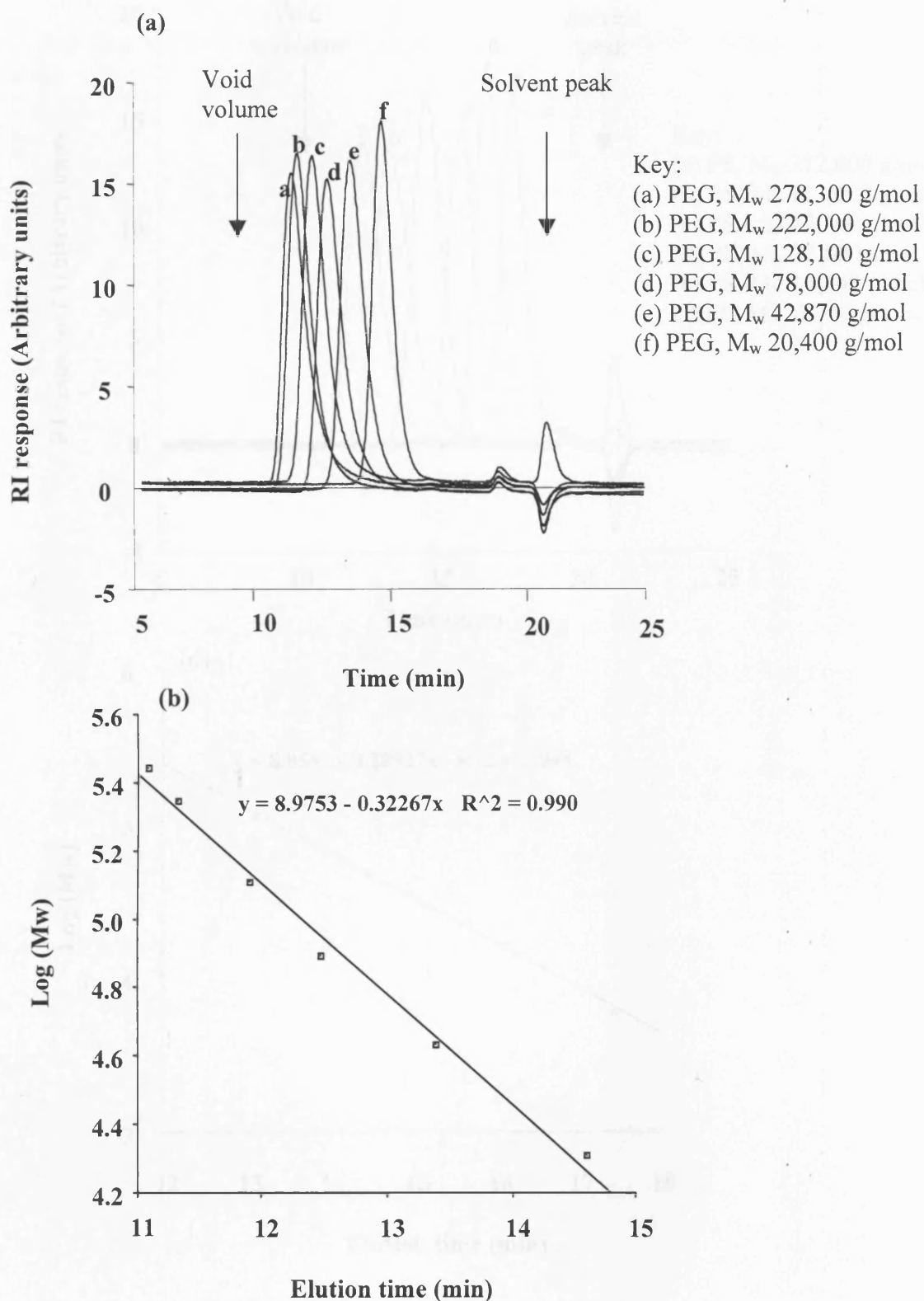


Figure 3.6 GPC of PEG and pullulan standards. Panel (a) show the GPC traces of PEG standards, and panel (b) a plot of elution time against log PEG M_w . Units of M_w are g/mol

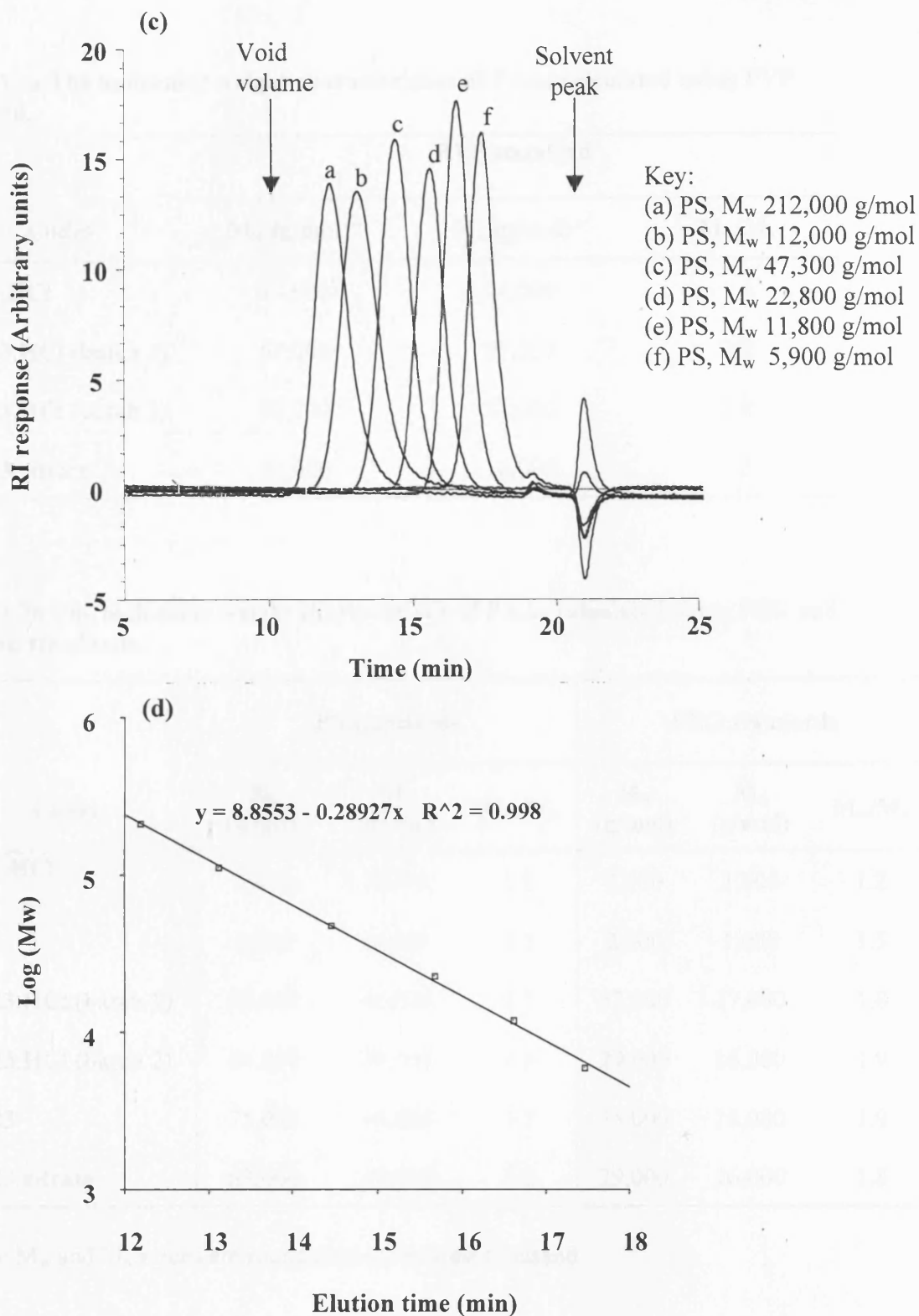


Figure 3.6 (continued). GPC of pullulan standards. Panel (c) shows the GPC traces of pullulan standards, panel (d) a plot of elution time against log pullulan M_w . Units of M_w are g/mol

Table 3.3a The molecular weight characteristics of PAAs calculated using PVP standard.

Codes	PVP standard		
	M_w (g/mol)*	M_n (g/mol)*	M_w/M_n
ISA1.HCl	23,000	14,000	1.6
ISA23.HCl (batch 1)	67,000	31,000	2.2
ISA23.HCl (batch 2)	62,000	32,000	2.8
ISA23.citrate	52,000	16,000	3.3

Table 3.3b The molecular weight characteristic of PAAs calculated using PEG and pullulan standards.

Codes	PS standards			PEG standards		
	M_w (g/mol)	M_n (g/mol)	M_w/M_n	M_w (g/mol)	M_n (g/mol)	M_w/M_n
ISA1.HCl	5,000	4,000	1.2	2,000	1,000	1.2
ISA1	5,000	3,000	1.5	2,000	1,000	1.5
ISA23.HCl (batch 1)	68,000	41,000	1.7	32,000	17,000	1.8
ISA23.HCl (batch 2)	64,000	39,000	1.6	29,000	16,000	1.9
ISA23	75,000	44,000	1.7	35,000	18,000	1.9
ISA23.citrate	63,000	40,000	1.6	29,000	16,000	1.8

* The M_w and M_n values are rounded to the nearest thousand

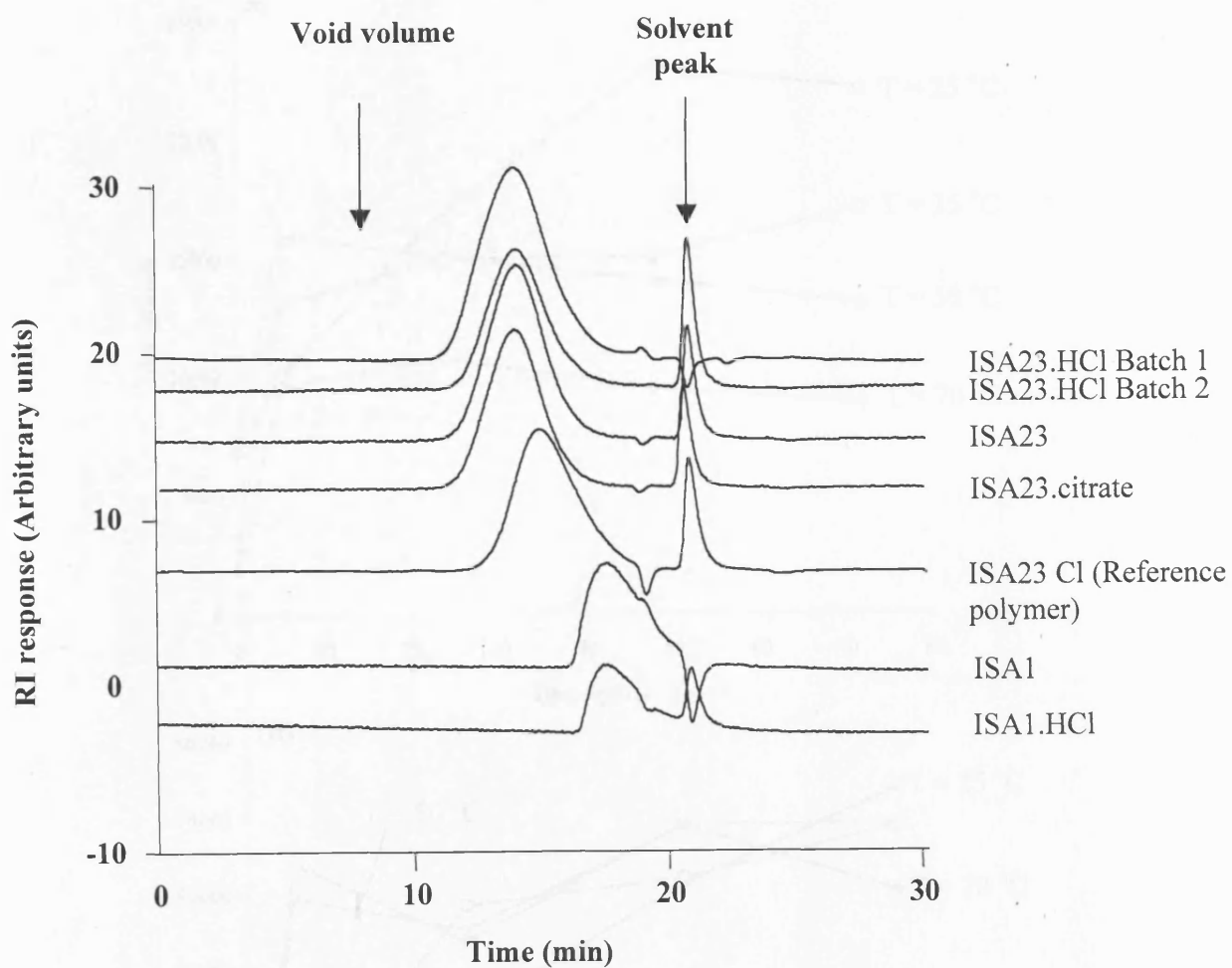


Figure 3.7 The GPC traces of PAAs.

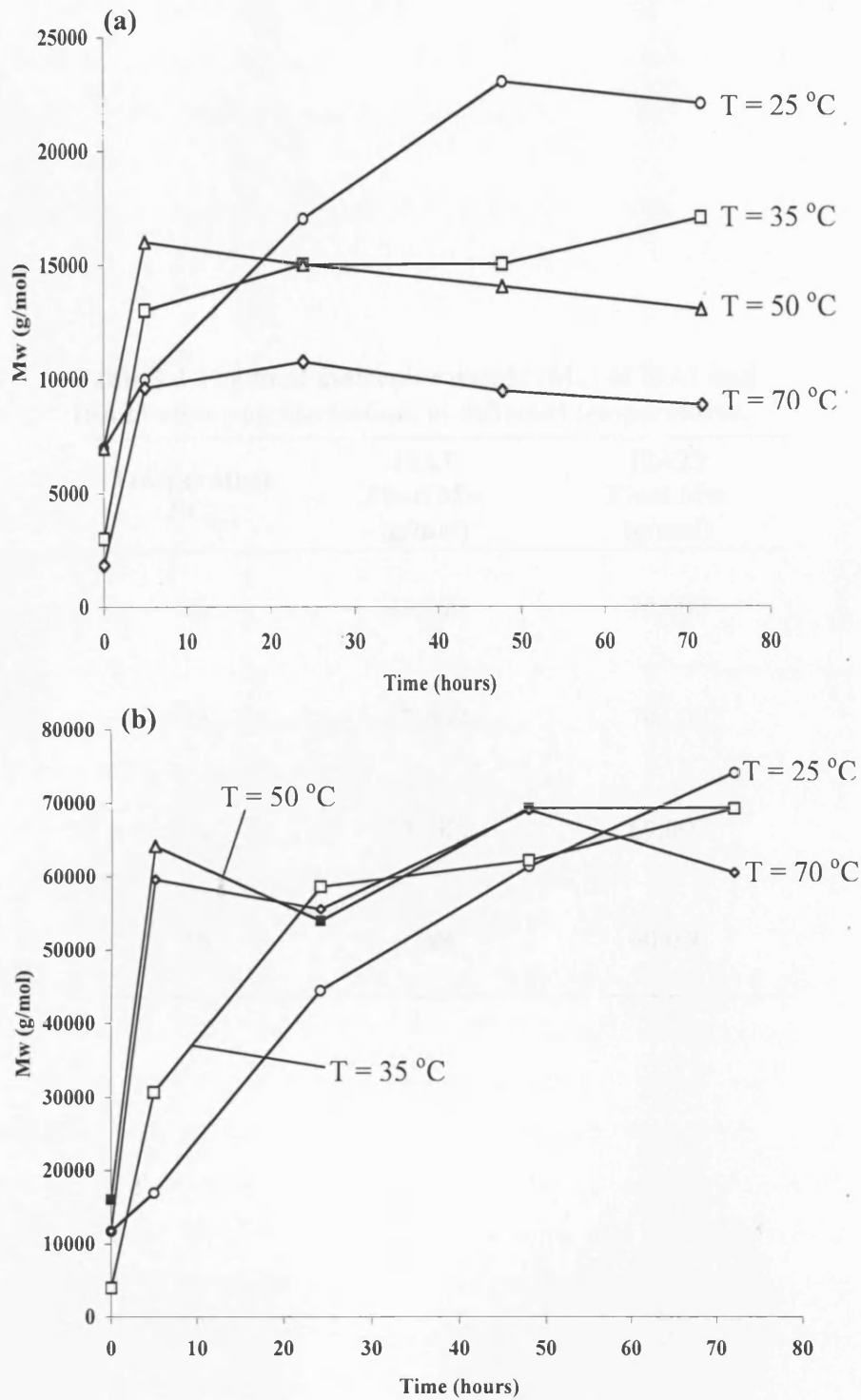


Figure 3.8 The effect of time and temperature on PAA polymerisation. The molecular weight of: ISA1 panel (a), and ISA23 panel (b) is shown, and the data points are a single GPC value collected at each time point

Table 3.4 The final molecular weight (M_w) of ISA1 and ISA23 after polymerisation, at different temperatures.

Temperature (°C)	ISA1 Final Mw (g/mol)	ISA23 Final Mw (g/mol)
25	22,000	74,000
35	17,000	70,000
50	13,000	69,000
70	9,000	60,000

of ISA1, but increasing the temperature above 35 °C did not affect the rate of polymerisation. Changes in temperature had the greatest effect on the maximum, and the final molecular weight of ISA1. Increasing temperature caused a decrease in molecular weight.

For ISA23, temperature did not increase the rate of polymerisation, and the final molecular weight of ISA23 was unaffected by varying the temperature.

3.3.3 Studies on the degradation of PAAs at room temperature and 37°C (pH 7.4 and 5.5)

GPC was also used to investigate the rate degradation of ISA23 over time at different pHs (7.4, 6.5 and 5.5), and temperatures (room temperature and 37°C). GPC showed that the elution time of ISA23.HCl (batch 1 and 2) and ISA23.citrate, remained constant with time (Figure 3.9a,b,c). This was not affected by varying pH. No degradation of ISA23.HCl (batches 1 and 2) was seen at 37 °C (results not shown), and again changing the pH had no effect on the degradation rate.

3.3.4 Evaluation of the haemolytic activity

The ISA23.HCl reference polymer did not cause RBC lysis at pH 7.4 or 6.5, but did cause a significant haemolysis at pH 5.5 (Figure 3.10). No haemolysis was observed in the PBS control or for dextran at any pHs. The haemolysis seen for PEI decreased with decreasing pH (22%, 8%, and 2.5% at pH 7.4, 6.5 and 5.5 respectively).

The new batches of PAA, ISA23.HCl (batch 1 and 2) and ISA23.citrate, displayed pH-dependent haemolysis. No haemolysis was seen at pH 7.4 and 6.5, but there was haemolytic activity at pH 5.5. It is important to mention that these pH values are nominal, and they are altered following the addition of the polymer (see discussion).

The effect of polymer concentration on the haemolytic activity was examined at pH 5.5. Generally, as the polymer concentration increases the percentage haemolysis also increases, and it reached a plateau at a polymer concentration of ~ 1.5 mg/ml (Figure 3.11).

3.4 Discussion

A library of PAAs were synthesised (Table 3.2) and analysed using biological, chemical and physical methods. It is quite difficult to characterise the molecular weight of PAAs accurately due to the lack of appropriate molecular weight standards.

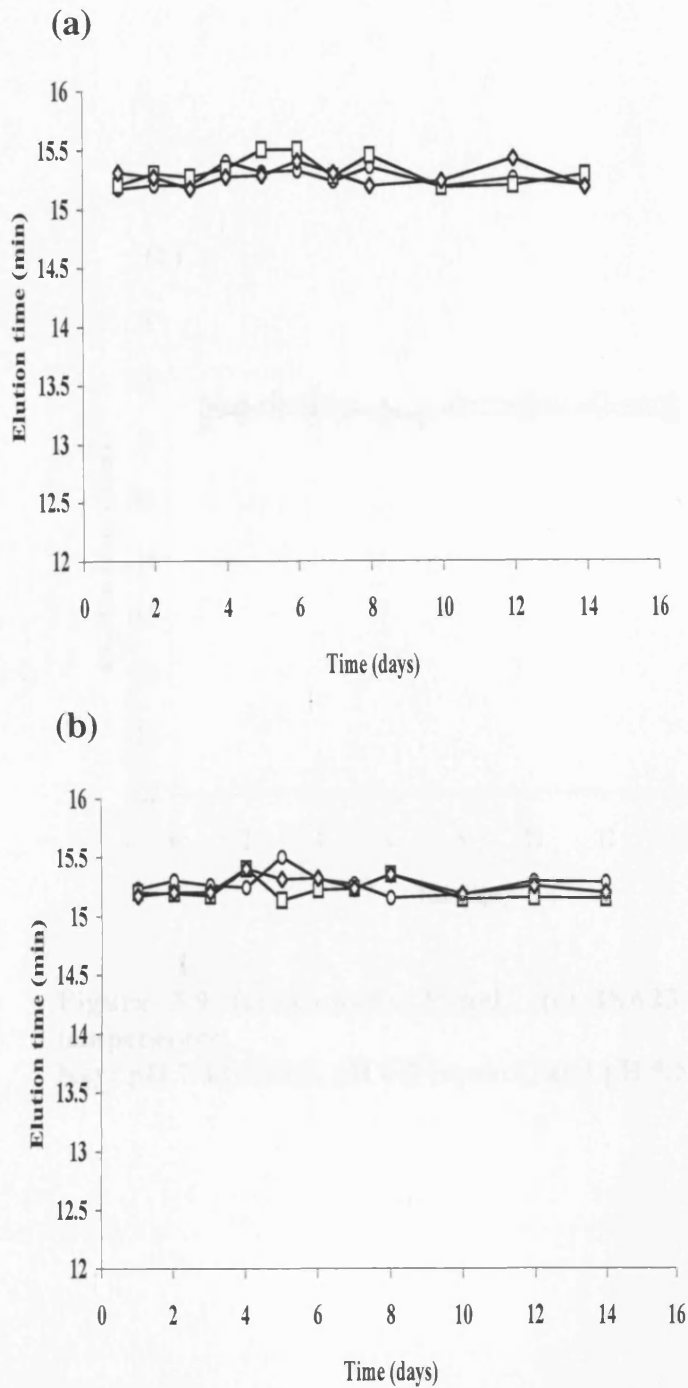


Figure 3.9 Evaluation of the degradation of ISA23 using GPC. Panel (a) ISA23.HCl (batch 1), panel (b) ISA23.HCl (batch 2), at room temperature
Key: pH 7.4 (circle), pH 6.5 (square) and pH 5.5 (diamond)

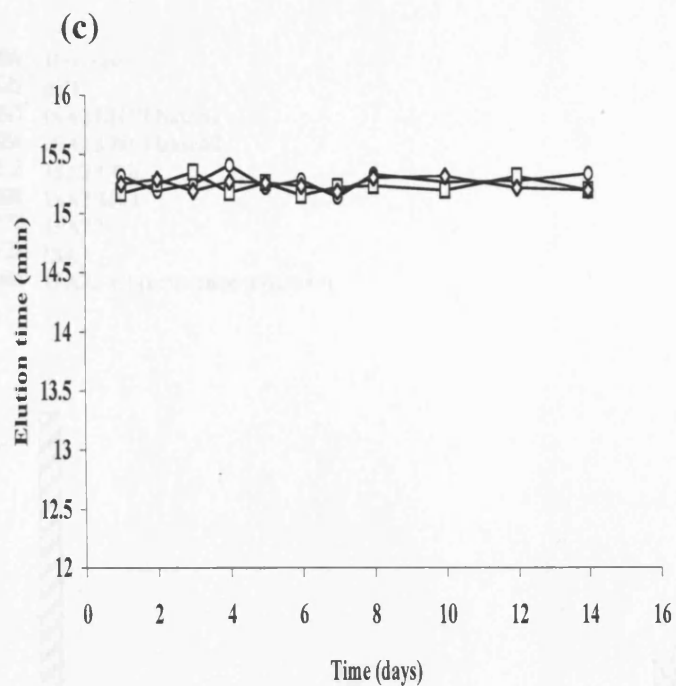


Figure 3.9 (continued). Panel (c) ISA23.citrate, at room temperature
Key: pH 7.4 (circle), pH 6.5 (square) and pH 5.5 (diamond)

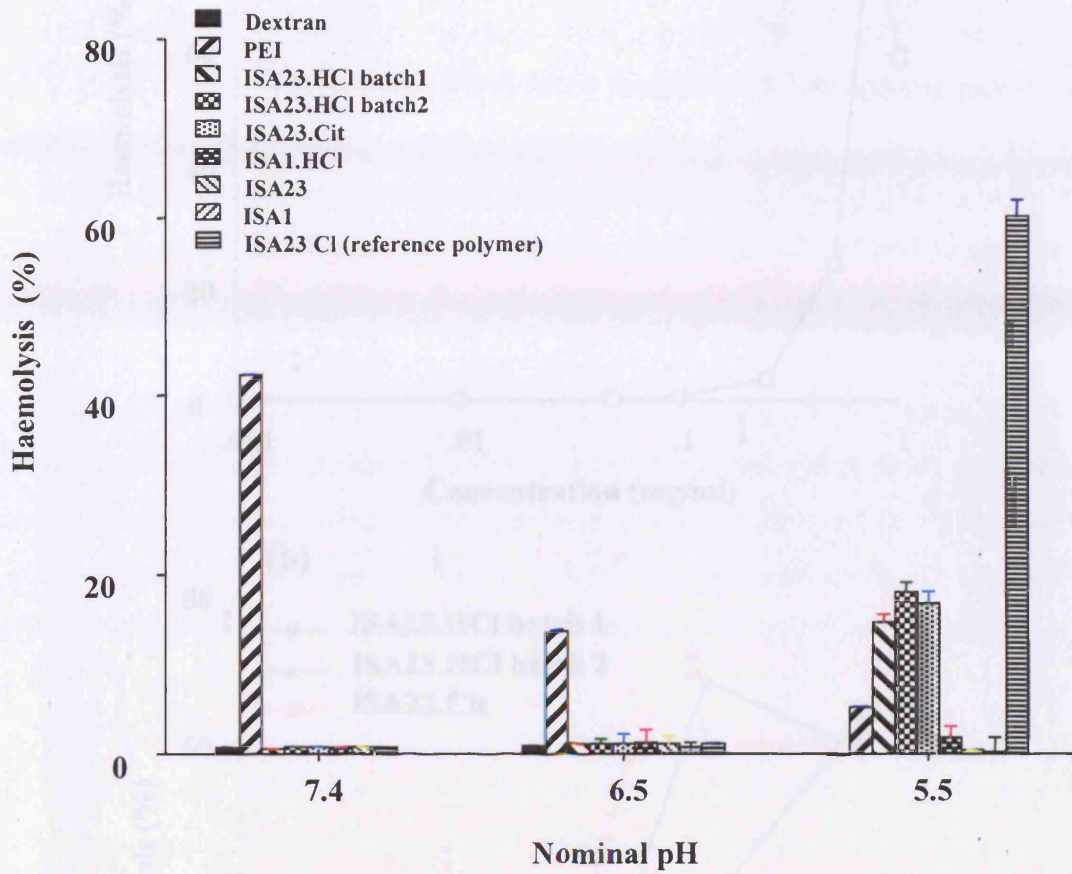


Figure 3.10 The haemoglobin release (1h) by PAA polymers (1 mg/ml) at different pH values. Data represent mean \pm standard error (n = 3)

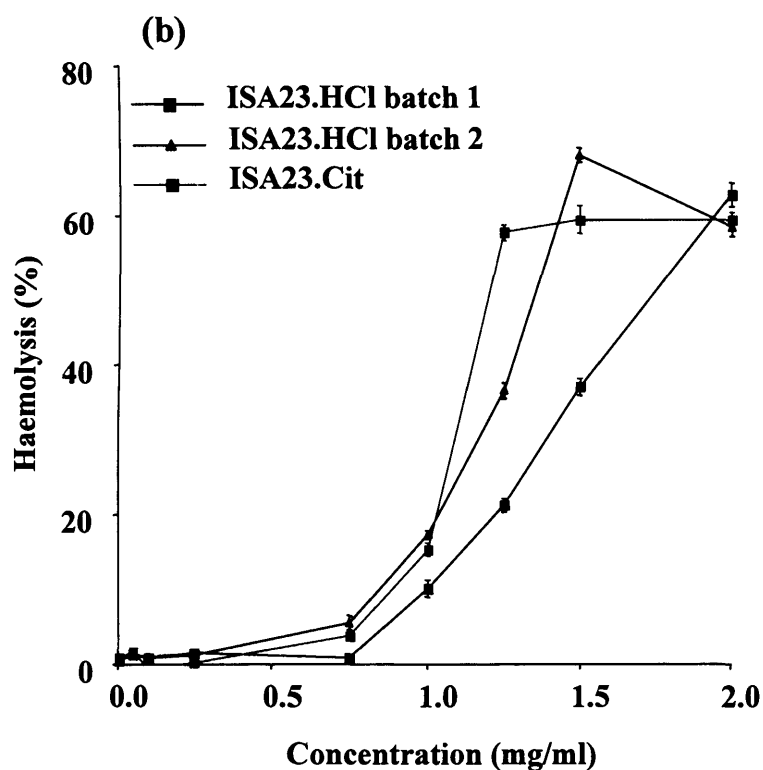
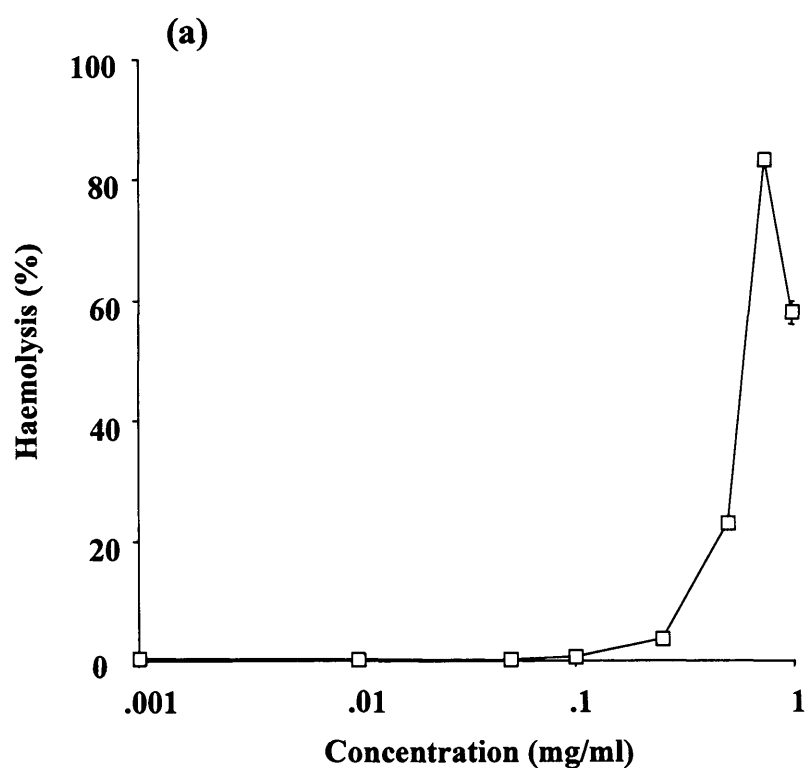


Figure 3.11 Concentration dependent haemolysis of ISA23. Panel (a), ISA23Cl (reference batch) at pH 5.5 (1 h incubation, n = 3), panel (b), concentration dependent haemoglobin release by PAA polymers at pH 5.5 (n = 3), ISA23.HCl batch 1 and 2, and ISA23.citrate, following 1 h incubation

Although PEG, pullulan and PVP standards were used here, differences in their solution properties (coil dimension) can introduce error when calculating the M_w and M_w/M_n .

Historically, PVP had been used in Milan as a standard to obtain the molecular characteristics of PAAs (reviewed in Franchini and Ferruti, 2004). In these experiments, PS and PEG standards were also used. PS calibration produced M_w and M_n values that were in the same range as the PVP standards (ISA23 50,000-75,000 g/mol; ISA1 5,000-23,000 g/mol). In contrast, the PEG standards gave much lower apparent molecular weight values for the PAAs. As mentioned before, this is due to the large hydrodynamic radius of PEG (Magazù, 2000; Rangelov and Brown, 2000). PEG is known to have a highly extended, flexible and hydrated polymer chain, and this gives the polymer a much higher radius in solution than would normally be seen for a random-coil polymer chain.

The PAAs synthesised here displayed a relatively high polydispersity (1.6-1.7, calculated using pullulan standard and 2-3.3, calculated using PVP standards). Ultrafiltration using a 10,000 or 5,000 g/mol membrane cut-off led to a reduction of polydispersity, but it was still in the range 1.3-1.5 (calculated using PS standards). Further fractionation or solvent precipitation could be used to decrease polydispersity, but this was not undertaken here.

For parental administration it is important to use either a biodegradable polymer or a polymer weight that allows renal elimination (reviewed in Duncan, 2005). Although it has been shown before that PAAs are “biodegradable polymers” (Ferruti et al, 1994), it is clear from the degradation experiments undertaken here that ISA23 did not degrade over the period examined. Changing the incubation pH, the counterion or increasing temperature to 37 °C (results not shown) did not accelerate degradation. These results are not consistent with previous studies. Ranucci et al (1991) have shown using viscosity measurements and GPC analysis that PAAs do degrade. It was also reported that pH had an effect on the extent and rate of degradation (Ranucci et al, 1991). There is one important difference between the PAAs synthesised here and those tested previously that might be responsible for this, the molecular weight. Ranucci et al (1991) tested PAAs of low M_w , i.e. in the range of 16,500 to 28,000 g/mol (Ranucci et al, 1991). This can be compared to the PAA M_w of 50,000 to 70,000 g/mol tested here. It is possible that the higher molecular weight might cause a change in polymer conformation, leading to intramolecular coil-coil interactions or differences in

hydration, that might have an impact on the PAA degradation behaviour. It is important to add, that the degradation experiments were conducted in the absence of enzymes that would also be present in the body. It would be interesting to repeat these experiments in different physiological solution (e.g. plasma), in the presence of enzymes and for longer times to see if this would affect the rate of degradation of ISA23.

The batches of ISA23 synthesised here displayed pH-dependant haemolytic properties consistent with the results described previously (Ferruti et al, 2000; Wan et al, 2004). However, there were some key differences. For example, the degree of haemolysis produced by ISA23.HCl batch 1 and 2 (1 mg/ml), at pH 5.5 was lower than reported previously (Wan et al, 2004) (Figure 3.10). This could be simply due the higher molecular weight of the polymer. Previous studies have shown that molecular weight of cationic polymers in general can play a key role in determining the haemolytic activity (Ferruti et al, 2000). However, in the case of PLL and PEI increasing molecular weight causes an increase in haemolysis (Hill et al, 1999). The amphoteric nature of PAAs might complicate things. In this case increasing molecular weight might cause the amphoteric polymer to aggregate, thus leading to a decrease in the number of positively charged amino groups available to interact with the negatively charged head groups of the RBC membrane. This would limit membrane interaction and limiting breakage.

In the context of these haemolysis experiments, it is important to note that the initial pH of the solutions used, and the final pH (following the addition of PAAs) is not the same. For example, in the experiments conducted at a starting pH 7.4, 6.5 and 5.5, the actual pH of the polymer solution decreased to ~ pH 6.5, 5 and 3.5 respectively. Even when a buffer of higher buffering capacity was used, it improved buffering towards PAA (1 mg/ml) at pH 7.4 and 6.5 but not at pH 5.5. This could be expected, as a PBS buffer has pKa values of 12.4, 7.2 and 2.1, and it is known that a buffer will work best at, or close to its pKa value (pKa 7.2). Although other buffers could have been explored, these experiments were designed to mimic the physiological situation where physiological buffering would be limited

When the degree of haemolysis was plotted against the final pH, it was clear that no significant haemolysis is produced until the final pH is below 4 (Figure 3.12). At lower pH haemolysis increased sharply. There is a direct correlation between, PAA protonation and haemolytic activity.

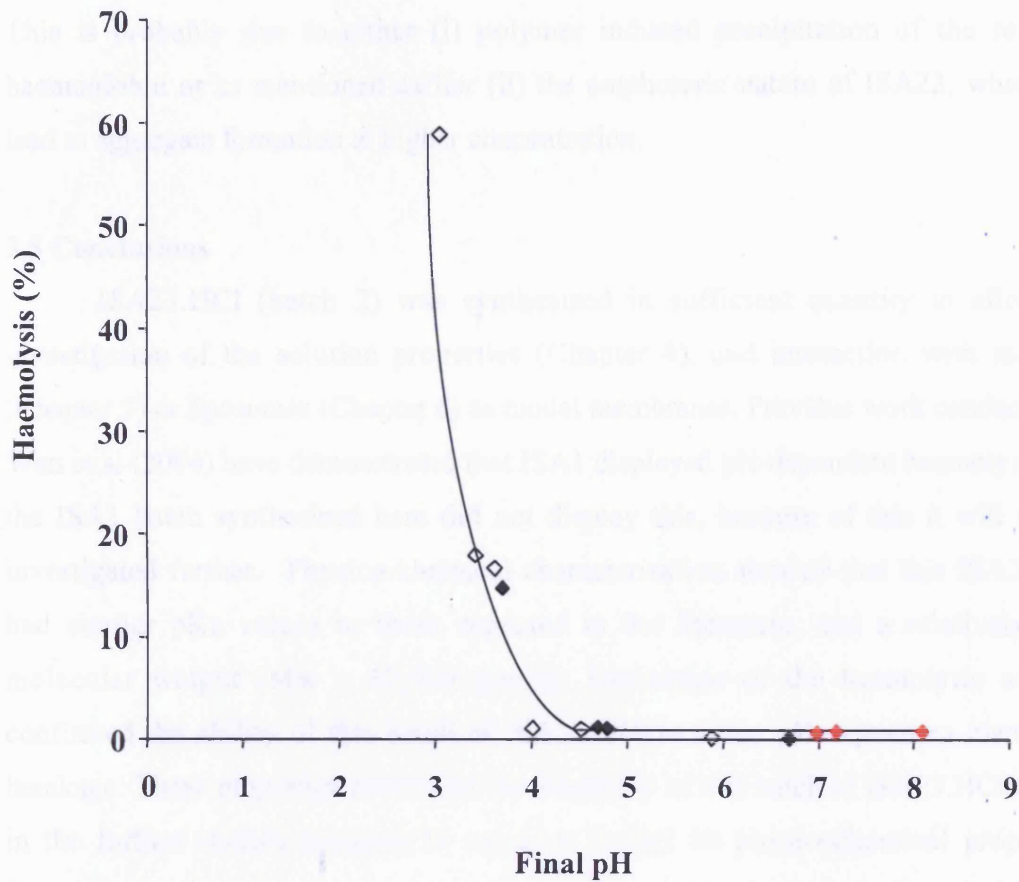


Figure 3.12 The relationship between PAA induced haemolysis and solution pH. Data show ISA23 (red diamonds), ISA23.HCl (empty black diamonds) and ISA23.citrate (solid black diamonds)

Increasing the polymer concentration caused an increase in haemolysis (Figure 3.11a,b). Although the haemolysis seemed to decrease after a certain concentration. This is probably due to either (i) polymer induced precipitation of the released haemoglobin or as mentioned earlier (ii) the amphoteric nature of ISA23, which can lead to aggregate formation at higher concentration.

3.5 Conclusions

ISA23.HCl (batch 2) was synthesised in sufficient quantity to allow the investigation of the solution properties (Chapter 4), and interaction with micelles (Chapter 5) or liposomes (Chapter 6) as model membranes. Previous work conducted by Wan et al (2004) have demonstrated that ISA1 displayed pH-dependent haemolysis, but the ISA1 batch synthesised here did not display this, because of this it will not be investigated further. Physico-chemical characterisation showed that this ISA23.HCl had similar pKa values to those repeated in the literature, and a relatively high molecular weight ($M_w \sim 62,000$ g/mol). Evaluation of the haemolytic activity confirmed the ability of this batch of ISA23.HCl to cause pH-dependent membrane breakage. These properties confirmed the suitability of this batch of ISA23.HCl for use in the further studies designed to examine further its physicochemical properties. Interestingly, the PAAs synthesised here did not undergo hydrolytic degradation over time (up to 2 weeks). This was not consistent with the literature. If the ISA23.HCl synthesised here was to be used *in vivo*, further studies would be required (over longer time and in the presence and absence of enzymes) to confirm that the polymer would eventually degrade.

Chapter 4
The investigation of the solution behavior of
ISA23.HCl using SANS

4.1 Introduction

Having synthesised the PAA, ISA23.HCl and shown that it displayed biological properties consistent with previous studies using this PAA (Ferruti et al, 2000; Richardson et al, 1999; Wan et al, 2004), the aim of this study was to investigate the conformation of ISA23.HCl in solution. In addition, the aim was to study how conformation would change according to polymer concentration and molecular weight at pHs (7.4 and 5.5) that the endosomolytic polymer would be exposed to at the cellular level.

Few studies have investigated the physico-chemical properties of ISA23 (see Chapter 1; section 1.5.3), although (potentiometric and calorimetric) ^{13}C -NMR have been used to study the protonation of several other PAAs (Barbucci et al, 1980). Also techniques such as GPC (Ferruti et al, 2000), light scattering (Ferruti et al, 2000) and viscosity measurements have been used to investigate the solution properties of specific PAAs (Barbucci et al, 1981b).

As mentioned earlier in Chapter 1, previous studies have shown that ISA23 can deliver genes (Richardson et al, 2001), and ISA1 can deliver non-permeant toxins such as ricin A chain and gelonin (Patrick et al, 2001) into the cytosol. However, Patrick et al (2001) found that the ability of the PAA ISA1 to deliver toxin molecules was poorly efficient. Many polymer molecules were required to deliver a single toxin molecule. Unless the efficiency can be improved, application of these PAAs as endosomolytic polymers for *in vivo* delivery is unlikely to succeed. To improve PAA design, it is crucial to better understand their precise mechanism of membrane destabilisation. Here SANS was used to investigate ISA23.HCl conformation in solution. The theoretical basis of SANS is introduced briefly below.

4.1.1 SANS

Two main techniques are used to produce neutrons for SANS, a nuclear reactor or a spallation neutron source. In the case of the nuclear reactor (Figure 4.1a), neutrons are released by fission of uranium-235, each fission event releases 2-3 neutrons (King, 2000) with the release of ~ 180 MeV of energy per fission (Dianoux, and Lander, 2002). The most powerful reactor in the world is the 57 MW High-Flux Reactor at Institute Max von Laue-Paul Langevine (ILL) in Grenoble, France (Ibel, 1994) (Figure 4.1b). Spallation neutron sources produce neutrons by the process of 'spallation'. This is a

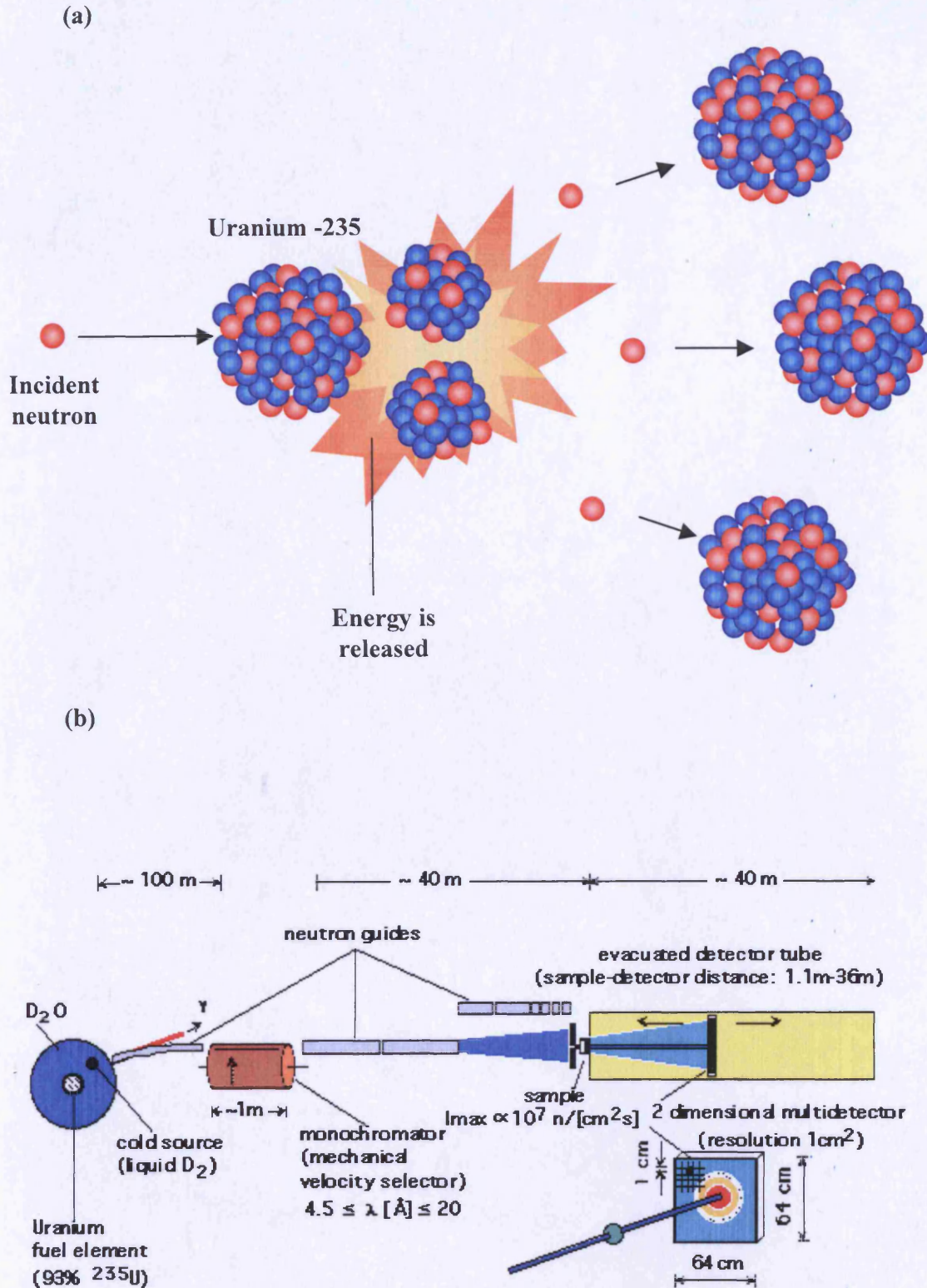


Figure 4.1 Schematic diagram of SANS instrumentation and neutron production at ILL. Panel (a) production of neutrons by fission process, panel (b) diagram of the D11 instrument (taken from <http://www.ill.fr/YellowBook/D11/>)

common reaction that occurs when high energy particles bombard heavy atoms (Dianoux, and Lander, 2002) (Figure 4.2a) and this generates an intense, high energy, proton beam (King, 2000). The most powerful spallation neutron source is ISIS, located near Oxford, in the UK (Boland and Whapham, 1992) (Figure 4.2b).

SANS has been used in many scientific disciplines (Shibayama et al, 1998) (Figure 4.3). It provides unique information on the structure and function of biological and synthetic macromolecules. In the context of this work, SANS has been widely used to study polyelectrolyte behaviour (Nishida et al, 2002; Nakamura et al, 2005), polymer-surfactant interactions (Aswal, 2003; Bergström et al, 2004), and dendrimer conformation (Ramzi et al, 2002; Hedden and Bauer, 2003). However, although these studies were mainly conducted in aqueous solution (D_2O), physiologically relevant salt concentrations and temperatures were not used.

During SANS the neutron beam is elastically scattered by the nucleus of any atoms in its path. Isotopes of the same element are scattered differently. The scattering of the neutron by single nucleus can be described in terms of the cross section of the nucleus (the apparent area that the nucleus presents to the neutron) (Griffiths and King, 2002). The strength of the nucleus-neutron interaction is characterised by the scattering length, which is independent of atomic number and varies randomly throughout the periodic table.

The scattering length densities differ for each particle of interest, and the solvent. This is described as the contrast $[(\rho_{\text{scatterer}} - \rho_{\text{solvent}})^2]$. It plays a key role in the determination of scattered radiation intensities, and the scattering length densities for any compounds. These parameters can be calculated as the following:

$$\rho = \sum_i b_i \frac{\rho_{\text{bulk}} N_A}{M} = N \cdot \sum_0 b_i \quad 4.1$$

where b_i is the coherent neutron scattering length of the nucleus (the coherent scattering lengths of some nuclei are shown in Table 4.1),

ρ_{bulk} is the bulk density of the scatterer,

N_A is Avogadro's number,

M is the molecular weight.

The difference between the coherent scattering length of hydrogen and deuterium is great (opposite side of the scale), so deuteration of molecules or solvent can be used in a system to allow the study of a specific part of the macromolecule or a single molecule

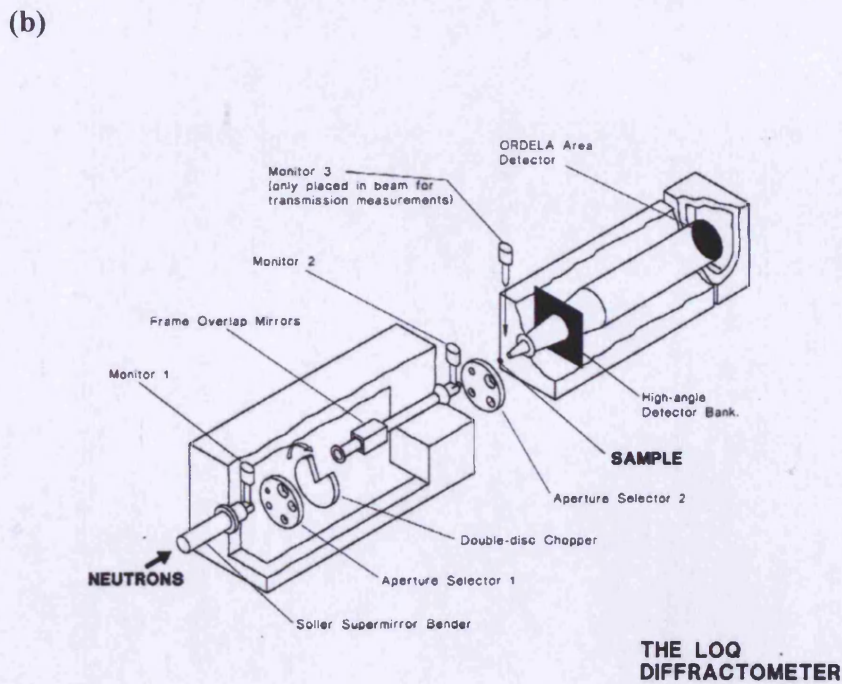
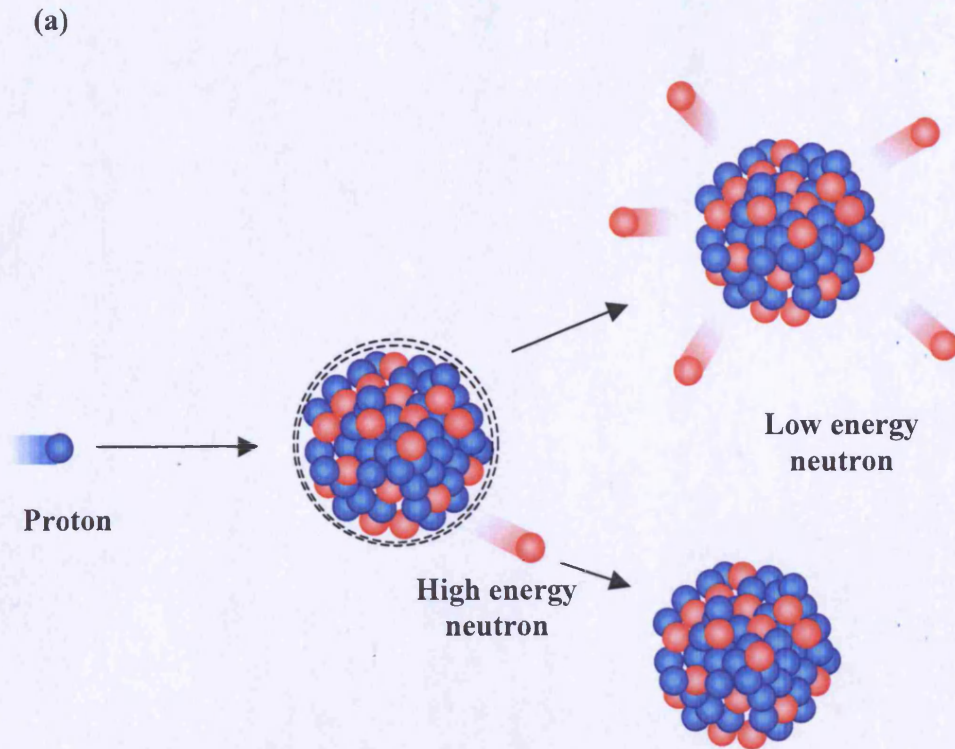


Figure 4.2 Schematic diagram of SANS instrumentation and the neutron production at ISIS. Panel (a) neutron production by spallation method, panel (b) diagram of the LOQ diffractometer (taken from <http://www.isis.rl.ac.uk/largescale/loq/loq.htm>)

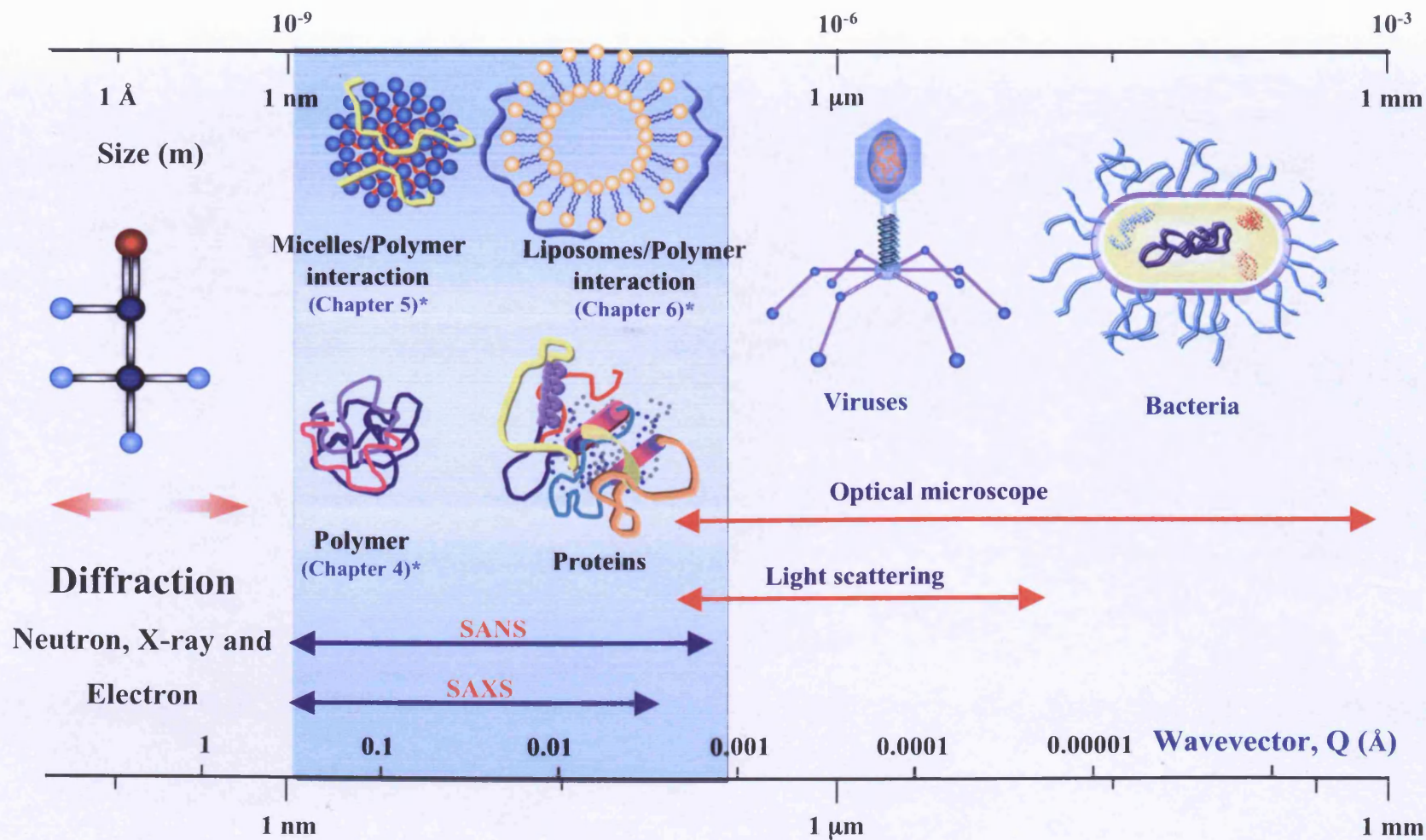


Figure 4.3 Schematic diagram summarising application of different scattering methods, according to their size.

* Indicates studies in this thesis

Table 4.1 The coherent scattering lengths of some common nuclei.

Nucleus	Coherent scattering lengths, $b / 10^{-15} \text{ M}$
^1H	-3.74×10^{-15}
^2D	6.67×10^{-15}
C	6.65×10^{-15}
N	9.37×10^{-15}
O	5.80×10^{-15}
Cl	9.58×10^{-15}
Na	3.63×10^{-17}
P	5.13×10^{-17}
S	2.80×10^{-17}
Cu	7.72×10^{-17}
La	8.27×10^{-17}
K	3.71×10^{-17}

* Adapted from Koester et al, 1991 and Sears, 1992

in a multi-components system (see examples in Figure 4.4).

Neutron scattering data are usually recorded in terms of wavevector (Q), (or scattering vector) which is the modulus of the resultant between incident (k_i) and scattered (k_f) wavevectors (Griffiths et al, 2002) (Figure 4.5), and $k_i = k_f$ for elastic scattering and $k_i = k_f = 2\pi n/\lambda$, where n is the refractive index of the medium. For the neutron the refractive index is 1. Q has a dimension of $(\text{length})^{-1}$; normally quoted in nm^{-1} or \AA^{-1} (King, 2000), and Q can be given by:

$$Q = |Q| = |k_f - k_i| = 4\pi n / \lambda \sin(\theta / 2) \quad 4.2$$

Where q is the scattering angle and λ is the neutron wavelength (Figure 4.6).

The substitution of equation (4.2) to Bragg's law of diffraction (equation (4.3)) produces a useful expression (equation 4.4), where d is a distance,

$$l = 2d \sin(\theta) \quad 4.3$$

$$d = 2\pi / Q \quad 4.4$$

Equation 4.3 highlights the simple relationship between the characteristic dimensions associated with d and Q (Griffiths and King, 2002). Both equation 4.2 and 4.4 are used to configure an instrument, to select a Q -range, and to size the scattering bodies in a sample from the position of any diffraction peak in Q -space (King, 2000). The distance (d) is inversely proportional to q , thus small q values are required to investigate the large-scale structure in a sample.

The number of neutrons that are incident on an area of detector can be measured, and this flux of neutrons can be described as:

$$I(\lambda, \theta) = I_0(\lambda) \Delta\Omega \eta(\lambda) T V \frac{\partial\sigma}{\partial\Omega}(Q) \quad 4.5$$

where $I(\lambda, \theta)$ is the flux,

$I_0(\lambda, \theta)$ is the incident flux,

$\Delta\Omega$ solid angle element that the neutrons are scattered onto,

η the detector efficiency, T is the sample transmission,

V is the sample volume and $\partial\sigma/\partial\Omega(Q)$ is the differential cross section and this is given

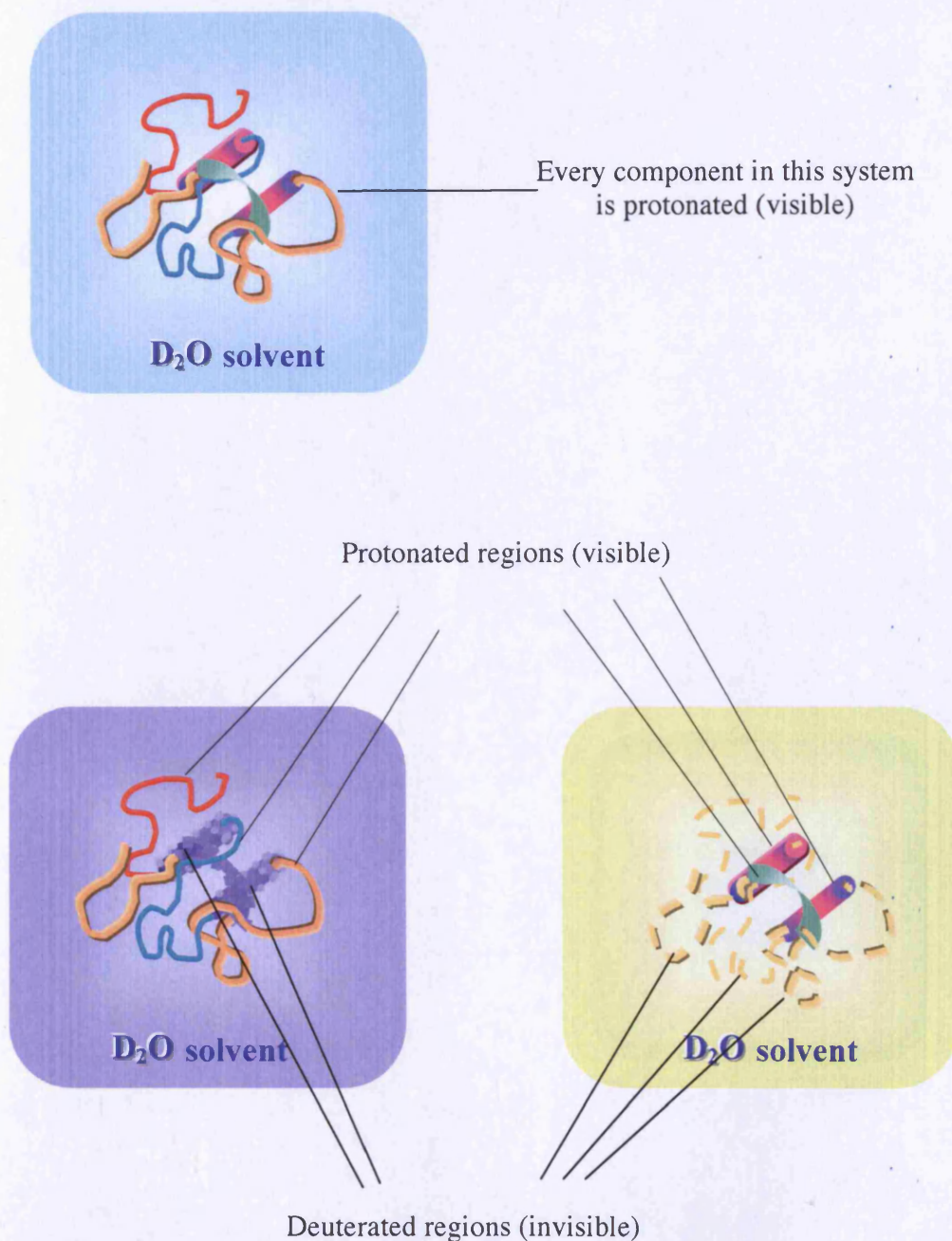
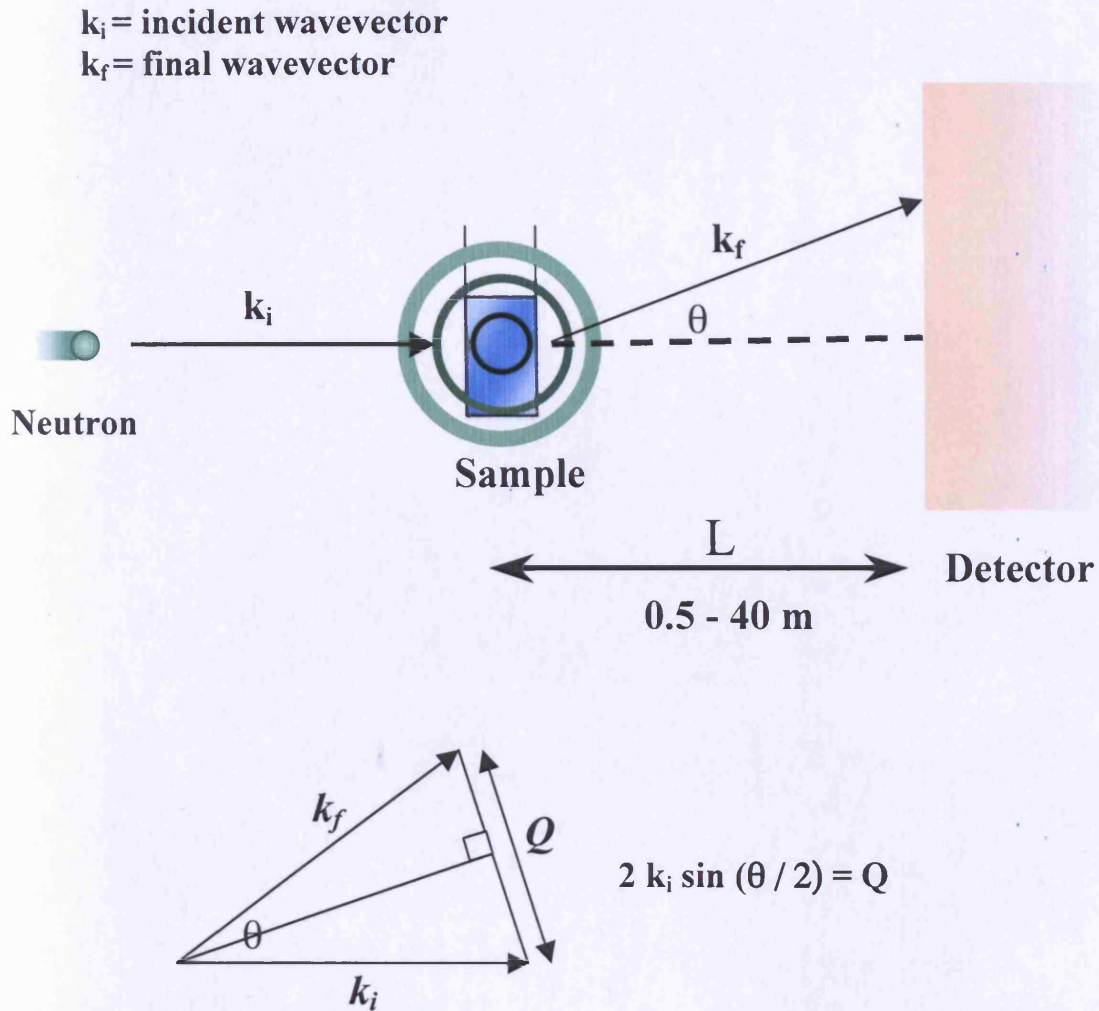


Figure 4.4 Schematic diagram showing the mechanism for studying a multicomponent system by varying the contrast. This is achieved by deuteration of the components that will not be studied (they turn invisible), and the regions of interest are protonated



Substitute k_i with $2\pi / \lambda$ to give $4\pi / \lambda \sin(\theta / 2) = Q$

Figure 4.5 The theory behind, and the mathematical derivation of the scattering wavevector (Q).

by:

$$\frac{\partial \sigma}{\partial \Omega}(Q) = N_p V_p^2 (\Delta \rho)^2 P(Q) S(Q) + B_{inc} \quad 4.6$$

where N_p is the number of scattering bodies,

V_p is the volume of scattering body,

$(\Delta \rho)^2$ is the contrast term (is the square of the difference in the neutron scattering length density), $P(Q)$ is the form factor,

$S(Q)$ is the structure factor and B_{inc} is the incoherent background

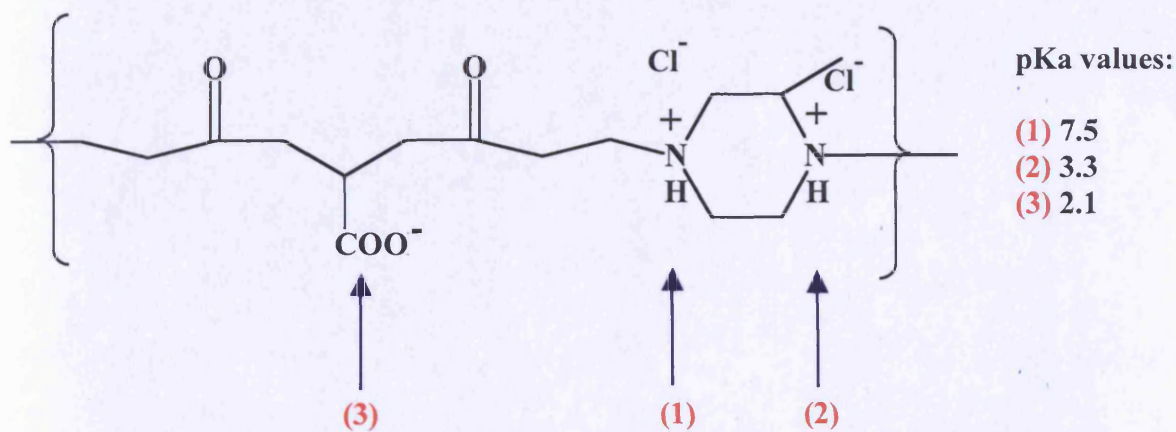
The form factor is used to describe how the scattering is modulated by interference effects arising from different parts of the same scattering body. Thus it depends on the shape of the scattering body (King, 2000).

First it was necessary to determine the most appropriate mathematical model to fit the SANS data derived from ISA23.HCl (batch 2) which was used for the studies and in subsequent chapters this polymer will only be known as ISA23.HCl. Rod, sphere, polyelectrolyte and Gaussian coil models were explored (Figure 4.6). The impact of data interpretation using each model on the calculated polymer coil radius was determined. As ISA23.HCl induces a pH-dependant haemolysis (Chapter 3), the effect of pH on the size of the polymer coil was also examined using SANS. It was also demonstrated in Chapter 3 that polymer concentration and molecular weight might also play an important role in the chemical, physical and biological behaviours of ISA23.HCl, so the effect of these parameters on the polymer conformation was also investigated using SANS.

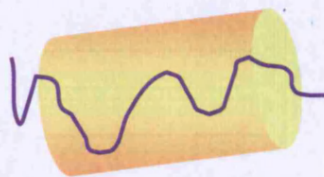
4.2 Methods

4.2.1 Sample preparation

ISA23.HCl ($M_w = 62,000$ g/mol, $M_n = 32,000$ g/mol) was synthesised and characterised as previously described (see Chapter 3). The ISA23.HCl samples used for SANS experiments were generally prepared by dissolving a known mass of polymer in PBS (D_2O , pH 7.4). Following the addition of ISA23.HCl, the pH dropped and it was subsequently adjusted to different pH values ranging from pH 2 to 13 by adding concentrated NaOH (5 M) or HCl (5 M). In certain experiments, scattering of the polymer solution at different concentrations (10, 25 and 50 mg/ml), at pH 7.4 and 5.5



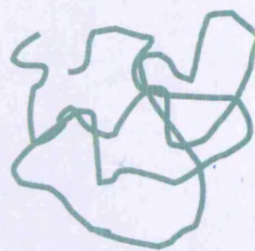
(a)



(b)



(c)



(d)

Figure 4.6 The theoretical shapes that ISA23.HCl might adopt. Panel (a) sphere, panel (b) Rod, panel (c) polyelectrolytes and panel (d) Gaussian coil

were measured.

To examine the effect of temperature, scattering of ISA23.HCl (50 mg/ml, at pH 7.4 and 5.5) was measured at 25 or 37 °C. To study the effect of molecular weight, SANS of an ISA23.HCl sample with lower molecular weight ($M_w = 21,000$ g/mol) was also measured at pH 5.5, for comparison.

4.2.2 SANS measurements of ISA23.HCl in solution

The SANS experiments were conducted using both the LOQ diffractometer at the ISIS Spallation Neutron Source (Oxfordshire), and the D11 and D22 diffractometers at the ILL (Grenoble). LOQ is a fixed-geometry, time-of-flight (TOF), instrument whereas the ILL (D11 and D22) is a steady-state reactor source. Neutron wavelengths between 2 and 10 Å (LOQ) and 8 Å (D11) or 6 Å (D22) were employed to span Q-ranges (see below) of approximately 0.001 to 0.6 Å⁻¹.

In all cases the samples were placed in 2 mm pathlength, UV-spectrophotometer grade, quartz cuvettes (Hellma, Ltd., UK), and mounted in aluminium holders on top of an enclosed, computer-controlled, sample changer. Sample volume was approximately 0.4 ml. Temperature control was achieved through the use of a thermostated circulating water bath pumping fluid through the base of the sample changer. Under these conditions, a temperature stability of ± 0.5 °C can be achieved. Experimental measuring times were approximately 40 min. Dependent on which instrument was used, all scattering data were :

- (a) normalised for the sample transmission and incident wavelength distribution
- (b) background corrected using a solvent filled quartz cell (this also removes the inherent instrumental background arising from vacuum windows, etc.)
- (c) corrected for the linearity and efficiency of the detector response using the instrument-specific software package

The data obtained were put onto an absolute scale by reference to the scattering from a well-characterised partially deuterated polystyrene-blend standard (LOQ) or 1 mm thick sample of water (D11, D22).

As it was mentioned earlier $P(Q)$ gives information about the size and shape of the polymer in solution. Given the knowledge of the chemical composition of the polymer and its concentration, some of the factors may be estimated. A fitting approach was therefore used to calculate the theoretical scattering from a model in terms of the

parameters describing the size and shape of the polymer. “Best fit” values of these parameters were then determined *via* a non-linear least squares iterative process.

The following formulae were explored as a possible fit for the raw data:-

(i) A spherical scatterer

$$P(Q) = \left[\frac{3(\sin(QR) - QR \cos(QR))}{(QR)^3} \right]^2 \quad 4.7$$

(ii) A rod shaped scatterer, where the object has negligible cross-section is given by:

$$P(Q) = \left[\frac{2S_i(QL)}{QL} - \frac{\sin^2\left(\frac{QL}{2}\right)}{\frac{QL}{2}} \right] \quad 4.8$$

where S_i is the sine integral function and L is the length of the rod.

(iii) A polyelectrolyte model, obtained by incorporating a finite cross-section to the rod:

$$P(Q) = \frac{1}{QL} \exp\left(\frac{-Q^2 R_g^2}{2}\right) \left(\frac{Q^2 x^2}{1 + Q^2 x^2}\right) \quad 4.9$$

(iv) A Gaussian coil model (derived by Debye, 1947), modified to include polydispersity;

$$P(Q) = \frac{2 \left[\left(1 + \frac{u}{v}\right)^{\left(\frac{-1}{v}\right)} + u + 1 \right]}{(1+v)u^2} \quad 4.10$$

where v is a measure of the polydispersity, $(M_w/M_n)-1$ and $u = \frac{Q^2 R_g^2}{(1+2v)}$ where R_g is the polymer radius of gyration.

4.3 Results

4.3.1 Data fitting of neutron scattering data using rod, sphere and Gaussian coil models

Figure 4.7, panel (a) shows neutron scattering data of ISA23.HCl (50 mg/ml), at

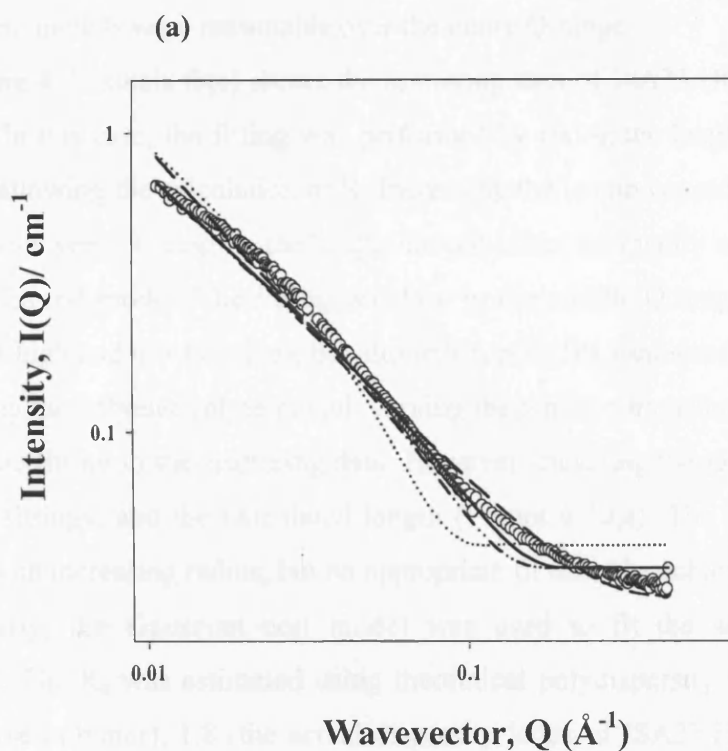


Figure 4.7 SANS data obtained for ISA23.HCl (50 mg/ml) in D_2O (pH 3.15) at 37°C . Panel (a) The lines represent the calculated behaviour for the solid sphere models (eqn 4.7) where $R = 10 \text{ \AA}$ (long dashed line) or $R = 25 \text{ \AA}$ (dash dot line) and $R = 40 \text{ \AA}$ (dotted line). The solid line represents the ‘best fit’ using this model

pH 3.15, analysed in terms of the spherical solid scatterer model. In this case, the principle fitting parameter is the radius, so three representative radii were examined (10 Å, 25 Å and 40 Å). A fit to the data without constraining the radius was also examined. None of these models were reasonable over the entire Q range.

Figure 4.7, panels (b,c) shows the scattering data of ISA23.HCl fitted using the rod model. In this case, the fitting was performed by fixing the length (L) to different values and allowing the calculation of R. Increasing the length caused a decrease in the radius and vice versa. Changing the length did not affect the quality of the fitting to the data using the rod model. The fitting was best in the middle Q range, but the quality decreased at high and low Q values, but altogether, poor fits were produced.

Using the polyelectrolyte model, varying the length parameter did not affect the quality of the fitting to the scattering data. However, changing the radius, significantly altered the fittings, and the calculated length (Figure 4.7d,e). The quality of the fits decreased with increasing radius, but no appropriate fit could be achieved.

Finally, the Gaussian coil model was used to fit the scattering data of ISA23.HCl. The R_g was estimated using theoretical polydispersity values of 1 (for a monodisperse polymer), 1.8 (the actual dispersity index of ISA23.HCl obtained from the GPC) and 3. The latter was chosen, it is arbitrarily value, which is greater than the true dispersity of ISA23.HCl. This value was used for comparison, and to examine the effect of the polydispersity on the quality of fittings and R_g . Overall this model produced a very good fit to the data in the whole Q range (Figure 4.7, panel (f)). Fixing the polydispersity to 1.8 (the true value) and 3 produced a better fitting compared to the fit seen when polydispersity was fixed to 1. The calculated radii of gyration were rather insensitive to the polydispersity values assumed, and M_w/M_n values of 1, 1.8 and 3, which gave R_g values of 78, 85 and 88 Å respectively.

4.3.2 The effect of pH on ISA23.HCl conformation

Figure 4.8 shows (a selection of) the data replotted in the form $\frac{I_{polymer}(Q)}{\varphi V (\rho_{polymer} - \rho_{solvent})}$ where φ is the polymer volume fraction and V is the sample volume, to remove the slight concentration and contrast variations within the pH series. Clearly, all the data have a very similar form suggesting that there was no significant change in polymer morphology with pH, simply a change in radius of gyration.

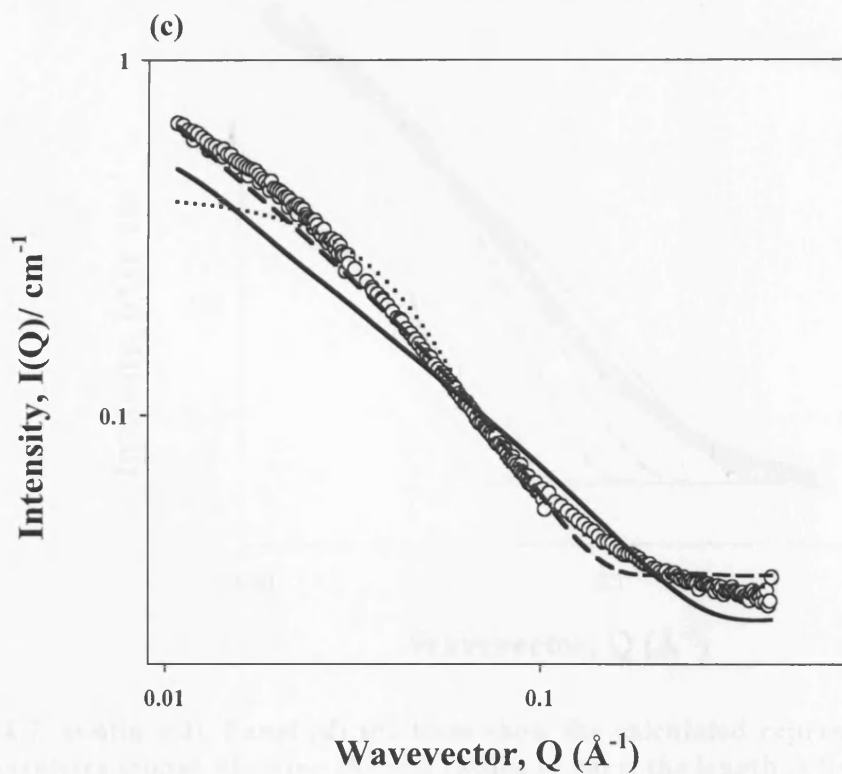
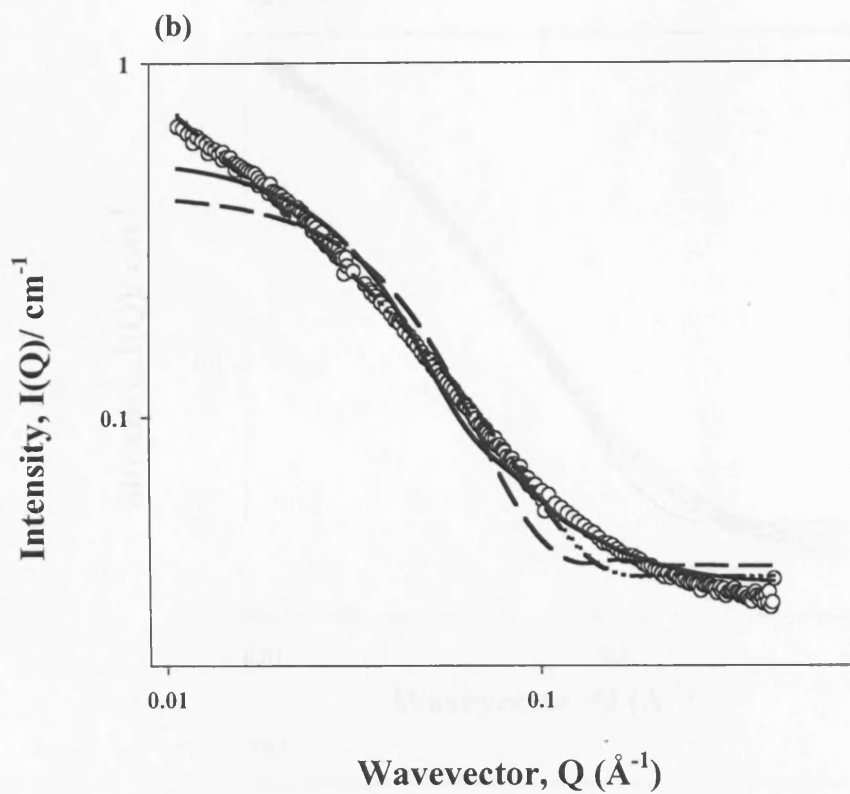


Figure 4.7 (continued). Panel (b) the lines show calculated representation of the rod model, with length fixed at $L = 10 \text{ \AA}$ (solid line), $L = 100 \text{ \AA}$ (dashed line), $L = 500 \text{ \AA}$ (dashed-dotted line), and $L = 1000 \text{ \AA}$ (dotted line). Panel (c) the lines represent calculated representation of the rod model, with radius fixed at $R = 10 \text{ \AA}$ (solid line), $R = 20 \text{ \AA}$ (dashed line) and $R = 50 \text{ \AA}$ (dotted line)



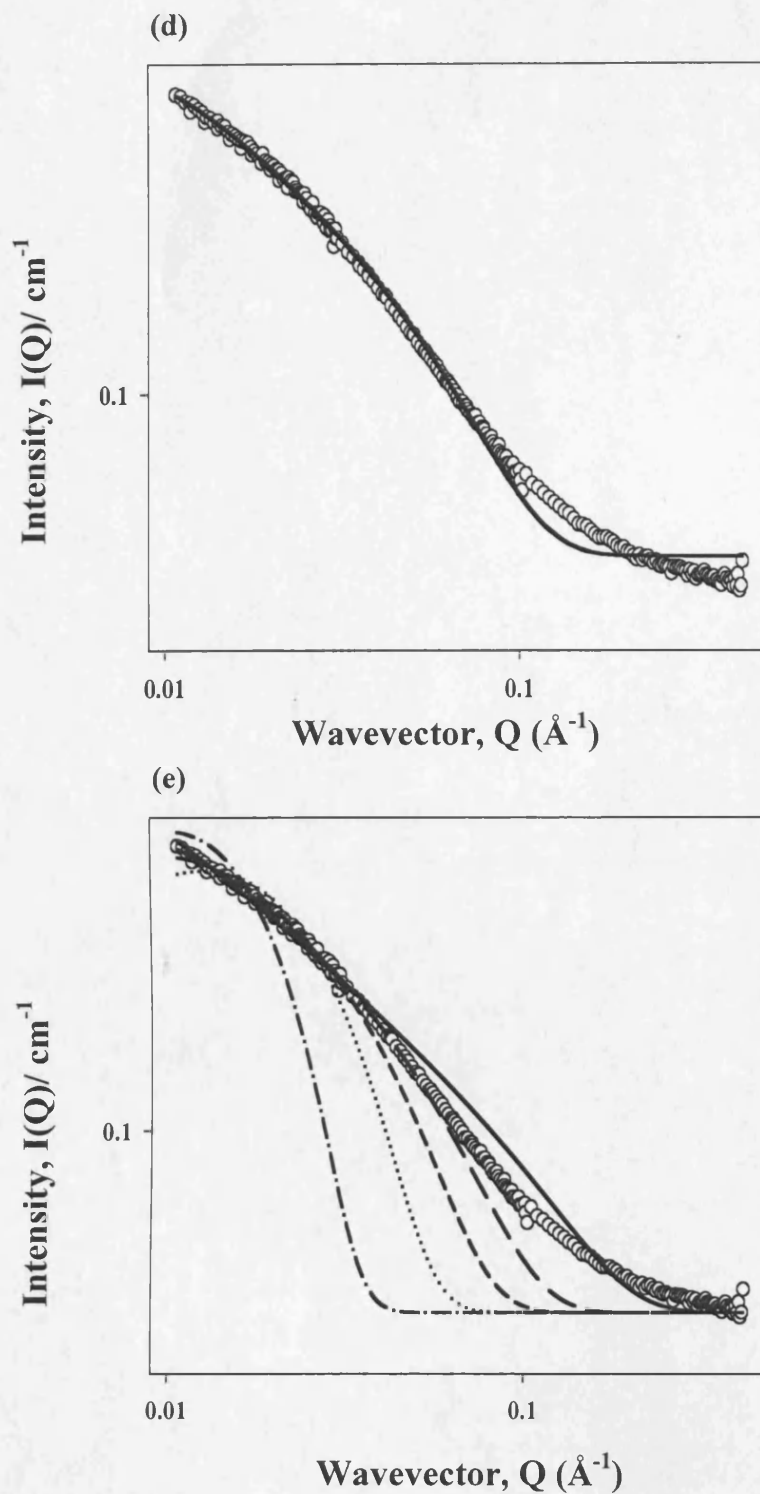


Figure 4.7 (continued). Panel (d) the lines show the calculated representation of the polyelectrolytes model, allowing the rod radius to vary, the length is fixed at $L = 10 \text{ \AA}$ (solid line), $L = 100 \text{ \AA}$ (dashed line) and $L = 500 \text{ \AA}$ (dotted line). Panel (e) the lines represent the calculated representation of the polyelectrolytes model, allowing the rod length to vary, the radius is fixed at $R = 10 \text{ \AA}$ (solid line), $R = 20 \text{ \AA}$ (long dashed line) and $R = 30 \text{ \AA}$ (short dashed line), $R = 50 \text{ \AA}$ (dotted line) and $R = 100 \text{ \AA}$ (dotted line)

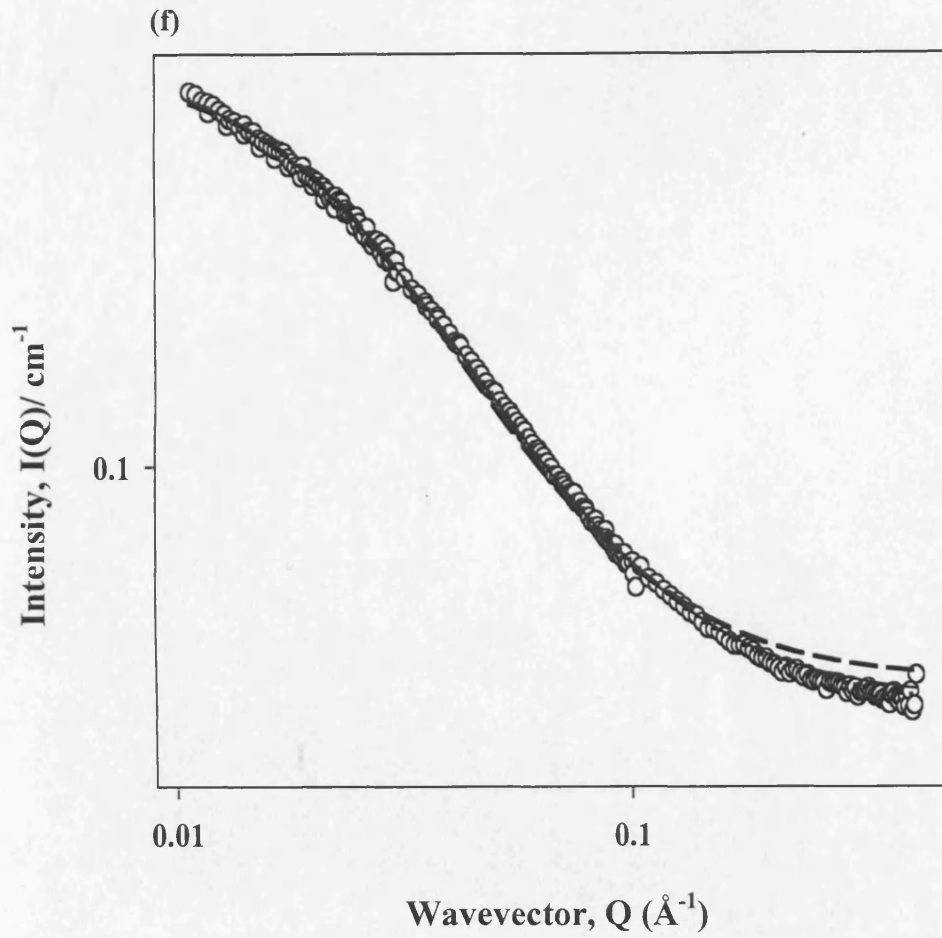


Figure 4.7 (continued). Panel (f) the lines show the representation based on a polydisperse Gaussian coil model constraining the polydispersity, $P = 1$ i.e. monodisperse (long dashed line), $P = 1.8$, the GPC derived estimate (solid line) and $P = 3$ (dotted line)

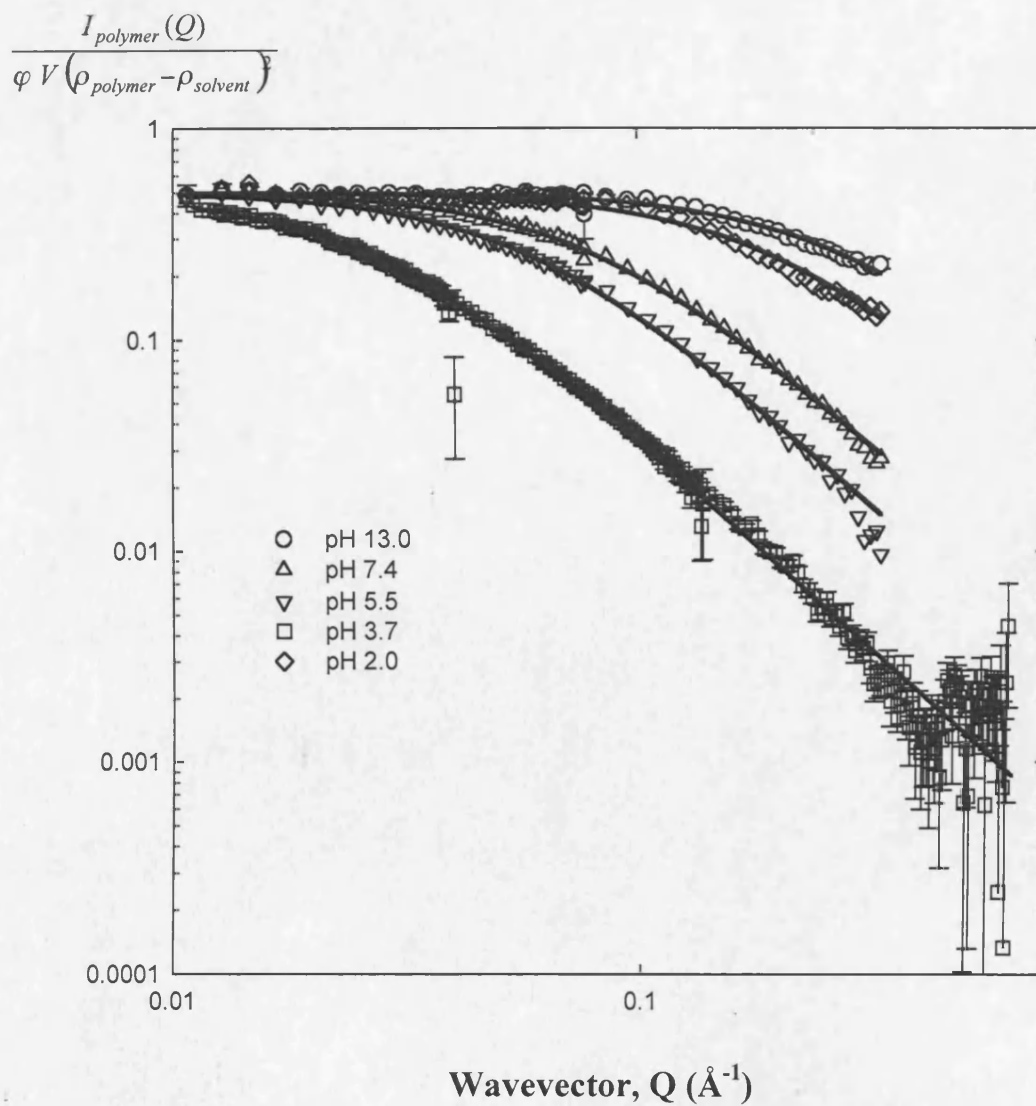


Figure 4.8 The effect of pH on the data form of ISA23.HCl. Normalized SANS data for polymer $I(Q)/[\phi V(\rho_{\text{polymer}} - \rho_{\text{solvent}})^2]$ for 5 wt % ISA23 polymer in D_2O as a function of pH. Diamonds, pH 2.0; squares, pH 3.7; inverted triangles, pH 5.5; triangles, pH 7.4; circles, pH 13.0

Some data extend to higher Q depending on the instrument configuration. A fit has been drawn through each dataset, and the obtained radii of gyration presented as a function of pH in Figure 4.9. On decreasing the pH from pH = 13 the radius of gyration increases. The size attained a maximum value $R_g=80 (\pm 3)$ Å at around pH = 3, roughly an order of magnitude greater than the pH = 13 value. Subsequently, the radius further decreases with decreasing pH (Figure 4.9).

As mentioned before, the pH of the polymer samples was determined by the addition of base. This does not only alter the pH, but also alters the ionic strength. Thus, to study the effect of pH alone, two ISA23.HCl samples were prepared. To the first sample (sample 1), a known amount NaOH was added (just enough to reach pH 12) and to the second sample (sample 2), NaCl solution was added (the amount added was equivalent to the added NaOH in sample 1, the pH of this sample is 3.3). To obtain ISA23.HCl samples at pH 7.4 and 5.5, a known amount of sample 1 and 2 were mixed together. It is clear from Figure 4.10, that the data forms were quite similar at the two pHs. This suggested a change in size and not the shape. Gaussian coil model was again used to fit the data at these pH values. The R_g changed from 22.4 Å (pH 7.4) to 39.1 Å (pH 5.5). These is in agreement with the R_g values mentioned earlier.

4.3.3 The effect of concentration, molecular weight and temperature on the polymer conformation

Figure 4.11 (a,b) shows the raw scattering data obtained for a series of ISA23.HCl samples of different polymer concentration recorded at ISIS. Table 4.2 shows the fitting parameters obtained. The data have been normalised to account for the volume fraction. They are relatively noisy due to the weak contrast $((\rho_p - \rho_m)^2)$. Nonetheless, as may be seen by the shapes of the curves and the fit parameters, it is clear that the shape of curves is not effected by the change of concentration that was examined. The Gaussian coil remained the most appropriate model to fit these data. There may be a small change in size with concentration but such a conclusion is at the resolution limit of these data. This pattern was observed at both pH values, but is more pronounced at pH 5.5 compared to that at pH 7.4. However, the error in this data is significant.

Changing temperature from 25 and 37 °C did not effect the conformation of ISA23.HCl, at pH 7.4 or pH 5.5 (Figure 4.12, Table 4.3).

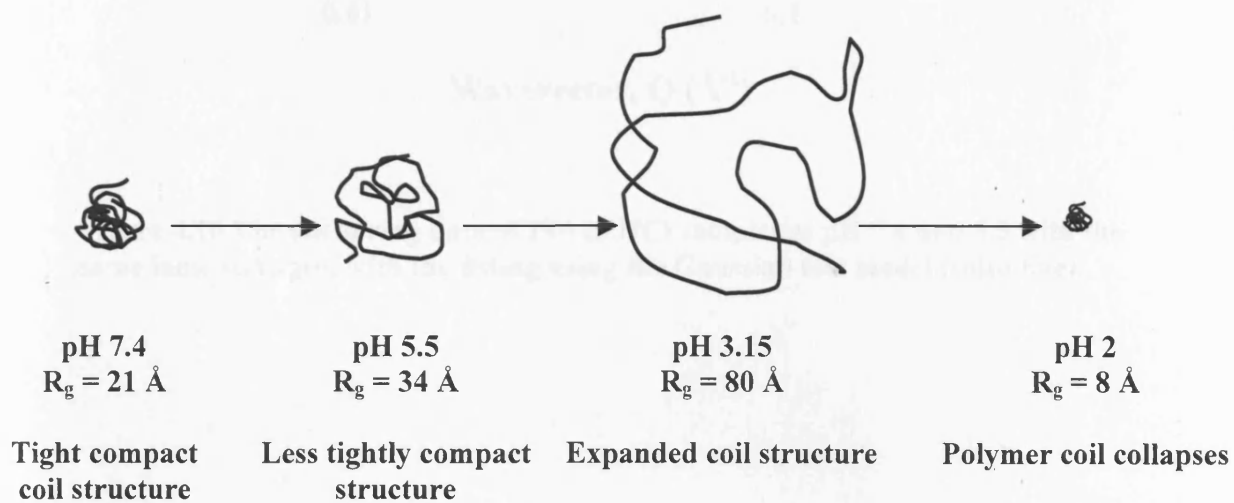
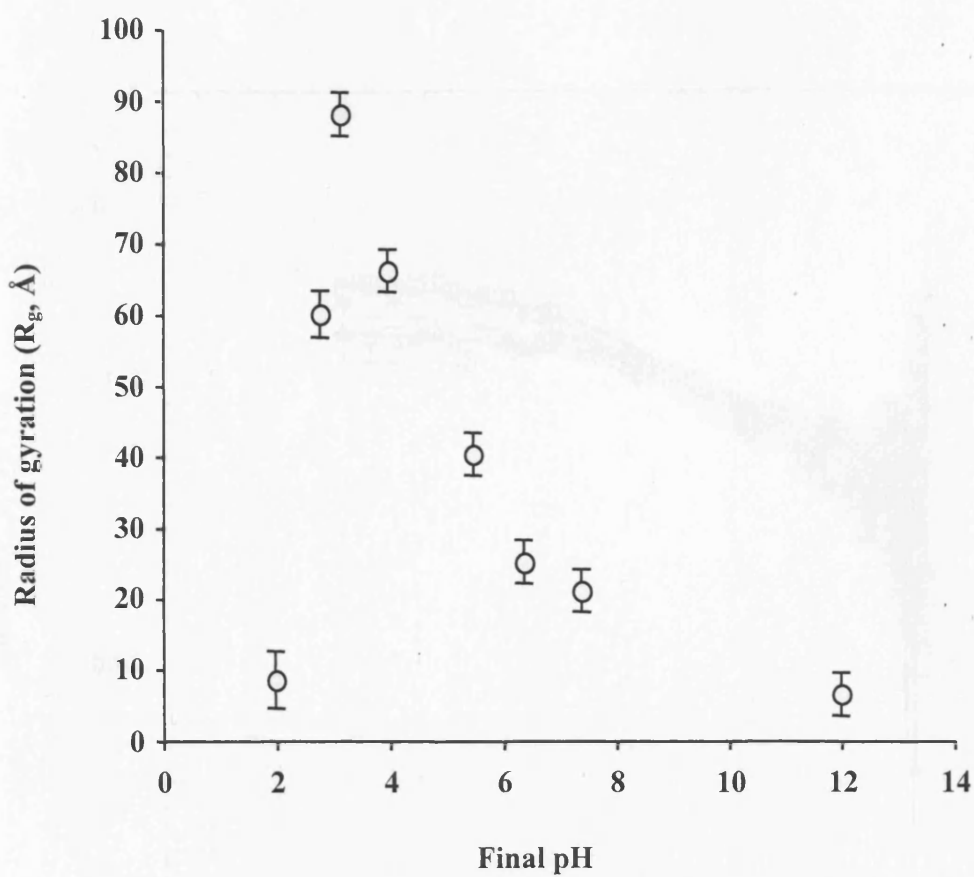


Figure 4.9 The effect of pH on PAA conformation.

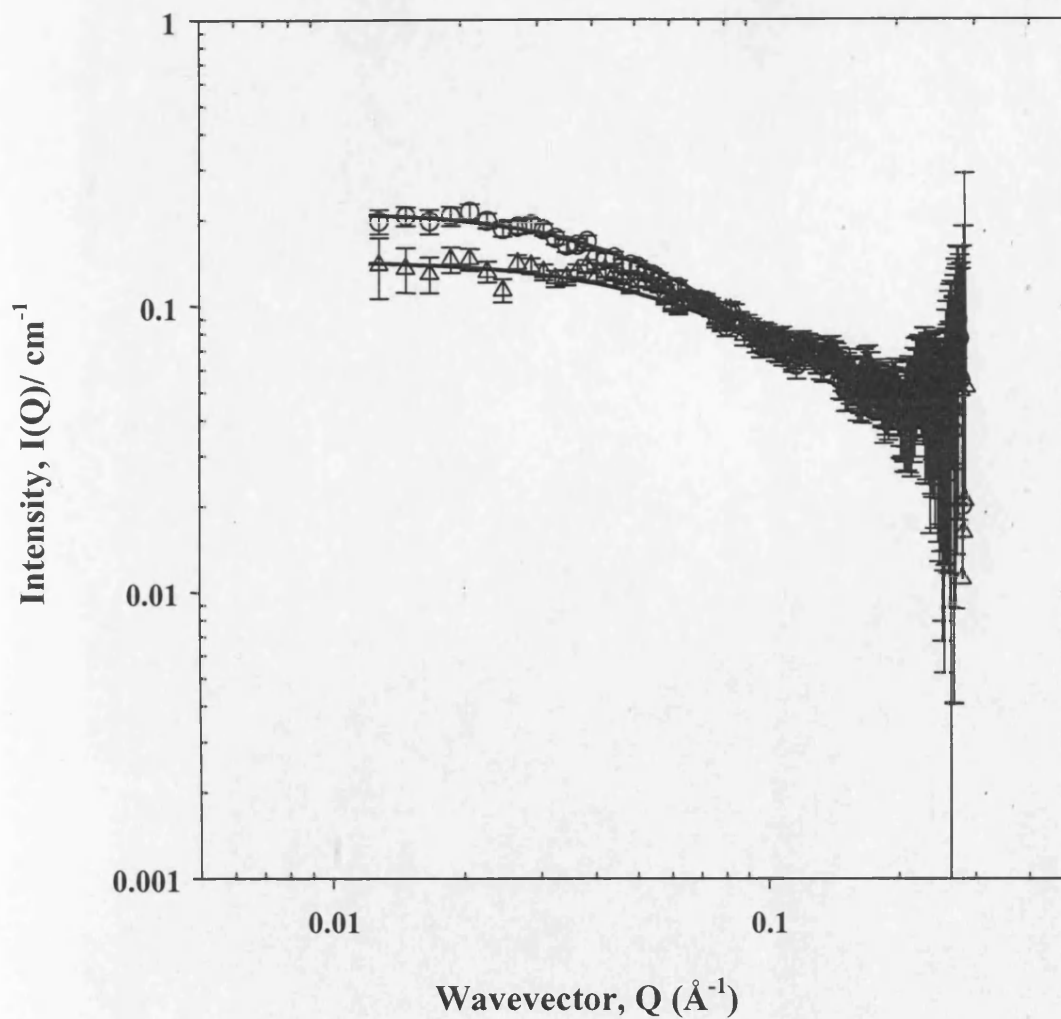


Figure 4.10 The scattering data of ISA23.HCl samples at pH 7.4 and 5.5 with the same ionic strength, with the fitting using the Gaussian coil model (solid line).

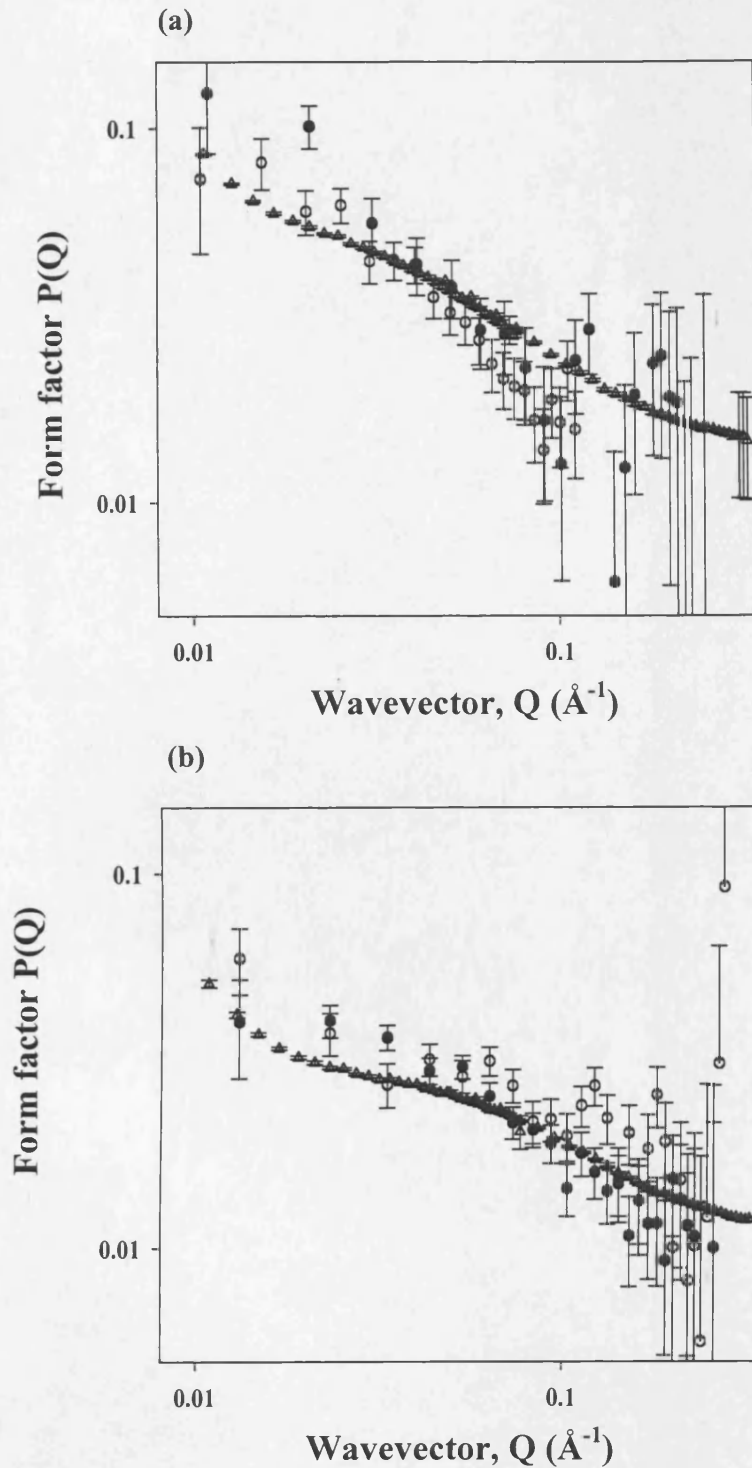


Figure 4.11 Effect of concentration and pH on the solution conformation of ISA23.HCl in D_2O ($37^\circ C$) evaluated by SANS. The data were interpreted using the Gaussian coil model. Panel (a) shows SANS data of 5 wt%, 2.5 wt% and 1 wt% ISA23.HCl at pH 5.5. Panel (b) shows SANS data obtained at 5 wt%, 2.5 wt% and 1 wt% ISA23.HCl and at pH 7.4

Table 4.2 The effect of concentration on the size of ISA23.HCl, at pH 7.4 and 5.5.

pH	Concentration (mg/ml)	R_g (Å)
7.4	10	$24.7 \pm 1.1^*$
	25	23.5 ± 3.6
	50	21.4 ± 1.1
5.5	10	40.0 ± 2.3
	25	38.5 ± 8.6
	50	32.8 ± 1.1

* Data represent $R_g \pm$ error in the fitting

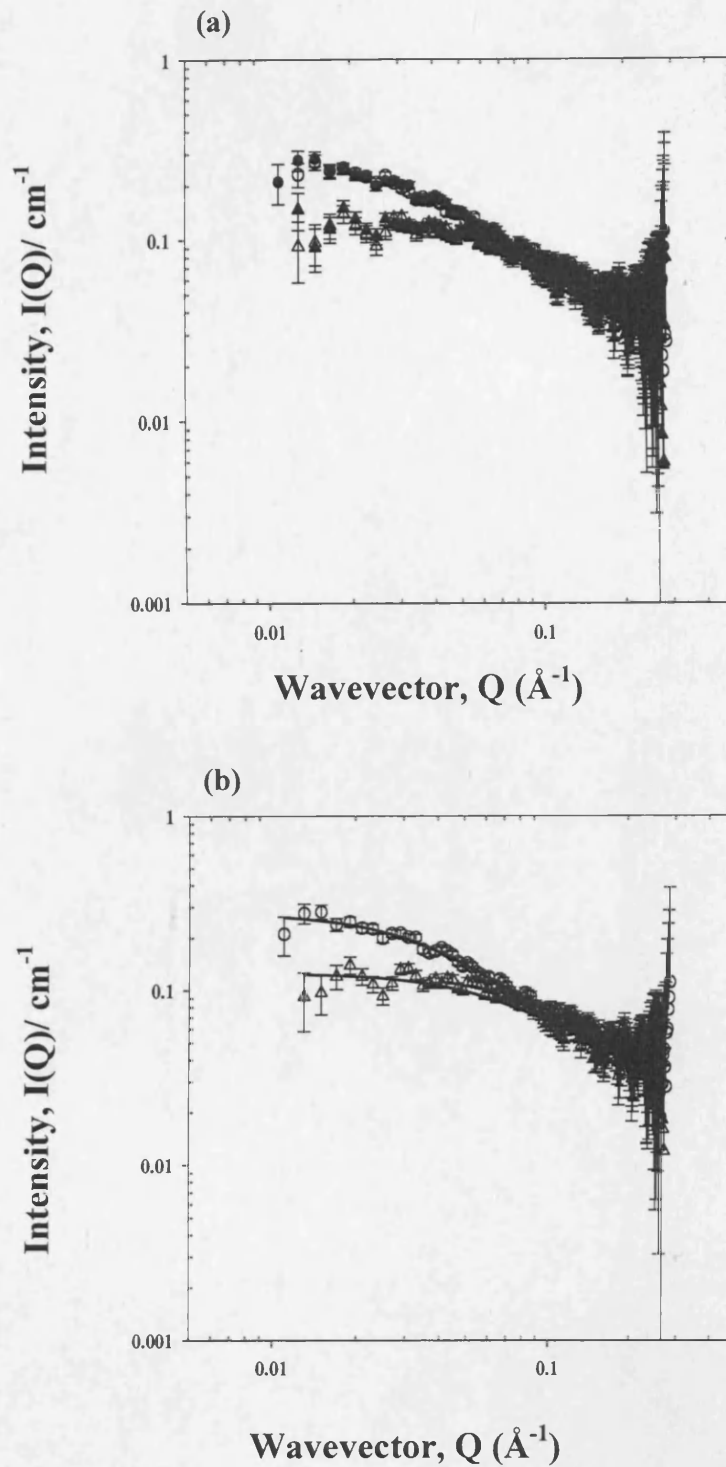


Figure 4.12 The effect of temperature on the scattering raw data obtained for ISA23.HCl at different pHs. Panel (a) shows pH 5.5 (25 °C; open circles, 37 °C; solid circles) and 7.4 (25 °C; open triangles, 37 °C; solid triangles), and panel (b) pH 7.4 (open triangles) and 5.5 (open circle), at 25 °C, solid lines represent the fittings obtained using Gaussian coil model

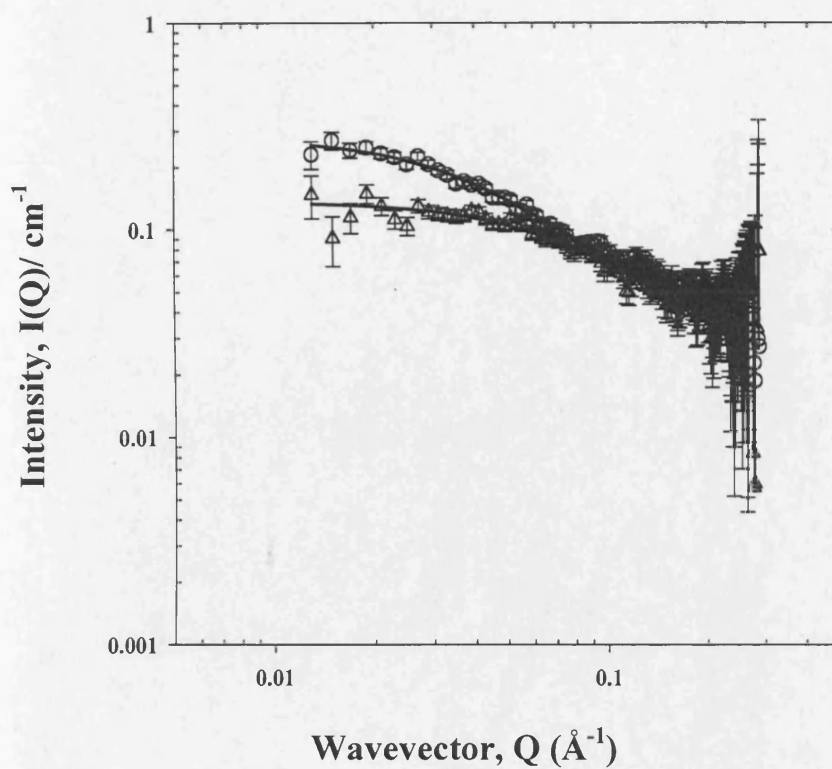


Figure 4.12 (continued). Panel (c) pH 7.4 (open triangles) and 5.5 (open circles), at 37 °C. The solid lines represent data fittings data using the Gaussian coil model

Table 4.3 Summary of the fitting parameters for ISA23.HCl calculated using Gaussian coil model.

Polymer (M_w)	pH	Temperature	Radius of gyration (Å)
ISA23.HCl [†] (21,000 g/mol)	5.5	37	32.2 ± 3.0*
ISA23.HCl [†] (71,000 g/mol)	5.5	25	40.6 ± 3.0
	5.5	37	40.1 ± 3.2
	7.4	25	21.8 ± 4.0
	7.4	37	22.0 ± 3.2

* Data represent $R_g \pm$ error in the fitting

[†] ISA23.HCl was the same batch, but the polymer was separated using membranes with different molecular weight cut-offs

Finally, when the effect of molecular weight of ISA23.HCl was studied, (Figure 4.13; Table 4.3), it appeared that ISA23.HCl size decreased as molecular weight decreased. This was to be expected, although, the difference in molecular weight of the two polymers was much greater than the difference in the radius of gyration seen. For example decreasing of the molecular weight from 71,000 g/mol to 21,000 g/mol caused a decrease R_g of only by 7 Å.

3.4 Discussion

These SANS experiments show that ISA23.HCl adopts a Gaussian coil-like structure in aqueous solution. Changing the pH, polymer concentration, polymer molecular weight, and temperature did not affect polymer shape, only the radius of the Gaussian coil (Griffiths et al, 2004). This was surprising, as ISA23.HCl is amphoteric in nature. It was expected that a rod or polyelectrolyte mathematical model would produce the best fit to the raw data. Upon protonation PAAs become charged, and a previous study using GPC with light scattering detection had concluded that ISA23.HCl adopts an elongated, rod-like structure (Ferruti et al, 2000). It is safe to say that this early conclusion was not true, as the data fit was not really good enough to state that the polymer would adopt this shape in aqueous solution.

Although changing the pH did not have any effect on PAA shape, it did greatly affect the polymer size. At high pH values (pH 13) the R_g was ~ 10 Å. This was very small, considering the high molecular weight of ISA23.HCl ($M_w = 71,000$ g/mol). It is interesting to note that PEG of the same molecular weight in a theta solvent would have an $R_g = 50$ Å (Griffiths et al, 2004). A PEO with the same degree of polymerisation as for ISA23 has a $R_g = 25$ Å (Griffiths et al, 2004). At pH 13, ISA23 is negatively charged with 100% of the carboxylic acid groups deprotonated. It would be expected that repulsion between these negative charges would cause the expansion of the polymer chain. However, the results show that the polymer chain is very compact with very small radius of gyration. It is possible that the number of the negative charges are not enough to cause repulsion or polymer expansion, but the exact reason for the small polymer size is still unclear.

As the pH was decreased the ISA23.HCl radius started to increase. Initially, between pH 10 to 6, this occurred slowly, but as the pH was lowered, the radius started to increase significantly. At \sim pH 9.4, the first nitrogen in ISA23.HCl starts to protonate and at pH 7.4, 50% of the first nitrogen will be protonated (Figure 4.14). Between pH

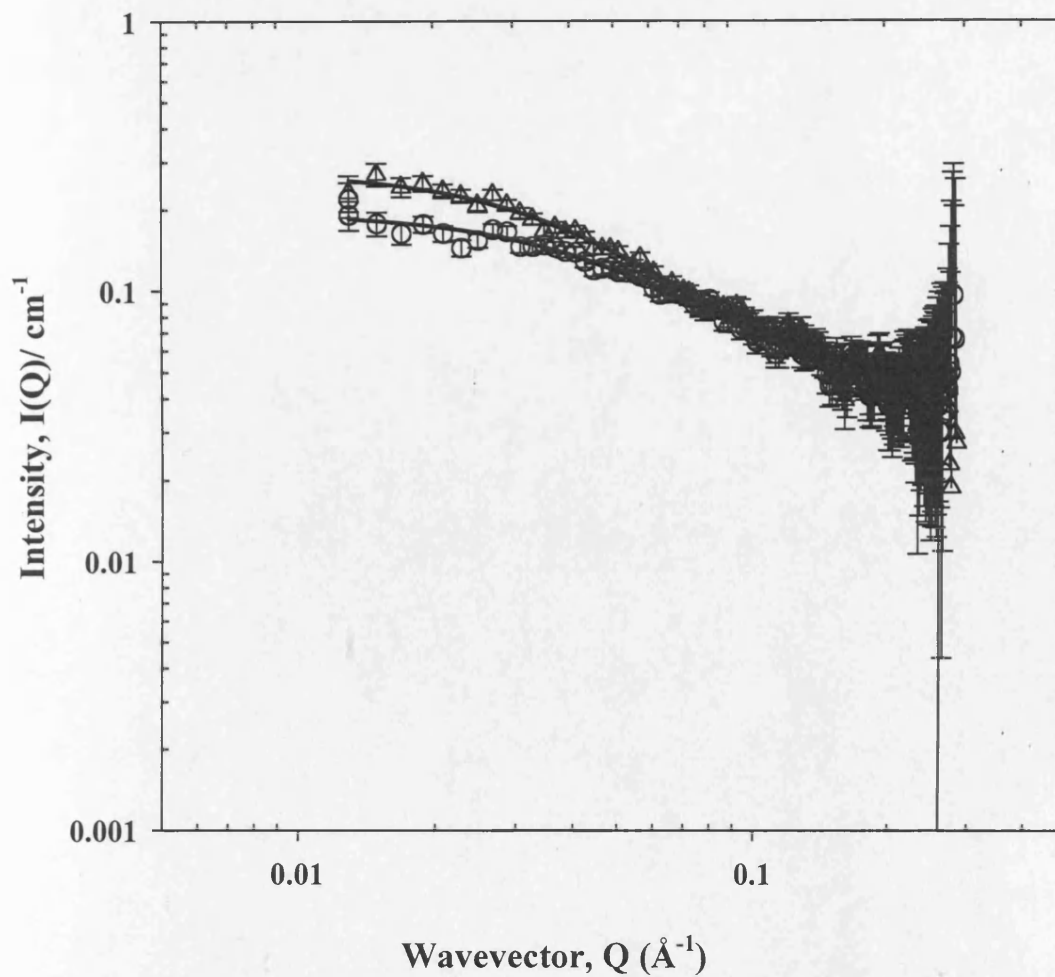


Figure 4.13 The effect of ISA23.HCl molecular weight on SANS. Data obtained at pH 5.5 for low molecular weight ISA23.HCl ($M_w = 21,000$ g/mol, open circles), and high molecular weight ISA23.HCl ($M_w = 71,000$ g/mol) (open triangles). The solid lines represent the fitting obtained using the Gaussian coil model

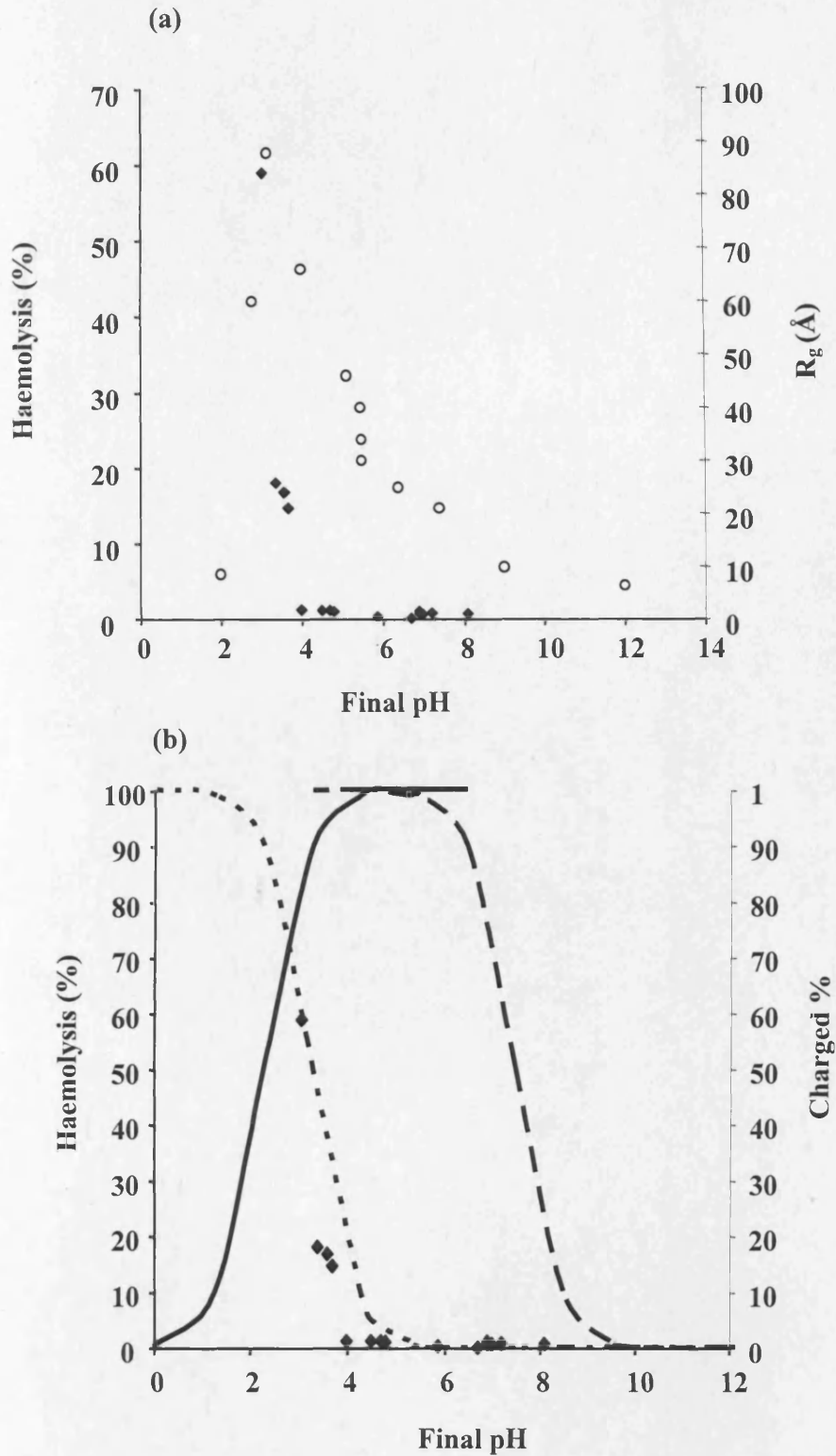


Figure 4.14 Correlation between ISA23.HCl haemolytic activity and its R_g and degree of protonation. Panel (a) haemolytic activity (filled diamonds) and R_g (open circles) of ISA23.HCl as a function of pH. Panel (b) The overlapping haemolysis activity (filled diamonds) and the percentage of negatively charged carboxylic acid groups (solid lines), the first positively charged nitrogen (long dashed lines) and the percentage of the second nitrogen (short dashed lines)

7.4 to 6 the overall ISA23.HCl charge remains negative and R_g measured was 21 to 24 Å. R_g continued to increase, and as pH reached 5.5, the R_g increased sharply as a result of repulsion between the like-charged groups along the polymer backbone. This sharp increase in R_g starts to occur when the second amino group begins to protonate at \sim pH 5.4. The maximum R_g was 80 Å seen at pH 3.15. This occurs close to the pKa value of the second amino group. However, as pH decreased further, R_g began to decrease. This was quite confusing as ISA23.HCl is becoming more positively charged as pH falls. However, by decreasing the pH further, the carboxylic acid groups gain a hydrogen, and at pH 2.1 half of the population of the carboxylic acid groups gain a proton and thus become neutral. This will make the polymer less hydrophilic (and more hydrophobic) and thus affects polymer solubility. This effect can result in the collapse of the polymer coil. The exact reason for this pattern of the behaviour is not known, but a combination of the inter-and intra-molecular interactions may be responsible.

Increasing ISA23.HCl concentration caused a slight increase in the R_g observed (Table 4.3). This effect was observed at both pH values, but was more pronounced at pH 5.5. Previous studies using light scattering and GPC, suggested that ISA23 tends to form aggregates (Mencdichi et al, 2005; Ferruti et al, 2000). However, the SANS experiments reported in this chapter did not confirm these observations. This variation in results could be due to the differences in how the experiments were conducted, e.g. concentration of the polymer, solvent used or the ionic strength.

As described in Chapter 3, pH affects the haemolytic activity of ISA23.HCl. This was consistent with previous observations (Ferruti et al, 2000; Richardson et al, 1999; and Wan et al, 2004). The increase in R_g and the increase in positive charge of ISA23.HCl as pH decreases is likely to be responsible for the polymer's membrane activity. However, there was no close correlation between the haemolytic activity and the R_g of ISA23.HCl (Figure 4.14). A better correlation was seen between polymer positive charge and haemolysis. The best correlation was found when ISA23.HCl haemolytic activity was related to the percentage of positive charge on the second nitrogen atom. One can say that for ISA23.HCl to cause a significant haemolysis, 100% of the first nitrogen must be positively charged together with \sim 20% of the second nitrogen. From these results it is possible to state the hypothetical number of positive charged groups that are required to cause RBC membrane breakage at a particular pH

value. Ideally an endosomolytic polymer should cause membrane permeabilisation at ~ pH 6.5. The observations made here can be used to tailor polymer structure to provide pKa values that should promote significant haemolysis between pH 6.5 to 5 without haemolysis at pH 7.4.

The data reported here are interesting as they demonstrate for the first time the correlation between PAA R_g and pH. Also they show the importance of protonation of the second aminic nitrogen in the process.

4.5 Conclusions

To define the conformation of PAAs under different environmental conditions the raw data obtained by SANS for ISA23.HCl (37 °C at 50 mg/ml) were analysed in terms of best fit of various models to the raw data. The Gaussian coil model gives the best fit for ISA23.HCl and the shape of the polymer was not affected by pH (pH 2 to 14) or polymer concentration examined (10 mg/ml to 50 mg/ml). These results help to better understand the mechanism of action of ISA23.HCl. It is clear that polymer R_g is pH-dependent, this coupled with the increase in the cationic nature of ISA23.HCl could be responsible for their membrane breakage activities. Thus the next step is to study the interaction between ISA23.HCl with micelles, a simple model membrane, using various physico-chemical techniques.

Chapter 5
Studies on the interaction between
ISA23 and model micelles

5.1 Introduction

The effect of pH, polymer concentration, ionic strength, temperature and molecular weight on the solution conformation of ISA23.HCl were investigated in Chapter 4. It was shown that pH was the dominant factor that affected the solution morphology (size and shape) of ISA23.HCl. However, it is probable that the conformation of the polymer at the interface will be different to that in solution.

Therefore, the main aim of this study was to examine the effect of pH on the interaction of ISA23.HCl and a series of “model” surfaces. Techniques that are well-established in the colloid field – surface tension (Goddard, 2002), small-angle neutron scattering (Haldar et al, 2004; Bergström et al, 2004), and electron paramagnetic resonance (Bales and Stenland, 1992; Griffiths et al, 2002) - were applied to study the biologically relevant systems being considered here. Micelles with surfaces that increased in complexity were used as model surfaces. Initially, a single type of surfactant was chosen to prepare micelles, but as biological membranes are rather heterogeneous in nature – they are principally a phospholipid surface populated with proteins and glycoproteins – some studies were also undertaken with surfactant mixtures containing bulky, spherical (C₁₂BNMG) or bulky, highly extended headgroups (C₁₂E₄). The surface composition of the surfactant micelles used were changed by varying the surfactant mole fraction. Finally, the most biologically relevant model was then systematically studied using spherical micelles composed of lyso-PC. These studies link most closely to those in Chapter 6, which used liposomes as model membranes.

To investigate ISA23.HCl surface interaction, surface tension measurements were first used to give a picture of how pH influenced the ISA23.HCl – surfactant interaction. Such an interaction might have an affect on the localised fluidity and the morphology of the micelle, and this can be quantified using EPR and SANS. So far such techniques and experimental models have rarely been used to help better understand the mechanism of action of endosomal polymers as non-viral vectors for protein or gene delivery. To better understand the background to these studies, first the micellar systems chosen as models will be described in more detail. The theoretical basis of the analytical techniques used are also briefly described.

5.1.1 Surfactants and Model surfaces

Surfactants or *surface active* agents are amphiphilic in nature, *i.e.* they contain both hydrophilic and hydrophobic regions, and due to this property, surfactant molecules adsorb at the gas-liquid interface (surface), liquid/liquid, solid/liquid or solid/air interface (Fainerman et al, 2002).

The surfactants used for these studies are shown in Figure 5.1. Initially, model surfaces composed only of SDS were used. This surfactant was chosen as it is a well known surfactant, and it is negatively charged in the pH range of interest. Then, the non-ionic surfactants, C₁₂BNMG, and C₁₂E₄, which have bulky headgroups, were also included to produce mixed surfaces. Finally, micelles composed of lyso-PC (zwitterionic surfactants) were used. Lyso-PC was chosen as its headgroup is the most abundant phospholipid headgroup found in biological membrane.

Generally, surfactants can be classified in terms of the nature of the headgroup:-

- Nonionic surfactants have an uncharged headgroup.
- Anionic surfactants possess a negatively charged headgroup. Examples of this group include sulfate and phosphate esters.
- Zwitterionic surfactants contain a polar region carrying negatively (usually carboxyl or sulfonic acid groups) and positively charged functional groups (usually quarternary amine groups). Examples of zwitterionic surfactants are betaines, sulphobetaines, and in the context of this thesis natural lipids such as lysophospholipids and phospholipids.

When surfactants are added to pure water, the surfactant molecules typically locate at the surface, and after a certain surfactant concentration, the critical micelle concentration (CMC), the surfactant molecules start to form aggregates called micelles (Figure 5.2). These micelles can have different shapes (e.g. spherical, cylindrical) that are determined by their surfactant chemistry, the “surfactant number” or the packing parameter (see Chapter 6 for details), solvent used, pH, temperature and type of salt present. The number of surfactant molecules needed to form the micelle is called the “aggregation number” This is usually high (~ 50 – 1000s), and is greatly influenced by a number of factors like pH, temperature, ionic strength and the nature and the purity of the surfactant.

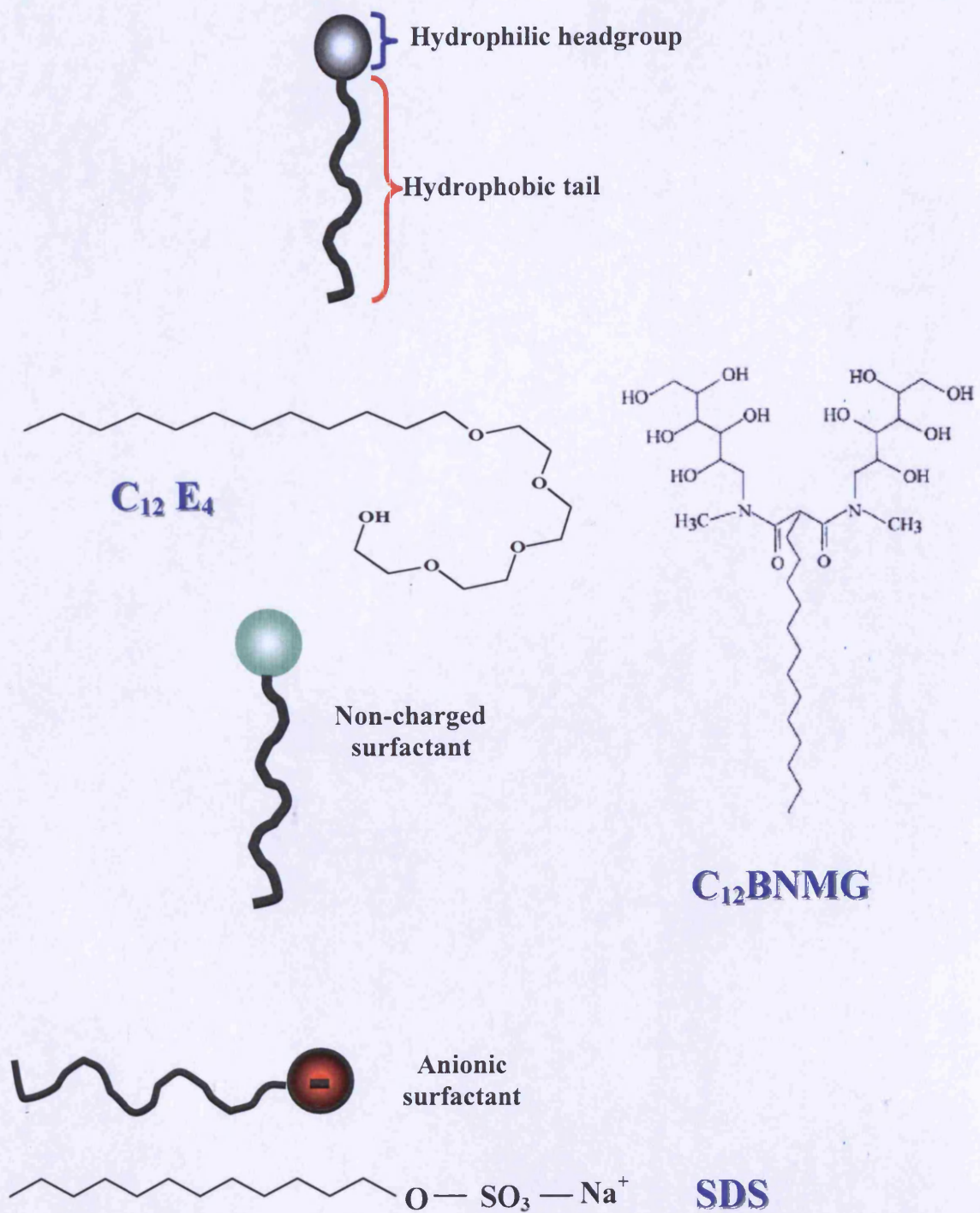
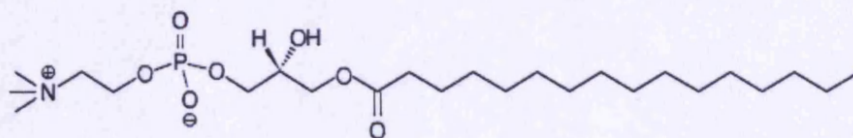
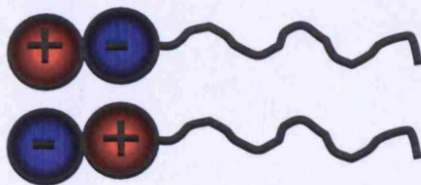
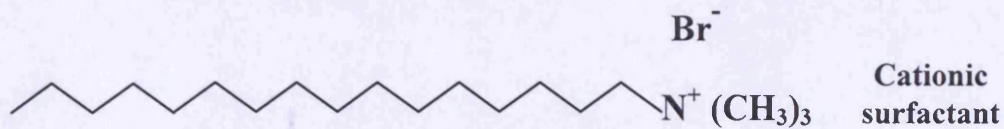


Figure 5.1a The chemical structure of non-ionic and anionic surfactants.

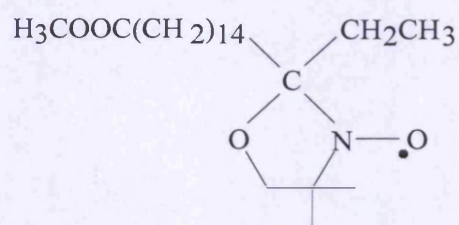
Zwitterionic
surfactant



Lyso-PC



**Cationic
surfactant**



16-DSE

Figure 5.1b The chemical structure of zwitterionic and cationic surfactants, and the spin-probe.

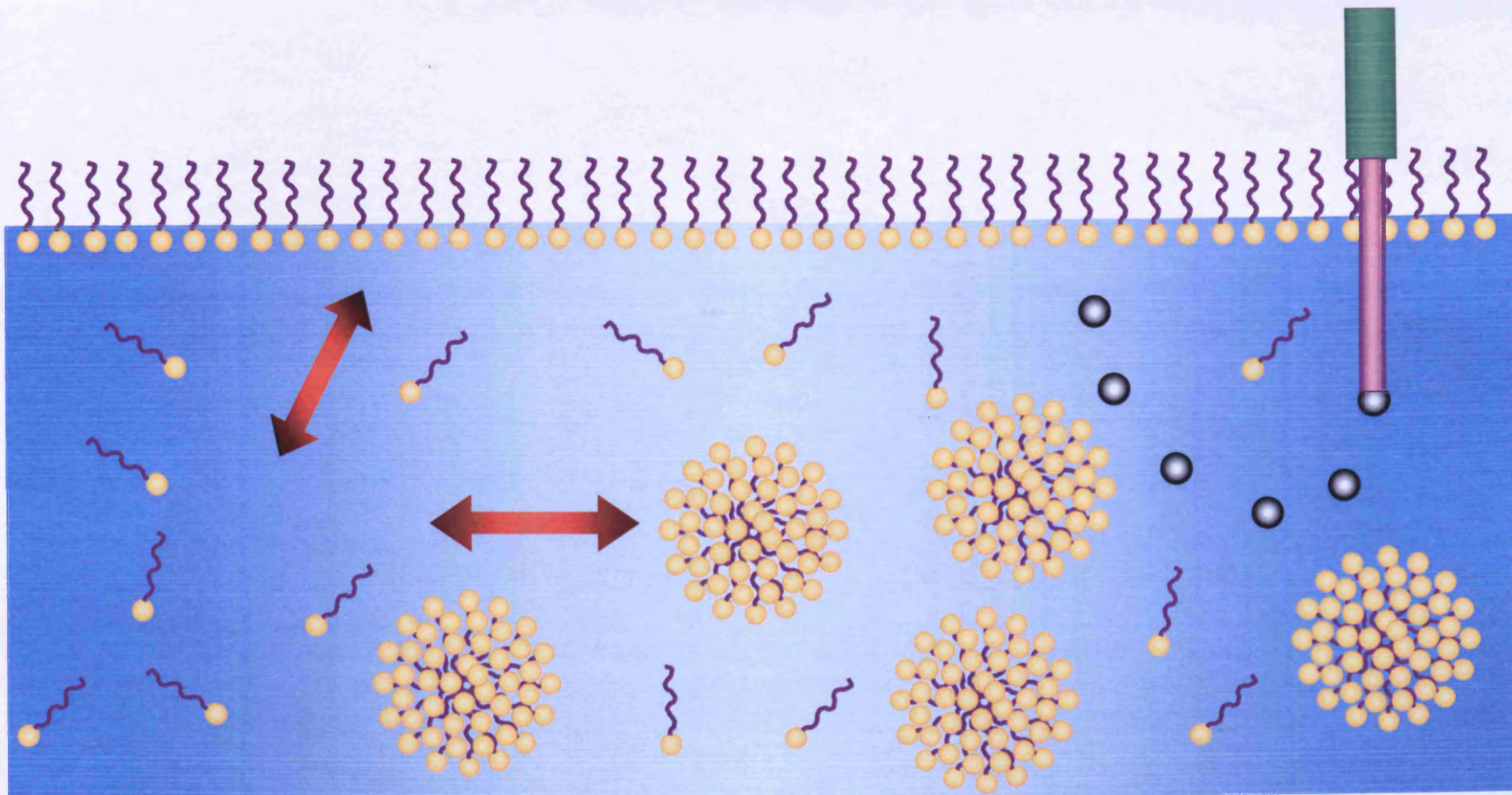


Figure 5.2 The distribution of surfactant molecules at the surface and the bulk of the solution, and the maximum bubble pressure technique used to measure the surface tension.

5.1.2 Methods used to characterise polymer-micelles interaction

Studies examining the surface tension were used to measure the onset of interaction, not only between the polymer and the surfactants present in the micelles, but also the interaction between ISA23.HCl with free surfactants found in the bulk solution, and the surfactants adsorbed on the surface (shown schematically in Figure 5.3). Surface tension (expressed in Nm^{-1}) is the storage of energy at the surface of liquids, and it accounts for observations such as the spherical shape of water droplets and the fact that some insects can walk on water. The surface tension of surfactants is measured using a variety of methods including static methods (capillary rise), detachment methods, (e.g. drop weight and drop volume) and dynamic methods, e.g. maximum bubble pressure. In this study, measurement of maximum bubble pressure (Figure 5.2) was chosen to measure surface tension. More detail of the theory of this method is given in Chapter 2, section 2.3.4.1.

EPR was used to study the effect of ISA23.HCl on the localised fluidity of the micelles. EPR is a spectroscopic technique that is very similar to the better known NMR (Lurie and Mäder, 2005). Whereas in NMR the electromagnetic radiation interacts with magnetic moments associated with the nuclei, in EPR the magnetic moment is produced by the electrons. Only molecules with unpaired electrons can produce an EPR signal. For example, free radicals, molecules with an odd number of electrons, triplet-state molecules and transition-metal complexes. In an EPR experiment, an external static magnetic field is applied across the sample to align the usually randomly oriented electrons to spin either clockwise or anticlockwise in respect to the direction of the magnetic field. EPR measures the amount of energy required to reverse the spin of unpaired electron (Dalton, 1985). In order to understand the energy splitting in a magnetic field, it is important to discuss the Zeeman energy effect. This is shown in Figure 5.4. Electrons are split into two populations, one occupying the lower energy level ($M_s = -1/2$) which occurs when the magnetic moment of the electron (μ) is aligned with the applied magnetic field, and a second occupying the higher energy level where the magnetic moment of the electron aligns against the external magnetic field ($M_s = +1/2$) (Hoff, 1989). The energy required to separate the two electron populations can be varied by changing the static magnetic field, and the energy required for the transition is given by:

$$\Delta E = h\nu = g\mu_B B$$

5.1

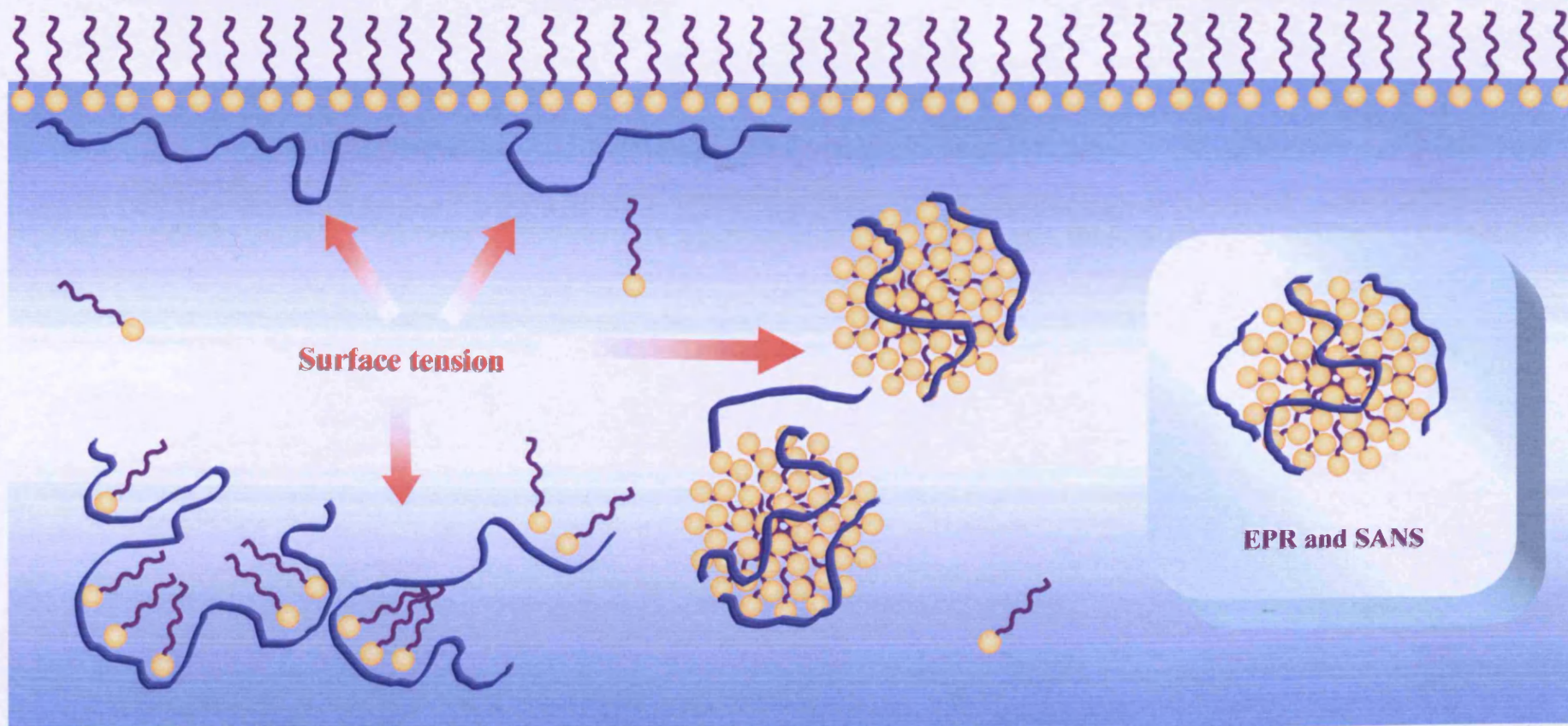


Figure 5.3 Schematic diagram showing the possible location where polymer interacts with surfactants, and the techniques used to investigate polymer-surfactant interaction.

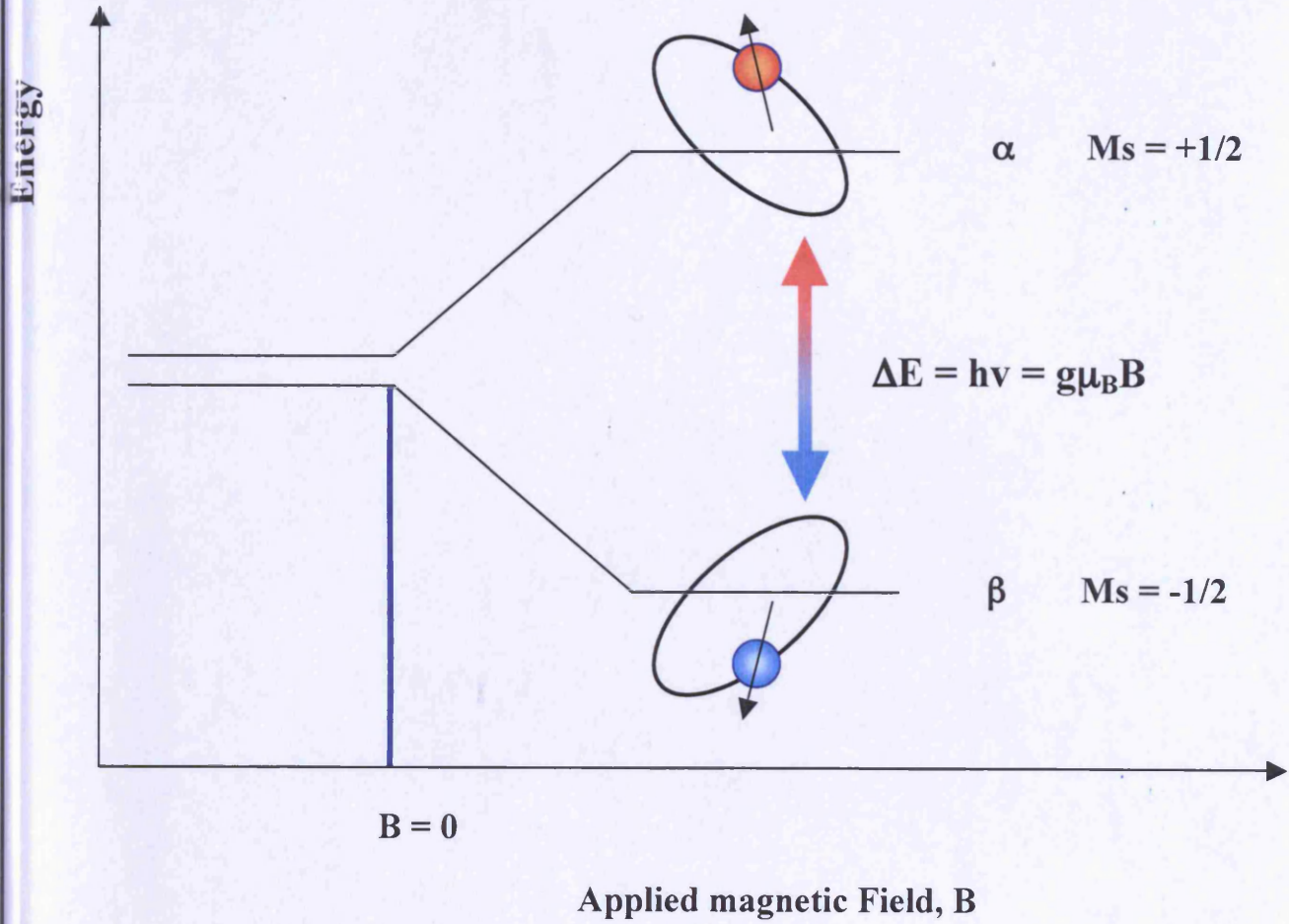


Figure 5.4 Zeeman energy levels.

where h is Plank's constant, g is the dimensionless "g-factor" characteristic of the electron's environment, μ_B is the Bohr magneton and B is applied magnetic field (Jeschke, 2003).

Information relating to the identity of the sample, and its composition, can be obtained from the hyperfine interaction or hyperfine coupling between the unpaired electron and its nuclei with non-zero nuclear spin. The hyperfine interaction causes the splitting of the line spectrum, and number of lines are equal to $2nI + 1$, where I is the nuclear spin quantum number and n = number of nuclei. There are two types of hyperfine interaction, isotropic (which involves electron in the s-orbital, A_{iso}) and anisotropic interactions (involves the electron in the d- and p-orbitals) (Berliner and Reuben, 1989). The shape (the intensity and the line-width), the position and the presence of multiplet structure in the lines of the EPR spectra can be used to extract information about the sample. For example, the intensity of the EPR line gives the amount of the paramagnetic species in the sample, and the line-width depends on the relaxation time of the spin. There are two types of relaxation processes, spin-spin and spin-lattice interaction.

Here, in the mixture of polymers and surfactants there are no paramagnetic species. Thus, in order to observe an EPR peak a spin-probe, 16-DSE must be included. This probe was picked as it has a narrow line-width and short correlation times. This is due its high intrinsic flexibility (Bales et al, 2000). Secondly, 16-DSE is hydrophobic in nature and only soluble when the surfactant concentration is greater than the CMC. For ^{14}N , the spin of the nucleus is 1, and accordingly the number of lines that will be observed is $2I+1 = 3$ and all nearly have equal intensities.

In these studies, the EPR spectrum was fitted using the LOWFIT program. An example of these fittings was not included here, as it was not possible to obtain the data output file using LOWFIT. The parameters obtained from the fittings can be used to calculate the rotational correlation time τ_C and τ_B (the rotational correlation time can be described as the time required for the molecule of the spin probe to rotate through one radian around its axis, (Gabre-Mariam et al, 1991) (see equation 5.2 and 5.3.1, see appendix III for details).

$$\tau_C = 1.16 C_{cor}$$

5.2

$$\tau_B = -1.27 B_{cor} \quad 5.3$$

$$C_{cor} = \frac{1}{2} \Delta H_{pp}^0(0) \left\{ \sqrt{\frac{V_{pp}(0)}{V_{pp}(+1)}} + \sqrt{\frac{V_{pp}(0)}{V_{pp}(-1)}} - 2 \right\} \quad 5.4$$

$$B_{cor} = \frac{1}{2} \Delta H_{pp}^0(0) \left\{ \sqrt{\frac{V_{pp}(0)}{V_{pp}(+1)}} - \sqrt{\frac{V_{pp}(0)}{V_{pp}(-1)}} \right\} \quad 5.5$$

EPR allows the characterisation of the surface hydration of a micelle (Bales et al, 1998), since there is a very good correlation between A_0 (the separation of the lines) and the polarity index. The latter defined as the ratio of the molar concentration of OH dipoles in a solvent or solvent mixture to that in water (Mukerjee et al, 1982; Bales et al, 1998). Basically the polarity (H) is the volume fraction occupied by water (Bales et al, 1998) in the polar shell. In this study the hyperfine spacing A^+ will be used to obtain the polarity index as it was shown previously that A_0 is more affected by the small second-order shifts due to motional effects (Bales et al, 1998; 2000) compared with A^+ . The polarity (H) can be calculated by:

$$H = ((A^+) - 14.309) / 1.418 \quad 5.6$$

5.2 Methods

5.2.1 Measurement of the surface tension of surfactants in the presence of ISA23.HCl

First, stock surfactant solutions were prepared by dissolving the appropriate mass of surfactant in distilled water to produce a total surfactant concentration of 20 mM.

100% SDS	116 mg, 20ml
SDS : C ₁₂ E ₄ (90% SDS)	104 mg of SDS and 21 mg of C ₁₂ E ₄ , 20ml
SDS : C ₁₂ E ₄ (75% SDS)	81 mg of SDS and 44 mg of C ₁₂ E ₄ , 20ml
SDS : C ₁₂ E ₄ (50% SDS)	58 mg of SDS and 72 mg of C ₁₂ E ₄ , 20ml
SDS : C ₁₂ BNMG (50% SDS)	58 mg of SDS and 132 mg of C ₁₂ BNMG, 20 ml
CTAB : C ₁₂ BNMG (50% SDS)	73 mg of CTAB and 72 mg of C ₁₂ BNMG, 5 ml
100% lyso-PC	119 mg, 12ml

To prepare the stock solution of ISA23.HCl, 80 mg was dissolved in 20 ml (0.4 w/v%) of double distilled water. For the surfactant mixture, and the polymer solution, the final pH was measured and adjusted accordingly to the desired value for each experiment using 1, 0.1 or 0.01 M HCl or NaOH.

The concentration of the surfactant mixture ranged from 0.002 mM to 10 mM, and the surface tension of this mixture was measured in the presence or the absence of ISA23.HCl as a function of pH. Serial dilutions were prepared to obtain different surfactant concentration, and 3 ml of each was added to a glass vial. The surface tension was measured using the maximum bubble pressure tensimeter (with a bubble life-time of 10 sec). For the samples containing a mixture of ISA23.HCl and surfactant, a 1.5 ml of surfactant and a 1.5 ml of ISA23.HCl (final polymer concentration of 0.2 w/v%) were added to a glass vial, they were left to equilibrate for 10 min, then the surface tension was measured as above. Measurements were made at pH 4, 5, 6, 7 and 8.

5.2.2 EPR spectroscopy of micelle-ISA23.HCl interaction

To study the effect of pH and ionic strength on the fluidity of SDS micelles, 5 ml of SDS (25 mM, 36 mg) was added to two glass vials containing pre-dried spin-probe 16-DSE (0.04 mg/ml). This was mixed and allowed to equilibrate (the ratio of SDS to spin probe was ~ 500:1). The pH of one sample was altered by the addition of HCl (1 M or 0.1 M). To the second sample, NaCl was added to give a NaCl concentration equivalent to the added HCl concentration. The EPR measurements were made as described below.

To investigate the ISA23.HCl/SDS interaction, 2.5 ml of SDS (50 mM, 36 mg) and 2.5 ml of ISA23.HCl (0.4 w/v%) were added to a glass vial containing pre-dried spin-probe (16-DSE). The EPR measurements were made as described below.

To study Lyso-PC micelle ISA23.HCl interaction, a 5 ml of lyso-PC (10 mM) was added to pre-dried 16-DSE (as above), and the pH was adjusted to the desired value by the addition of 0.1 M and 1 M HCl or NaOH. For the EPR of lyso-PC in the presence of ISA23.HCl, 2.5 ml of lyso-PC (20 mM), and 2.5 ml of ISA23.HCl (0.4 w/v%) were added to the glass vial containing dried spin-probe.

For EPR evaluation, an aliquot of each sample was taken using a capillary tube (~ 10 μ l), which was then sealed at both ends by holding the capillary near the flame from a bunsen burner. EPR measurements were made using Bruker EMX spectrometer

at 25°C. For each sample 5 scans were performed and the spectra were saved in ASCII format. LOWFIT was used to fit the spectra.

5.2.3 SANS of ISA23.HCl-micelle interaction

To study SDS micelle-ISA23.HCl interaction, three stock solutions of SDS (50 mM) were prepared in D₂O (SDS, 58 mg, 4 ml, d-SDS, 63 mg, 4 ml), and the pH was adjusted to the required value (pH 7.4, 5.5 or 4). ISA23.HCl solutions were also prepared (concentration of 2 w/v %) at pH 7.4, 5.5 or 4. Prior to the SANS measurements, 1.5 ml of SDS and 1.5 ml ISA23.HCl solution were mixed.

To study lyso-PC micelles-ISA23.HCl interactions, a 20 mM of lyso-PC (20 mg, 2 ml) was prepared at pH 5.5 or 7.4. 2 w/v % solution of ISA23.HCl (40 mg, 2ml, at pH 7.4 and 5.5), PEI (40 mg, 2ml), dextran (40 mg, 2ml) and TX-100 (40 mg, 2ml) stock solutions were also prepared in D₂O. Prior to the SANS measurements, 1.5 ml of the lyso-PC solution with 1.5 ml of the polymer solution were mixed.

In both cases, SANS measurements were performed on the LOQ diffractometer at the ISIS, at 37°C, each sample took around 40 – 60 min to run. The scattering data were normalised for the sample transmission and incident wavelength distribution, background corrected and were also corrected for the linearity and efficiency of the detector response.

5.3 Results

First, the results obtained when measuring the interaction with the simplest SDS micelles model are presented, followed by the heterogeneous micelle model and then the lyso-PC micelle models. For each micellar model, the data obtained using each technique are described individually. The overall picture is presented in Section 5.4.

5.3.1 Interaction of ISA23.HCl with SDS surfactants

A pH range of pH 4 to 7.4 was chosen as this is the range where ISA23.HCl changes from a positively to a negatively charged polymer. At pH 4, a very strong interaction was seen between ISA23.HCl and the SDS mixture in the surface tension studies. Precipitation or phase separation occurred over surfactant concentration from 0.1 mM to 0.8 mM (Figure 5.5a). At pH 5 and 6, the surface tension of SDS altered

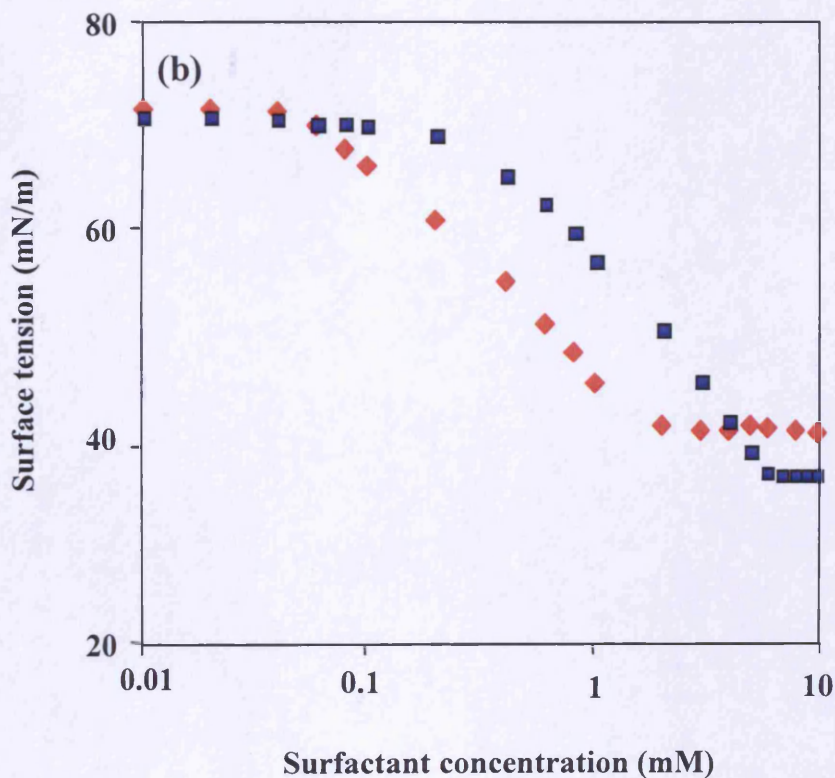
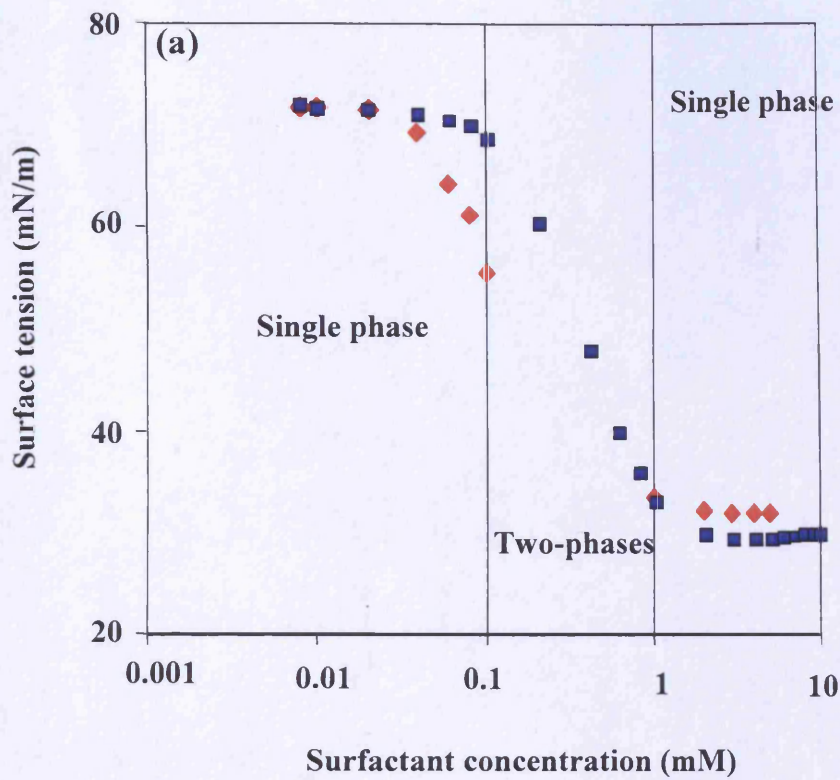


Figure 5.5 Effect of ISA23.HCl on the surface tension of SDS surfactant solution. Panel (a) surface tension of SDS in the presence (red diamond) and absence (blue squares) of ISA23.HCl at pH = 4 (strong interaction with phase separation). Panel (b) surface tension of SDS in the presence (red diamond) and absence (blue squares) of ISA23.HCl at pH 5.5 (weak interaction)

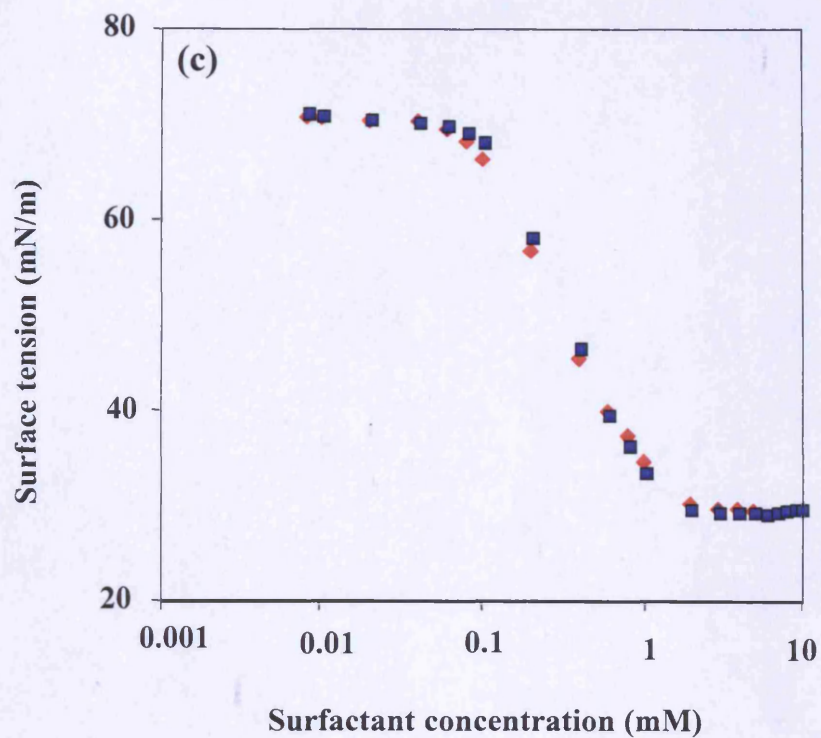


Figure 5.5 (continued). Panel (c) the surface tension curve of SDS in presence (red diamond) and absence (blue squares) of ISA23.HCl at pH = 7.4 (no interaction)

following the addition of ISA23.HCl, but phase separation did not occur at any of the surfactant concentrations examined (Figure 5.5b). And finally at pH 7.4, no interaction occurred between ISA23.HCl and SDS, as the surface tension of SDS was the same in the presence and absence of ISA23.HCl (Figure 5.5c).

Likewise, in the SANS studies, at pH 7.4 (Figure 5.6a) the scattering did not change when ISA23.HCl was added. However, at pH 5.5 and 4 (Figure 5.6b,c), changes in the scattering were evident. The magnitude of the change increased with the decrease in pH. Two shell ellipsoid with a charged sphere H-P $S(Q)$ was used to fit the SANS data acquired from SDS micelles - in the presence and absence of ISA23.HCl. The scattering from SDS/ISA23.HCl mixture was predominately from the SDS micelles, as the polymer is a weak scatterer (Chapter 4). Changing the pH alone (just the effect of pH, no polymer was involved) did not affect the overall morphology of the SDS micelles. However at pH 4, the aggregation number (N_{agg}) is higher than the N_{agg} SDS micelles at pH 5.5 and pH 7.4 (Table 5.1).

At pH 4, ISA23.HCl caused an increase of the radius of SDS micelles and ellipticity (and due to this, the N_{agg} also increases), but the thickness of the shell decreased by 1.4 Å (from 3.6 Å to 2.2 Å). At pH 5.5, the ellipticity (and N_{agg}) increased in the presence of ISA23.HCl. Finally at pH 7.4, ISA23.HCl did not have any effect on the morphology (radius and ellipticity) of the SDS micelles.

In the d-SDS/ISA23.HCl system, the scattering from d-SDS was much weaker and the polymer conformation played greater importance. At pH 5.5 and 7.4 the scattering from d-SDS/ISA23.HCl resembled that of ISA23.HCl alone (random coil) at these pHs. However, at pH 4, the scattering data of the d-SDS/ISA23.HCl resembled that of the SDS micelles (spherical model). A Gaussian coil model produced the best fit for d-SDS/ISA23.HCl data at pH 7.4 and 5.5, and the radius of gyration calculated using this model is 25 Å and 35.6 Å respectively (Figure 5.7a,b). For the d-SDS/ISA23.HCl system the best fit to the data at pH 4, was the two shell ellipsoid, charged sphere model (Figure 5.7c). A model that also incorporated a contribution for the polymer scattering produced in an equally good fit of this data, similar conclusions were drawn from the two models. The polymer scattering resembled that of the SDS micelle. However, the overall radius of the sphere, and the ellipticity, did increase following the addition of ISA23.HCl (Table 5.2).

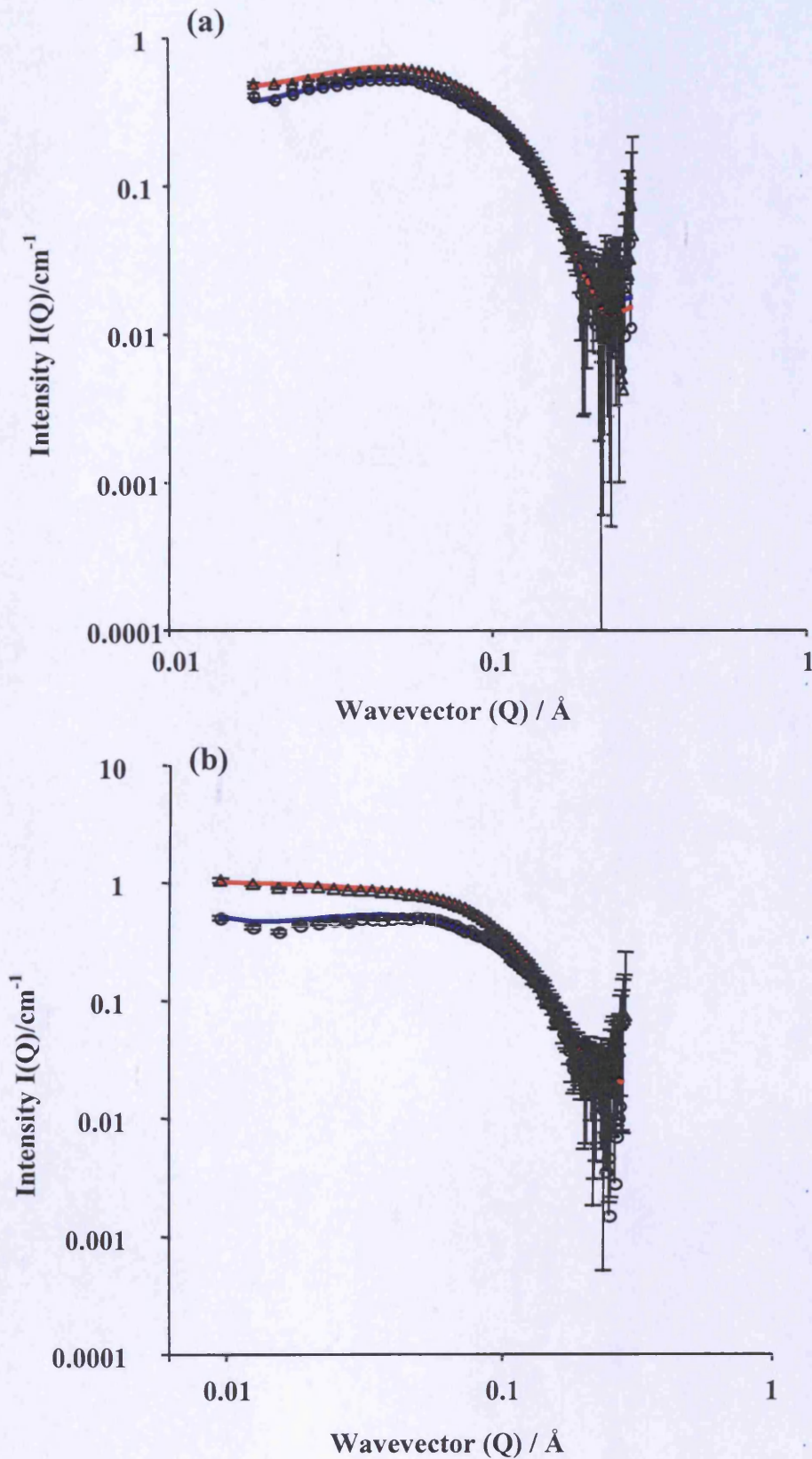


Figure 5.6 The effect of ISA23.HCl on the SANS data of the SDS micelles. SANS data of SDS in the presence (open triangle) and absence (open circles) of ISA23.HCl at pH 7.4 (panel a) and pH 5.5 (panel b), plus their fittings (solid blue or red line)

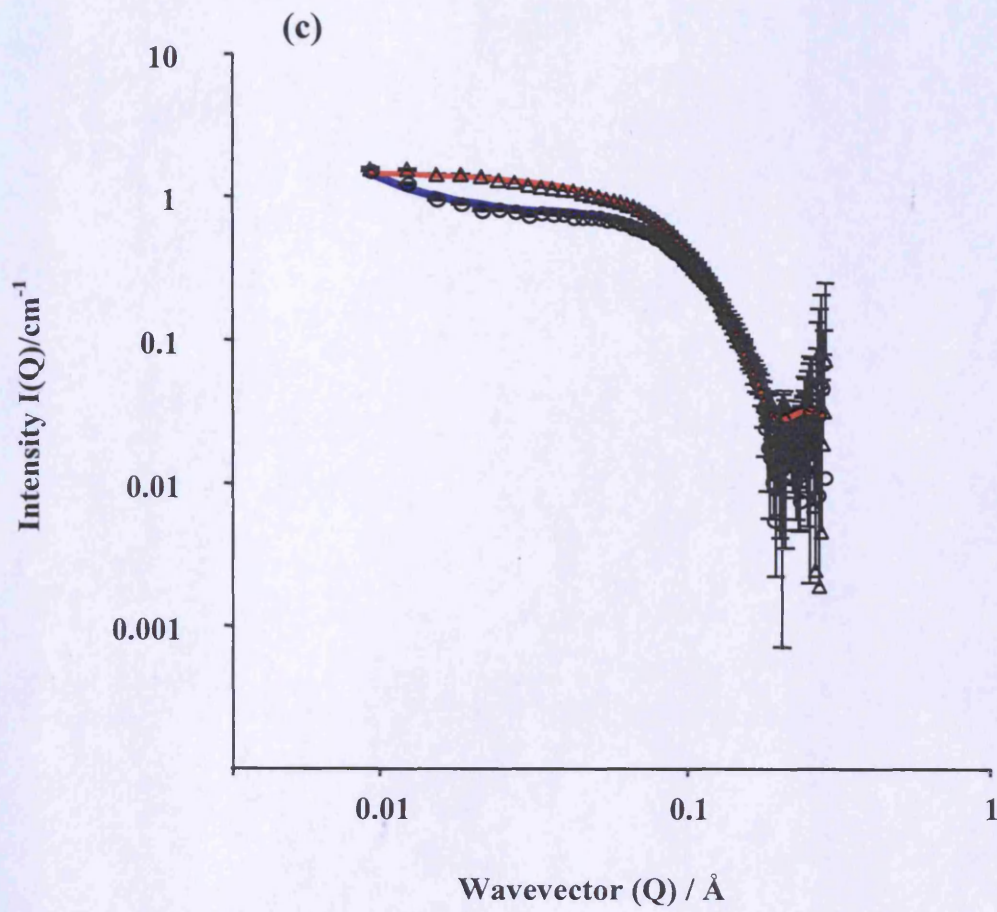


Figure 5.6 (continued). Panel (c) the SANS data of SDS in the presence (open triangle) and absence (open circles) of ISA23.HCl at pH 4, plus their fittings (solid blue or red line)

Table 5.1 The summary of the parameters calculated from the model fittings to the SDS in the presence and absence of ISA23.HCl at pH 4, 5.5 and 7.4.

Parameter	SDS, pH 4	SDS + ISA23.HCl, pH 4
Radius of the core (Å)	16.7	16.5
Thickness of the shell (Å)	3.6	2.2
Ellipticity (X)	1.77	2.6
Radius of the sphere (Å)	19.3	24.8
N_{agg}	95	120
	SDS, pH 5.5	SDS + ISA23.HCl, pH 5.5
Radius of the core (Å)	16.6	16.7
Thickness of the shell (Å)	3.4	2.7
Ellipticity (X)	1.66	2.2
Radius of the sphere (Å)	20.2	22.8
N_{agg}	75	110
	SDS, pH 7.4	SDS + ISA23.HCl, pH 7.4
Radius of the core (Å)	16.7	16.7
Thickness of the shell (Å)	3.4	3.4
Ellipticity (X)	1.37	1.40
Radius of the sphere (Å)	18.8	17.1
N_{agg}	75	77

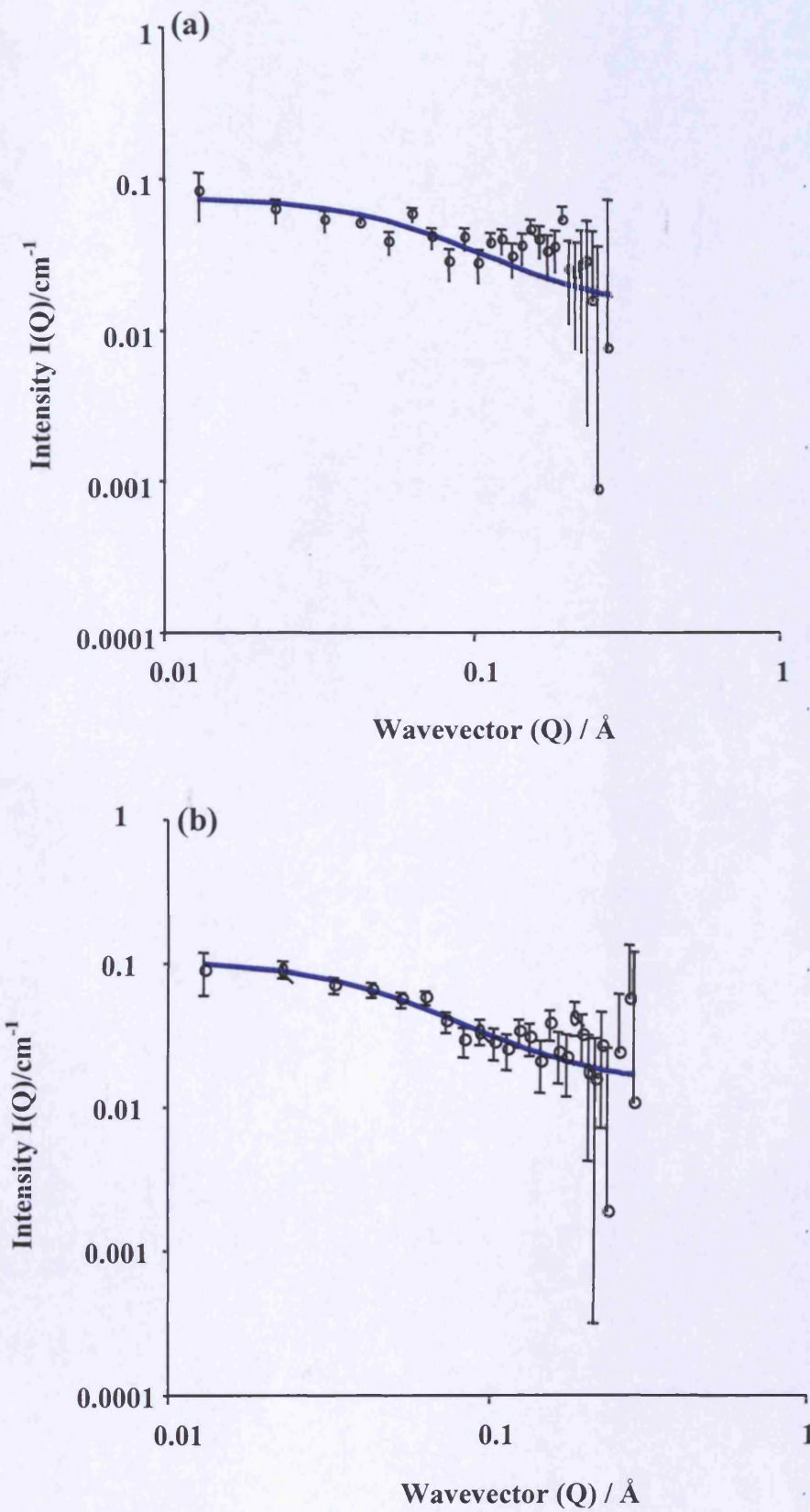


Figure 5.7 The SANS data of d-SDS micelles in the presence of ISA23.HCl. Panel (a) at pH 7.4, and panel (b) pH 5.5, plus their fittings (solid blue line)

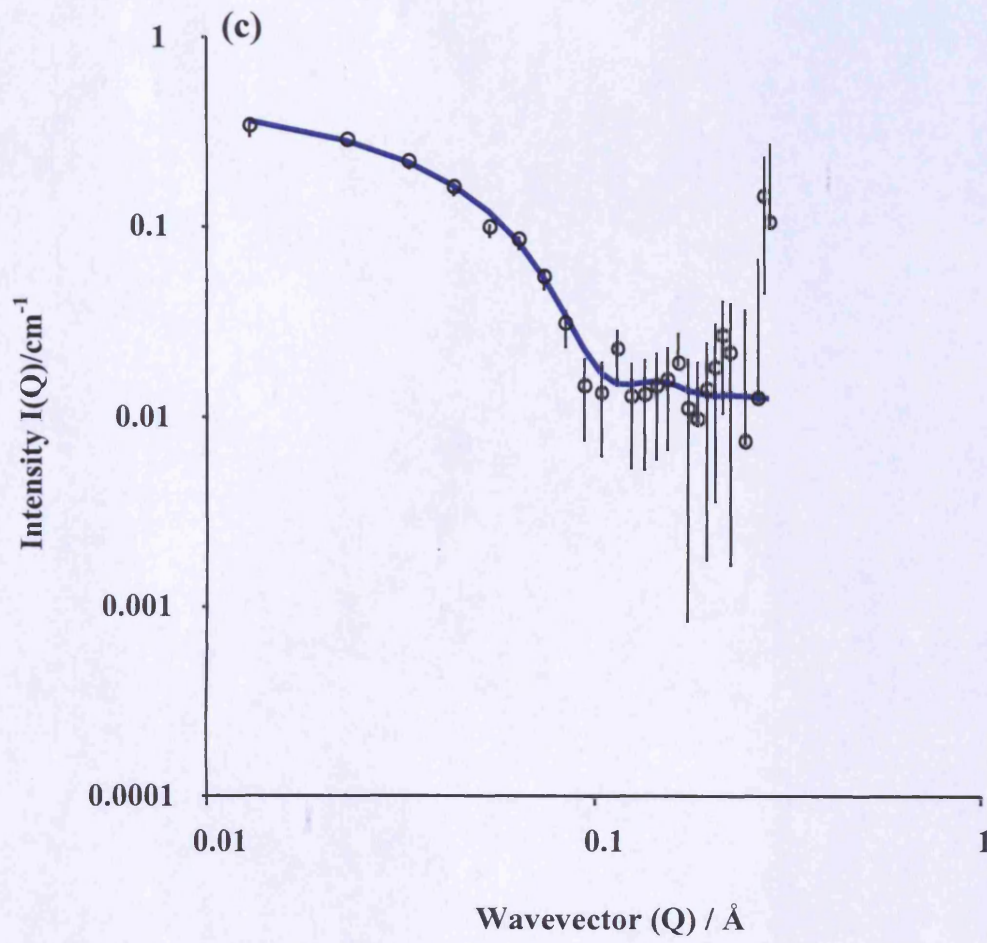


Figure 5.7 (continued). Panel (c) the SANS data of d-SDS in the presence of ISA23.HCl at pH 4, plus the fitting (solid blue line)

Table 5.2 The summary of the parameters calculated from the model fittings to the d-SDS micelles in the presence of ISA23.HCl at pH 4, 5.5 and 7.4.

Parameter	d-SDS + ISA23.HCl pH 4	d-SDS + ISA23.HCl pH 5.5	d-SDS + ISA23.HCl pH 7.4
Radius of the core (Å)	16.5	N/A*	N/A
Thickness of the shell (Å)	2.3	N/A	N/A
Ellipticity (X)	2.5	N/A	N/A
Radius of gyration (Å)	23.3	35.6	25.0

*N/A = not applicable

The EPR spectroscopy gave additional information. When the spin-probe (16-DSE) was allowed to dissolve in the hydrophobic region of the SDS micelles, changing the pH did not affect the EPR spectra obtained (Figure 5.8 and 5.9). To alter the pH a certain amount of HCl was added, which inherently also changes the ionic strength, these two processes cannot be decoupled. However, changing either the pH or the ionic strength did not effect the EPR spectra, A^+ and rotational correlation time of 16-DSE.

The EPR spectra of SDS micelles measured in the presence of ISA23.HCl (between pH 4 and 6.5), produced a spectrum where it was not possible to fit the third peak using LOWFIT program. The shape of the third line or peak changed with decreasing pH (Figure 5.10 and Figure 5.11a,b,c,d). Consequently, it was not possible to calculate the corrected rotational correlation time of 16-DSE between pH 4 and 6.5. However, between pH 7 and 8 the EPR spectra were fitted using LOWFIT. The corrected rotational correlation time (0.39 to 0.47 nanoseconds) measured was not affected by the addition of ISA23.HCl to SDS micelles at pH 7-8. The polarity of SDS micelles in the presence of ISA23.HCl increased with increasing pH (Figure 5.12). The greatest change in polarity occurred between pH 4.4 and 5, increasing from 0.001 to 0.34. The polarity increased by the least amount between pH 7.4 and 8 (from 0.69 to 0.72).

5.3.2 Interaction of ISA23.HCl with SDS/C₁₂E₄ as heterogeneous system

When measuring surface tension, at pH 4, it was shown that a very strong interaction occurred between ISA23.HCl and the surfactant mixture SDS:C₁₂E₄, at all ratios, 1:1, 3:1 and 9:1. This resulted in precipitation or phase separation over a certain range of surfactant concentration, which was between 0.8 mM and 0.1 mM.

At pH 5 (for 50% and 75% SDS), the surface tension of the surfactants did not change following the addition of ISA23.HCl. This was also true at pH 6 and 7.4. For 90% SDS, at pH 5, a clear interaction is observed but not at pH 6 or 7.4.

5.3.3 Interaction of ISA23.HCl with SDS/C₁₂BNMG and CTAB/C₁₂BNMG as heterogeneous system

Initially the surface tension of the sugar surfactant C₁₂BNMG was measured (CMC = 3 mM). The surface tension of the C₁₂BNMG was not effected by the presence of ISA23.HCl, indicating no interaction (Figures 5.13).

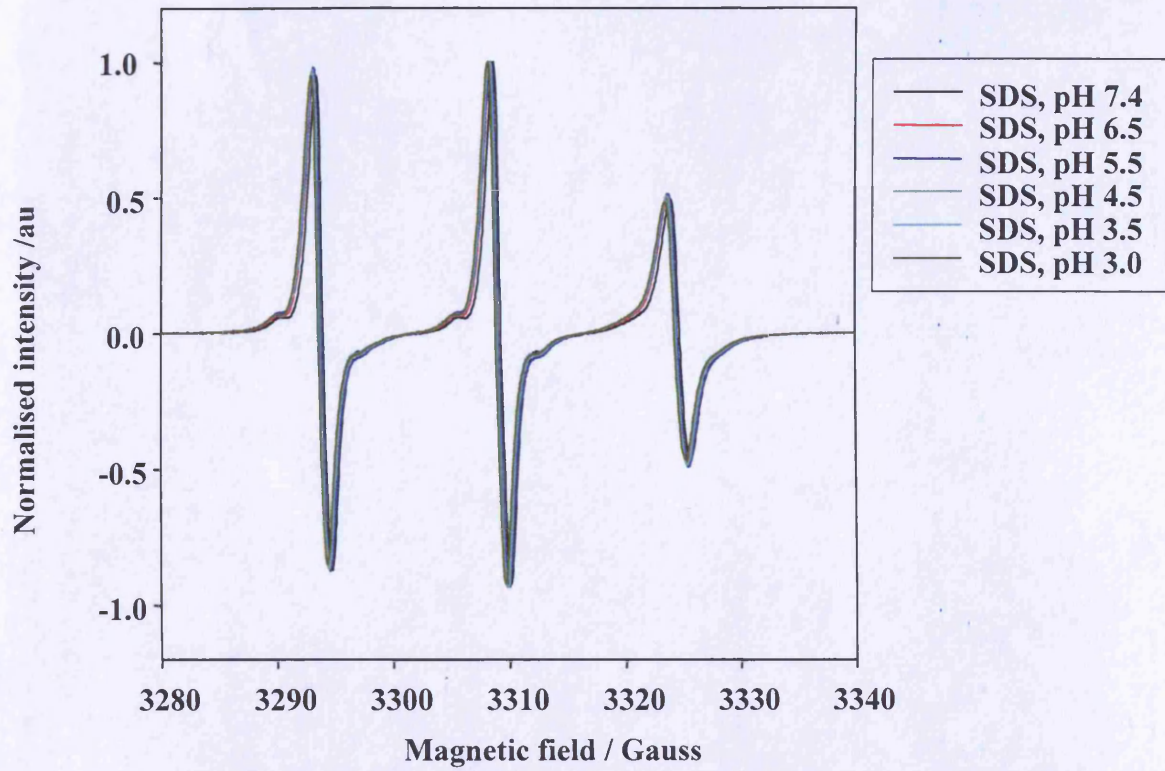


Figure 5.8 EPR spectra of SDS micelles as a function of pH.

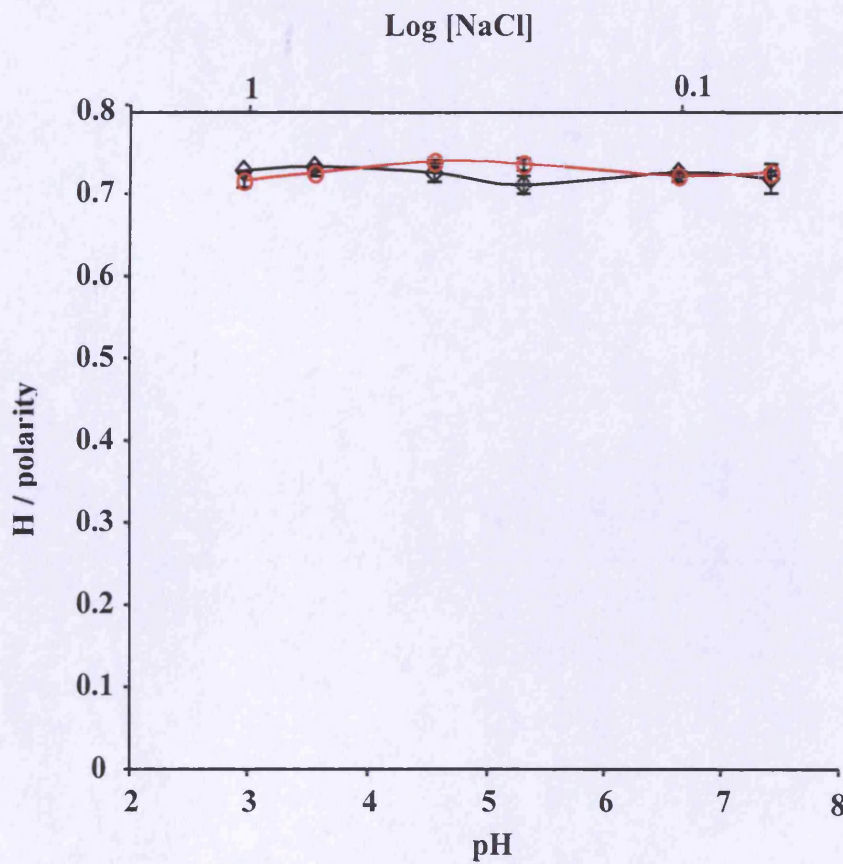


Figure 5.9 The polarity of SDS + HCl (open diamond) as a function of pH and the polarity (open circle) of SDS plus NaCl with concentration that is equivalent to that of HCl.

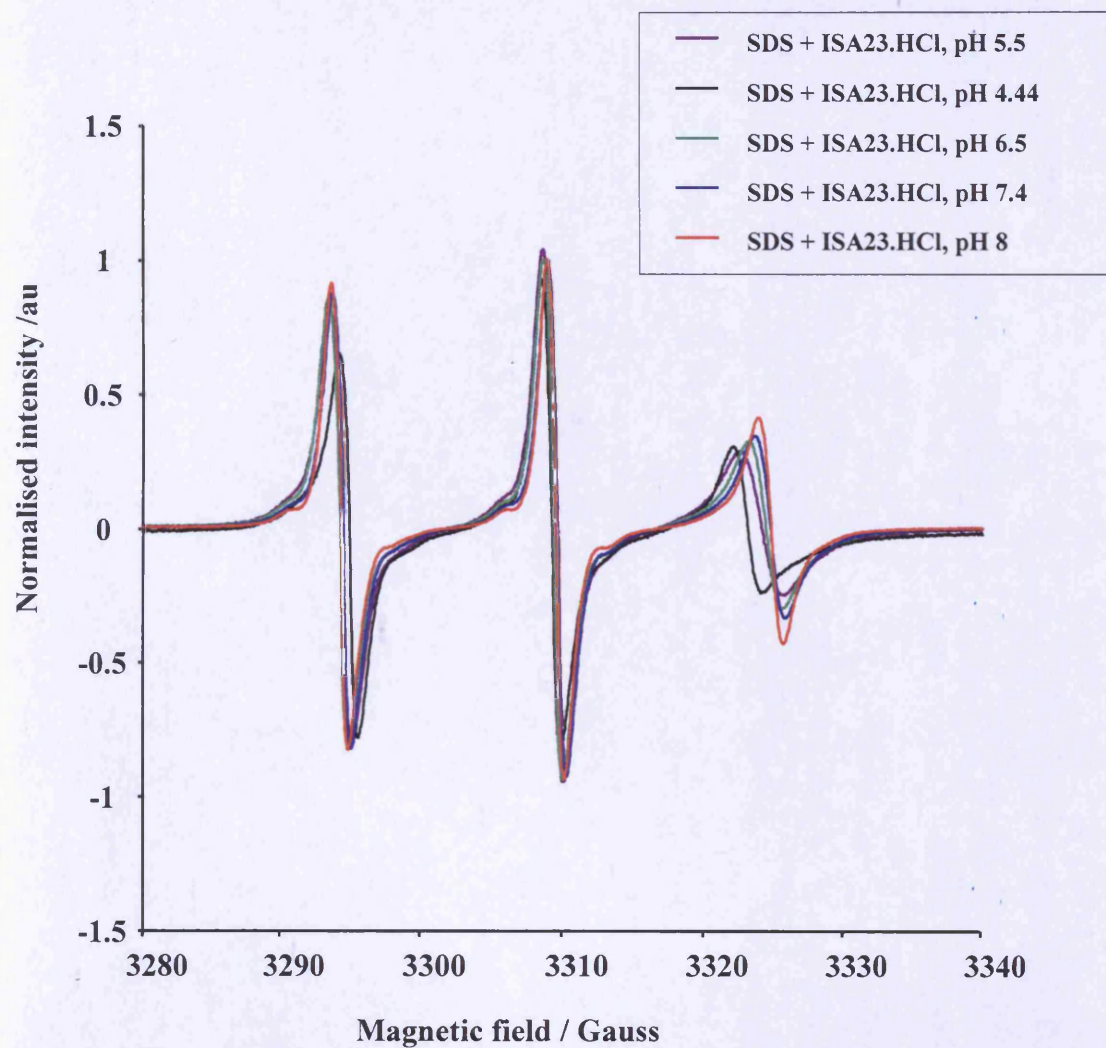


Figure 5.10 The EPR of SDS in the presence of ISA23.HCl as a function of pH.

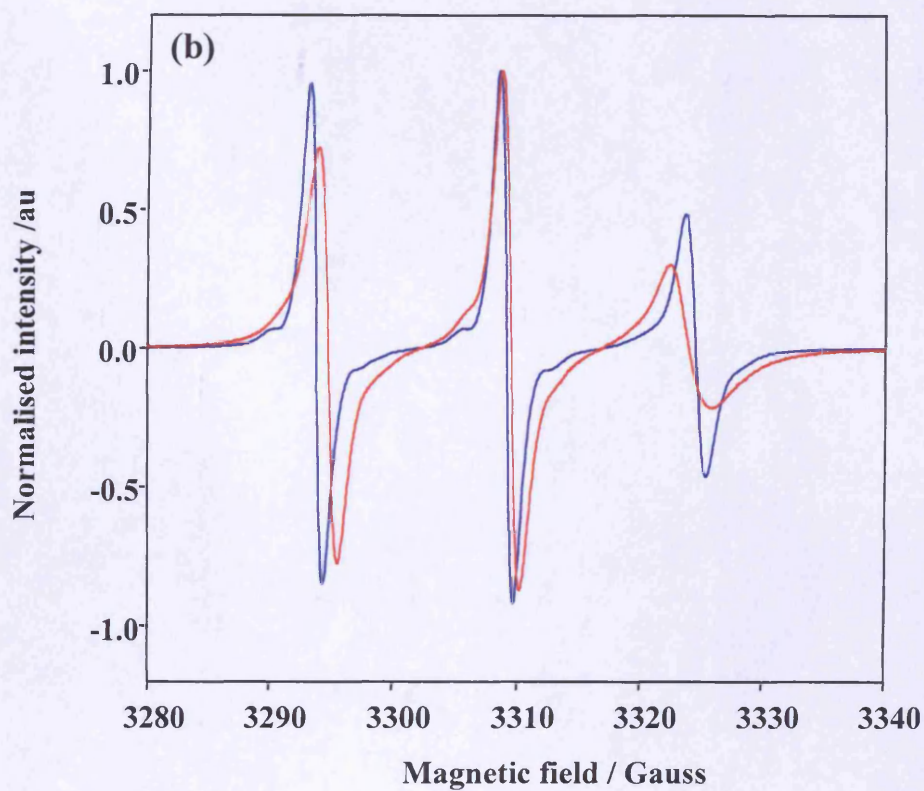
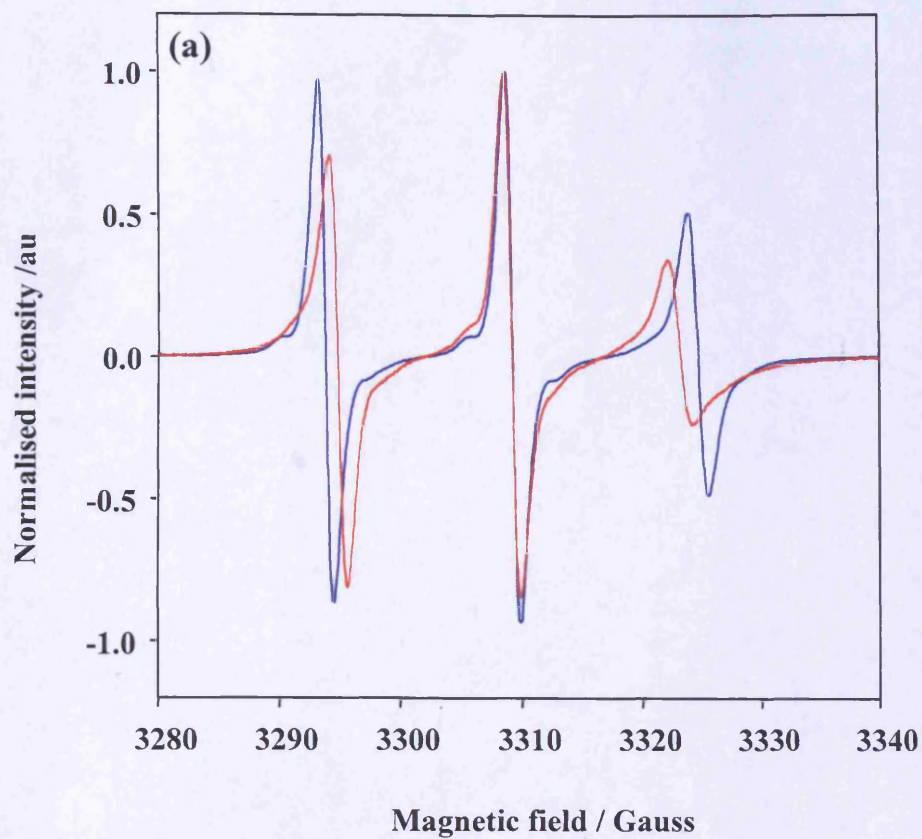


Figure 5.11 The effect of ISA23.HCl on the fluidity of SDS micelles, as a function pH. EPR spectra of SDS in the presence (red line) and absence (blue line) of ISA23.HCl at pH 4.5 (panel a) and pH 5.5 (panel b)

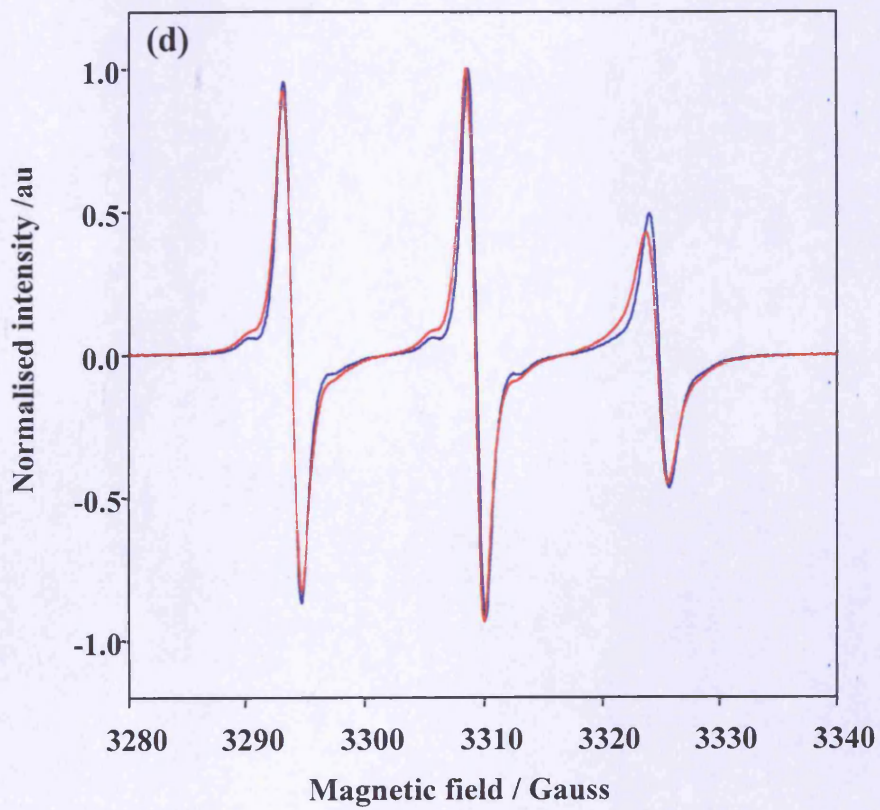
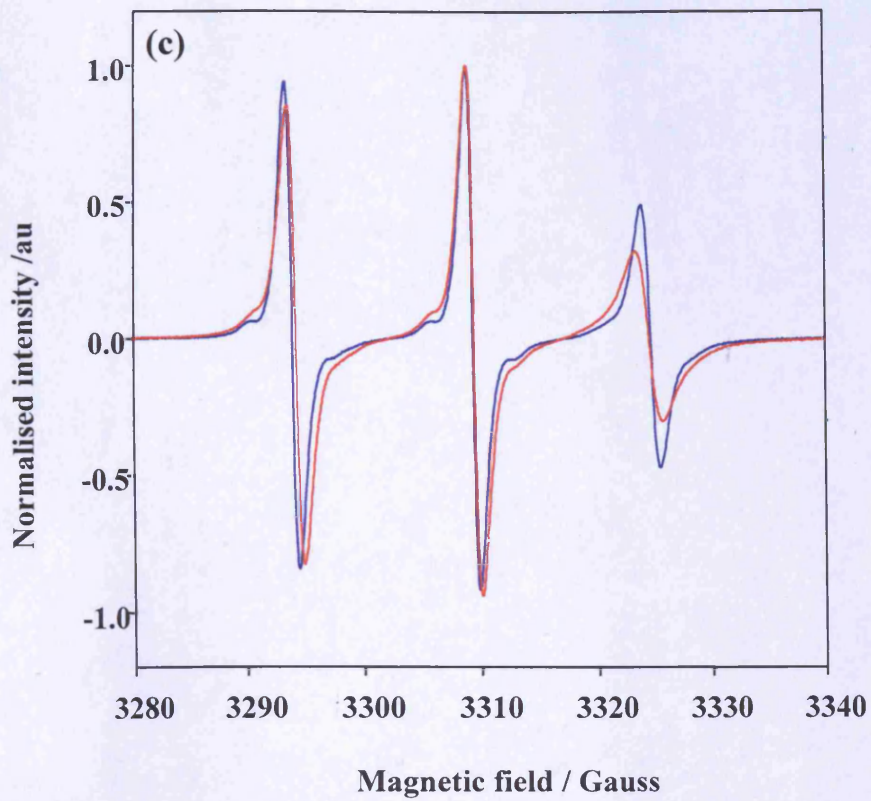


Figure 5.11 (continued). The EPR spectra of SDS in the presence (red line) and absence (blue line) of ISA23.HCl at pH 6.5 (panel c) and pH 7.4 (panel d)

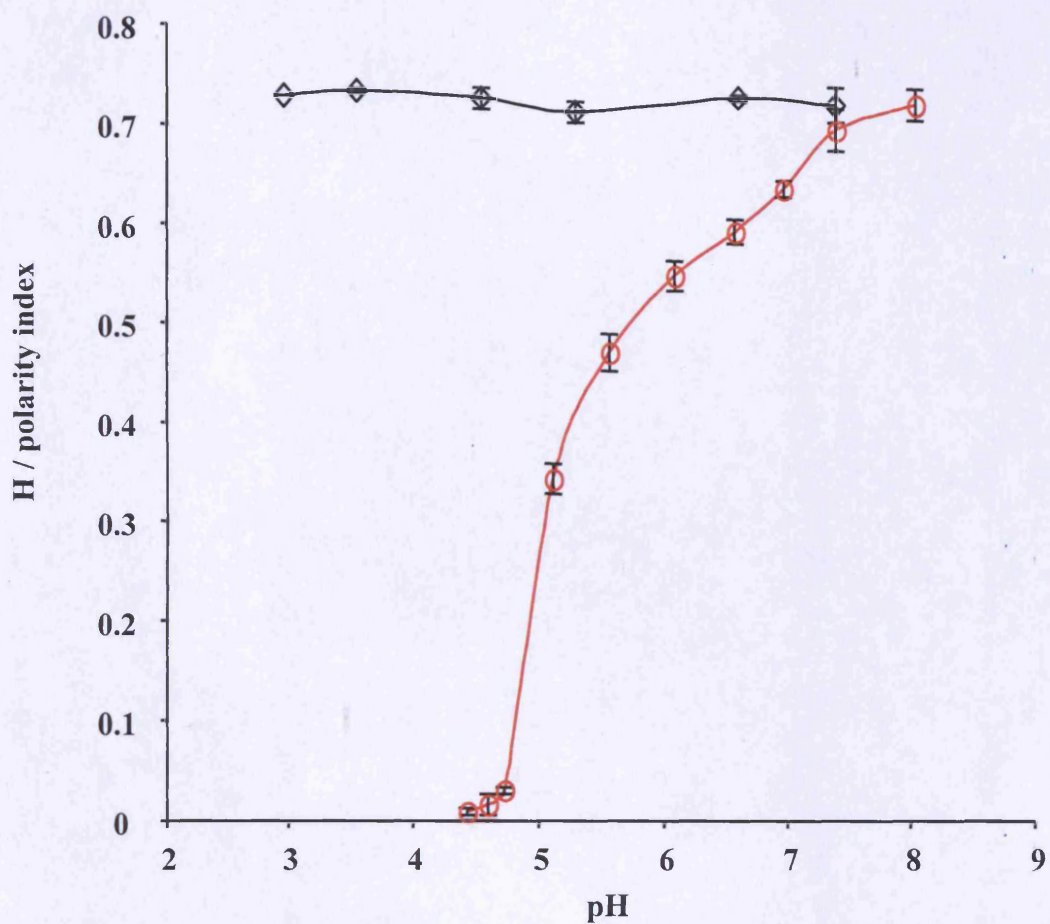


Figure 5.12 The polarity of SDS micelles in the presence (open circles) and absence of ISA23.HCl (open diamond) as a function of pH (the ratio between SDS and ISA23.HCl is 3.6:1).

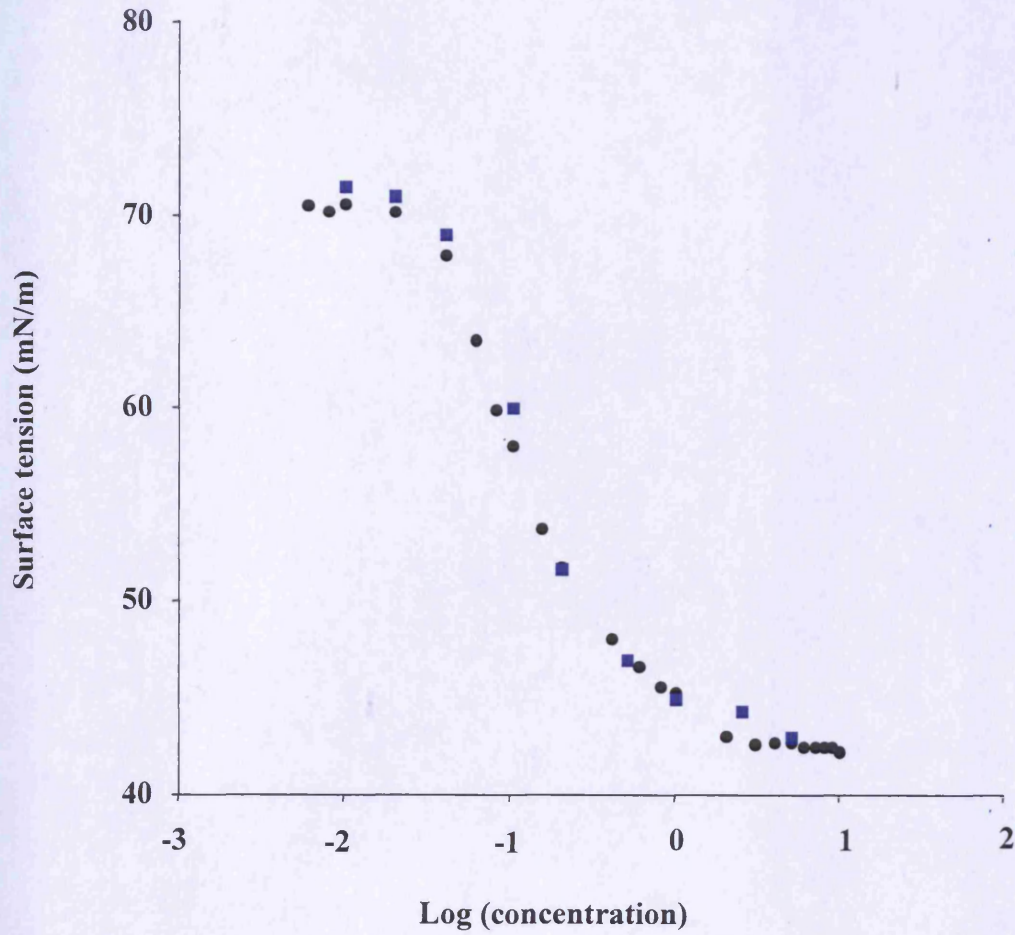


Figure 5.13 The surface tension of C₁₂BNMG in the presence (black circles) and absence (blue squares) of ISA23.HCl.

When the effect of pH on the interaction between ISA23.HCl and the SDS surfactant micelle was investigated, at pH 7.4, the surface tension of SDS/C₁₂BNMG was exactly the same in the presence and absence of ISA23.HCl. The same was also true at pH 5.5 (Figure 5.14a,b). However, at pH 4, there was a clear change in the surface tension in the presence of ISA23.HCl (Figure 5.14c). At pH 2 and 3, following the addition of ISA23.HCl, precipitation / phase separation occurred (i.e. the solution turned cloudy).

For the CTAB/C₁₂BNMG system, at pH 5.5, the surface tension of the surfactant mixture was altered slightly by the addition of ISA23.HCl (Figure 5.15). At pH 7.4, following the addition of ISA23.HCl, precipitation was observed.

5.3.4 Interaction of ISA23.HCl with Lyso-PC micelles

Lyso-PC is a phospholipid - based surfactant but unlike usual phospholipids, the lyso-PC contains only one hydrophobic chain. Due to the molecular shape of this surfactant molecule (cone shape), these form spherical micelles, and not the lamellar sheet or liposomes that are observed with normal phospholipids with two fatty acid chains. Due to this property, and the fact that phosphatidylcholine is the most abundant phospholipid found in the biological membrane, lyso-PC was chosen as a more realistic surfactant model to investigate ISA23.HCl / membrane interaction.

The CMC of lyso-PC was shown to be ~ 2 mM, and it was invariant with pH. The surface tension of lyso-PC was not affected by the addition of ISA23.HCl at either pH 7.4 (Figure 5.16a), or pH 5.5 (Figure 5.16b).

Following the determination of ISA23.HCl interaction by SANS, the model used to fit the data (in the absence and the presence of ISA23.HCl) was the same as used for the SDS/ISA23.HCl system (see section 5.3.1). A number of parameters (e.g. scattering length density) were fixed to values that correspond to the lyso-PC micelles.

In the absence of polymer, the scattering of lyso-PC micelles did not change the pH 7.4, but the ellipticity was slightly affected by the reduction in pH. It increased from 1.3 (at pH 7.4) to 1.6 at (pH 5.5) (Table 5.3). The form of the scattering data of lyso-PC was also not altered by the presence of ISA23.HCl across the pH range 7.4 - 5.5 (Figure 5.17a,b). The shape of the micelle remained unaltered, and in the presence of ISA23.HCl and the same model was used to fit the data (Table 5.3).

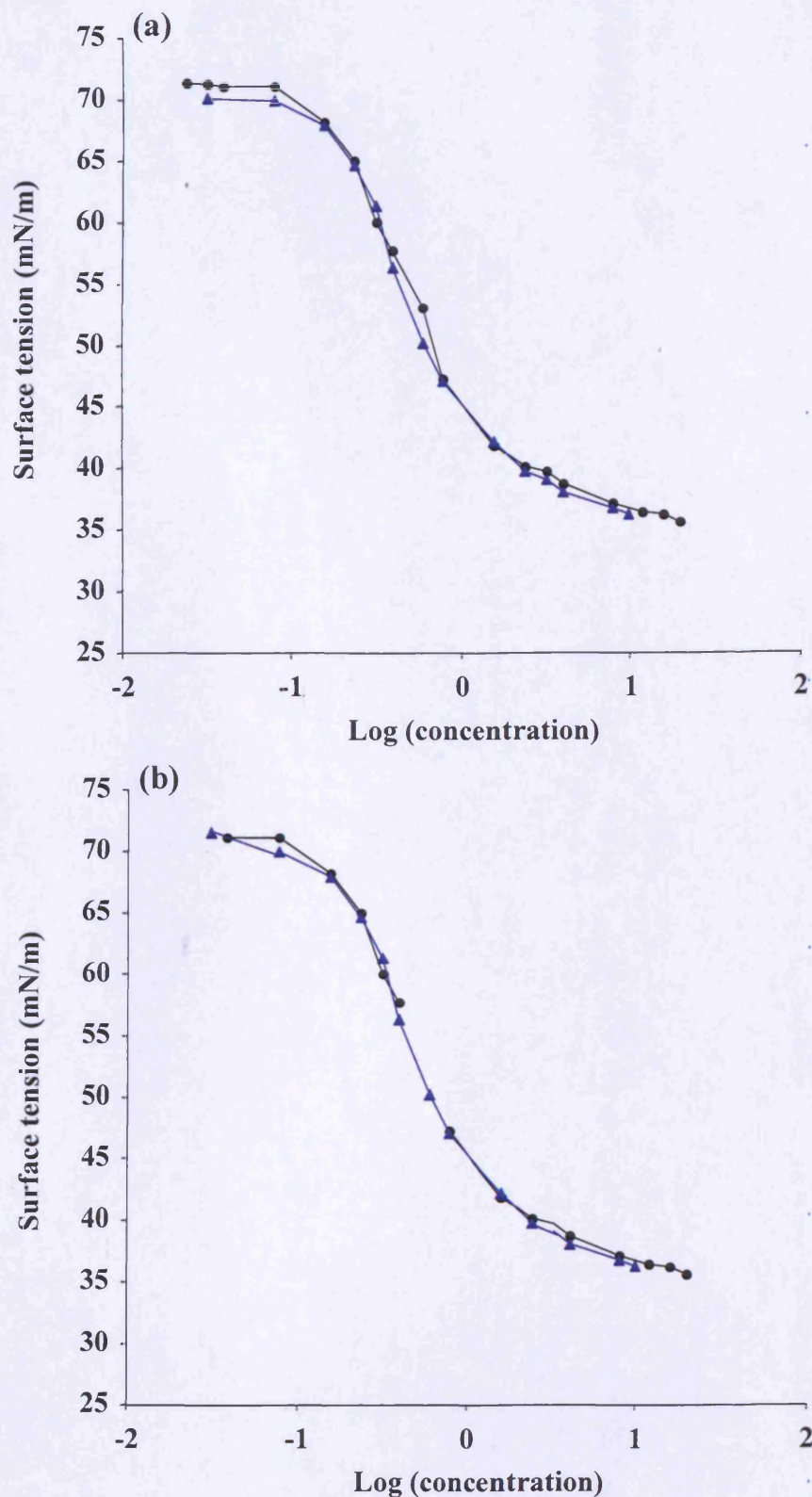


Figure 5.14 The surface tension curve of SDS/C₁₂BNMG in the presence (blue triangles) and absence (black circles) of ISA23.HCl at pH 5.5 (panel a) and pH 7.4 (panel b).

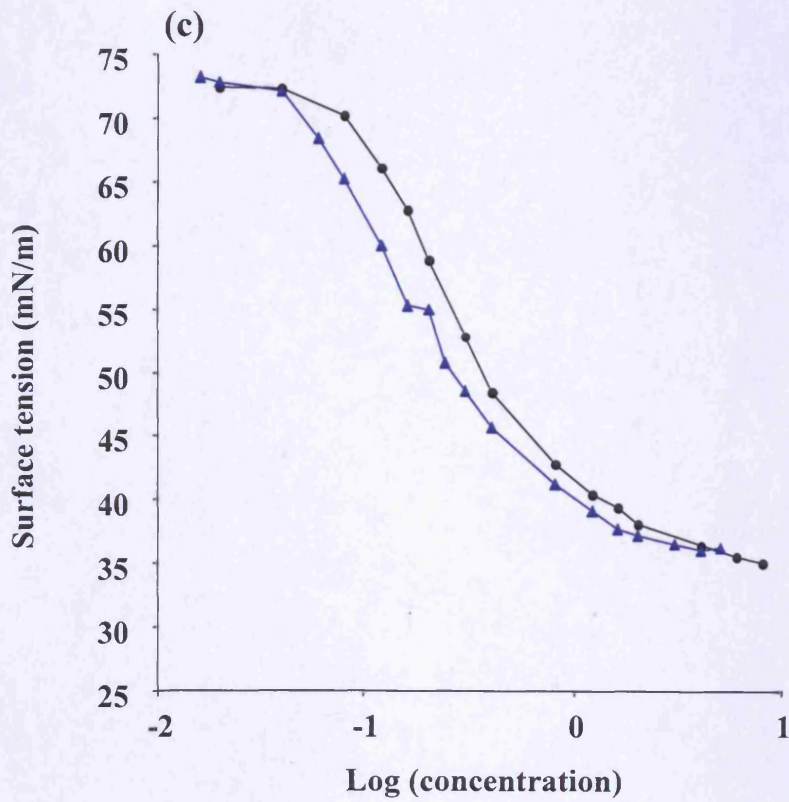


Figure 5.14 (continued). Panel (c) the surface tension curve of SDS/C₁₂BNMG in the presence (blue triangles) and absence (black circles) of ISA23.HCl at pH 4, it is very clear from this graph that there is an interaction

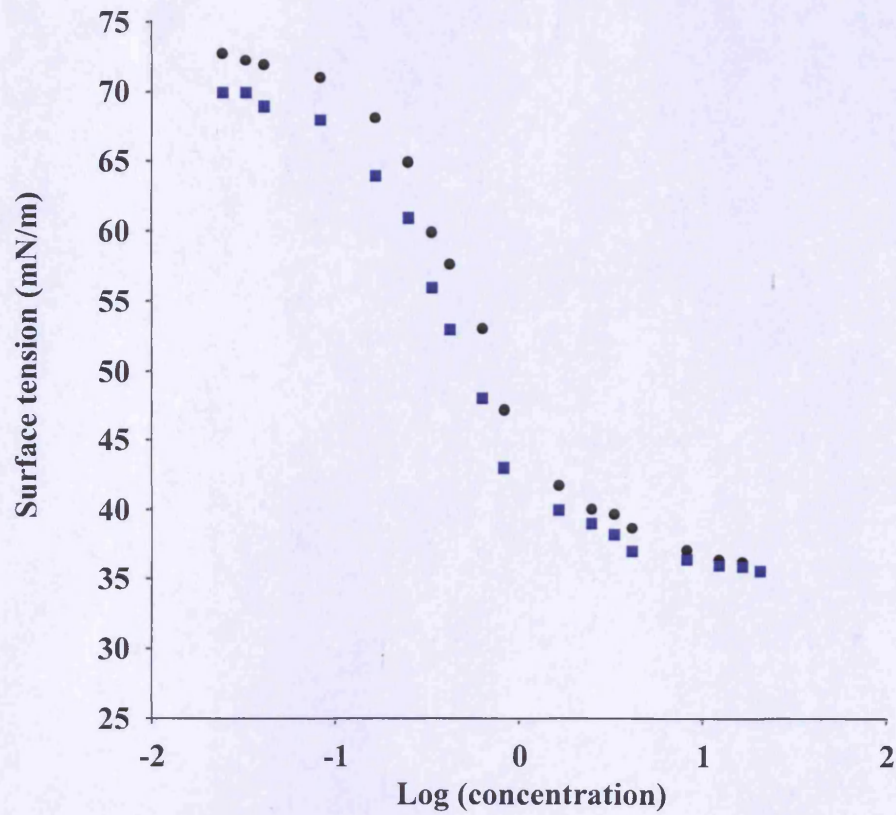


Figure 5.15 The surface tension curve of CTAB/C₁₂BNMG in the presence (blue squares) and absence (black circles) of ISA23.HCl at pH 5.5.

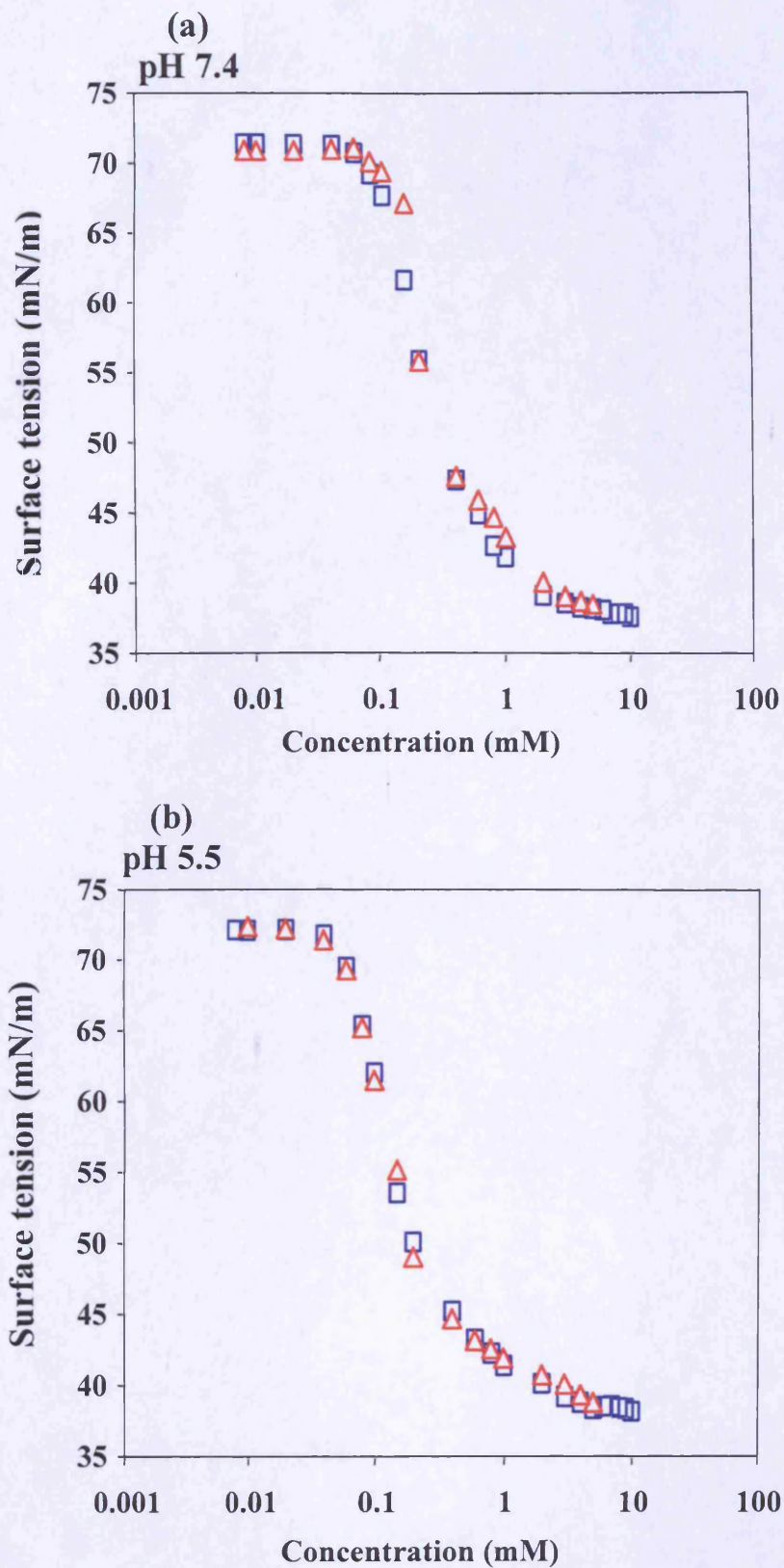


Figure 5.16 The effect of ISA23.HCl on the surface tension of lyso-PC. The surface tension of lyso-PC in the presence (open red triangles) and absence (open blue squares) of ISA23.HCl at pH 7,4 (panel a) and 5.5 (panel b), no interaction occurs between the polymer and the surfactant, at both pH values

Table 5.3 Summary of the parameters calculated from model fittings to lyso-PC in the presence and absence of ISA23.HCl at pH 5.5 and 7.4.

Parameter	Lyso-PC, pH 5.5	Lyso-PC + ISA23.HCl, pH 5.5
Radius of the core (Å)	20.5	21.9
Thickness of the shell (Å)	12.8	13.1
Ellipticity (X)	1.6	1.6
	Lyso-PC, pH 7.4	Lyso-PC + ISA23.HCl, pH 7.4
Radius of the core (Å)	20.4	21.1
Thickness of the shell (Å)	12.7	13.1
Ellipticity (X)	1.3	1.5

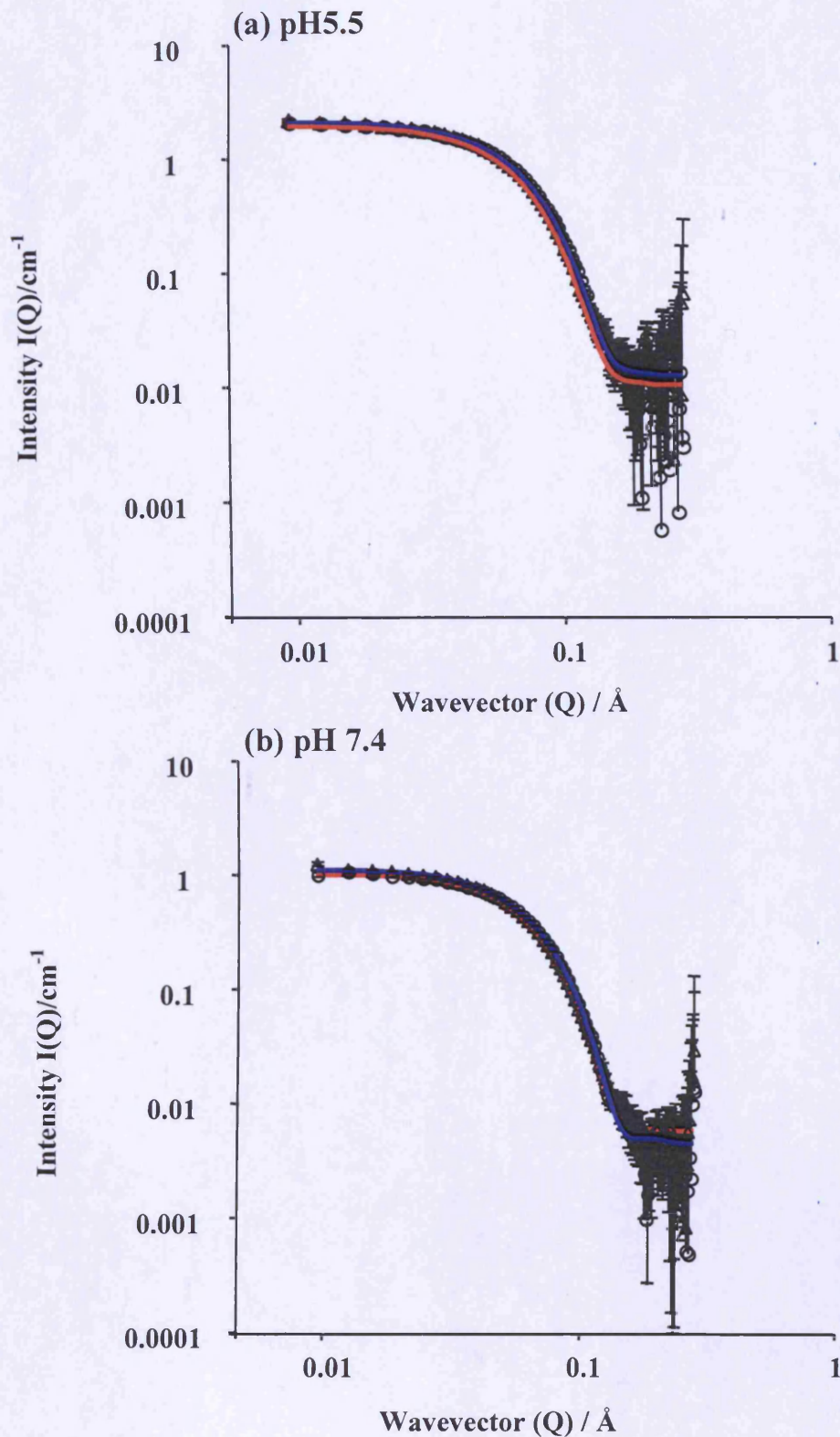


Figure 5.17 The effect of ISA23.HCl on the morphology of lyso-PC micelles. SANS data of lyso-PC micelles in the presence (open triangles) and absence (open circles) of ISA23.HCl at pH 5.5 (panel a) and pH 7.4 (panel b), plus their fittings (solid blue or red line), it is hard to distinguish between the SANS data of lyso-PC in the presence and absence of ISA23.HCl at both pH values

The LOWFIT program did not produce a fit for the EPR spectra of lyso-PC in the presence and absence of ISA23.HCl as a function of pH. Changing pH and the presence of ISA23.HCl, the line position, spacing and shape of EPR spectra were not altered (Figure 5.18 - 5.20). The polarity was calculated using equation 5.6 (see earlier), and this did not vary with pH or following the addition of ISA23.HCl.

5.4 Discussion

When examining the interaction of ISA23.HCl with charged micelles composed of SDS and/or $C_{12}E_4$ or $C_{12}BNMG$, by measuring surface tension, three different responses were observed, depending on the pH, and the composition of the micelles. These are summarised in Figure 5.21. Strong interaction, in this case at low SDS concentrations, where a single homogenous phase existed, and the positive charge on ISA23.HCl exceeded the amount of the negatively charged SDS particles. When the polymer-surfactant system had a positive charge it was soluble. As the concentration of SDS was increased, precipitation began to occur (two phases), and phase separation occurred close to the charge neutralisation. Both, inter-and intra-molecular interaction in the system accounts for this observation, as it is governed by the subtle balance between hydrophilic and electrostatic interaction (Bai et al, 2002). When the concentration of SDS was increased further, the polymer-surfactant system returned to single homogenous phase. In this case the negative charge of the SDS exceeds the positive charge of ISA23.HCl, and this leads to the stabilisation of the system (Figure 5.22).

For the weak interaction of ISA23.HCl and SDS, at a concentration above the CMC, the surface tension of the surfactant micelles increased following the addition of ISA23.HCl. This can be explained by the binding of the free surfactants molecules to ISA23.HCl, which caused the reduction of surface activity of the surfactant resulting in an increase in surface tension. Below the CMC, the surface tension of the surfactants decreased in the presence of ISA23.HCl. Since ISA23.HCl is not surface active, this observation indicates that the complex formed between the surfactants and ISA23.HCl accumulates at the surface causing a decrease in surface tension.

When there was no association between ISA23.HCl and surfactant (no interaction). This occurred due to the reduced cationic nature of ISA23.HCl, there was not sufficient positive charge of the polymer to cause interaction with the surfactant,

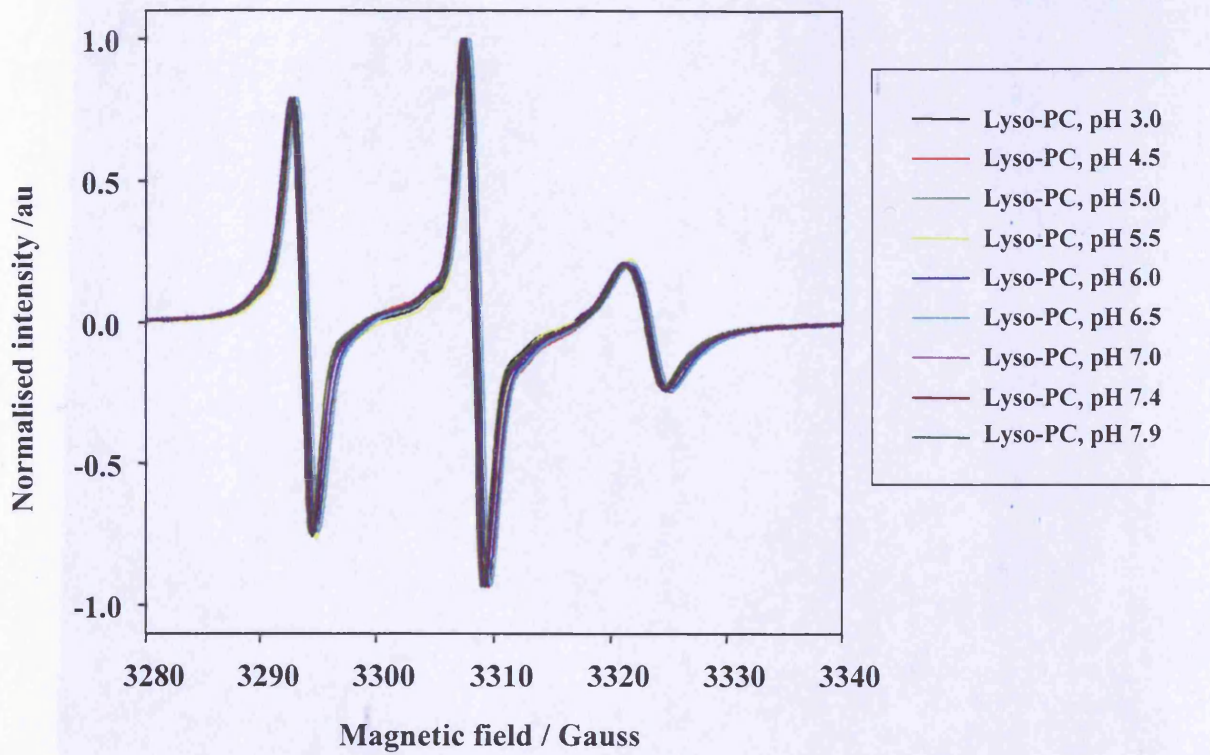


Figure 5.18 The EPR spectra of lyso-PC micelles as a function of pH.

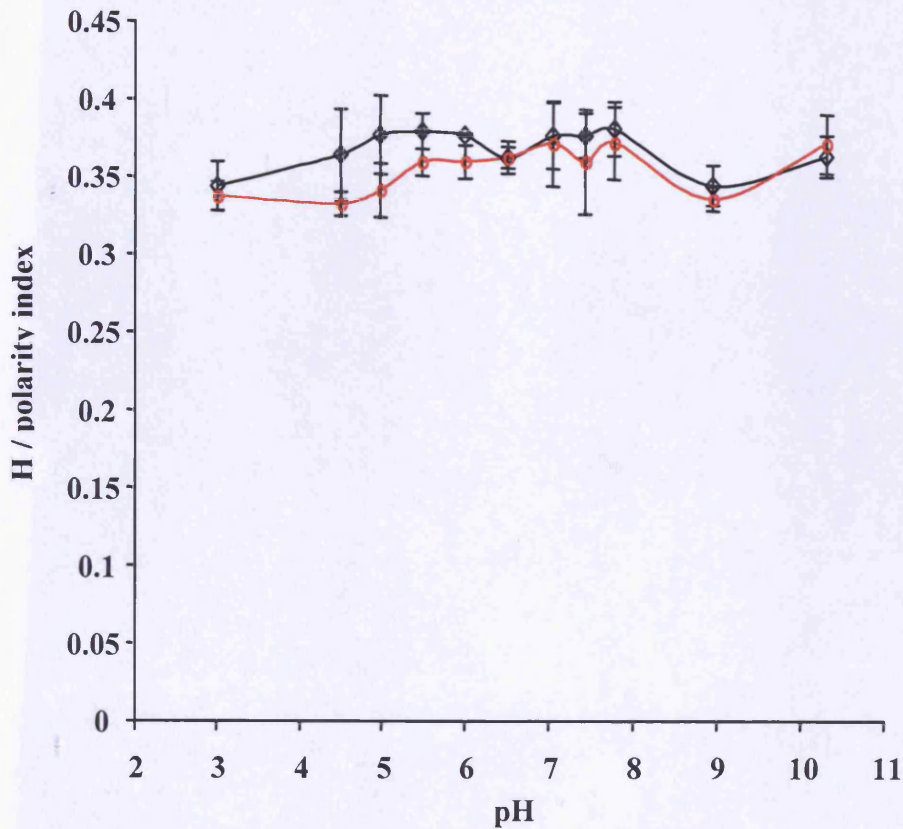


Figure 5.19 The polarity of lyso-PC micelles in the presence (open red circles) and absence of ISA23.HCl (open black diamonds) as a function of pH.

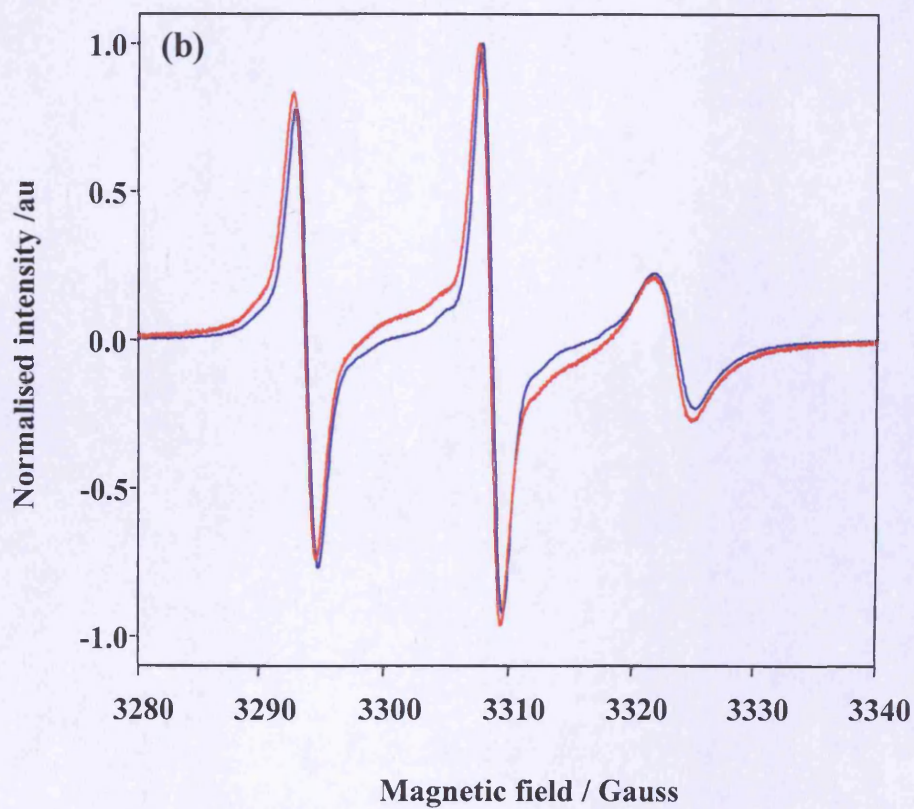
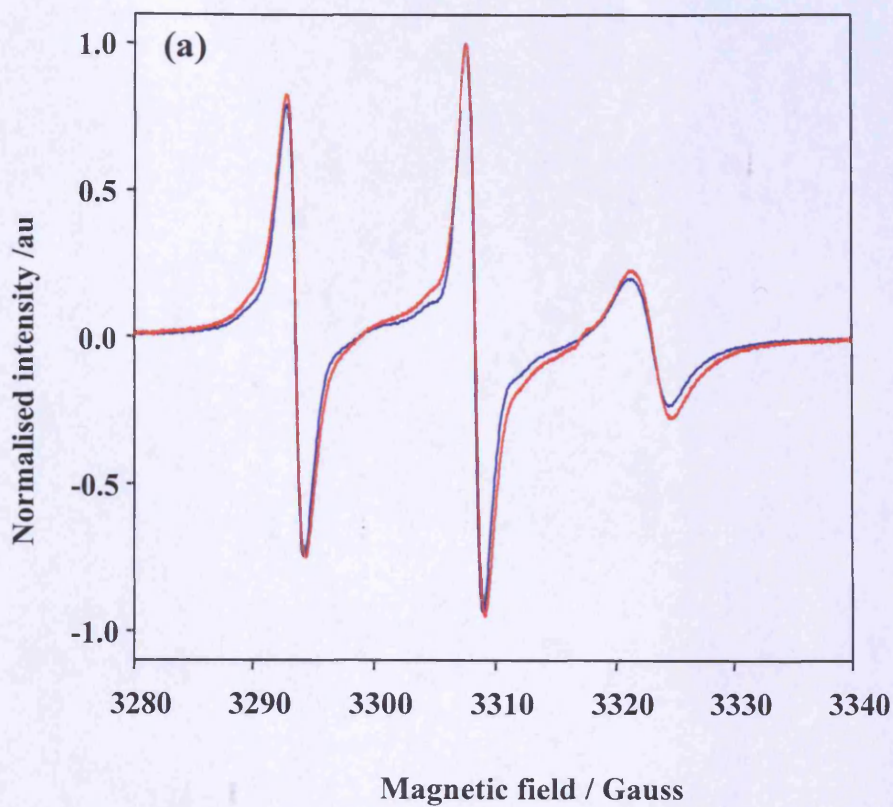


Figure 5.20 The EPR spectra of lyso-PC in the presence (red line) and absence (blue line) of ISA23.HCl at pH 5.5 (panel a) and pH 7.4 (panel b).

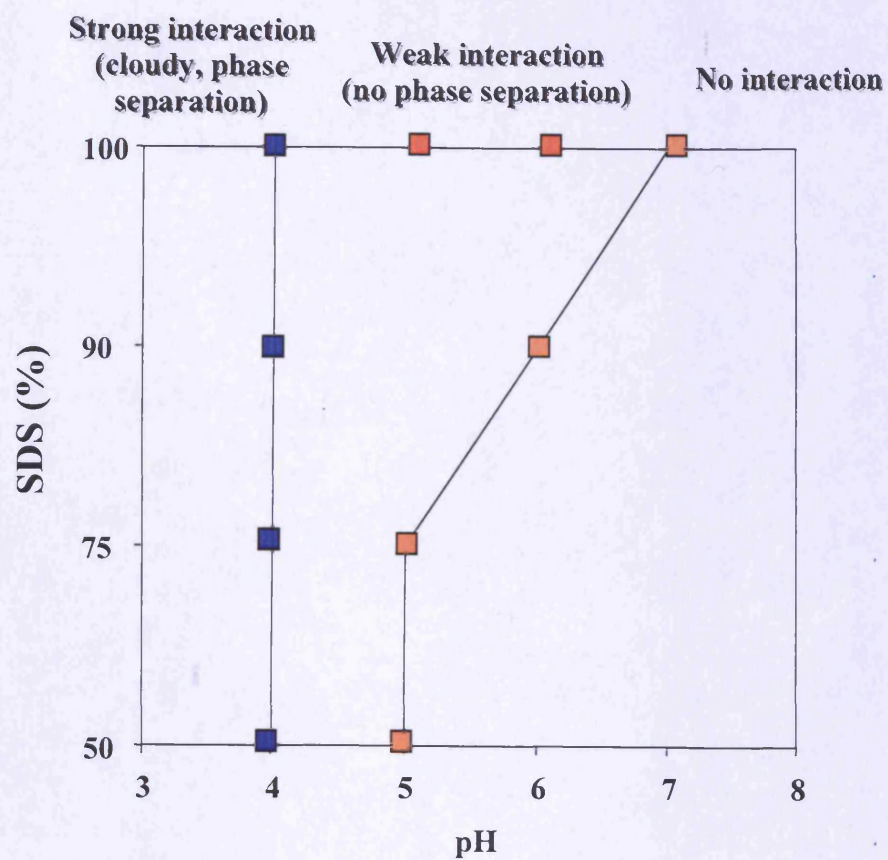


Figure 5.21 Summary of the ISA23.HCl interaction with SDS/C₁₂E₄ micelles using surface tension.

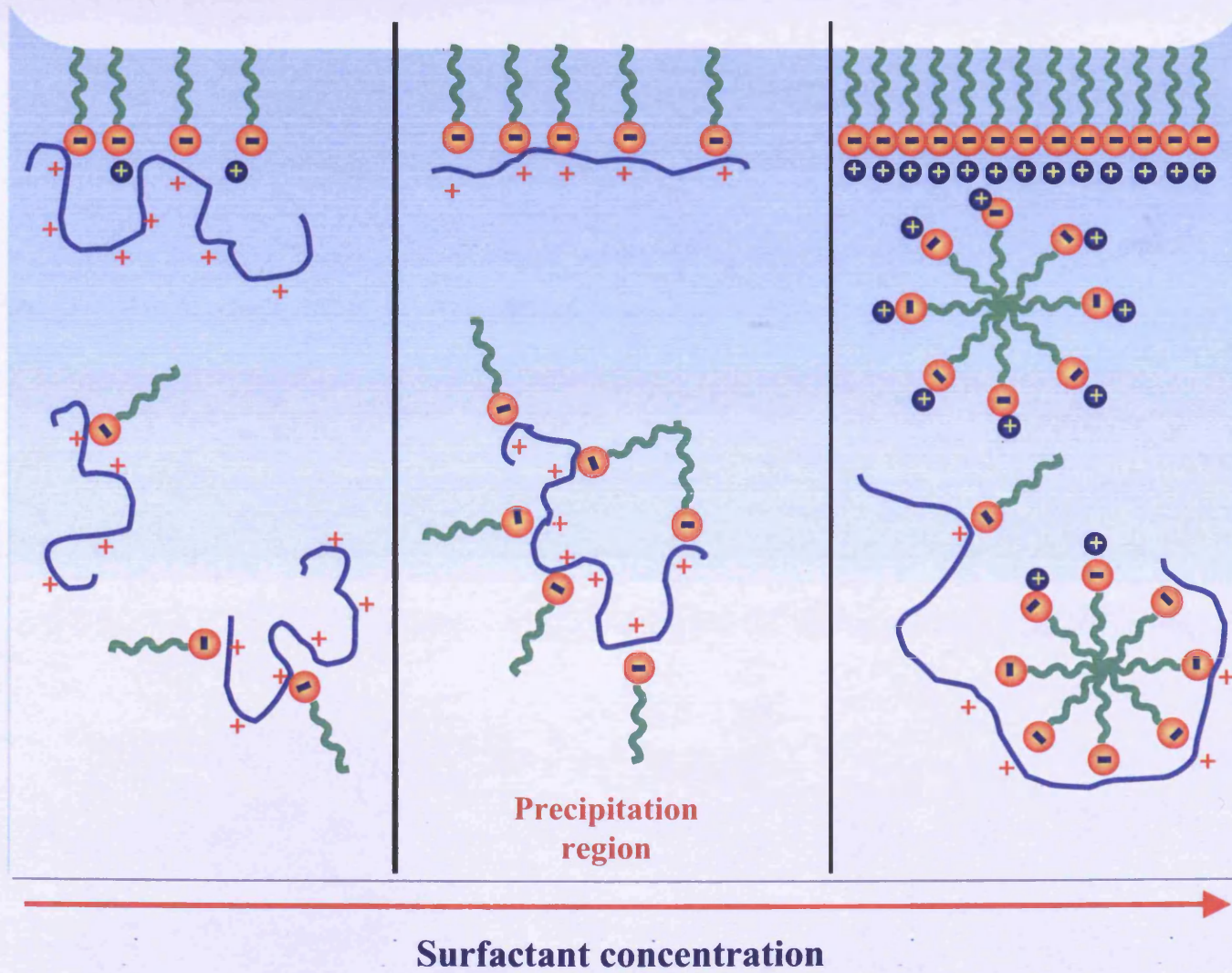


Figure 5.22 The schematic diagram which represent the hypothetical interaction of ISA23.HCl with SDS molecules as a function of surfactant concentration (adapted from Goddard, 2002).

thus the surface tension remained exactly the same in the presence of ISA23.HCl.

Polyelectrolytes and oppositely charged surfactants form aggregates that occur at a point known as the critical aggregation concentration (CAC), which is usually below the CMC (Voisin and Vincent, 2003). However, in the case of the SDS-ISA23.HCl and SDS-C₁₂E₄-ISA23.HCl systems, a CAC was not observed. It is not clear why. Possibly there was not a high enough surfactant concentration reached to detect it. However, this could also be due to the nature of interaction between the surfactants and the polymer, or the fact that the aggregates formed were too small to be detected by the surface tension measurements.

The effect of ISA23.HCl on the fluidity of the SDS micelles measured by EPR was pH-dependent. At low pH values, it was not possible to fit the EPR spectra of SDS micelles using LOWFIT program. This may have been due to the fact that the addition of ISA23.HCl could either change the motion of the spin-probe from isotropic to anisotropic, or it caused a decrease or an increase in the motion of the 16-DSE molecules themselves. From these studies, it is not possible to determine the exact reason, or if it is a combination of the two. As it was mentioned earlier, EPR can also be used to obtain information on the hydration of the micelle and how this was effected by the presence of ISA23.HCl. At low pH following the addition of ISA23.HCl, the polarity is low (the number of water molecules on the surface of the micelle), so the water molecules at the surface of the micelles would be replaced by ISA23.HCl molecules. As the pH increases, ISA23.HCl become less positively charged and the interaction with the oppositely charged surfactants becomes weaker. This would cause a decrease in the number of polymer molecules at the surface of the micelles, and they would be replaced by water molecules (Figure 5.23).

From the SANS results, ISA23.HCl and SDS micelles produced three interaction responses, these were further investigated using SANS. At pH 4 (strong interaction with precipitation), the SANS showed that ISA23.HCl caused the SDS micelle overall sphere size to increase and become more elongated. The data indicated that the polymer wrapped around the micelle changing its overall radius. This could be due to the intercalation of the polymer into the shell of the micelle, which is due to the charge interaction of the polymer and the SDS headgroups (Figure 5.23).

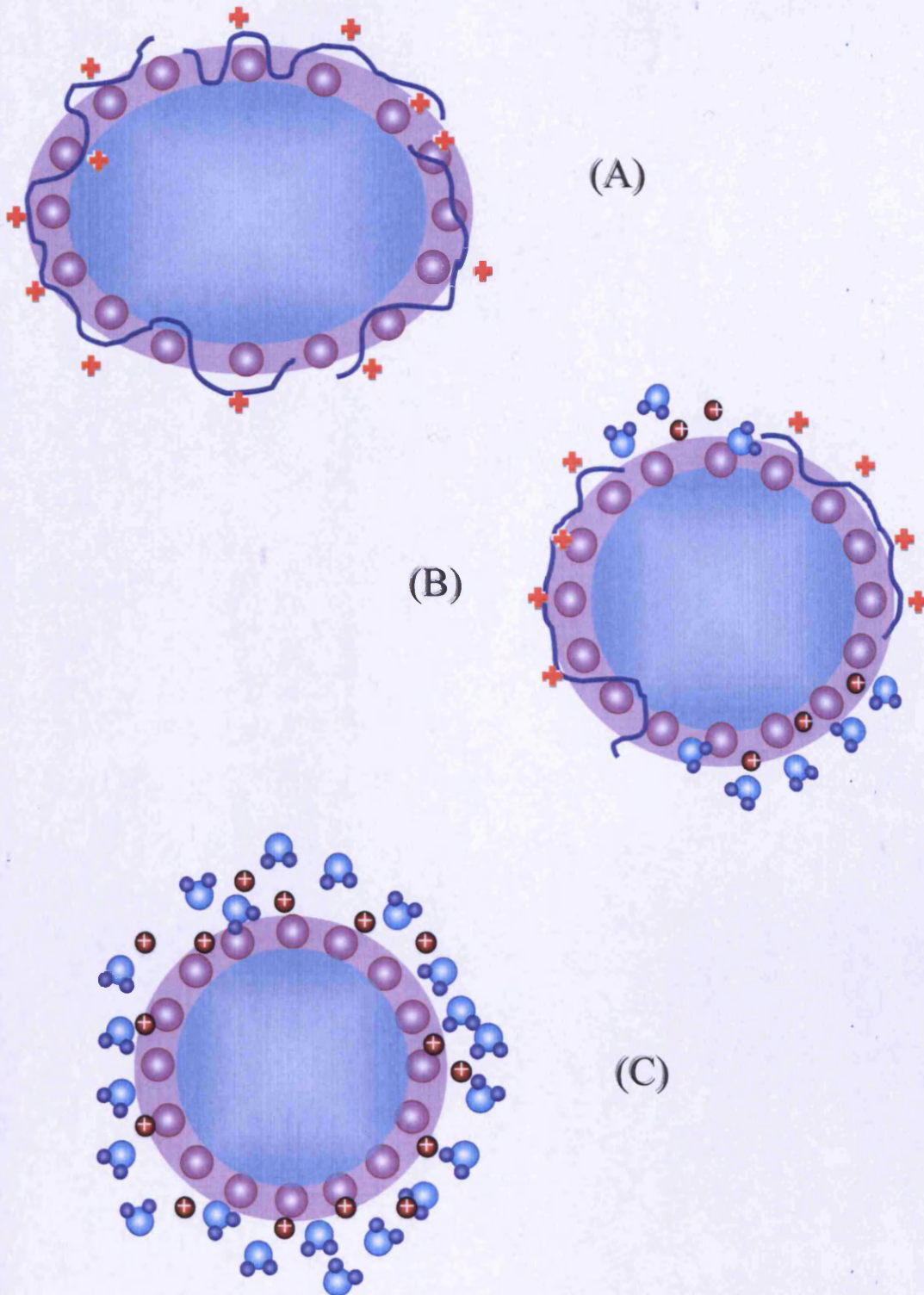


Figure 5.23 The possible structures that represent the three different possible responses observed in SANS and EPR study. The strong interaction (pH 4, panel A), the weak interaction (pH 5.5, panel B) and no interaction (pH 7.4, panel C)

At pH 5.5 (weaker interaction, no phase separation), SANS data suggested the size of the SDS micelle was slightly affected by ISA23.HCl but at lesser extent than seen at pH 4 (Figure 5.23).

At pH 7.4, SANS showed that ISA23.HCl had no effect on the size of SDS micelles. At this pH, only 50% of one of the amine groups of the ISA23.HCl is positively charged, and at this pH all the carboxylic groups are negatively charged, thus the polymer carries an overall negative charge. As SDS is also negatively charged, repulsion would be presented, which is in agreement with the SANS observation (Figure 5.23).

For the lyso-PC-ISA23.HCl, the surface tension studies showed no interaction at pH 7.4 and 5.5, the surface tension of lyso-PC was not affected by the presence of ISA23.HCl. These observations were reinforced by the EPR and SANS studies. The EPR spectra of lyso-PC micelles in the presence and the absence of ISA23.HCl could not be fitted using LOWFIT. Again it is quite difficult to know why. The shape of the EPR spectra of the lyso-PC micelles remained the same following the addition of ISA23.HCl (this includes line shape, position and spacing), so it is possible to conclude that the speed and the type of motion of the lyso-PC molecules was not affected by ISA23.HCl. Overall, the polarity, shape and size of Lyso-PC micelles were also unaltered by the addition of ISA23.HCl, at both pHs. Where it was expected that no interaction would occur between lyso-PC and ISA23.HCl at pH 7.4 (due to the overall negative charge that is carried by the polymer) lack of interaction at pH 5.5 was perhaps surprising. At this pH, the polymer is more cationic in nature. However, it is important to note that the ISA23.HCl synthesised here did not produce significant haemolysis until the pH reached ~ 4 (Chapter 3). Either the polymer did not carry sufficient cationic charge to promote interaction with lyso-PC or the amphoteric polymer prefer self-association at this pH. When the interaction between lyso-PC and ISA23.HCl was measured at pH 3 and 4 using both surface tension and EPR (results not shown), still no interaction was seen. Perhaps this is also due to the zwitterionic nature of lyso-PC. The headgroup of lyso-PC is composed of positively charged groups (quaternary ammonium group, $(^+N)R_4$) and negatively charged groups (phosphodiester phosphate, pKa value of 1-1.7) (Marsh, 1990). Thus between pH 7.4 and 3, the lyso-PC molecule will carry both positive and negative charge, and the net charge is zero. The careful examination of the

structure of lyso-PC suggests, it might be quite difficult for ISA23.HCl to access and interact with the negatively charged headgroup due to the steric hindrance caused by the quaternary ammonium group. This would explain the lack of interaction seen. Molecular modelling could be used to investigate this further.

SANS of lyso-PC in the presence of TX-100, PEI or dextran were also conducted. These compounds were picked because they were used as “controls” in the haemolysis experiments (described in Chapter 3). TX-100 caused complete haemolysis. The SANS results show an interaction, as the scattering data of lyso-PC changed in the presence of TX-100 (Table 5.4, Figure 5.24a), it is possible that the micelles are not solely composed of lyso-PC but a mixture of lyso-PC and TX-100 molecules, which is due to TX-100 being a non-ionic surfactant. Dextran is a non-ionic polymer and was used as the negative control in the haemolysis experiments (produced ~ 0% haemolysis, see Chapter 3). It is expected that no interaction will occur between lyso-PC micelles and dextran, which is shown by the SANS data (Figure 5.24b). Finally, PEI was used as the positive control. It is clear from both the scattering data and the fitting parameters that there is no interaction between the micelles and the polymer, as there was no change in micelle shape and size (Figure 5.24c). This is unexpected, as PEI is a cationic polymer, and has a pKa value of ~ 9, so at pH 7.4 about 99% of the amine groups are positively charged. In the haemolysis assay (Chapter 3), PEI caused ~ 42% haemolysis at pH 7.4. It is quite hard to explain why no interaction exists between lyso-PC and PEI. It is possible that the high molecular weight of PEI, (M_w 750,000 g/mol) and its branched structures might cause the amine groups to be sterically hindered from the interaction with the opposite charges of the micelles. But this does not explain the haemolytical activity observed with PEI at pH 7.4. It is clear that the target also plays a key role, and just like for ISA23.HCl, the nature of lyso-PC can account for this result.

5.5 Conclusions

The strength of interaction between ISA23.HCl and the SDS, SDS/C₁₂E₄ and SDS/C₁₂BMNG depend on the pH and the composition of the surfactant mixture, thus the amount of the negative SDS particles and the amount of positive charges of ISA23.HCl polymer (can be varied by changing the pH or the concentration of the polymer), play a key role on polymer/micelle interaction. The window at which interaction occurs between polymer and surfactant, without phase separation is small,

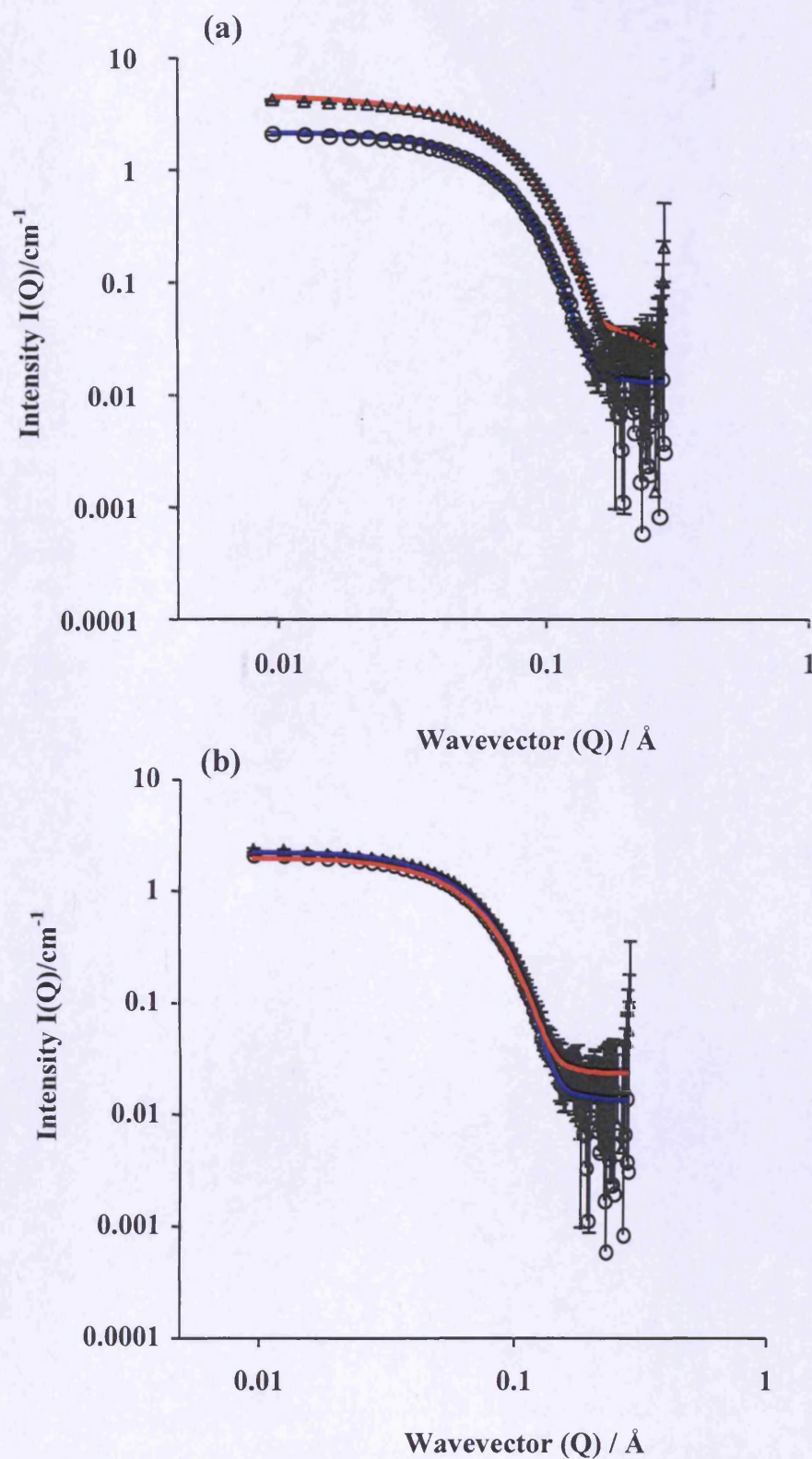


Figure 5.24 The effect of the control polymers used in the haemolysis assay on the morphology of lyso-PC micelles. SANS data of lyso-PC micelles in the presence (open triangles) and absence (open circles) of TX-100 (panel a) and dextran (panel b), plus their fittings (solid blue or red line), it is hard to distinguish between the SANS data of lyso-PC in the presence and absence of dextran

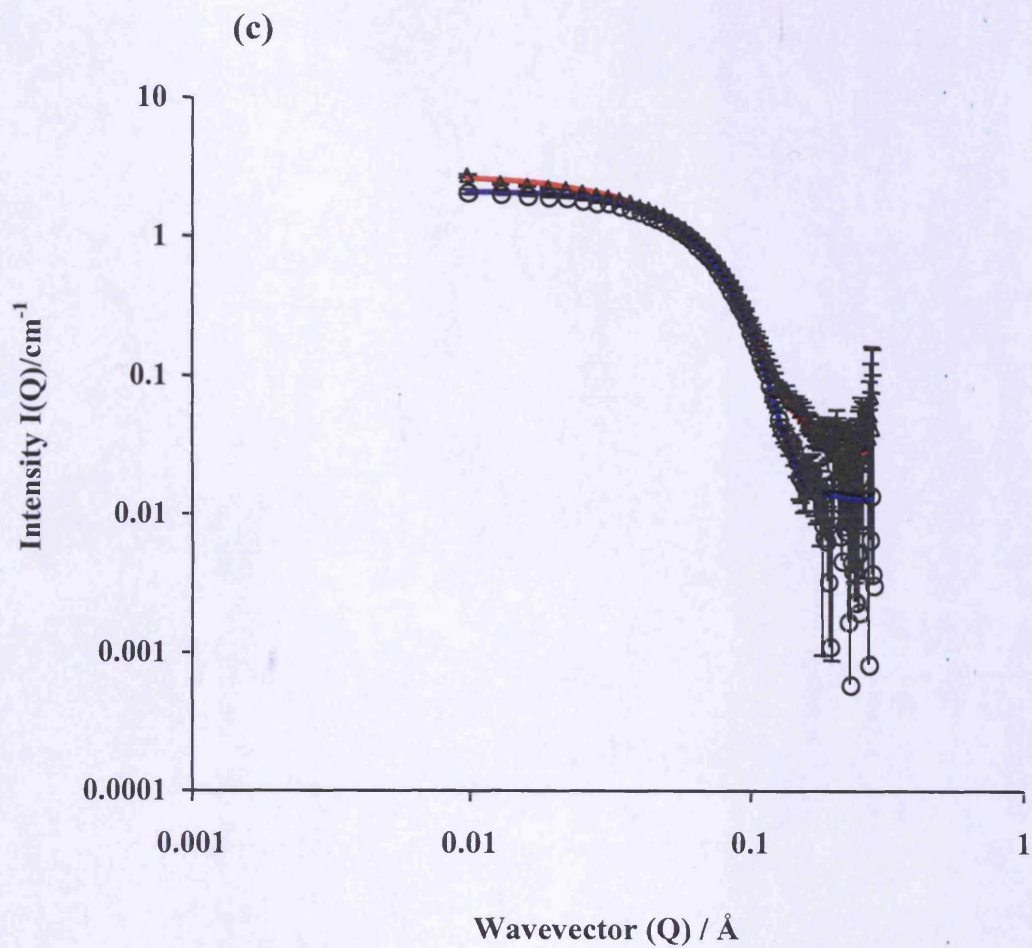


Figure 5.24 (continued). Panel (c) the SANS data of lyso-PC micelles in the presence (open triangles) and absence (open circles) of PEI, plus their fittings (solid blue or red line)

Table 5.4 Summary of the parameters calculated from the model fittings to the lyso-PC in the presence of TX-100, dextran and PEI.

Parameter	Lyso-PC + TX-100	Lyso-PC + dextran	Lyso-PC + PEI
Radius of the core (Å)	20.1	21.9	20.1
Thickness of the shell (Å)	11.1	12.6	12.7
Ellipticity (X)	1.2	1.2	1.3

but this increases with the increase of the negatively charged SDS molecules. So it is quite important to achieve the correct balance between the negative charges of the micelles to the positive charge on the polymer to cause sufficient interaction to measure using surface tension, but not too strong to cause phase separation. Changing the pH, i.e. the charge on the polymer has greater effect on the interaction between surfactants and ISA23.HCl than varying the amount of negative charges of the model surfaces. At acidic pH, ISA23.HCl is adsorbed at the surface of the micelles affecting the motion of the surfactant micelles and affecting their size, elongating its spherical shape. No interaction was observed with more biologically relevant lyso-PC surfactants at pH 5.5, and also there was no interaction observed between lyso-PC and PEI (positive control). These results are not as expected but the nature and the molecular structure of lyso-PC molecules is such that there is no displaceable water.

Chapter 6
Studies on the interaction
between ISA23 and liposomes

6.1 Introduction

In the previous chapter the interaction between ISA23.HCl and well-defined interfaces composed of non-ionic, anionic, cationic and zwitterionic surfactants was studied. A number of conclusions were drawn. Here, the validity of these conclusions was investigated further using more complex and biologically related models i.e. liposomes composed of the main phospholipids commonly found in the biological membranes, and what the endosomolytic polymer would meet during endocytic uptake.

6.1.1 Biomembranes and their organisation

Biological membranes (see Figure 1.2b in Chapter 1) are very complex heterogeneous structures composed of lipids, phospholipids and proteins. The main constituents are phospholipids, of which phosphoglycerides are the largest group, (Pollard and Earnshaw, 2002). They include phosphatidic acid (PA), phosphatidylglycerol (PG), phosphatidylethanolamine (PE), phosphatidylcholine (PC), phosphatidylserine (PS) and phosphatidylinositol (PI) (Figure 6.1) (Pollard and Earnshaw, 2002). Another important constituent of membranes are the saccharides containing lipids, the glycolipids, e.g. the sphingolipids and glycerol glycolipids.

As amphiphilic molecules, phospholipids have both hydrophilic and hydrophobic groups, they tend to orient and self-organise in polar and non-polar solvents, due to the hydrophobic and hydrophilic interactions (Dumitriu, 2002). The geometric packing constraint is an important factor in determining the structural organisation and the phase transition (White and King, 1985; reviewed in Seddon, 1990), and shape plays a key role in determining these parameters (Figure 6.2) (Shumilina and Shchipunov, 1997). Phospholipids usually adopt concentric bilayer vesicles in water (Dumitriu, 2002), but lamellar or hexagonal II phases are also observed depending on the length and the composition of the phospholipids hydrocarbon chain, the water content and temperature (Cullis and DeKruiff, 1978 and Seddon, 1984).

In general, the morphology of the aggregation formed by amphiphiles is determined by the ratio between the size of the hydrophilic and hydrophobic moieties, semi-empirically quantified via the packing parameter P . P is defined by $P = v / a l$, where v is the volume of the hydrophobic moiety, l is the length of the hydrophobic chain and a is the effective area of the cross-section of the polar group (Bhattacharya and Haldar, 2002) (Figure 6.2).

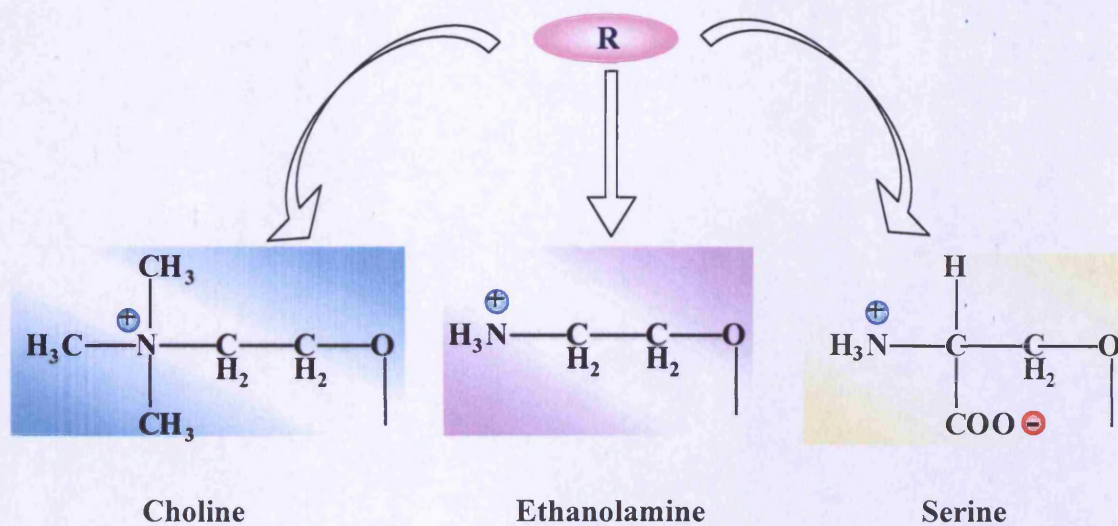
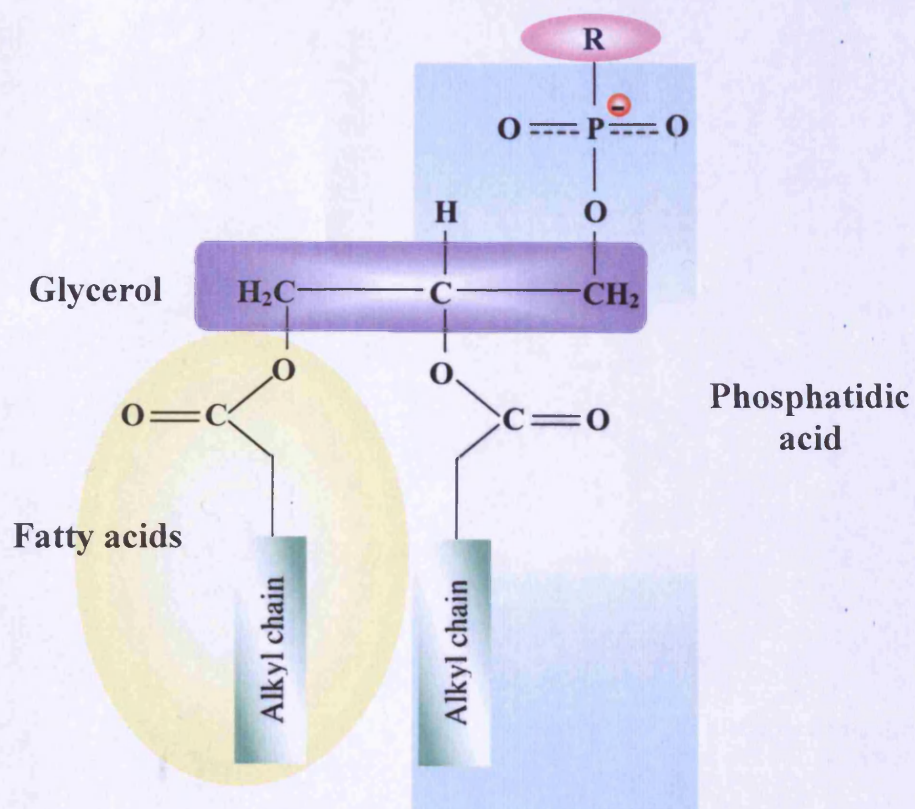
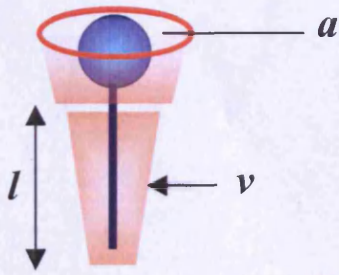
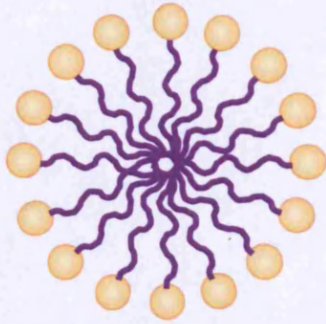


Figure 6.1 The major phospholipids found in biological membranes. Phosphatidyl derivatives of choline, ethanolamine or serine (adapted From McGilvery and Goldtein, 1981)

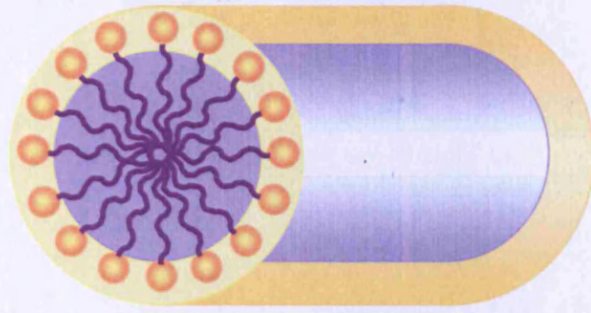
packing parameter P
 $P = v / a \cdot l$



Cone shape
 $P < 1/3$



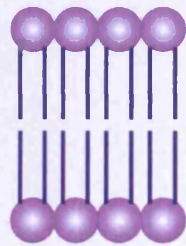
Spherical micelle



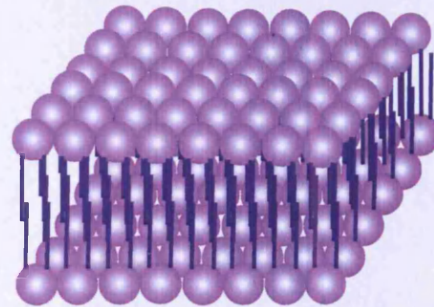
Rodlike micelles



Cylinder shape
 $P \sim 1$



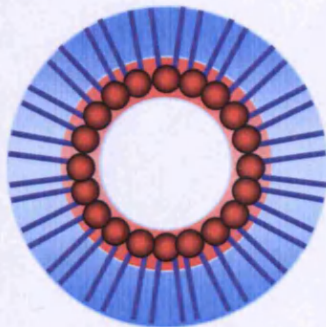
Lamellar



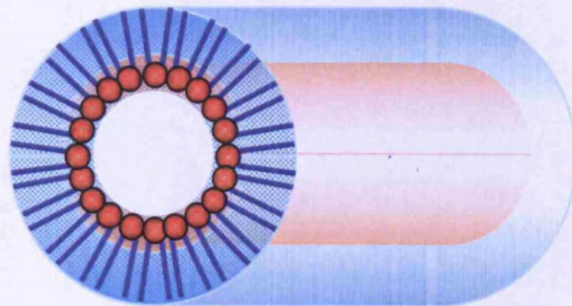
Bilayer



Inverted truncated cone
 $P > 1$



Inversed micelles



Rodlike inversed micelles

Figure 6.2 Schematic representation the packing parameter of amphiphiles. It can be seen that different aggregates can be formed depending on the shape of the amphiphiles (adapted from Lang et al)

For normal spherical micelles, $P < 1/3$, whilst for a bilayer $P \sim 1$. For values of $P > 1$, inverse structures are favoured (Dumitriu, 2002) (Figure 6.2). An amphiphile with a large headgroup and short saturated hydrophobic tail tends to form a spherical micelle, while an amphiphile with a small polar headgroup and a long saturated group will favour an inverted hexagonal morphology. Thus, factors that affect P include the size and nature of the polar headgroup, the length of the hydrocarbon chain(s), the presence of unsaturation and branching within the hydrophobic chain(s), temperature, pH and the presence of electrolytes (Bhattacharya and Haldar, 2002). It is therefore quite important to consider the molecular geometry of amphiphiles such as phospholipids, to understand better the organisation of phospholipid in biological membranes, which in turn defines their function and interaction with other molecules present in the membrane.

An important thermodynamic parameter of a lipids is its “transition temperature” (T_m). At low temperatures ($T < T_m$), the lateral movement of the hydrocarbon chain is restricted leading to a structure known as the gel phase. At high temperature, the hydrocarbon chain is mobile and disordered; and it is known as the fluid or liquid-crystalline phase (Dumitriu, 2002). Table 6.1 shows the main transition temperatures of the three phospholipids used in this study. Factors that affect the phase transition are those that also determine P , e.g. the type of hydrophilic headgroup, the presence of saturation and the length of hydrocarbon tail. T_m increases with chain length, as solid phases are stabilised by the additional increment in the van der Waals interaction between the hydrocarbon chains (Gauger et al, 2001). For certain phospholipids, e.g. PE, it is also possible to have a lamellar to non-lamellar hexagonal phase transition. Lipids that can adopt a hexagonal phase make up a substantial part of the biological membrane (30% of the total lipids) (Winter, 2002), therefore PE has an important role in determining the physical properties of the membrane, and the activity of membrane peptides and proteins (reviewed in Epan, 1998).

6.1.2 Selection of lipids compositions for these studies

To study ISA23-membrane interaction, liposomes composed of phospholipids, PC, PE and PS, were prepared. These phospholipids were picked as they are the most common or abundant phospholipids found in the biological membranes (plasma, endosome and lysosome) that ISA23.HCl will encounter at the cellular level (Table 6.2). The issues that need to be taken into account while choosing the phospholipids are

Table 6.1 Transition temperature of the phospholipids used to prepare the model liposomes in this study. It is important to consider the T_m while preparing the model liposomes

Phospholipid	Carbon : unsaturated	Transition Temperature T_m ($^{\circ}\text{C}$)
DPPC	16:0	41
DPPE	16:0	54
DPPS	16:0	63

Table 6.2 Summary of the major components of the three biological membranes, plasma, endosome and lysosome.

	Composition (in percentage) of the different biological membranes*		
	Plasma	Endosomal	Lysosomal
Phosphatidylcholine	39.89	55.41	31.34
Phosphatidylethanolamine	19.37	22.35	16.96
Phosphatidylinositol	4.36	1.35	4.68
Phosphatidylserine	8.73	4.7	11.54
Sphingomyelin	15.21	16.02	26.82
cholesterol	12.43	0	8.68
Total	100	100	100

* Adapted from Quinn, 1976; Robinson, 1975; Gallegos et al, 2002; Bergstrand et al, 2003; Evans and Hardison, 1984; Urade et al, 1988

the headgroup and the length and the presence of double bond in the fatty acid chain (i.e. unsaturated or saturated fatty acid chain). The exact phospholipids picked were DPPC, DPPE and DPPS. All these phospholipids have two unsaturated 16-carbon atoms in their fatty acid. These phospholipids were also used due to their availability of the deuterated form, allowing examination of the morphology of ISA23.HCl in the presence of the model liposomes.

Using liposomes as model membranes, has the advantage of being able to prepare different models of liposomes with a phospholipids composition similar to that of specific biological membranes (plasma, endosome and lysosome). However there are disadvantages of using liposomes as models. For example, in the case of plasma model-liposomes, liposomes surface curvature will be different (higher) from the cell surface. ISA23.HCl approaching the cell surface would be located towards the outside face of the plasma membrane as it is in the case of the liposomes.

In the case of endosome and the lysosome, the model-liposomes morphology is similar to that of intracellular vesicles. However, an endosomolytic polymer would normally be located inside the vesicles. In these experiments ISA23.HCl is added to the outside of the liposomes. Therefore, the curvature and the surface tension of the membrane will be different compared to the normal physiological situation. This will likely effect how the polymer associate / interact with and cause damage to the lipid bilayer.

Another major difference between the real biological membrane and the model liposomes, is the absence of proteins and cholesterol in the model system, where they are found in all biological membranes, and this will also have an effect on the action of the polymer.

The aims of this study were:

- (i) Prepare liposomes composed of DPPC, DPPE and DPPS, with a composition similar to that of the plasma, endosome and lysosome membranes (see Table 6.2 for the phospholipids composition of the three biological membrane).
- (ii) The stability of the liposomes were assessed as a function of time and pH.
- (iii) Prepared liposomes with calcein-entrapped liposomes. By studying the release rate of the dye and the use of different dyes with different molecular weight, it was possible to get information on the mechanism by which the polymer causes membrane destabilisation, and the size of the pore caused by the polymer.

- (iv) SANS was used to study the effect of the ISA23.HCl on the morphology of plasma model-liposomes (at pH 7.4, 37 °C), endosomal model-liposomes (at pH 5.5 and 4) and lysosomal model-liposomes (at pH 5.5 and 4).
- (v) Through the use of deuterated phospholipids, SANS experiments permit the study of the target/model membrane (plasma-, endosomal-, and lysosomal- model liposomes) and the morphology of ISA23.HCl.
- (vi) Finally, the interaction between endosomal- and lysosomal model-liposomes and the “controls” in the haemolysis experiments (TX-100, dextran and PEI), were also investigated in order to compare their interaction to that of ISA23.HCl.

6.2 Methods

6.2.1 Preparation of liposomes and stability testing

Preparation of liposomes

Liposomes composed of protonated and deuterated DPPC/DPPE/DPPS with the phospholipids composition similar to that of the plasma, endosomal and lysosomal membranes (Table 6.3 presents the composition) were prepared using a freeze/thaw extrusion method. The size of the resultant liposomes was characterised using PCS, for full details regarding the preparation of liposomes please see Chapter 2, section 2.3.3.

Stability testing of the liposomes.

To test the stability of liposomes during storage at 4 °C, their stability was assessed over two days (following liposome preparation), at pH 7.4, 5.5, 4 and 3. The stability assessment was performed by measuring the size of the liposomes using PCS at room temperature. A stock liposome solution was prepared at pH 7.4 (10 mM in 2 ml), the desired pH of the other samples was achieved by the addition of HCl. The stability of these liposomes (all with a final phospholipids concentration of 4 mM) was analysed using PCS.

Preparation and purification of calcein-entrapped liposomes

The calcein-entrapped liposomes were prepared in exactly the same manner as empty liposomes, with two differences 1) the aqueous phase contained 4 mM calcein and 2) an extra step was required to remove the free (non-entrapped) calcein from the calcein entrapped-liposomes. Several methods were attempted to remove the material:

- 1) Ultracentrifugation:

Table 6.3 The molar ratio of the three phospholipids used to prepare the liposomes.

Liposomes		Molar ratio
		DPPC : DPPE : DPPS
Plasma	Protonated	0.59 : 0.28 : 0.13
	Deuterated	0.59 : 0.28 : 0.13
Endosome	Protonated	0.67 : 0.27 : 0.06
	Deuterated	0.67 : 0.27 : 0.06
Lysosome	Protonated	0.52 : 0.28 : 0.19
	Deuterated	0.52 : 0.28 : 0.19

- a) 35,000 rpm for one hour (Kusonwiriawong et al, 2003)
- b) 200,000 g (43,000 round per minutes, rpm) for 20 minutes (Tokudomea and Sugibayashia, 2004)

2) Centri-prep Filtration

Centrifuged at a speed of 2000 rpm for 20 min.

3) PD50 and PD25 columns

For both columns, the liposomes were diluted 1 in 5, and 0.5 ml of this solution was added to the column. PBS (pH 7.4) was used as the mobile phase.

To break the liposomes and estimate the entrapped calcein, the liposomes fraction was diluted 1 in 50, and 10 μ l of 5% TX-100 was added to 2 ml of the diluted liposomes solution. The fluorescence of the sample was measured at room temperature.

6.2.2 SANS measurements

The neutron scattering of deuterated and protonated liposomes in the presence and absence of ISA23.HCl was measured (Table 6.4). All the samples were prepared in D₂O, and the pH of the samples was altered using 1, 0.1 M of HCl or NaOH. Prior to SANS measurements, 1 ml of liposomes solution (4 mM) and 1 ml of either D₂O (SANS of the liposomes alone) or 1 ml ISA23.HCl (the SANS of liposomes in the presence of polymer) for solution (5 wt%) were added to glass vial, and this was allowed to equilibrate for about 10 min. Then, 0.5 ml of the sample was added to UV-spectrophotometer grade, quartz cuvettes. SANS measurements were conducted at 37 °C on the LOQ diffractometer, at the ISIS. For the protonated liposomes systems the scattering was measured for 30 min and for the deuterated liposomes system it was for 45 min.

6.3 Results

6.3.1 Liposome characterisation

Following the hydration step the liposomes obtained were large with an average diameter of 262 nm. Following 5 cycles of freezing and thawing, three liposome populations were formed having an average diameter of 285, 361 and 609 nm respectively. After 10 cycles of liposomes extrusion through 200 nm membrane, the diameter of the liposomes was on average 217 nm (Figure 6.3a). Finally, following 20 cycles of extrusion through 100 nm, the size of the liposomes decreased to an average

Table 6.4 Experiments undertaken to study liposomes ISA23 interaction.

	Liposomes	pH	Polymer
Plasma	Protonated	7.4	± ISA23.HCl
	Deuterated	7.4	± ISA23.HCl
		7.4	PEI, Dextran and TX-100
Endosome	Protonated	5.5	± ISA23.HCl
		4	± ISA23.HCl
		5.5	± ISA23.HCl
	Deuterated	4	± ISA23.HCl
		7.4	PEI
Lysosome	Protonated	5.5	± ISA23.HCl
		4	± ISA23.HCl
		5.5	± ISA23.HCl
	Deuterated	4	± ISA23.HCl

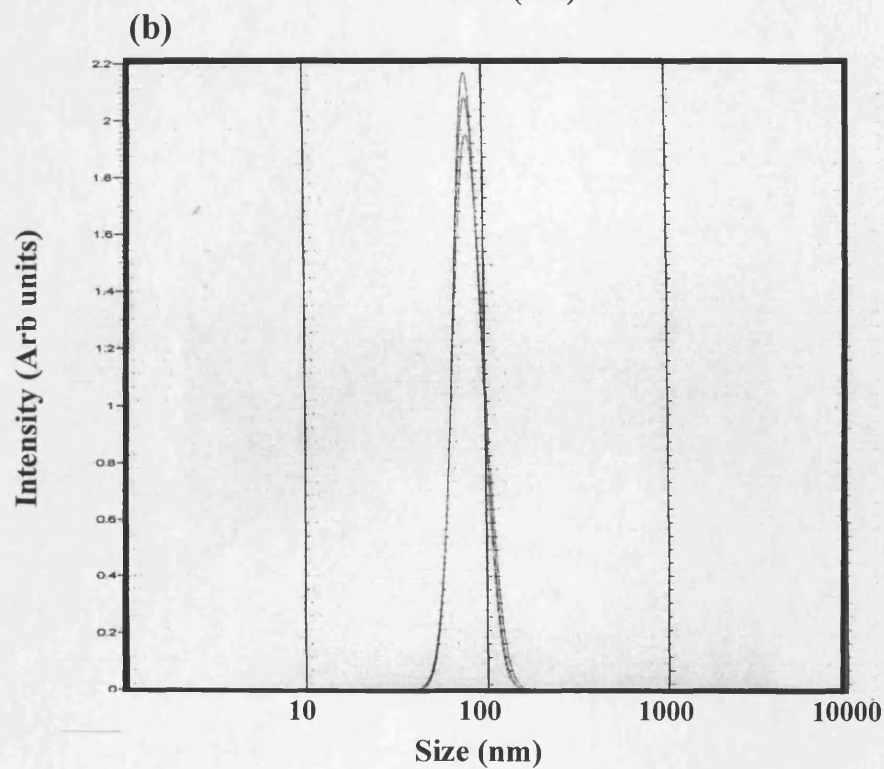
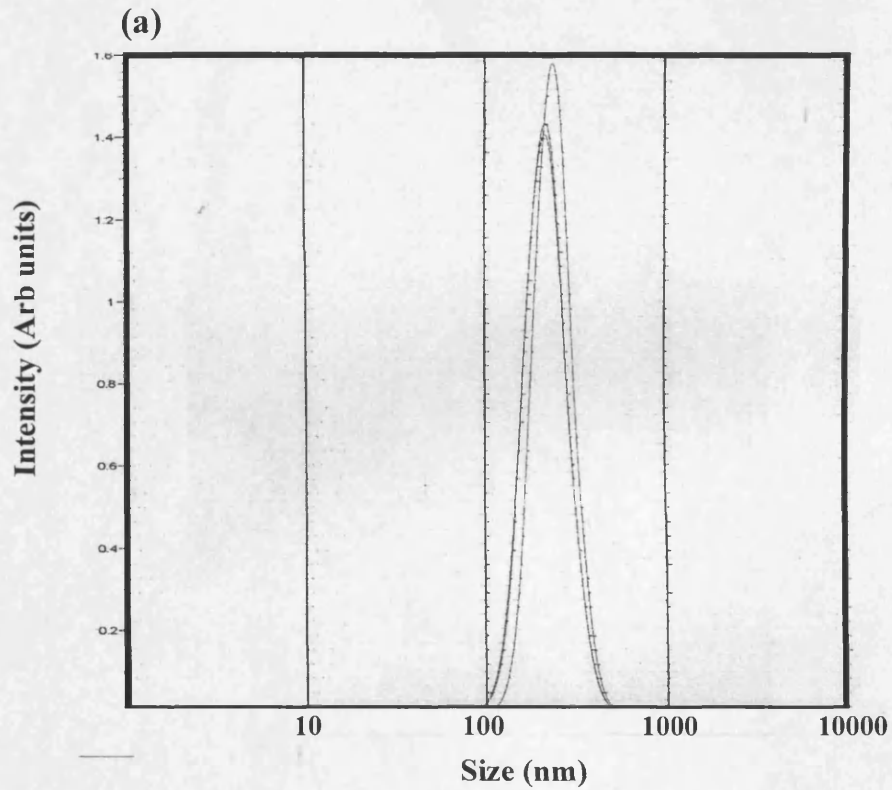


Figure 6.3 The effect of extrusion on liposome size distribution. Panel (a) the size distribution of endosome- model liposomes following 10 cycles of extrusion through 200 nm membrane, and 20 cycles of extrusion through 100 nm membrane (panel b) (the three lines represents three repeats)

of 78 nm in diameter (Figure 6.3b). Similar results were also observed for plasma and endosome model-liposomes (results not shown).

6.3.2 Stability of liposomes

The stability of the liposomes was examined at pH 7.4, 5.5, 4 and 3. Plasma membrane model-liposomes (Figure 6.4) were stable at pH 7.4, 5.5 and 4 over the test period, however, at pH 3, the liposomes were slightly less stable, as can be seen due to liposome aggregation.

The endosome model-liposomes (Figure 6.5) were also stable at 4 °C at pH 7.4 and 5.5 two days after preparation. At pH 4, the liposomes were only stable over a day, and a small population of larger liposomes were formed after this time. Finally at pH 3, the liposomes were not stable following 8 h (results not shown).

The lysosomal model-liposomes (Figure 6.6) were stable at 4 °C at 7.4, 5 and were quite stable at pH 4, although at this pH, on day two, the liposomes did slightly increase in size due to aggregation. Again these liposomes were unstable at pH 3 and their size decreased with time.

6.3.3 Preparation of calcein entrapped liposomes

In order to remove un-entrapped calcein several methods were attempted. The ultracentrifugation step, separation was produced but the liposomes were destroyed by this process. The use of Centri-prep Filtration was also unsuccessful, the liposomes were stuck on the membrane of the centri-prep and it was not possible to extract them.

Finally the purification using PD50 and PD25 columns, this process took over two days to complete for a very diluted liposome sample. The fluorescence of the purified calcein entrapped liposomes was measured in the presence and absence of TX-100. The fluorescence of the liposomes with entrapped calcein was not affected by TX-100, this indicates that calcein was not released from the liposomes.

6.3.4 SANS analysis of protonated and deuterated liposomes mimicking biological membranes

First it was necessary to define a mathematical model able to fit both deuterated and protonated liposomes (plasma, endosomal, and lysosomal-model membranes). It

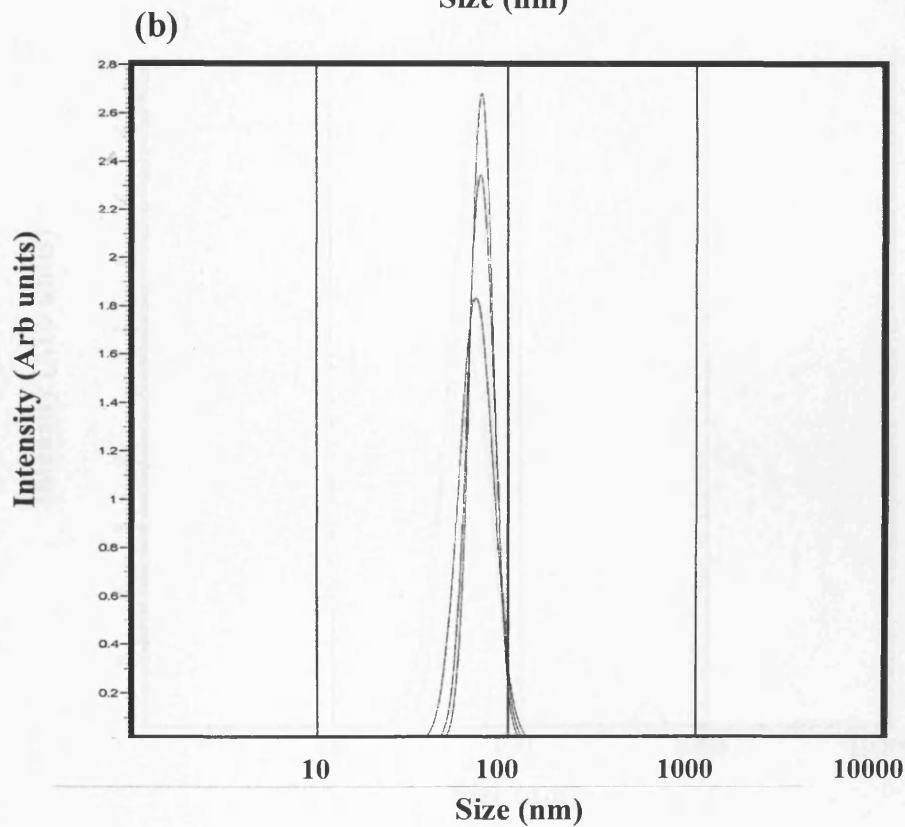
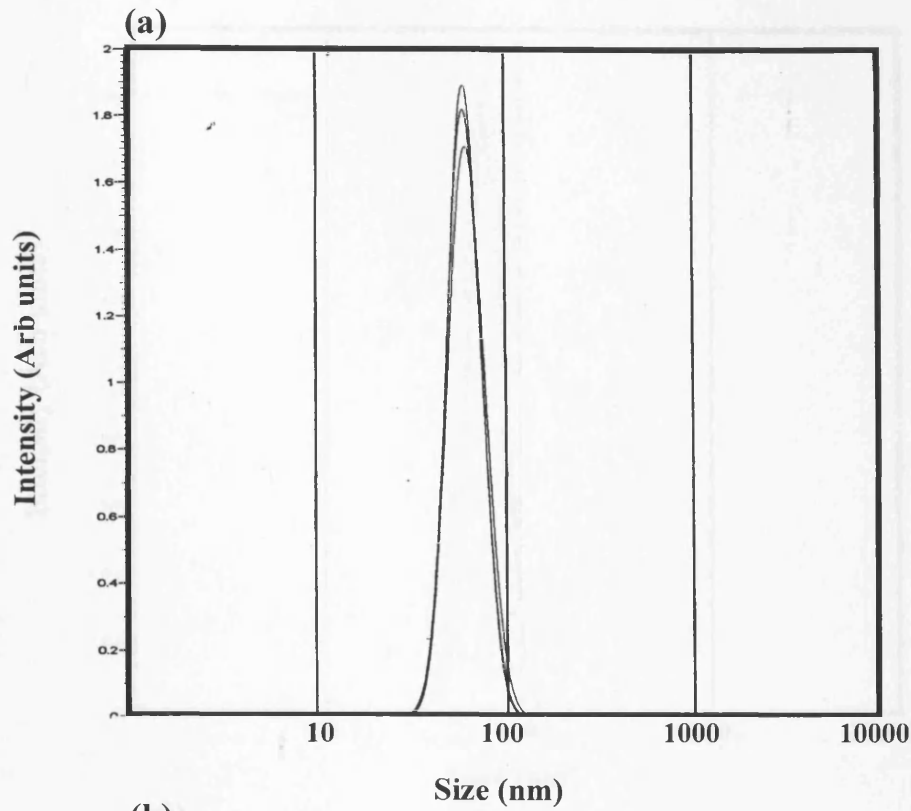


Figure 6.4 The stability of plasma-model liposomes at 4 °C. Panel (a) show pH 7.4 and panel (b) shows pH 5.5, after 0, 1 and 2 days. The three lines represents three repeats.

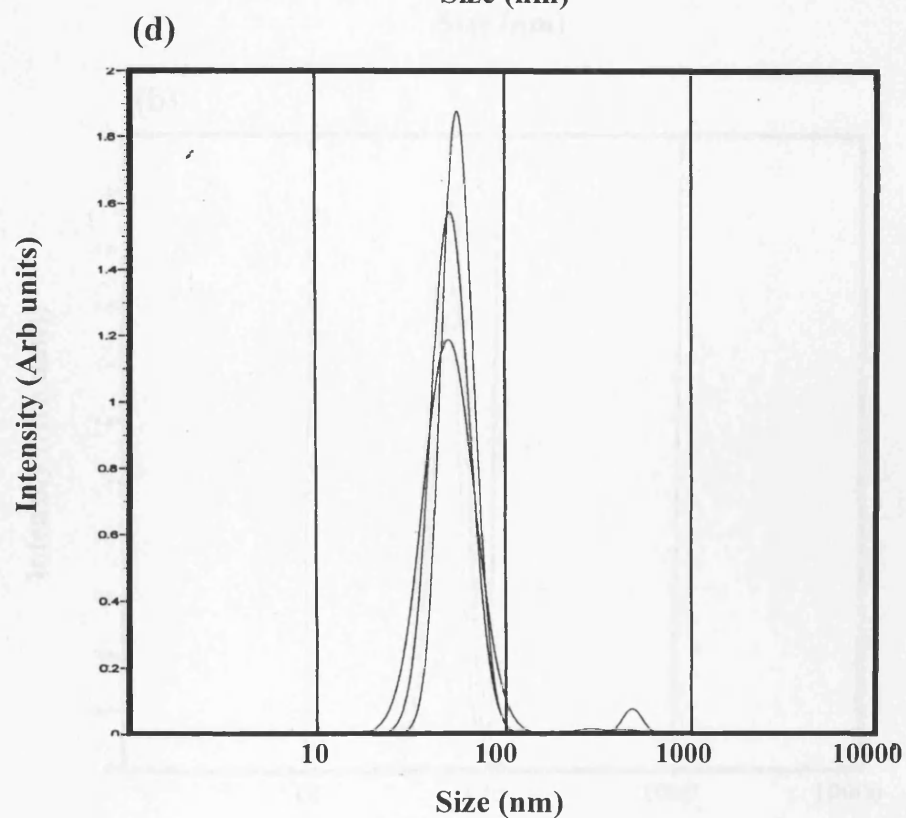
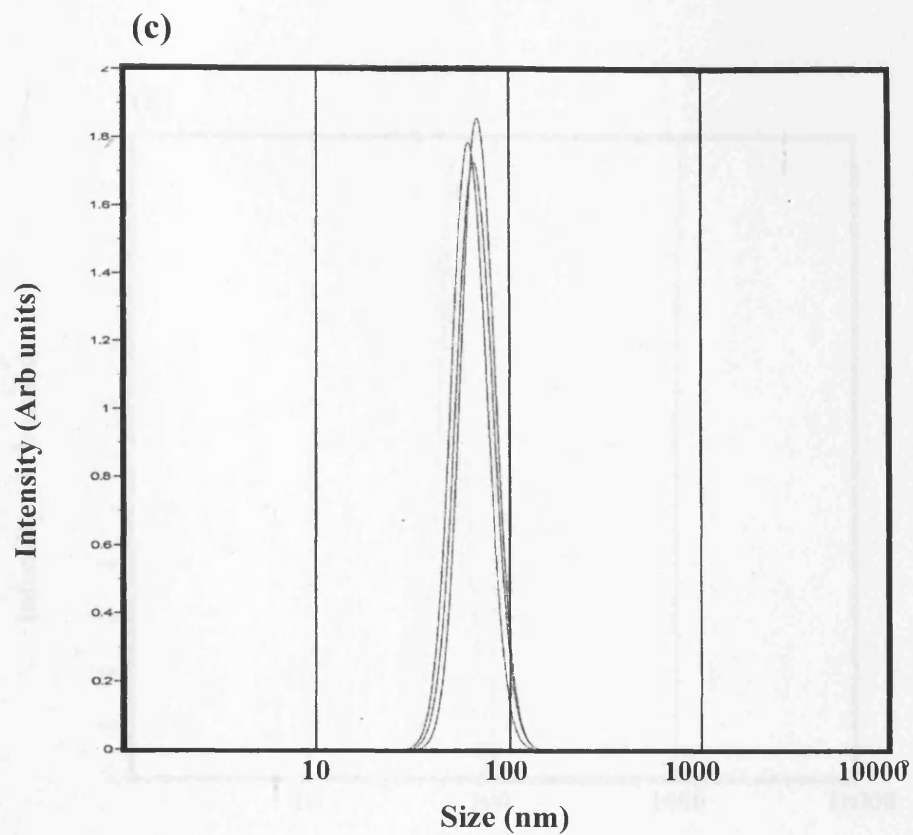


Figure 6.4 (continued). Panel (c) at pH 4 and panel (d) at pH 3, after 0, 1 and 2 days. The three lines represents three repeats

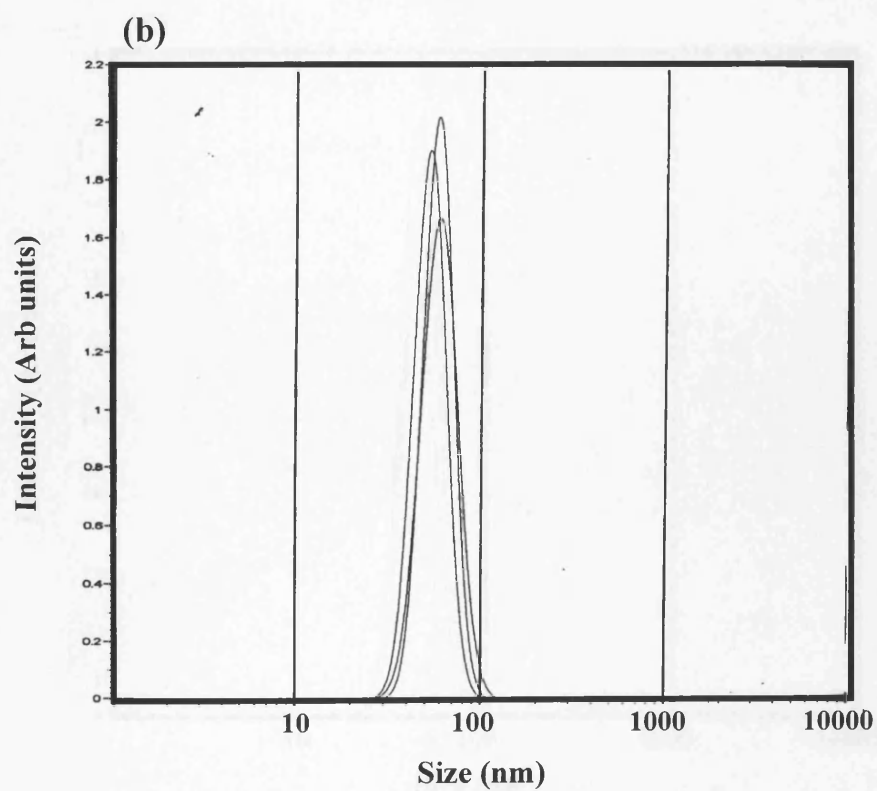
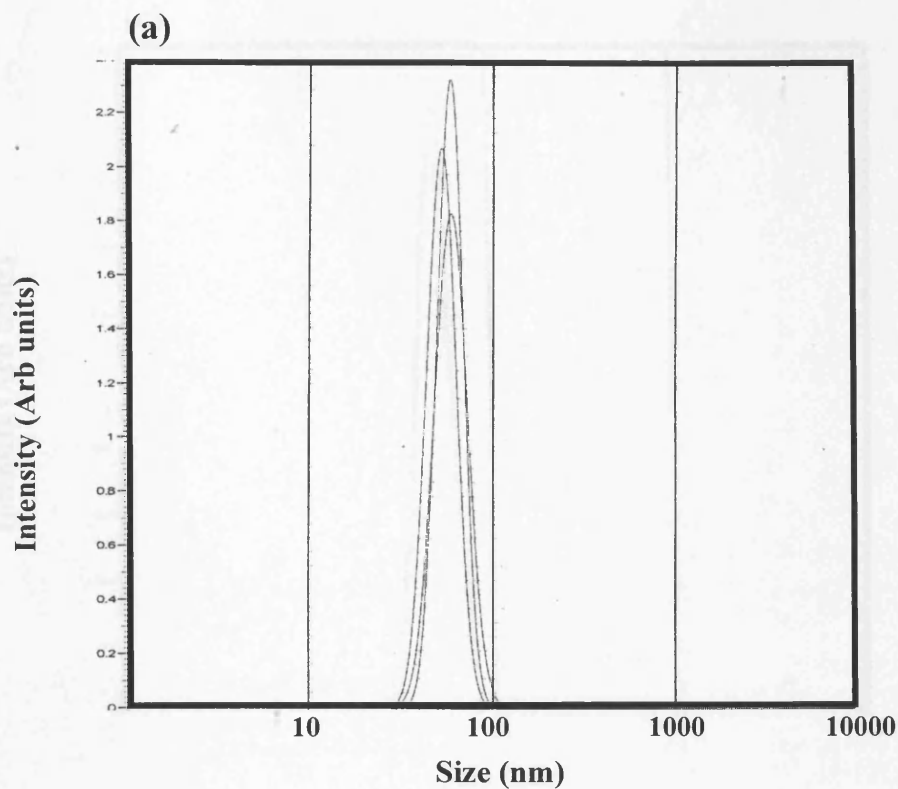


Figure 6.5 The stability of endosomal-model liposomes. Panel (a) at pH 7.4 and panel (b) at pH 5.5, after 0, 1 and 2 days. The three lines represents three repeats

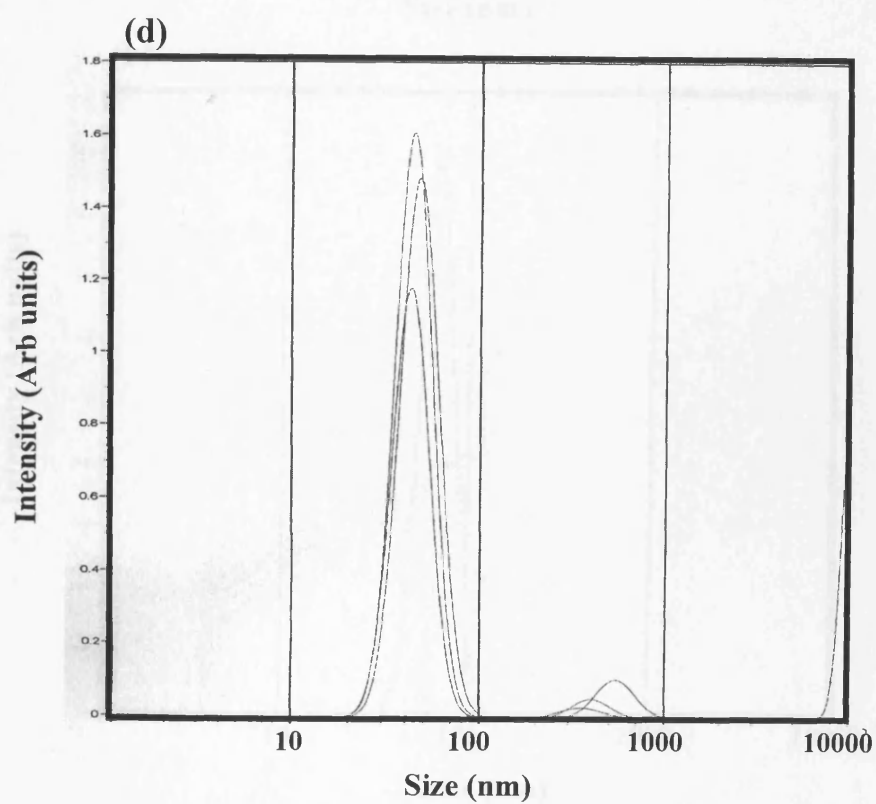
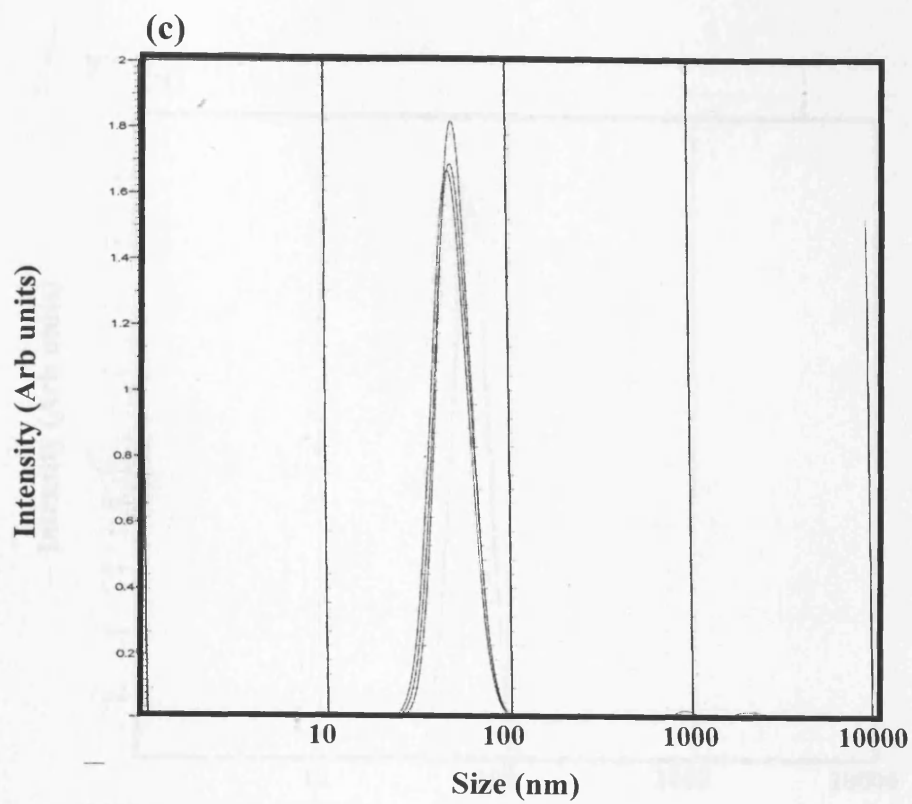


Figure 6.5 (continued). Panel (c) at pH 4 and panel (d) at pH 3, after 0, 1 and 2 days. The three lines represents three repeats

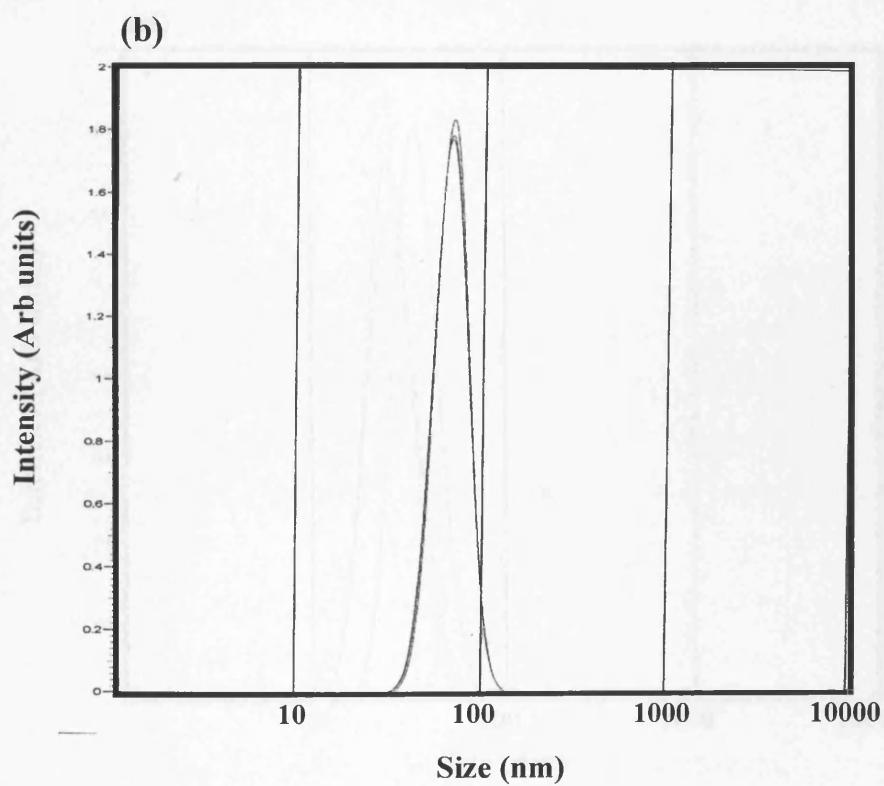
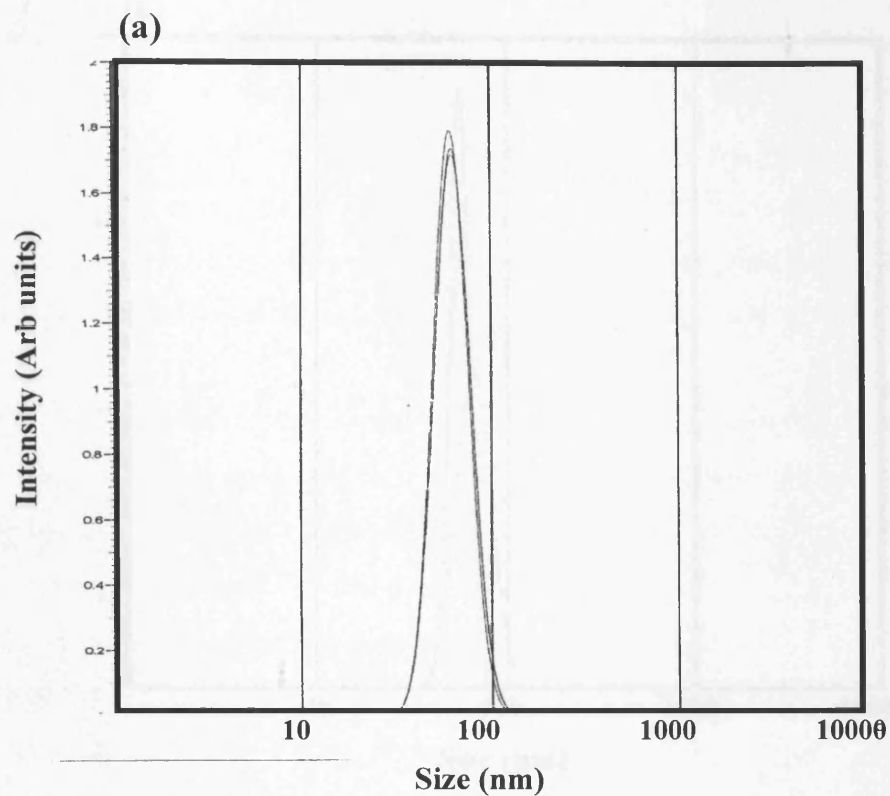


Figure 6.6 The stability of lysosomal-model liposomes. Panel (a) at pH 7.4 and panel (b) at pH 5.5, after 0, 1 and 2 days. The three lines represents three repeats

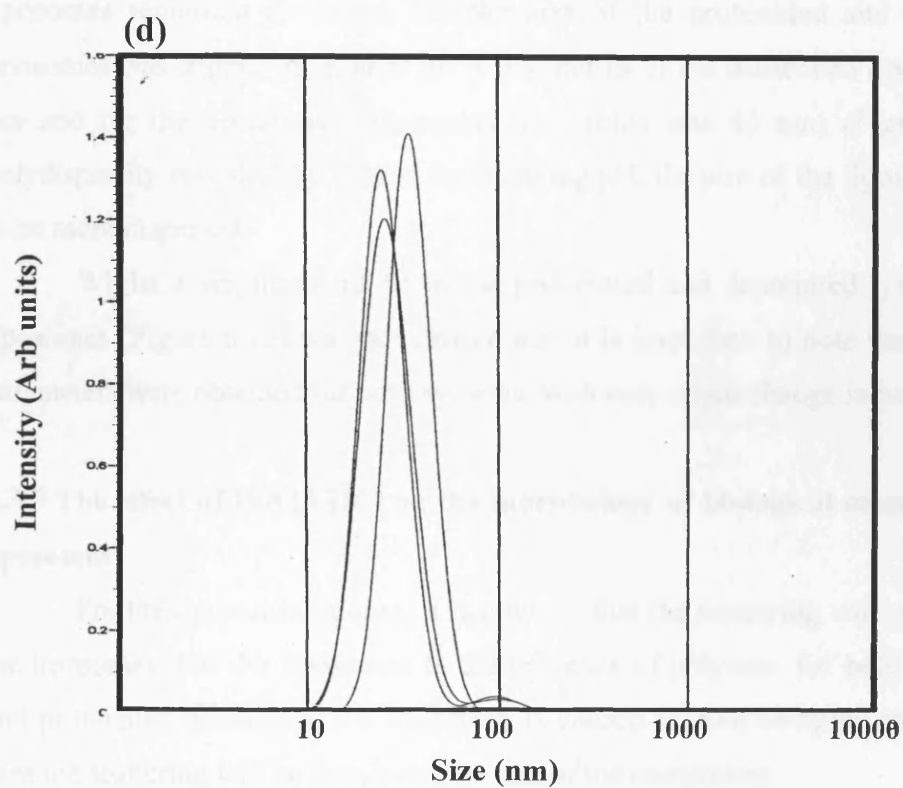
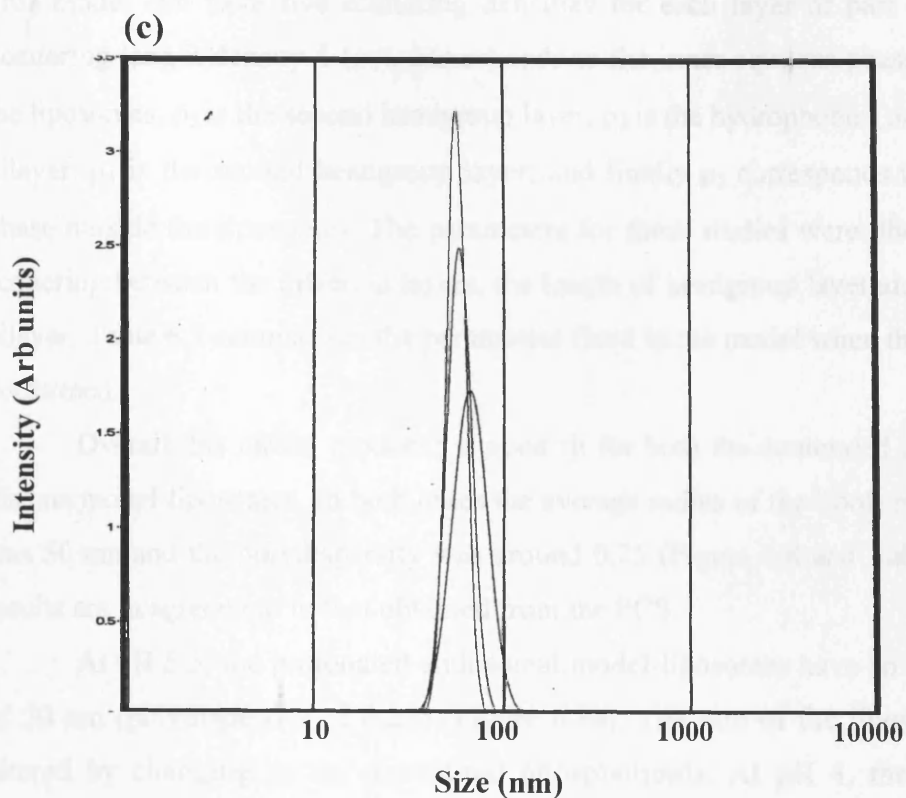


Figure 6.6 (continued). Panel (c) at pH 4 and panel (d) at pH 3, after 0, 1 and 2 days. The three lines represents three repeats

was found that the Schultz polydisperse 3 shell sphere model was suitable (Figure 6.7). This model can have five scattering densities for each layer or part of the model. Scattering length density 1 (ρ_1), corresponds to the inner aqueous phase entrapped in the liposomes, ρ_2 is the second headgroup layer, ρ_3 is the hydrophobic (or hydrocarbon) bilayer, ρ_4 is the second headgroup layer, and finally ρ_5 corresponds to the aqueous phase outside the liposomes. The parameters for these studies were: the difference in scattering between the different layers, the length of headgroup layer and hydrocarbon bilayer. Table 6.5 summarises the parameters fixed in the model when the fittings were performed.

Overall this model produced a good fit for both the deuterated and protonated plasma model-liposomes. In both cases the average radius of the liposomes determined was 50 nm and the polydispersity was around 0.25 (Figure 6.8 and Table 6.6). These results are in agreement to that obtained from the PCS.

At pH 5.5, the protonated endosomal model-liposomes have an average radius of 50 nm (polydispersity of 0.25) (Figure 6.9a). The size of the liposomes was not altered by changing to the deuterated phospholipids. At pH 4, the shape of the liposomes remained the same, but the size of the protonated and the deuterated liposomes was slightly smaller at pH 4 (the radius of the deuterated liposomes was 44 nm and for the protonated liposomes the radius was 45 nm) (Figure 6.9b). The polydispersity was slightly altered by changing pH, the size of the liposomes appeared to be more dispersed.

Whilst a simultaneous fit to the protonated and deuterated lysosome model-liposomes (Figure 6.10) was not carried out, it is important to note that identical size parameters were obtained for both systems, with only slight change in polydispersity.

6.3.5 The effect of ISA23.HCl on the morphology of biological membranes model liposomes

For the liposomes (alone), it is obvious that the scattering will only come from the liposomes. For the liposomes in the presence of polymer, for both the deuterated and protonated liposomes, the scattering is caused by two components, but for each case the scattering will be dominated by one of the component.

The scattering data obtained for the protonated plasma membrane- model

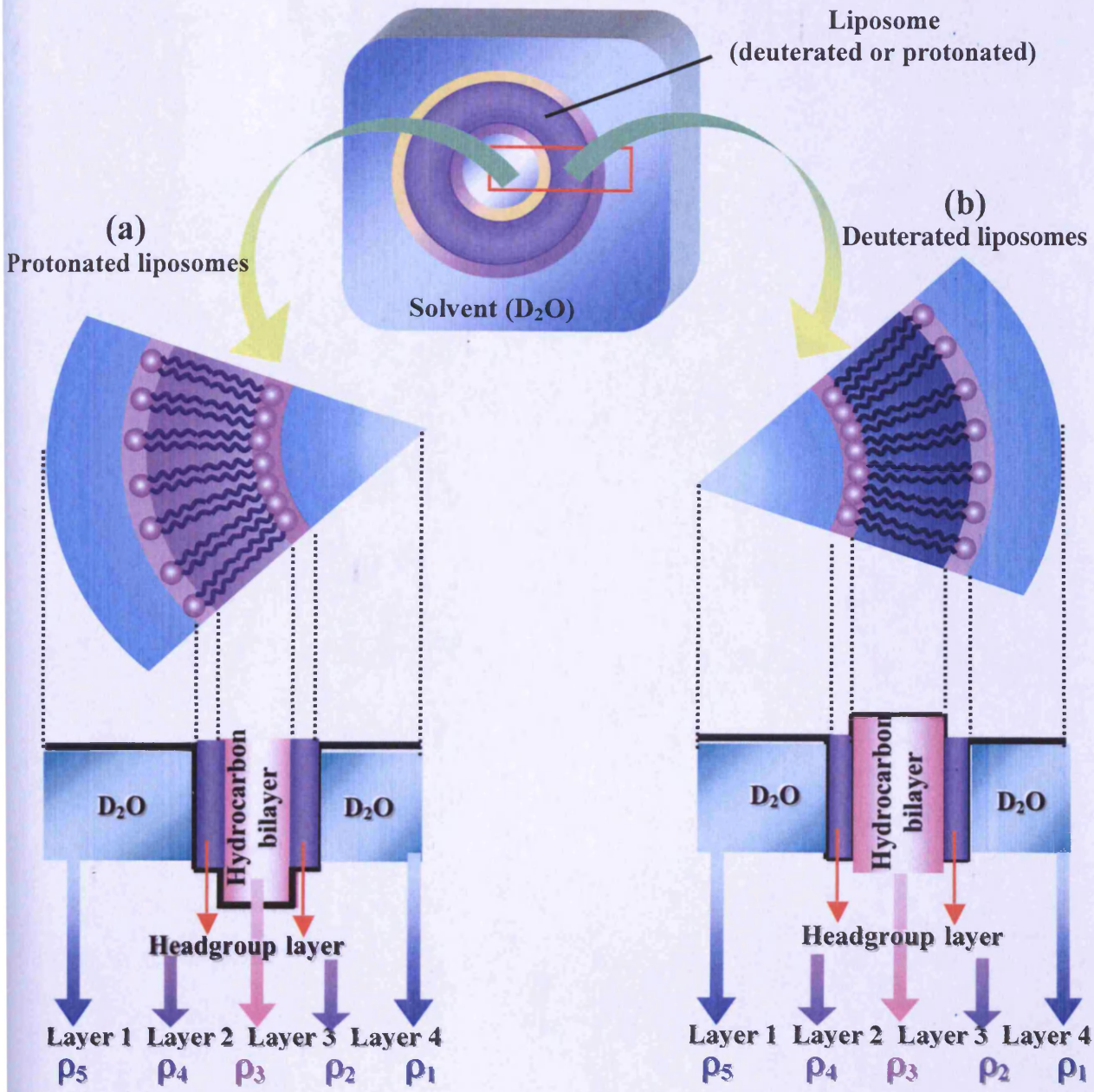


Figure 6.7 Schematic representation of the changing scattering length densities of the different layers of liposomes in solution (the Schultz polydisperse 3 shell sphere model). Panel (a) the scattering length density of liposomes composed of protonated phospholipids, panel (b) the scattering length density of the liposomes composed of phospholipids containing deuterated hydrocarbon chains

Table 6.5 Summary of the fixed parameters used to fit the SANS data obtained using liposomes.

System	Parameters									Length of headgroup layer (Å)	Length of hydrocarbon bilayer (Å)
	ρ_1	ρ_2	ρ_3	ρ_4	ρ_5	$\rho_1 - \rho_2$	$\rho_2 - \rho_3$	$\rho_3 - \rho_4$	$\rho_4 - \rho_5$		
DPPC										7.6*	33*
DPPE										6.1*	33
DPPS										4.4**	33
Protonated liposomes[†]											
Plasma	6.4	1.21	-0.086	1.21	6.4	5.19	1.3	-1.3	-5.19	6.8	33
Endosome	6.4	1.12	-0.086	1.12	6.4	5.28	1.21	-1.21	-5.28	7.0	33
Lysosome	6.4	1.29	-0.086	1.29	6.4	5.11	1.38	-1.38	-5.11	6.6	33
Deuterated liposomes[†]											
Plasma	6.4	1.21	7.4	1.21	6.4	5.19	-6.19	6.19	-5.19	6.8	33
Endosome	6.4	1.12	7.4	1.12	6.4	5.28	-6.28	6.28	-5.28	7.0	33
Lysosome	6.4	1.29	7.4	1.29	6.4	5.11	-6.11	6.11	-5.11	6.6	33

* Obtained or calculated from Nagle and Wiener, 1988 ** calculated from Petrache et al, 2004

[†] Calculated using equation 4.1 (Chapter 4, section 4.1.1) and obtained from (based on) Griffiths et al, 2005 and Ristori et al, 2005

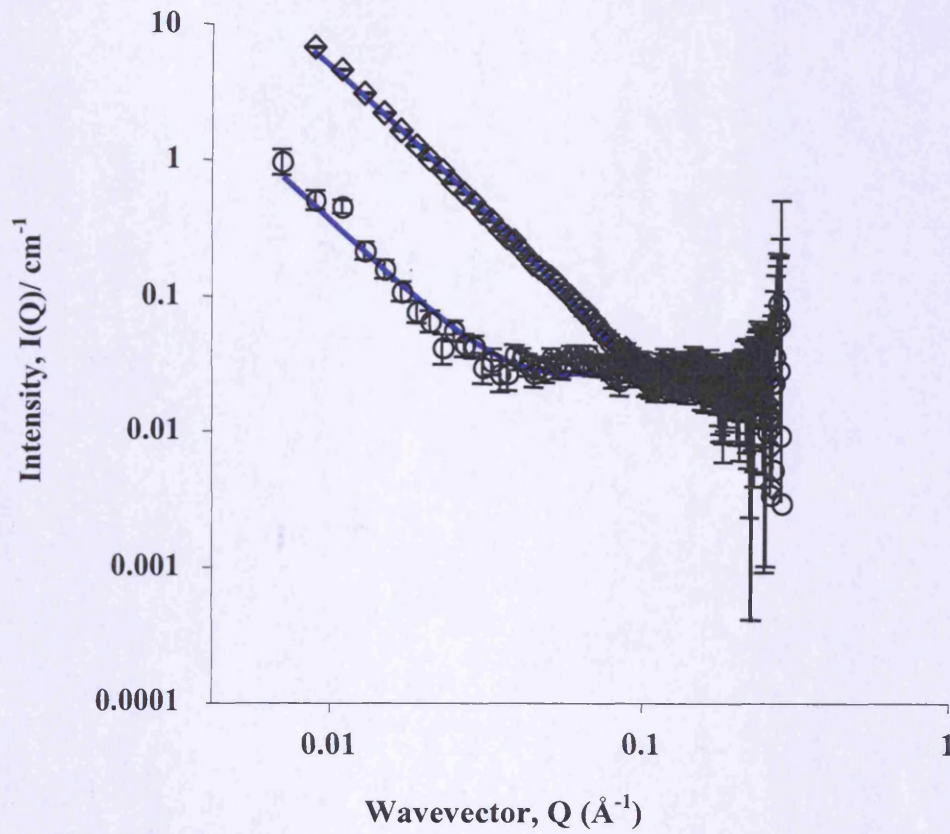


Figure 6.8 SANS data obtained using the plasma membrane-model liposomes. The scattering data of the deuterated (circles) and protonated (diamonds) liposomes are shown at pH 7.4, plus their fittings (solid blue line) using Schultz polydisperse 3 shell sphere mathematical model

Table 6.6 Summary of liposome characteristics, calculated from the Schultz polydisperse 3 shell sphere mathematical model.

System	pH	Radius (nm)	Polydispersity
Protonated-Plasma	7.4	50	0.25
Protonated-Endosome	5.5	50	0.25
	4	45	0.3
Protonated-Lysosome	5.5	50	0.25
	4	50	0.25
Deuterated- Plasma	7.4	50	0.26
Deuterated-Endosome	5.5	50	0.25
	4	44	0.4
Deuterated -Lysosome	5.5	50	0.26
	4	50	0.26

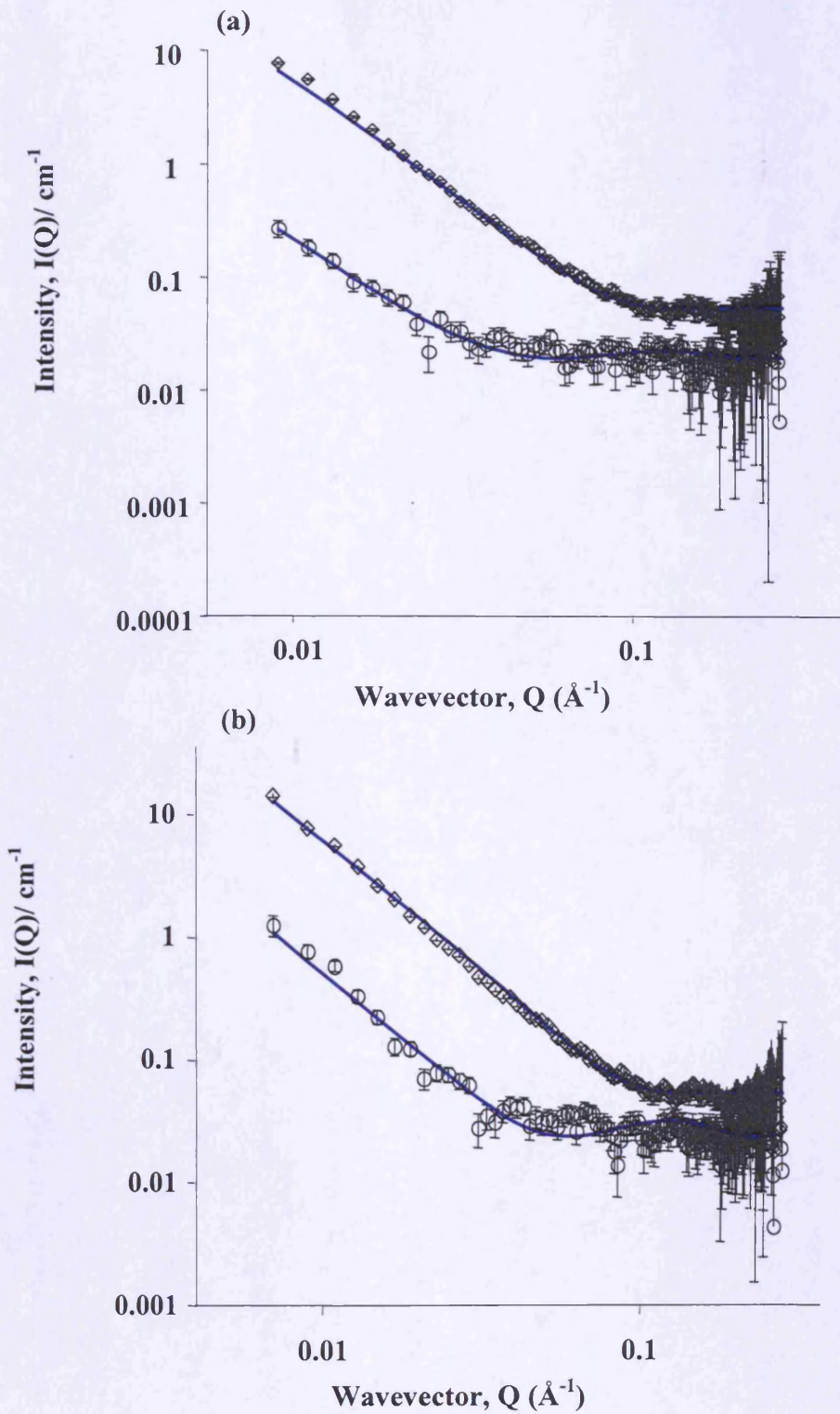


Figure 6.9 SANS data obtained using the endosomal membrane-model liposomes. The scattering data of the deuterated (circles) and protonated (diamonds) liposomes at pH 4 (panel a) and pH 5.5 (panel b) are shown plus their fittings (solid blue lines) using Schultz polydisperse 3 shell sphere mathematical model

liposomes changed very slightly in the presence of ISA23.HCl at pH 7.4 (Figure 6.11a). Between wavevector 0.025 \AA^{-1} to 0.29 \AA^{-1} the scattering from these liposomes was slightly higher than the scattering of the liposome alone. At a very low Q value ($Q < 0.015 \text{ \AA}^{-1}$), the liposome scattering in the presence of ISA23.HCl was slightly lower than that of the liposomes alone.

Very little scattering was produced from the deuterated plasma membrane-model liposomes (Figure 6.11b) at high/middle Q values (0.033 \AA^{-1} - 0.29 \AA^{-1}) and in this Q range the scattering seen was predominately from the polymer. Beyond this Q range, scattering was caused by the polymer and the protonated headgroups of the phospholipids in the liposomes. At very low Q values (between 0.07 \AA^{-1} – 0.01 \AA^{-1}) there was no difference between the scattering from the liposomes in the presence and absence of ISA23.HCl, indicating no interaction.

At pH 5.5, (Figure 6.12a) the scattering of the protonated endosome-model liposomes changed significantly in the presence of ISA23.HCl. Between Q values of 0.04 \AA^{-1} and 0.28 \AA^{-1} (Q), liposomes scattering was higher in the presence of ISA23.HCl and is higher than seen for the liposomes alone. Scattering of deuterated liposomes changed in the presence of ISA23.HCl (Figure 6.12b) due to both the scattering caused by the polymer, and also possibly a changed morphology of the bilayer. At pH 4, addition of ISA23.HCl appeared to affect the shape or size of the liposomes to a lesser extent than seen at pH 5.5. For the protonated liposomes, the scattering data form was almost identical to that of the liposomes in the presence of ISA23.HCl (Figure 6.13a).

Addition of ISA23.HCl to the protonated lysosomal-model liposomes at pH 5.5, did not seem to affect the scattering observed (Figure 6.14). In contrast to the endosomal-model the scattering of the lysosomal-model was affected by ISA23.HCl more at pH 4 than pH 5.5 (Figure 6.15). The same affect was observed with the deuterated lysosomal-model liposomes in the presence and absence of ISA23.HCl.

For the deuterated liposomes-ISA23.HCl system, it was possible to examine the effect of the liposome on the morphology of the polymer. The scattering data of ISA23.HCl can be extracted by subtracting the scattering data of the deuterated liposomes (alone) from data of the deuterated liposomes in the presence of ISA23.HCl, and this data was then fitted.

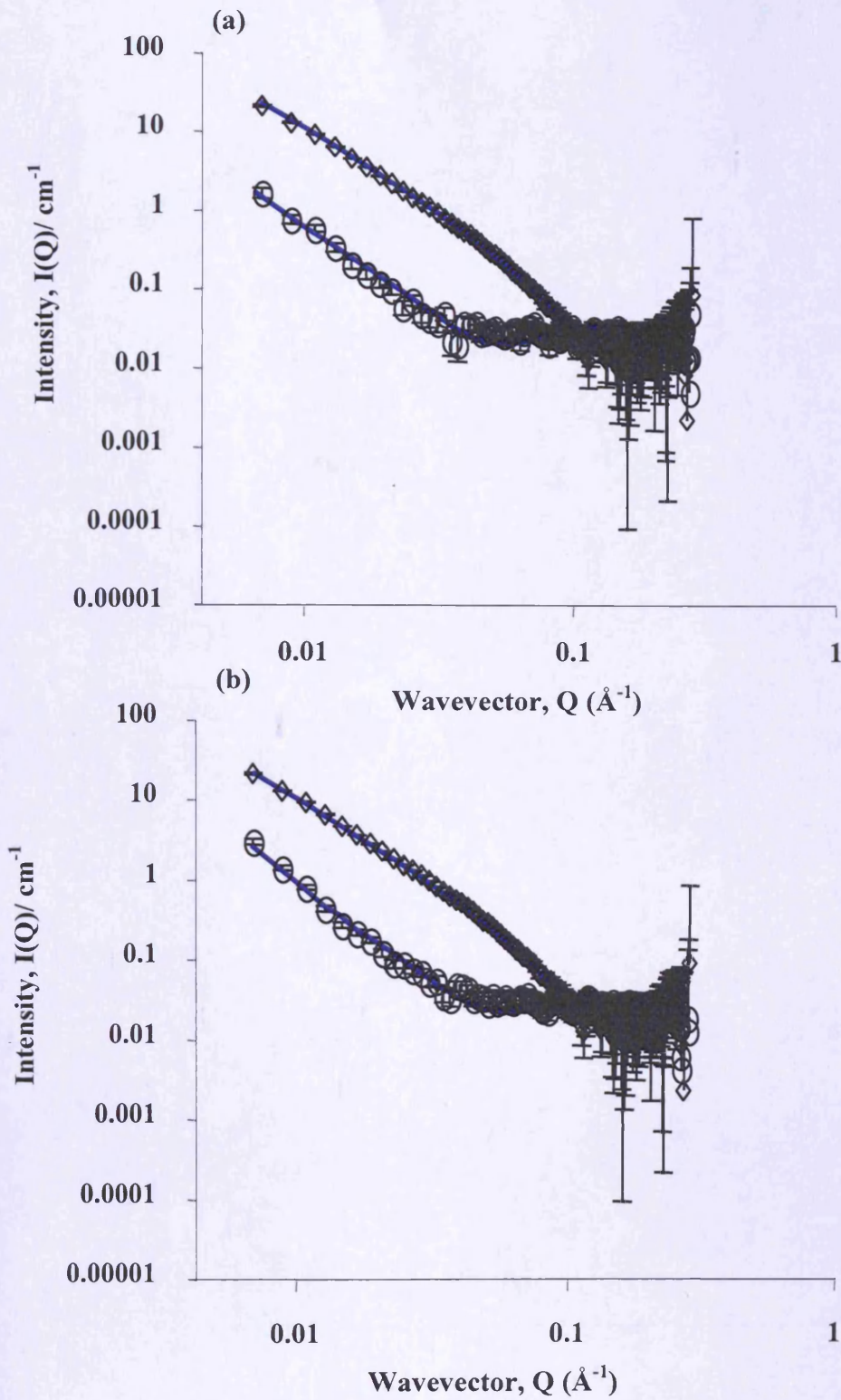


Figure 6.10 SANS data obtained for the lysosomal membrane-model liposomes. The scattering data of the deuterated (circles) and protonated (diamonds) liposomes at pH 4 (panel a) and pH 5.5 (panel b) are shown plus their fittings (solid blue lines) using Schultz polydisperse 3 shell sphere mathematical model

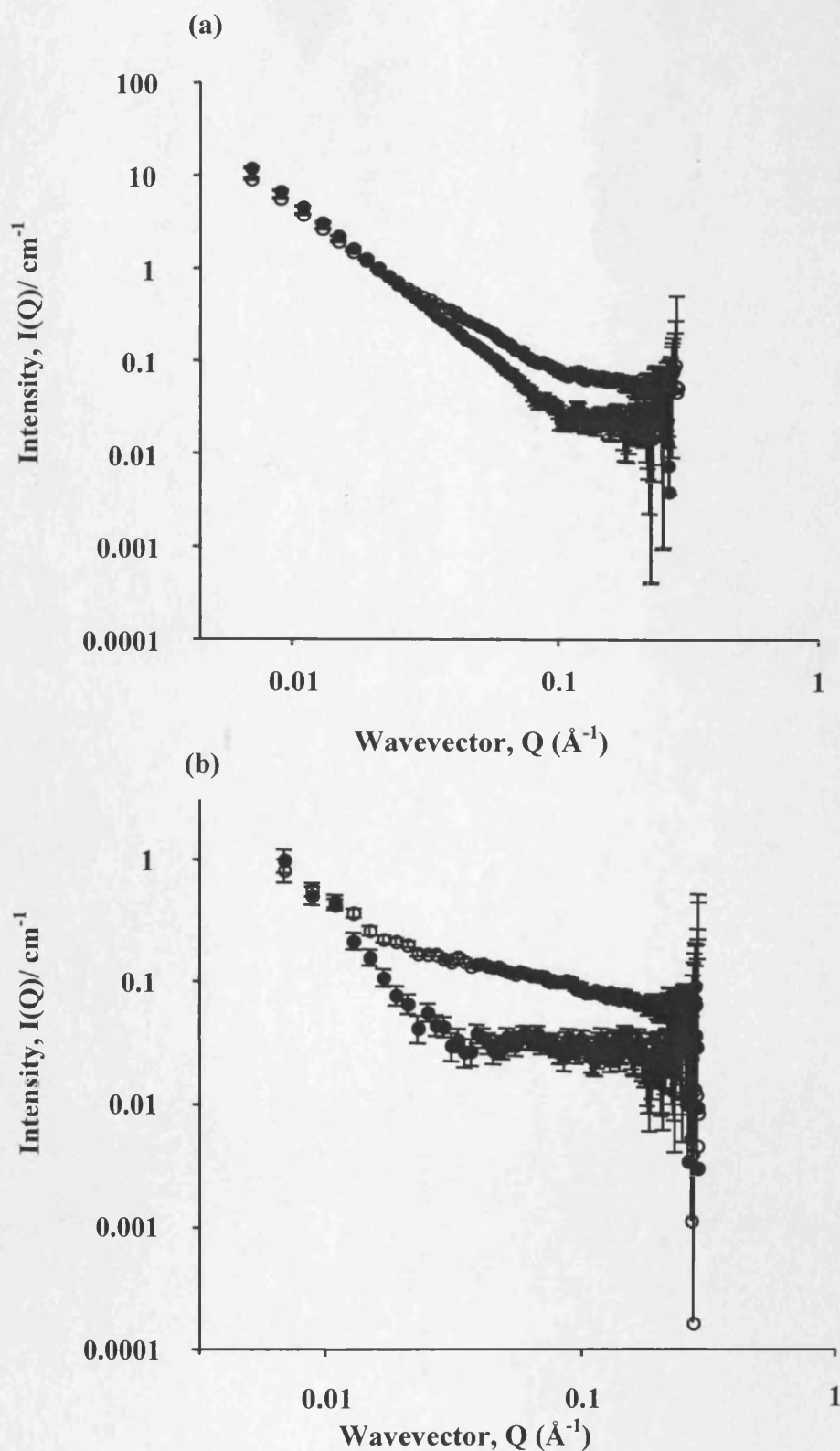


Figure 6.11 The effect of ISA23.HCl on the scattering of plasma membrane-model liposomes. SANS data of protonated (panel a) and deuterated (panel b) liposomes were obtained in the presence (empty circles) and absence (solid circles) of ISA23.HCl at pH 7.4

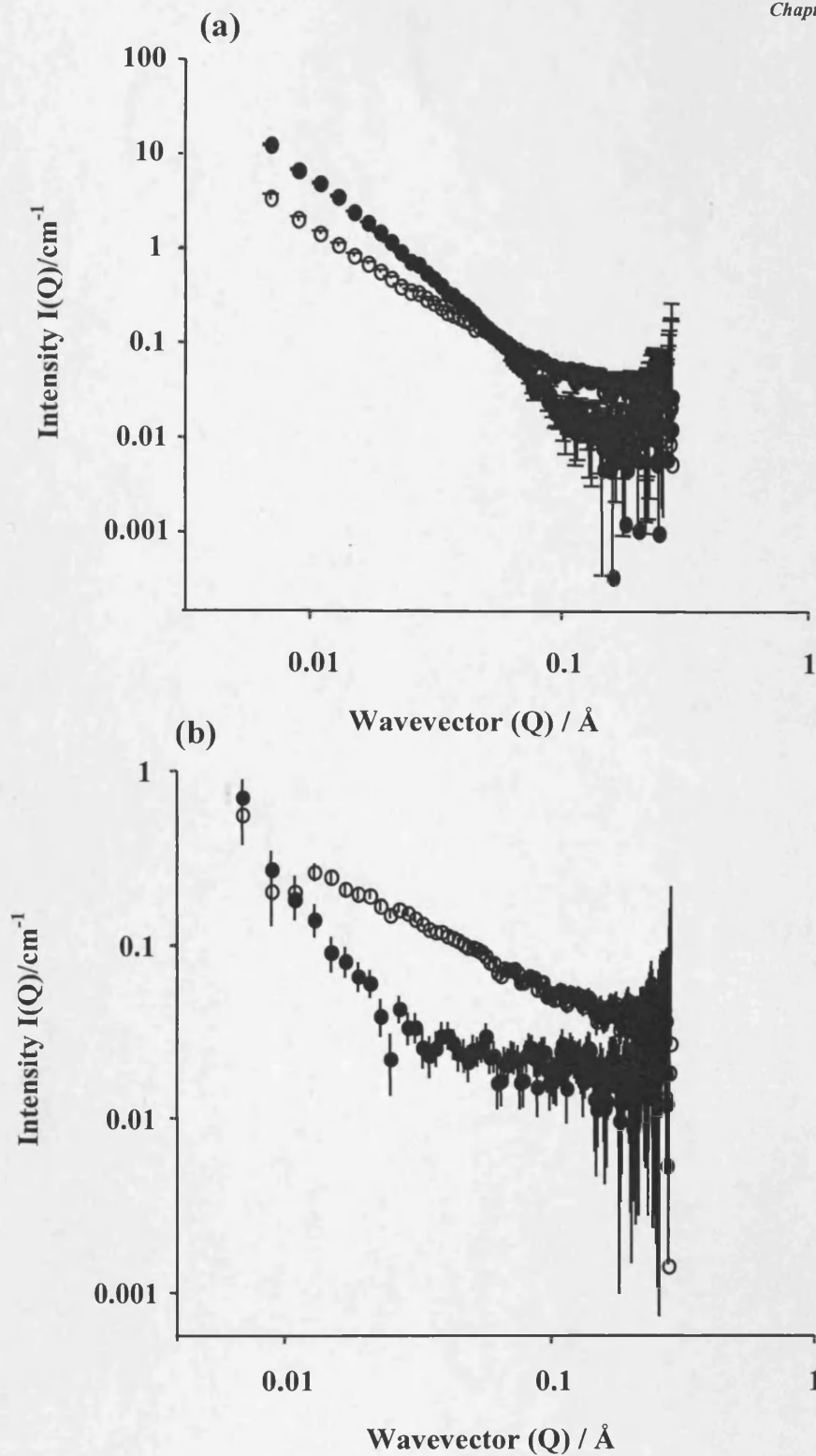


Figure 6.12 The effect of ISA23.HCl on the scattering of endosomal membrane-model liposomes. SANS data of protonated (panel a) and deuterated (panel b) liposomes were obtained in the presence (empty circles) and absence (solid circles) of ISA23.HCl at pH 5.5

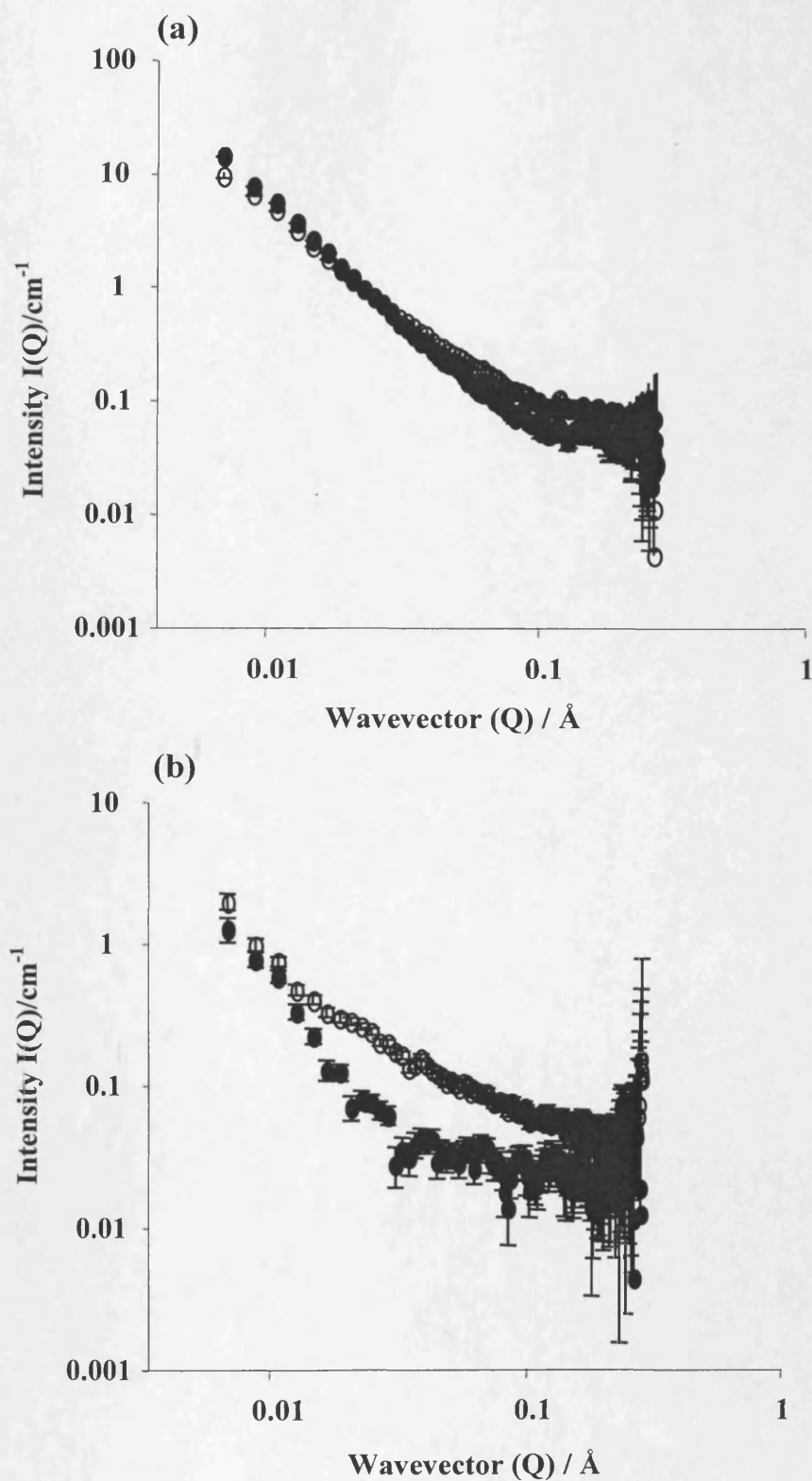


Figure 6.13 The effect of ISA23.HCl on the scattering of endosomal membrane-model liposomes. SANS data of protonated (panel a) and deuterated (panel b) endosomal model-liposomes were obtained in the presence (empty circles) and absence (solid circles) of ISA23.HCl, at pH 4

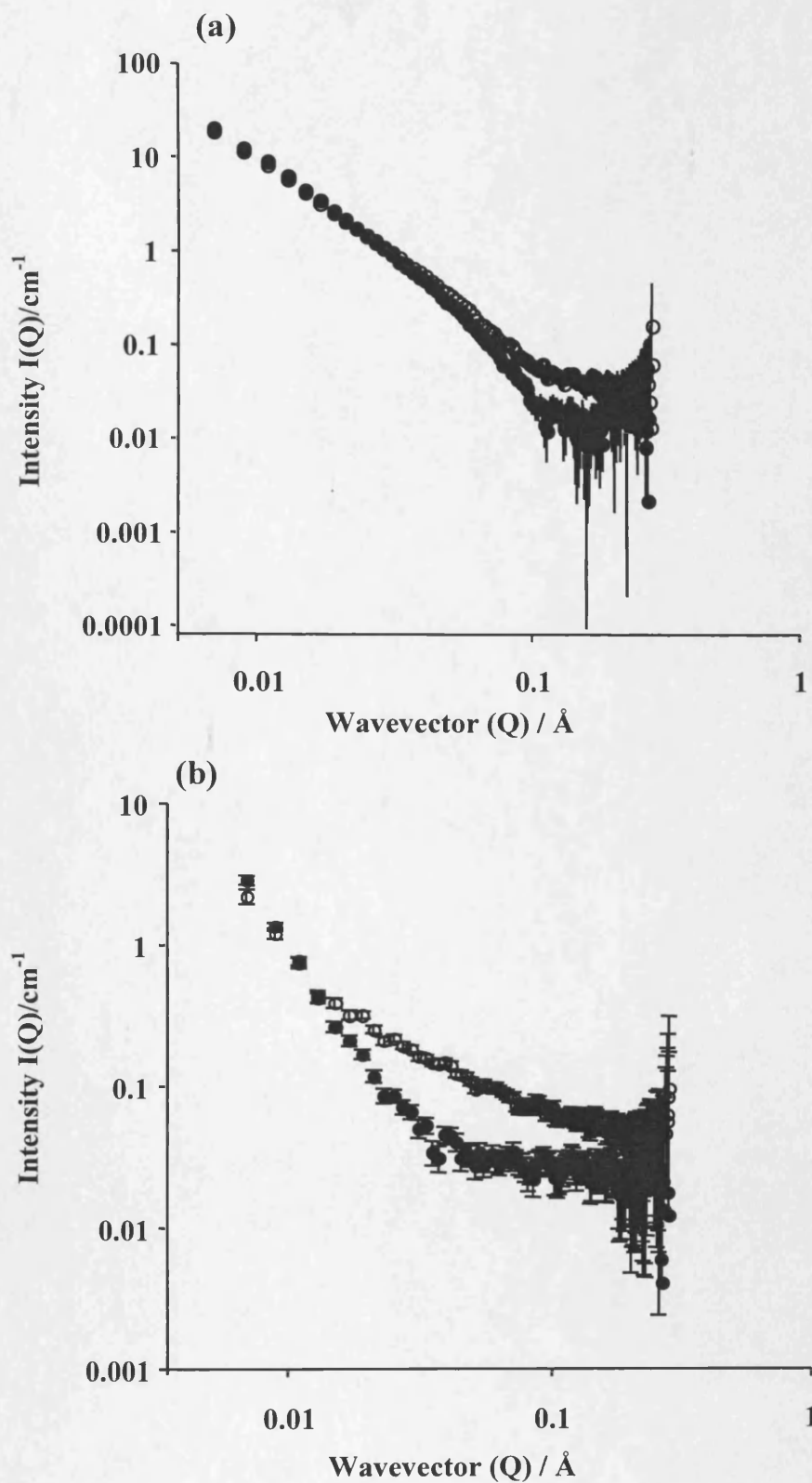


Figure 6.14 The effect of ISA23.HCl on the scattering obtained from lysosomal membrane-model liposomes. SANS data of protonated (panel a) and deuterated (panel b) liposomes were obtained in the presence (empty circles) and absence (solid circles) of ISA23.HCl at pH 5.5

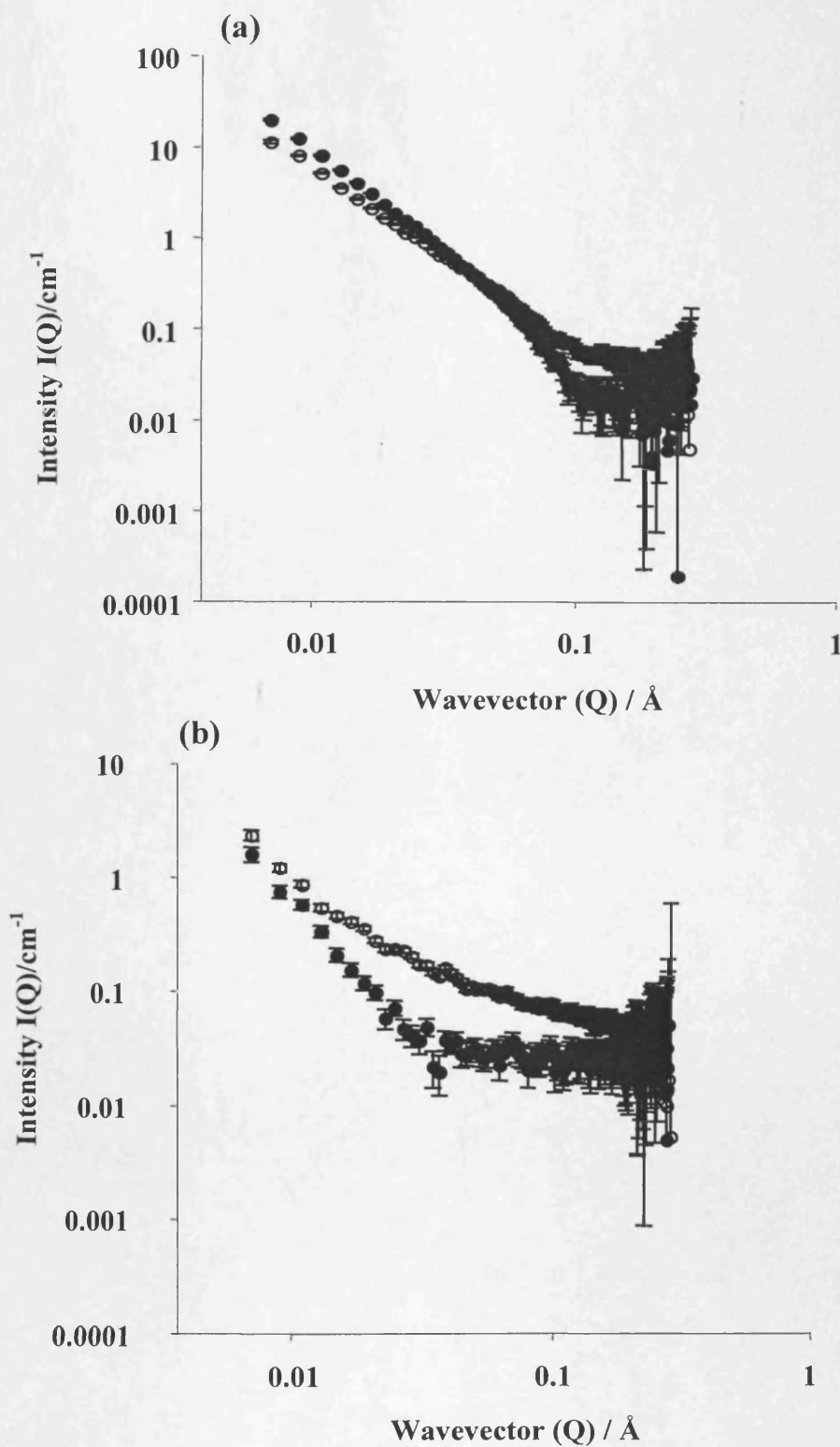


Figure 6.15 The effect of ISA23.HCl on the scattering of lysosomal membrane-model liposomes. SANS data of protonated (panel a) and deuterated (panel b) liposomes were obtained in the presence (empty circles) and absence (solid circles) of ISA23.HCl, at pH 4

The Gaussian coil model was used to fit the extracted ISA23.HCl data. It produced a good fit for all the data sets (results not shown). Table 6.7 summarises the R_g of the polymer measured in the presence and absence of the model-liposomes. At pH 7.4, the R_g of ISA23.HCl changes only very slightly in the presence of plasma model-liposomes. However at pH 5.5, ISA23.HCl appeared to have increased in size by a factor of 1.4 in the presence of the endosome- and lysosome-model liposomes. The polymer also increased in size at pH 4 in the presence of lysosome model-liposomes (increased from 6.6 nm to 7.3 nm), but not for the endosome model-liposomes. In the latter case, the size of polymer remained unaltered (the R_g decreased by 0.4 nm).

An attempt was made to try and fit the scattering data of the liposomes in the presence of ISA23.HCl using Schultz polydisperse 3 shell sphere but this was unsuccessful. A modification to the model maybe required, or a new mathematical model might be necessary to fit these data. In both cases it would be important to include the polymer scattering to get good fits with accurate parameters (i.e shape and size, radius and polydispersity). It became clear that interpreting these results was far harder than anticipated.

6.4 Discussion

Liposomes were prepared with a phospholipid composition chosen to mimic the biological membrane that ISA23 would encounter during endocytic internalisation. All these liposomes were stable (at pH 7.4, 5.5 and 4) over two days, and thus stable enough to enable the ISA23.HCl –liposome interaction studies conducted using SANS. None of the liposomes (plasma membrane-, endosomal membrane- and lysosomal membrane-model liposomes) were stable at pH 3. This was probably due to an increased rate of hydrolysis of the ester bonds in the phospholipids in acidic media causing liposomes disintegration, aggregation and/or fusion (Zhang and Pawelchak, 2000).

Calcein-entrapped liposomes

The aim of this experiment was to study polymer model liposomes interaction by investigating the release of calcein entrapped in the liposomes (Karoonthaisiri et al, 2003). It is possible to get information on the rate at which the polymer causes liposomes destabilisation by measuring the rate of the calcein release from the

Table 6.7 The summary of the R_g of ISA23.HCl, in the presence and the absence of the different model liposomes at pH 7.4, 5.5 and 4.

Polymer	pH	Liposomes	R_g (nm)	Effect of ISA23.HCl on the scattering data of the protonated liposomes
ISA23.HCl (alone)	7.4	-	2.1	N/A*
ISA23.HCl	7.4	deuterated plasma membrane	2.7	No change in scattering
ISA23.HCl (alone)	5.5	-	3.0	N/A
ISA23.HCl	5.5	Deuterated endosome membrane	4.3	Significant changes in scattering
ISA23.HCl	5.5	deuterated lysosome membrane	4.4	No change in scattering
ISA23.HCl (alone)	4	-	6.6	N/A
ISA23.HCl	4	deuterated endosome membrane	6.2	Slight change in scattering
ISA23.HCl	4	deuterated lysosome membrane	7.3	Slight change in scattering

* N/A - not applicable

liposomes (Karoonthaisiri et al, 2003). If different molecular weight dyes were used (e.g. different molecular weight FITC-dextran, also one with molecular weight similar to that of PAAs), it is likely to get information on mechanism of action of the polymer, i.e. does it cause a complete destruction of the liposomes or does it form pores, and if so then it would be likely to get an idea on the size of these pores. Also, the stability of the liposomes can be studied by measuring the leakage of calcein as a function of time and pH.

The preparation of calcein-entrapped liposomes was not successful. The fluorescence of calcein-entrapped liposomes in the presence of TX-100 did not increase. It is not clear why this occurs, but is it possible that at 5% w/v of TX-100 was not enough to cause liposome breakage. Thus PCS was used to examine the effect of TX-100 (5% w/v) on the size distribution of liposomes. It is clear from Figure 6.16 that the size changes from 70 nm (monodisperse population) to 10, 20 30 nm and 1000 nm (very polydisperse population), so it is obvious that the liposomes are broken by TX-100. Another possible explanation is that TX-100 is interacting with calcein, but the effect of TX-100 is more noticeable in the liposome preparation, as the TX-100 might be forming micelles with the phospholipids of the liposomes thus can entrap the calcein causing a decrease in the fluorescence.

It is also possible that the calcein might leak out the liposomes due to the low molecular weight of calcein, absence of cholesterol in the liposome preparation and the purification of the liposomes.

SANS studies of polymer-model membrane interaction

SANS was used to study the morphology of model-liposomes/ISA23.HCl system. For the protonated liposomes (alone) the scattering came from both the headgroup and hydrocarbon tail of the phospholipids (Figure 6.17a). For the protonated system in the presence of ISA23.HCl, the scattering is predominately from the liposome as the polymer is a weak scatterer, but the presence of ISA23.HCl does slightly contribute to the scattering data (Figure 6.17b). For the deuterated system, the tails of the lipids are deuterated but the headgroup is protonated, so for the deuterated liposomes (alone) a little scattering was still expected (Figure 6.17c), and for the deuterated liposomes in the presence of ISA23.HCl, the scattering is from both the headgroup of the phospholipids and the polymer (Figure 6.17d).

Very little interaction occurred between ISA23.HCl and plasma model-

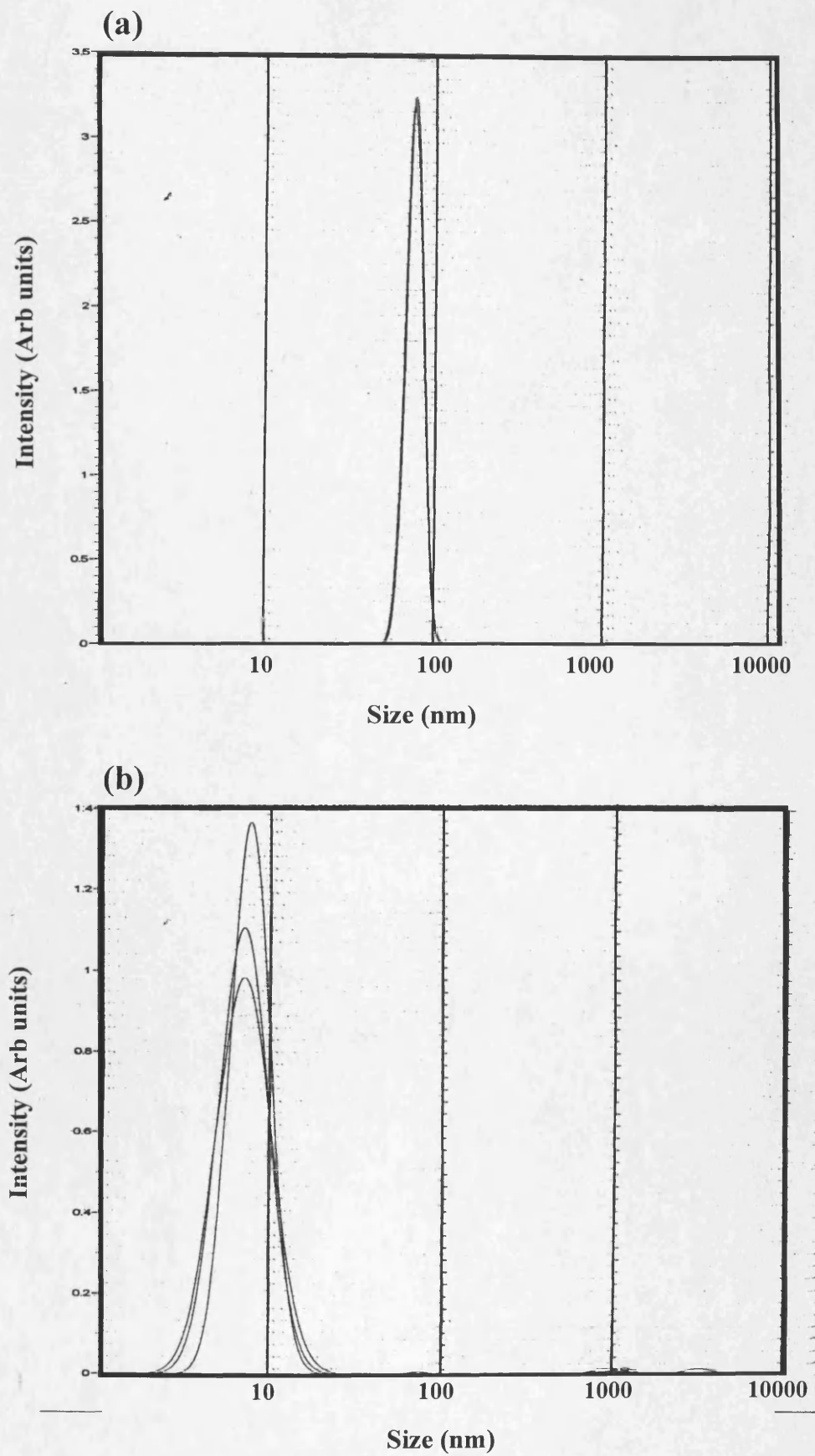


Figure 6.16 The size distribution of liposomes measured by PCS in the presence (panel b) of and absence (panel a) of TX-100. The three lines represents three repeats

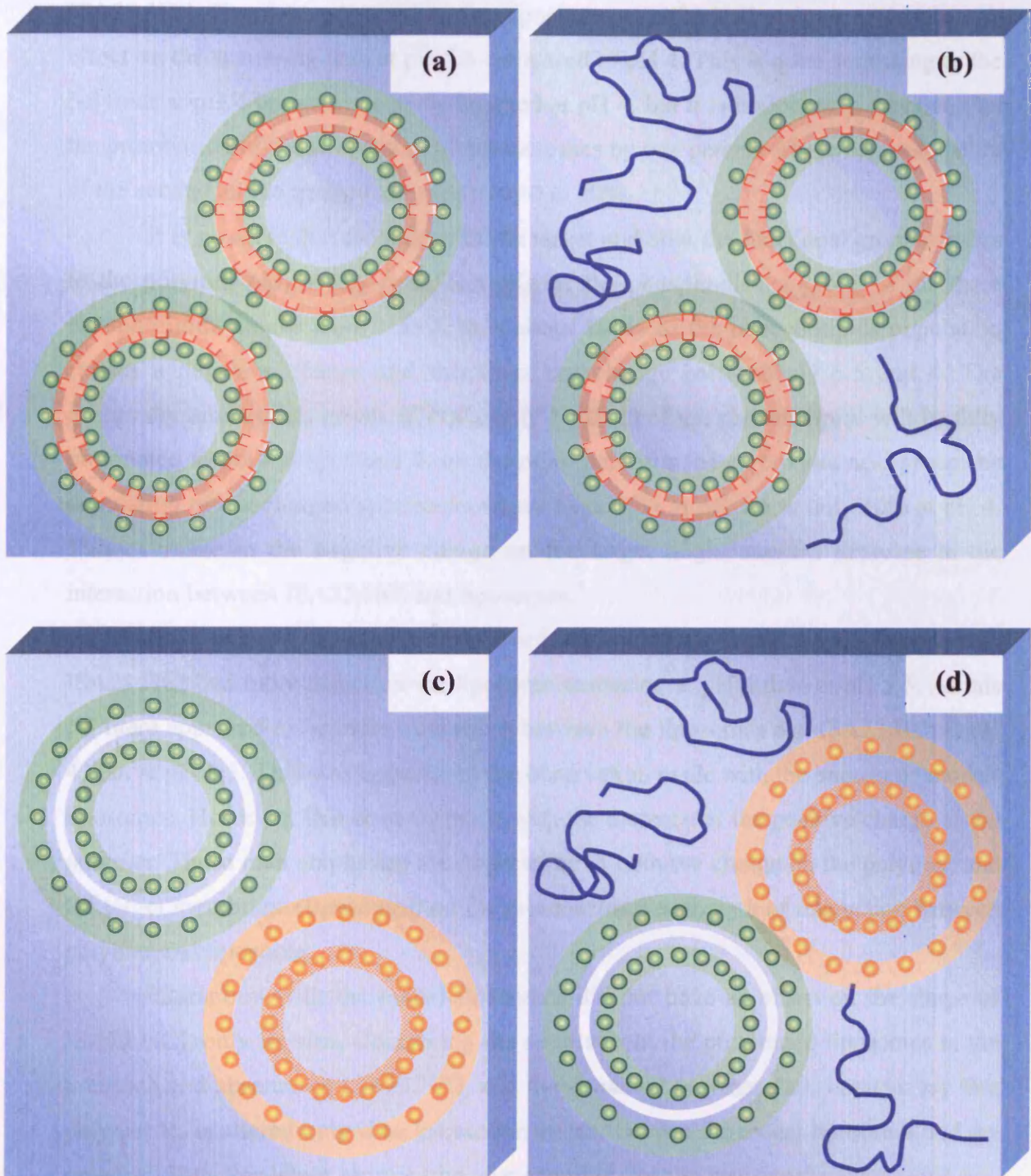


Figure 6.17 The schematic diagram representing parts of the liposomes/polymer system responsible for scattering in the protonated (panel a and b) and the deuterated liposomes (panel c and d).

liposomes at pH 7.4, as the scattering data does not change in the presence of ISA23.HCl. For the endosome model-liposomes, ISA23.HCl appears to have more effect on the scattering data at pH 5.5 compared to pH 4. This is quite surprising as the polymer at pH 4 is more positively charged at pH 4, but it is important to mention that the protonation of the first amino group increases by one percent where the protonation of the second amino group increased from 0 to 10%.

It is possible that the charge of the target and how the functional group appears to the polymer play a key role. The pKa of the phosphodiester group of the three phospholipids ranges from 1 to 2, thus about 100% of the phospholipids population carries a negative charge and this does not change between pH 5.5 and 4. The quaternary ammonium group, (N^+)R₄ or (N^+)RH₃ of the phospholipids will be fully protonated at both pH 5.5 and 4, on the other hand for the carboxylic acid group the population of the charged species decreases from 50% at pH 5.5 to only 10% at pH 4. This decrease in the negative charge on the target might cause a decrease in the interaction between ISA23.HCl and liposomes.

An opposite trend, was observed with the lysosomal model liposomes. ISA23.HCl had more affect on the liposome scattering at pH 4 than at pH 5.5. At this pH there appeared to be more interaction between the liposomes and ISA23.HCl at pH 4 than at pH 5.5. This was opposite to the observation made with the endosome model-liposomes. However, this does correlate with the increase of the positive charge of the polymer. These data emphasise the importance of both the charge on the polymer, and the target membrane (liposomes) on the presence/or the strength of interaction between polymer and liposome.

Interaction with the model-liposomes did not have an effect on the shape of ISA23.HCl, only its size. Combining the results from the protonated liposomes in the presence and absence of ISA23.HCl, and the extracted polymer data, one can say that polymer R_g is altered only if an interaction exists between the model liposomes and the polymer. But, this is not always true. For example, for the lysosomal model at pH 5.5, the scattering data from the protonated system indicate no interaction (as the scattering was exactly the same in the presence and absence of ISA23.HCl). However, the R_g of the polymer increased by 1.4 nm. These observations indicate the importance of distinguishing between the existence of an association / interaction with measurable physical changes and association / interaction with no measurable physical change.

During interaction it is possible that the polymer binds to the liposomes by electrostatic interaction and this could cause breakage by the removal of phospholipids from the bilayer (Figure 6.18). It is unlikely that the polymer causes a complete destruction of the liposomes.

As in Chapter 5, the SANS of model liposomes in the presence of polymers (control polymers used in the haemolysis assay in Chapter 3) was also measured.

The negative control (dextran) did not interact with the model liposomes, as the data had similar form to that of the endosome (alone) (Figure 6.19a).

The addition of TX-100 caused a complete destruction of the liposomes (Figure 6.19b) as the data form of the liposome completely changed in the presence of ISA23.HCl. This result is in agreement with that obtained from examining the effect of TX-100 on the size distribution of the liposomes using PCS. It is possible that TX-100 breaks the liposomes by forming micelles with the phospholipids (in the liposomes).

For the positive control, PEI, the results are quite interesting. No interaction was observed (Figure 6.19) between ISA23.HCl and lysosome model-liposomes, but the scattering of the endosome model-liposomes does alter quite significantly in the presence of ISA23.HCl. The only difference between the two models is the amount of the DPPC and DPPS (DPPS is higher in the lysosomal model liposomes compared to that of endosomal model-liposomes, and the opposite is true for DPPC). The scattering of the endosome model-liposomes is higher (in the whole Q range) in the presence of PEI, this could be due to the association of the polymer with phospholipids headgroups, thus the polymer could be wrapped or located on the liposomes, and this causes the increase in the scattering from the system. As the data form of the endosome model-liposomes in the presence and the absence of the PEI is almost identical, this could indicate that PEI is not breaking the bilayer, so there is only association / little interaction, but no physical change in the liposomes bilayer.

The scattering data from lysosomal model-liposomes was not at all effected by the presence of ISA23.HCl, this is not as expected as the lysosomal model contain more DPPS, which carries two negatively charged groups, on the other hand DPPC only carries one negatively charged group, thus there should be more association / interaction between PEI with the lysosome liposomes compared to that with endosome model, however the opposite was observed.

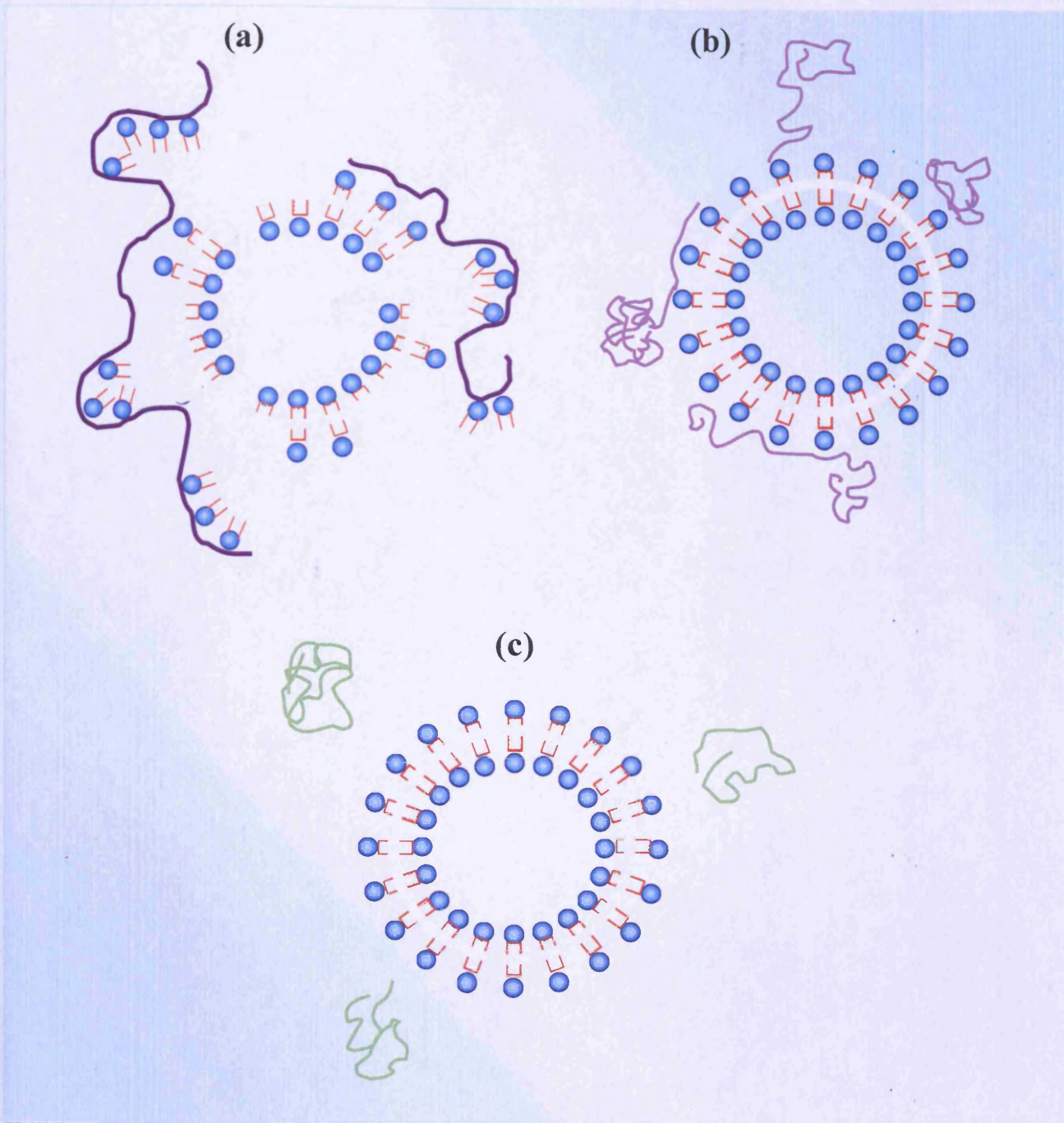


Figure 6.18 The hypothetical representation of the different possible interaction between ISA23.HCl and model-liposomes. Panel (a) association and interaction between ISA23.HCl and model liposomes, causing the destabilisation of the bilayer, panel (b) association with little interaction between ISA23.HCl and model liposomes, but with no destabilisation of the bilayer, and panel (c) no association and interaction between ISA23.HCl and model liposomes

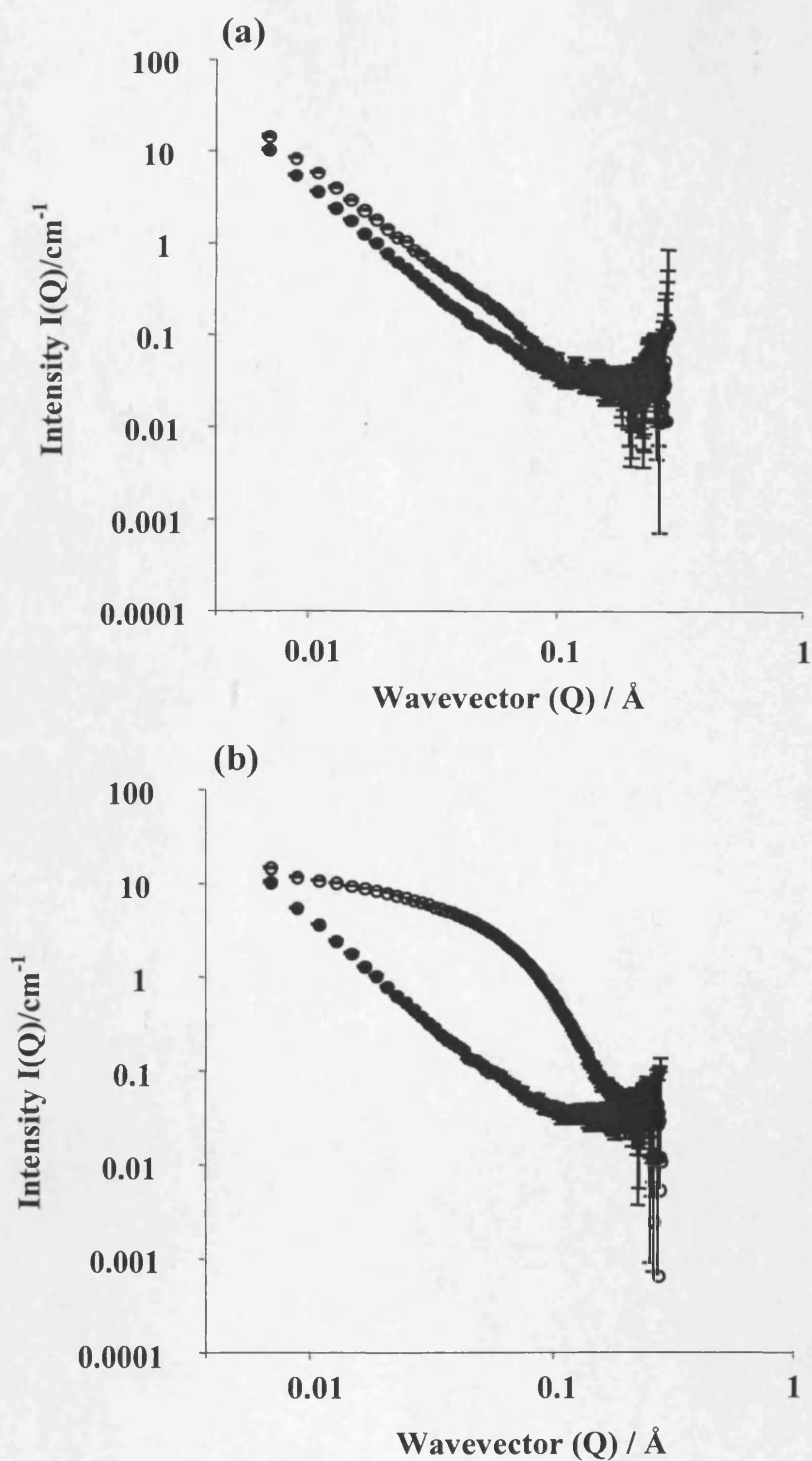


Figure 6.19 The effect of control polymers on the scattering of endosome membrane-model liposomes. SANS data of liposomes obtained in the presence (empty circles) and absence (solid circles) of dextran (panel a) or TX-100 (panel b)

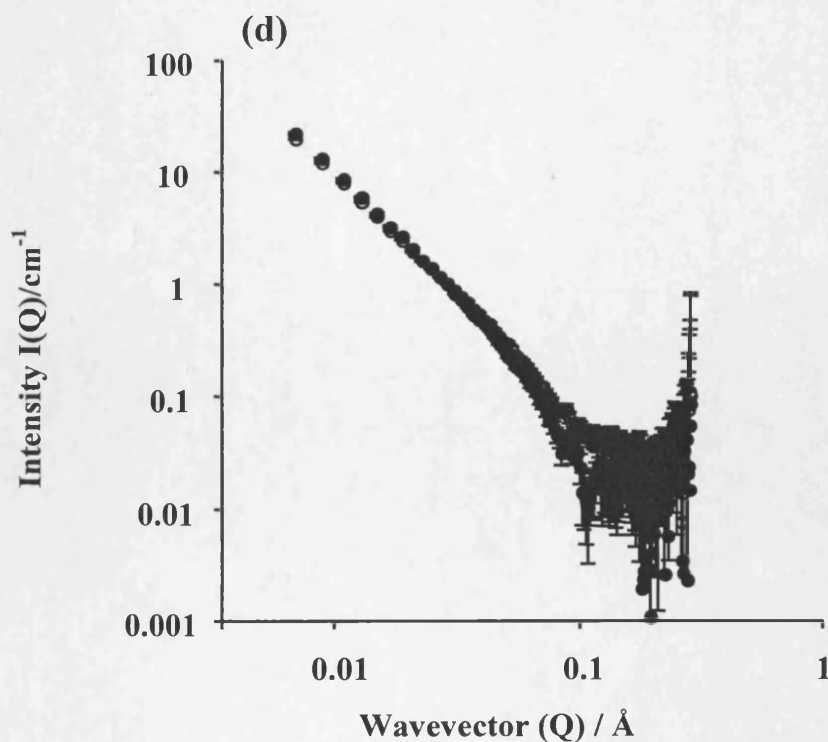
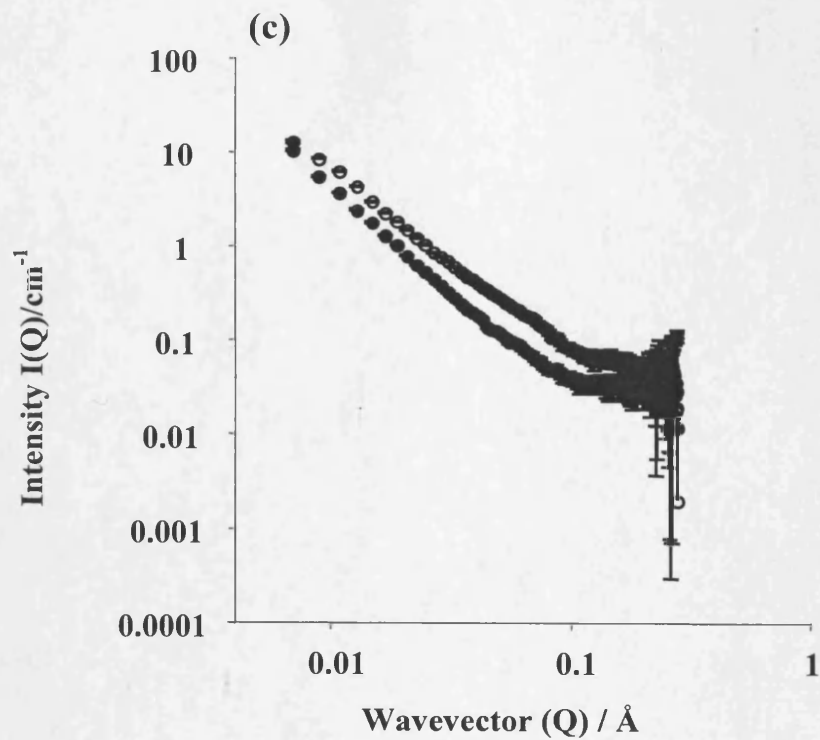


Figure 6.19 (continued). SANS data of endosome membrane-model liposome in the presence (empty circles) and absence (solid circles) of PEI at pH 7.4 (panel c). Panel (d) lysosome membrane-model liposomes in the presence (empty circles) and absence (solid circles) of PEI, at pH 7.4

6.5 Conclusions

To conclude it was possible to prepare liposomes with the desired phospholipids composition and they were stable at the pH values used to conduct polymer-liposomes study. The preparation of calcein-entrapped liposomes was not successful as a number of problems were encountered in the preparation process and solving this would require more time or changing the composition of the liposomes, but this would be something to do for the future.

The existence or the strength of interaction depends on both the charge of the polymer and the charge of the liposomes (the target), also the flexibility of the polymer and how the charges appear to the membrane. Also, the accessibility of the phospholipids charged groups to the polymer is also important for polymer-membrane interaction. It is important to acknowledge that an association / interaction between model liposomes and polymer is possible but without physical change in the liposomes or change in the polymer morphology.

Chapter 7
General Discussion

Chapter 7 General Discussion

Increased understanding of the human as a “biological system” is leading to advances in science and technology that can be used to develop new diagnostics and medicines, to improve the design of endosomolytic polymers for cytosolic delivery of genes and proteins.

The aim of gene therapy is often delivery of a specific sequence of DNA into the nucleus of a cell to correct the faulty gene. This seems a relatively simple and straight forward idea. It would be easy to realise if the body did not have so many defence systems (i.e RES) and biological barriers (i.e. the therapeutic agent could freely enter the cell), and was allowed free access to the cytoplasm and the nucleus without any challenge. Then the process would be simple, and there would not have been the need to conduct the studies described here. Numerous studies have been conducted using viral and non-viral vectors, and it has proven very difficult to overcome the many different obstacles in the biological system and thus it is hard to produce safe and efficient transfection agents. As discussed in Chapter 1, there are a number of advantages and disadvantages associated with both viral and non-viral vectors. Many challenges remain to be solved, but each step is a little piece in this large complex jigsaw puzzle. Section 7.3 describes the contributions this study has made to the scientific field, but first the other recent developments with non-viral are briefly summarised.

7.1 Recent development in the non-viral vectors

The development of effective non-viral vectors is still considered an important part of the development of successful gene therapy. Over the last 3 years, most studies have focused on the development of cationic polymers by the preparation of hybrid derivatives, and also using derivatives enclosing targeting ligands (reviewed in Park et al, 2006). Most studies have tried to correlate structure with biological properties such as cytotoxicity and transfection efficiency. The most popular cationic polymer, PEI, displays a high transfection efficiency compared to other polycationic polymers, but many derivatives have been very cytotoxic. Although PEI's have relatively high transfection efficiency compared to other polymers, their transfection efficiency is still low compared to the viral vectors (Boussif et al, 1995; Godbey et al, 1999b; 2001). A number of approaches are being employed to try and solve this problem. For example,

the conjugation of PEI to polymers such as PEG (Ogris et al, 1999; Kim et al, 2004), dextran (Tseng and Jong, 2003), polyacrylic acid (Trubetskoy et al 2003), dextran sulfate (Tiyaboonchai et al, 2003) and poly(N-(2-hydroxypropyl)methacrylamide) (pHPMA) (Oupicky et al, 2002b; Carlisle et al, 2004) (reviewed in Lungwitz, 2005). Generally, hybrid polymer systems have been successfully synthesised that can increase stability of the polyplex in the circulation, reduce non-specific interaction with blood cells, reduce RES clearance and reduce general toxicity. However, the ability of these PEI-based polyplexes to transfect cells is still poor (Ogris et al, 2003). To try and solve this problem, targeting moieties, such as transferrin (Kircheis et al, 2001), antibodies (Merdan et al, 2003; Chiu et al, 2004) and folate (Benns et al, 2001; Kim et al, 2005) have been included (reviewed in Park et al, 2006). Although this approach can significantly increase transfection efficiencies in vitro, with minimal toxicity, these new hybrid constructs will be able to target the desired cells in vivo. These systems provide potential candidates for gene delivery, but they are still far from ideal.

The second most widely studied cationic polymer is PLL. Just like PEI, the main disadvantages of PLL is its high toxicity. Similar approaches (as applied to PEI) have been used to improve PLL. PEGylation of PLL caused a decrease in toxicity and the PLL-PEG copolymer was able to protect/stabilise DNA better, and gave higher transfection efficiencies compared to the PLL alone (Lee et al, 2001).

Chitosan is another cationic polymer that is being widely studied. A number of modified chitosans have been reported, but generally they show lower transfection efficiencies compared to PEI. Quaternised chitosan derivatives displayed improved gene delivery and reduced toxicity in MCF-7 cells compared to PEI (Kean et al, 2005). However, lactosylated chitosans failed to enhance transfection in HepG2 cells (Erbacher et al, 1998; reviewed in Gupta et al, 2005).

Research into new PAA chemistry (not conducted in this study) continues. Emilietri et al (2005) prepared new PAAs containing disulfide linkages in their main chain with the aim of providing carriers for drugs and peptides. Their degradation behaviour was investigated, and it was shown that PAAs containing disulfide groups were susceptible to reductive cleavage in the presence of thiols (Emilietri et al, 2005).

As it was discussed before (Chapter 1, section 1.5), ISA1 and ISA23 are

relatively non-toxic and they display pH-dependant membrane activity. ISA1 is able to deliver non-permeant toxins, but displays poor transfection efficiency, whereas ISA23 is able to transfect cells, avoids hepatic clearance, and targets tumours by the enhanced permeation retention effect but ISA23 did not promote intracellular delivery of non-permeant toxins (Richardson et al, 1999; Patrick et al, 2001a). It appeared that both polymers ISA1 and ISA23 have some desirable properties that the other is lacking (Lavignac et al, 2004). This initiated the synthesis of new block and random copolymers composed of ISA1 and ISA23, in order to assess whether new PAAs could be made with increased toxin delivery efficiency (Lavignac et al, 2004). The random and block copolymers are not cytotoxic and still displayed pH-dependant haemolytical activity, but to a lesser degree compared to ISA23. Only one block copolymer composed of ISA1 : ISA23 of 1 : 2 ratio, was able to deliver toxins, better than the parent polymers (Lavignac et al, 2004). This was however a marginal improvement.

Several attempts to improve endosomolytic efficiency of ISA1 and ISA23 were carried out by conjugating with the polymer melittin (Lavignac et al, 2005). ISA1-melittin showed a better gelonin delivery than ISA1, but ISA23-melittin was still unable to deliver gelonin. Just like ISA23, this conjugate showed pH-dependant haemolysis (non-haemolytic at pH 7.4), and had low cytotoxicity (Lavignac et al, 2005).

The idea of PAA block and random copolymers is interesting, and it provides a bench mark to establish new approaches to combine crucial and desirable properties of different PAAs (or monomers).

7.2 Mechanism of action of ISA23.HCl as an endosomolytic polymer

The main objective of this study was to establish the mechanism by which PAAs caused pH-dependant membrane breakage by studying their physico-chemical properties. It was hoped that an insight into the molecular mechanisms would allow prediction of chemical improvements to structure.

At the cellular level, the PAA polymer will first encounter the plasma membrane. It was shown using SANS, that at pH 7.4, ISA23 did not appear to interact with the plasma membrane-model liposomes. Therefore it is likely that the polymer is internalised by fluid-phase endocytosis, although a non-specific adsorptive pinocytosis process could still play a part (no evidence was found here).

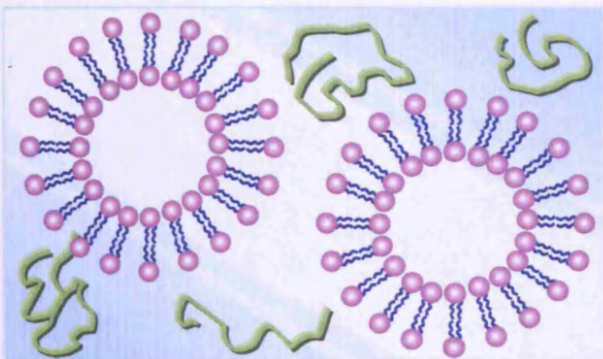
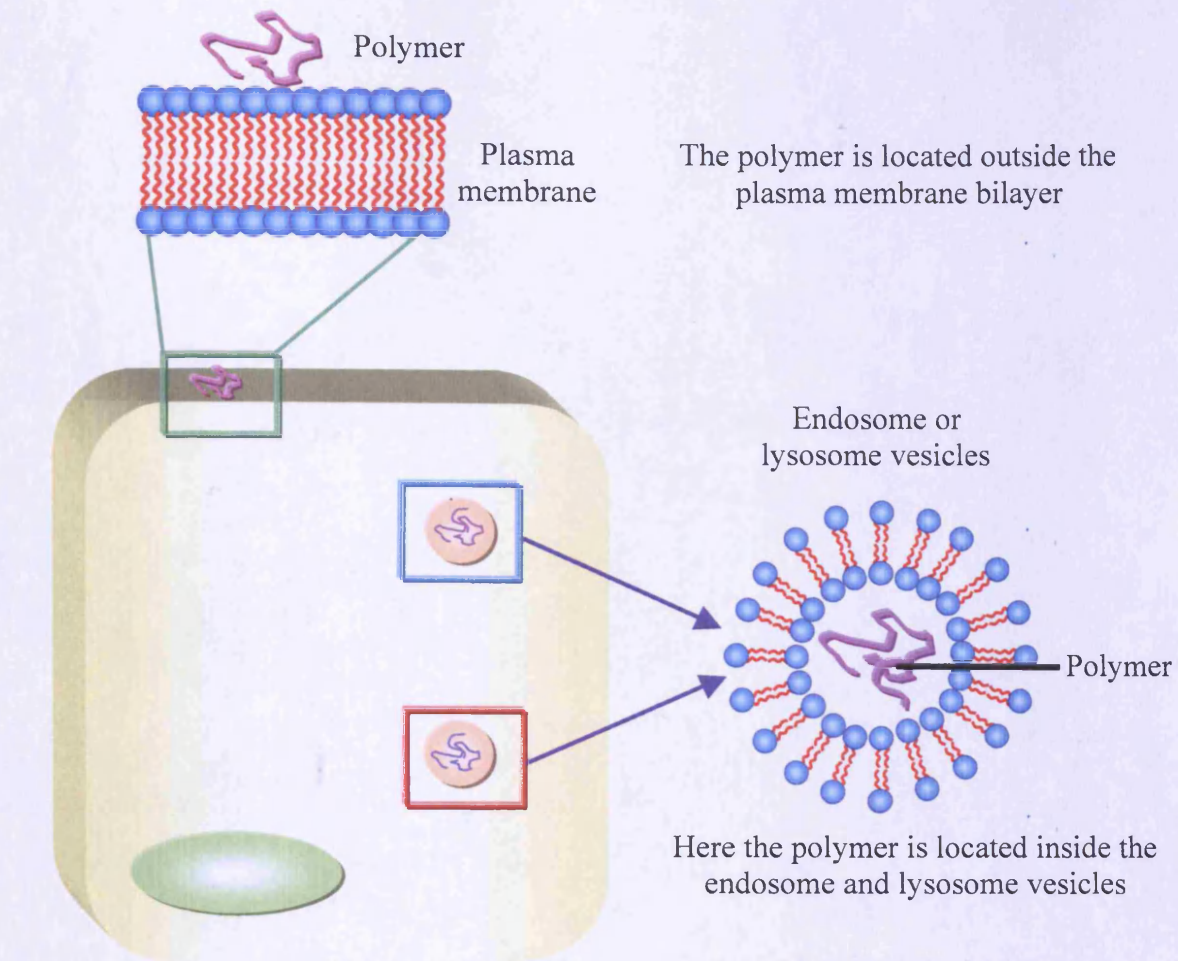
The decrease in pH to 6.5 as would be seen in the early endosome caused the

slight increase in ISA23 size (but the polymer shape remained unaltered) as a Gaussian coil was still the best model (Chapter 4) (Griffiths et al, 2004; Khayat et al, 2006). As the pH was decreased further as would be seen in the late endosome (pH 6.5 – 5.5), the size of ISA23 increased further to 3.6 nm (measured alone in solution) and/or 4.3 nm (measured in the presence of endosomal model liposomes). It is unlikely that this increase in size would be sufficient to cause endosomal breakage as the overall diameter of the endosome is around 100 nm. As discussed in Chapter 1, the proton sponge hypothesis and the pore formation through the membrane bilayer are unlikely to be the mechanism of action of PAAs. Induction of membrane curvature/membrane bending, is the most likely hypothesis, with the decrease in pH in the endosomal/lysosomal system, the cationic nature of the PAA will increase, causing an increase in size, but not shape (it does not become more elongated or rod-like). It is possible that the polymer expansion will expose the positive charges, allowing the chain to associate/bind to the vesicle membrane by the electrostatic interaction (between the opposite charges on the polymer and the phospholipids). As interaction increases, the polymer may destabilise the bilayer by inducing strains/curvatures and/or due to the removal of phospholipids. If an increase in tension occurs, this will be followed by the perturbation of the vesicle.

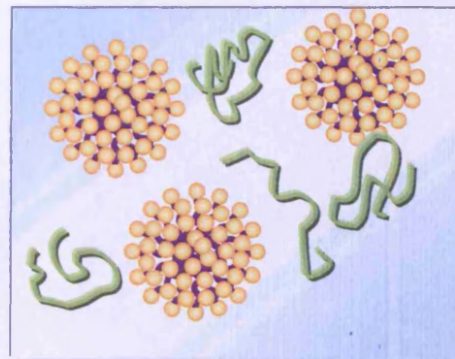
This is a reasonable hypothesis based on the results obtained in this study. However, the experimental design could still be improved. For example, as it was mentioned in Chapter 6, the ISA23.HCl-liposomes interaction was studied by the addition of the polymer to the outside of the liposomal preparation. At the cellular level, the PAA will be concentrated inside the endosomes and lysosomes. The external surface curvature of a bilayer is very different, and this will probably have a major effect on the polymer and the way the polymer interacts with the target (Figure 7.1). In addition, the surface tension inside the vesicle will be affected by the polymer-membrane interaction. This in turn will affect the way the vesicles are destabilised.

Before we go any further it is important to ask if the objectives of this study were fulfilled? Unfortunately there is no clear answer to this question; some of the aims were achieved, while others were partially achieved.

Studies investigating the effect of pH on the morphology/size of the ISA23



Polymer-liposomes (plasma, endosome and lysosome) interaction



Polymer-micelles interaction

To investigate the polymer-model membrane interaction, the polymer were located outside the model

Figure 7.1 The comparison between what the polymer encountered during intracellular trafficking and it comparison to the experiments conducted here.

polymer coil were successfully accomplished. Wan et al (2004) used SANS for the first time to investigate PAA solution conformation. These studies confirmed the previous results, but there were also new findings. For example, my studies also examined the affect of polymer concentration and temperature on the morphology of the polymer (Khayat et al, 2006). In both cases the PAA size and shape were not affected.

The next objective was to establish how the PAA caused pH-dependent membrane breakage. This was partially answered, it is clear that the increase in the positive nature of polymer is the key factor promoting interaction. Overall, the results obtained using the three membrane models (RBCs, micelles/surfactants, and liposomes) were in agreement. However, there were a few exceptions. The micelles composed of lyso-PC alone, did not interact with ISA23 at pH 5.5 (Khayat et al, 2005). This was shown using three techniques:- surface tension, EPR and SANS. Interestingly, ISA23 did interact with the endosome membrane-model liposomes and micelles composed of SDS, at this pH. There was also no interaction observed between lysosome membrane-model liposomes and ISA23.HCl at pH 5.5. The scattering of both endosome- and lysosome models was only slightly altered by ISA23.HCl at pH 4, where the polymer is even more cationic in nature.

Another interesting observation was made in the experiments investigating ISA23.HCl interaction with the surfactant micelles composed of the positively charged CTAB surfactant (Chapter 5). It was found that there was clear interaction between the model micelle and the polymer at pH 7.4, and to a lesser extent at pH 5.5. These results show that the carboxylic acid group of ISA23.HCl was able to promote interaction with the positively charged micelles. It was also found that an increase of the positive charge of the amphoteric ISA23.HCl decreased the extent of interaction. This being the case, then is it also possible that the carboxylic acid groups of ISA23 might also have a negative effect on the interaction between the cationic groups of the polymer with the model membrane? It is well known that the physiological membrane often carries an overall net negative charge. Hence, cationic polymers are mainly used to promote interaction and destabilisation. However, phospholipids can also carry a positively charged group, so it might also be possible that there is an interaction between this group and the negatively charges carried on the polymer. Is it also possible that there could be a PAA-PAA chain interaction, which results in aggregation. However as it

was shown in Chapter 4, there was no evidence of this.

Do these experiments give some hint as to the improved design of a PAA? It appears that the increase in positive charge on PAA between 7.4 and 5.5 does not occur rapidly enough to ensure efficient endosomal breakage at pHs less than 5.5. For optimum polymer-membrane interaction, both the target membrane and the polymer would play a part. Both the charge ratio on membrane and the polymer, and the accessibility of one to the other would be very important. Recent studies (unpublished) have shown lower molecular weight PAAs to be most effective.

7.3 Conclusions and future studies

These studies will play an important role in the forward progression of the field of endosomolytic polymers. Particularly for PAAs, but the techniques established can be much more generally applied. These studies are the first to use SANS to study the morphology and size changes of an endosomolytic polymer. Also it was the first time that polymer-membrane interactions had been probed in this way. The morphology of model membrane (liposomes and micelles) was investigated in the presence of polymer, and the effect of the model membrane on the morphology of the polymer was also examined. Surface tension and EPR techniques are commonly employed to investigate colloidal system, but here they were used to investigate endosomolytic polymer-model membrane interaction in a new way.

Usually biologists use RBC lysis to investigate polymer-membrane interaction. It is arguable that this is far from a 'normal' cell membrane, and intracellular vesicle membranes will be different in composition. Here other models were developed. First micelles were used as a simple model to obtain a general picture of polymer-membrane interaction. This was tuned by varying the micelle composition and the ratio of the surfactant mixture. Thus it was possible to systematically study the effect of target on the strength of interaction.

The use of liposomes as model membranes to study polymer interaction was not original. However we believe that no one has used liposomes prepared to contain a phospholipid composition chosen to mimic the plasma, endosome and lysosome membranes respectively. Both the micelles and liposomes were also prepared with deuterated surfactants and phospholipids, to allow contrast matching and thus they could be used to extract information on the polymer.

This was a multidisciplinary project, and it highlights the importance of collaboration across different scientific disciplines. In this case biology, chemistry and physics were combined to try and better understand an endosomolytic polymer. In addition, the mathematical modelling was much more complex than the usual statistical methods commonly employed in scientific research.

The results presented here have opened many further questions and would be a great opportunity for further research. Polymer-membrane interaction using liposome as a model, provides the greatest potential for further work. Listed below are a number of different experiments that could have been done (if time had permitted) to further improve our understanding of PAA as an endosomolytic polymer:

- 1) Time was needed for the fitting of the scattering data obtained from the liposomes in the presence of the polymer. The calculated parameters could then be compared to those of liposomes alone.
- 2) It would have been interesting to use PCS to study the effect of ISA23.HCl on the size distribution of plasma, endosome and lysosome membrane-model liposomes at pH 7.4, 6.5, 5.5 and 4. These results can be then compared to the result obtained from SANS.
- 3) Difficulties were encountered in the preparation of calcein-entrapped liposomes, with further work this could be solved and such models used to study the release rate of the entrapped fluorescence dye by ISA23. Liposomes containing a macromolecular probe (e.g. FITC-dextran) could also be used.
- 4) It would be interesting to try and entrap the PAA inside of the liposomes to study its effect on the inner face. By carefully changing the pH inside the liposomes, the polymer-membrane interaction could be investigated by measuring the release of radiolabeled-PAA. This is a more realistic model for both the endosome and lysosome vesicles.
- 5) In addition it would be interesting to investigate the effect that cholesterol, proteins, lipid rafts, and the distribution of phospholipids between the inner and outer leaflet of the bilayer had on polymer-membrane interaction. These studies would be more complex.
- 6) EPR could also be used to study the effect of polymers on the fluidity of the bilayer of the model liposomes.

- 7) Another topic, which remained unexplored would be the use of molecular modelling to examine sterically how the phospholipids in the membrane bilayer might access and interact with ISA23.

Although many experiments remain, this thesis has started a new field that brings together physico-chemical methods and the understanding and design of endosomolytic polymers. Hopefully in the future this approach will help realise improved efficiency of cytosolic delivery systems.

Bibliography

Bibliography

A.E.Aneed, An overview of current delivery systems in cancer gene therapy, *Journal of controlled release*, 2004, **94**, 1-14.

B.Alberts, D.Bray, J.Lewis, M.Raff, K.Roberts and J.Dwatson, Vesicular traffic in the secretory and endocytotic pathways, In *Molecular biology of the cell*, New York: Garland Publishing, Inc., 1994, 3rd edition, 604-654.

A.B.Auerbach, Production of functional transgenic mice by DNA pronuclear microinjection, *Acta Biochimica Polonica*, 2004, **51**, 9-31.

F.Aulenta, W.Hayes and S.Rannard, Dendrimers: a new class of nanoscopic containers and delivery devices, *European Polymer Journal*, 2003, **39**, 1741-1771.

V.K.Aswal, Salt effect in ionic mixed micelles, *Chemical Physics Letters*, 2003, **371**, 371-377.

G.Bai, Y.Wang, and H.Yan, Thermodynamics of Interaction between Cationic Gemini Surfactants and Hydrophobically Modified Polymers in Aqueous Solutions, *The Journal of Physical Chemistry B*, 2002, **106**, 2153-2159.

B.L.Bales and C.Stenland, The spin probe-sensed polarity of sodium dodecyl sulfate micelles is proportional to the one-fourth power of the surfactant concentration, *Chemical Physics Letters*, 1992, **200**, 475-482.

B.L.Bales, L.Messina, A.Vidal, M.Peric and O.R.Nascimento, Precision Relative Aggregation Number Determinations of SDS Micelles Using a Spin Probe. A Model of Micelle Surface Hydration, *The Journal of Physical Chemistry B*, 1998, **102**, 10347-10358.

B.L.Bales, A.Shahin, C.Lindblad and M.Almgren, Time-Resolved Fluorescence Quenching and Electron Paramagnetic Resonance Studies of the Hydration of Lithium Dodecyl Sulfate Micelles, *The Journal of Physical Chemistry B*, 2000, **104**, 256-263.

R.Barbucci, P.Ferruti, M.Micheloni, M.Delfini, A.L.Segre and F.Conti, Thermodynamic and ¹³C n.m.r. data on the protonation of polymeric bases whose repeating units behave independently towards protonation, *Polymer*, 1980, **21**, 81-85.

R.Barbucci, M.Casolaro, P.Ferruti, V.Barbone, F.Lelj and L.Oliva, Macroinorganics 7. Property-structure relationships for polymeric bases whose monomeric units behave independently toward protonation, *Macromolecules*, 1981a, **14**, 1203-1209.

R.Barbucci, M.Casolaro, M.C.Beni, P.Ferruti, M.Pesavento, T.Soldi and C.Riolo, Protonation and complex formation with heavy-metal ions of two tetra-functional amines and of a new structurally related ion-exchange resin, *J.C.S. Dalton*, 1981b, 2559-2564.

R.Barbucci, M.Benvenuti, G.Casini, P.Ferruti and F.Tempesti, Heparinizable materials (IV). Surface-grafting on polyfethylene terephthalate) of heparin-complexing

poly(amido-amine) chains, *Biomaterials*, 1985, **6**, 102-104.

R.Barbucci, A.Baszkin, M.Benvenuti, M.de L.Costa and P.Ferruti, Surface characterization of heparin-complexing poly(amido amine) chains grafted on polyurethane and glass surfaces, *Journal of Biomedical Materials Research*, 1987, **21**, 443-457.

R.Barbucci, Workshop on the characterization of biomaterials in contact with blood, *Biomaterials*, 1990, **11**, 138-151.

W.M.Becker, L.J.Kleeinsmith, J.Hardin, E.Mulligan, L.Cox, E.Dahlgren, S.Weisberg, L.Kenney (Eds), Membranes: their structure, function and chemistry, In *The World of the cell*, Addison Wesley longman, Inc., San Francisco, 2000, 4th edition, 163-200.

J.-P.Behr, Gene transfer with synthetic cationic amphiphiles: prospects for gene therapy, *Bioconjugate Chemistry*, 1994, **5**, 382-389.

J.-P.Behr, The proton sponge: a trick to enter cells the viruses did not exploit, *Chimica*, 1997, **51** (N1-2), 34-36.

T.Benachir, and M.Lafleur, Study of vesicle leakage induced by melittin, *Biochimica et Biophysica Acta*, 1995, **1235**, 452-460.

J.M.Benns, J.S.Choi, R.I.Mahato, J.S.Park and S.W.Kim, pH-sensitive cationic polymer gene delivery vehicle: *N*-Ac-poly(-histidine)-graft-poly(-lysine) comb shaped polymer, *Bioconjugate Chemistry*, 2000, **11**, 637-645.

J.M.Benns, A.Maheshwari, D.Y.Furgeson, R.I.Mahato, S.W.Kim, Folate-PEG-folate-graft-polyethylenimine-based gene delivery, *Journal of Drug Targeting*, 2001, **9**, 123-139.

N.Bergstrand, M.C.Arvidsson, J-M.Kim, D.H.Thompson and K.Edwards, Interactions between pH-sensitive liposomes and model membranes, *Biophysical Chemistry*, 2003, **104**, 361-379.

M.L.Bergström, M.U.R.Kjellin, P.M.Claesson and I.Grillo, Small-Angle Neutron Scattering Study of Mixtures of Cationic Polyelectrolyte and Anionic Surfactant: Effect of Polyelectrolyte Charge Density, *The Journal of Physical Chemistry B*, 2004, **108**, 1874-1881.

L.J.Berliner and J.Reuben (Eds), Spin labeling : theory and applications, Biological magnetic resonance, New York : Plenum, 1989, **8**.

S.Bhattacharya and J.Haldar, Molecular design of surfactants to tailor its aggregation properties, *Colloids and Surfaces A: Physicochemical and Engineering Aspects*, 2002, **205**, 119-126.

E.J.Blott and G.M.Griffiths, Secretory Lysosomes, *Nature Reviews Molecular Cell Biology*, 2002, **3**, 122-131.

B.C.Boland and S.Whapham (Eds), "User Guide to Experimental Facilities at the ISIS", Rutherford Appleton Laboratory Report RAL-92-041, 1992.

O.Boussif, F.Lezoualc'h, M.A.Zanta, M.D.Mergny, D.Scherman, B.Demeneix, M.M.Breuer and A.D.Jenkins (Eds), Polymer Science, a material science handbook, 1972, **2**, 1136.

O.Boussif, F.Lezoualch, M.A.Zanta, M.D.Mergny, D.Scherman, B.Demeneix and J-P.Behr, A versatile vector for gene and oligonucleotide transfer into cells in culture and in vivo: polyethylenimine, *The Proceedings of the National Academy of Sciences of the United States of America*, 1995, **92**, 7297-7301.

M.D.Brown, A.G.Schatzlein and I.F.Uchegbu, Gene delivery with synthetic (non viral) carriers, *International Journal of Pharmaceutics*, 2001, **229**, 1-21.

A.Brownlie, I.F.Uchegbu and A.G.Schätzlein, PEI-based vesicle-polymer hybrid gene delivery system with improved biocompatibility, *International Journal of Pharmaceutics*, 2004, **274**, 41-52.

M.Buzzacchi, P.Schmiedel and W.von Rybinski, Dynamic surface tension of surfactant systems and its relation to foam formation and liquid film drainage on solid surfaces, *Colloids and Surfaces A: Physicochem. Eng. Aspects*, 2006, **273**, 47-54.

P.Campeau, P.Chapdelaine, S.Seigneurin-Venin, B.Massie and J.P.Tremblay, Transfection of large plasmids in primary human myoblasts, *Gene Therapy*, 2001, **8**, 1387-1394.

M.R.Capecci, High efficiency transformation by direct microinjection of DNA into cultured mammalian cells, *Cell*, 1980, **22**, 479-488.

R.C.Carlisle, T.Etrych, S.S.Briggs, J.A.Preece, K.Ulbrich and L.W.Seymour, Polymer-coated polyethylenimine/DNA complexes designed for triggered activation by intracellular reduction, *Journal of gene Medicine*, 2004, **6**, 337-344.

C.Y.Cheung, N.Murthy, P.S.Stayton and A.S.Hoffman, A pH-sensitive polymer that enhances cationic lipid-mediated gene transfer, *Bioconjugate Chemistry*, 2001, **12**, 906-910.

T.V.Chirila, P.E.Rakoczy, K.L.Garrett, X.Lou and I.J.Constable, The use of synthetic polymers for delivery of therapeutic antisense oligodeoxynucleotides, *Biomaterials*, 2002, **23**, 321-342.

S.J.Chiu, N.T.Ueno and R.J.Lee, Tumor-targeted gene delivery via anti-HER2 antibody (trastuzumab, Herceptin) conjugated polyethylenimine, *Journal of Controlled Release*, 2004, **97**, 357-369.

Y.W.Cho, J-D.Kim and K.Park, Polycation gene delivery systems: escape from endosomes to cytosol, *Journal of Pharmacy and Pharmacology*, 2003, **55**, 721-734.

R.J.Christie and D.W.Grainger, Design strategies to improve soluble macromolecular

delivery constructs, *Advanced Drug Delivery Reviews*, 2003, **55**, 421-437.

L.Ciani, S.Ristori, A.Salvati, L.Calamai and G.Martini, DOTAP/DOPE and DC-Chol/DOPE lipoplexes for gene delivery: zeta potential measurements and electron spin resonance spectra, *Biochimica et Biophysica Acta (BBA) – Biomembranes*, 2004, **1664**, 70-79.

S.D.Conner and L.S.Schmid, Regulated portals of entry into the cell, *Nature*, 2003, **422**, 37-44.

P.R.Cullis and B.DeKruiff, The polymorphic phase behaviour of phosphatidylethanolamines of natural and synthetic origin. A ^{31}P NMR study, *Biochimica et Biophysica Acta*, 1978, **513**, 31-42.

L.R.Dalton (Ed), EPR and advanced EPR studies of biological systems, Boca Raton, Fla. : CRC Press, 1985.

F.Danusso and P.Ferruti, Synthesis of tertiary amino polymers, *Polymer*, 1970, **11**, 88-113.

P.R.Dash, M.L.Read, L.B.Barrett, M.A.Wolfert and L.W.Seymour, Factors affecting blood clearance and *in vivo* distribution of polyelectrolyte complexes for gene delivery, *Gene Therapy*, 1999, **6**, 643-650.

P.Debye, Molecular-weight determination by light scattering, *Journal of Physical Chemistry*, 1947, **51**, 18-32.

A.J.Dianoux and G.Lander (Eds), Neutron data booklet, ILL, 2002, 1st edition, 1.1-2.

P.Dubruel, B.Christiaens, B.Vanloo, K.Bracke, M.Rosseneu, J.Vandekerckhove and E.Schacht, Physicochemical and biological evaluation of cationic polymethacrylates as vectors for gene delivery, *European Journal of Pharmaceutical Sciences*, 2003, **18**, 211-220.

S.S.Dukhin, V.B.Fainerman and R.Miller, Hydrodynamic processes in dynamic bubble pressure experiments1. A general analysis, *Colloids and Surfaces SURFACES A: Physicochemical and Engineering Aspects*, 1996, **114**, 61-73.

R.Duncan, P.Ferruti, D.Sgouras, A.Tuboku-Metzger, E.Ranucci and F.A.Bignotti, Polymer-Triton X-100 conjugate capable of PH-dependent red blood cell lysis: a model system illustrating the possibility of drug delivery within acidic intracellular compartments, *Journal of Drug Targeting*, 1994, **2**, 341-347.

R.Duncan, The dawning era of polymer therapeutics, *Nature reviews*, 2003a, **2**, 347-360.

R.Duncan, Polymer-anticancer drug Conjugates, In *Handbook of Anticancer Drug Development*, D.Budman, H.Calvert and E.Rowinsky (Eds), 2003b, 239-260.

R.Duncan, Targeting and intracellular delivery of Drugs, In *Encyclopedia of Molecular*

Cell Biology and Molecular Medicine, R.A.Meyers (Ed), 2005, 2nd edition, **14**, 163-204.

E.Emilitri, E.Ranucci and P.Ferruti, New Poly(amidoamine)s Containing Disulfide Linkages in Their Main Chain, *Journal of Polymer Science Part A: Polymer Chemistry*, 2005, **43**, 1404-1416.

R.M.Epand, J.J.Cheetham, R.F.Epand, P.L.Yeagle, C.D.Richardson, A.Rockwell and W.F.DeGrado, Peptide models for the membrane destabilizing action of viral fusion proteins, *Biopolymers*, 1992, **32**, 309-314.

R.M.Epand, Lipid polymorphism and protein–lipid interactions, *Biochimica et Biophysica Acta (BBA) - Reviews on Biomembrane*, 1998, **1376**, 353-368.

P.Erbacher, S.Zou, T.Bettinger, A.M.Steffan and J.S.Remy, Chitosan-based vector/DNA complexes for gene delivery: biophysical characteristics and transfection ability, *Pharmaceutical Research*, 1998, **15**, 1332-1339.

W.H.Evans and W.G.M.Hardison, Phospholipids, cholesterol, polypeptide and glycoprotein, composition of hepatic endosome subfraction, *Biochemical Journal*, 1985, **232**, 33-36.

V.B.Fainerman, R.Miller and E.V.Aksenenko, Simple model for prediction of surface tension of mixed surfactant solutions, *Advances in Colloid and Interface Science*, 2002, **96**, 339-359.

N.Fang, J.Wang, H-Q.Mao, K.W.Leong and V.Chan, BHEM-Chol/DOPE liposome induced perturbation of phospholipid bilayer, *Colloids and Surfaces B: Biointerfaces*, 2003, **29**, 233-245.

J.Felay, F.Bray, P.Pusani, D.M Parkin, IARC CancerBase, Globocan : Cancer incidence, Mortality and Prevalence Worldwide, Version 1.0. No.5. IARCpress: Lyon, France, 2000.

P.L.Felgner, T.R.Gadek, M.Holm, R.Roman, H.W.Chan, M.Wenz, J.P.Northrop, G.M.Ringold and M.Danielsen, Lipofection: a highly efficient, lipid-mediated DNA-transfection procedure, *Proceedings of the National Academy of Sciences of the United States of America*, 1987, **84**, 7413-7417.

J.Feng and X.Fan, Direct deconvolution of Tung's integral equation using a multi-Gaussian function model for instrumental band broadening in gel-permeation chromatography, *Journal of Chromatography*, 1990, **522**, 57-65.

P.Ferruti and R.Alimardanov, *Chim. Ind. (Milan, Italy)*, 1967, **49**, 831.

P.Ferruti, F.Danusso, G.Franchi, N.Polentarutti and S.Garattini, Effects of a series of new synthetic high polymers on cancer metastases, 1973, *Journal of Medicinal Chemistry*, **16**, 496-499.

P.Ferruti, Biomedical and Pharmacological Application of tertiary Amino polymers", In *Polymeric Amines and Ammonium Salts*, E.J.Goethals (Ed), Pergamon Press, Oxford,

New York, 1980, 305.

P.Ferruti, N.Danzo, L.Oliva, R.Barucci and V.V.Barone, *Ibid*, 1981, 593

P.Ferruti, R.Barbucci, N.Danzo, A.Torrisi, O.Puglisi, S.Pignataro and P.Spartano, Preparation and ESCA characterization of poly(vinyl chloride) surface-grafted with heparincomplexing poly(amido-amine) chains, *Biomaterials*, 1982a, **3**, 33-37.

P.Ferruti, C.Bertoglio Riolo, T.Soldi, M.Pesavento, R.Barbucci, M.C.Beni and M.Casolaro, Protonation and heavy metal ions complex-formation behaviour of three cross-linked resins of poly(amido-amine) structure, *Journal of Applied Polymer Science*, 1982b, **27**, 2239-2248.

P.Ferruti, G.Scapini, M.C.Tanzi and L.Rusconi, TMSynthetic or Semisynthetic Polymers of Medical Significance^o, in: Proceedings I.U.P.A.C. Macromol. Symp. 28th, *International Union of Pure Appl. Chem*, 1982c, 373.

P.Ferruti, I.Domini, R.Barbucci, M.C.Beni, E.Dispensa, S.Sancasciani, M.A.Marchisio and M.C.Tanzi, Heparin absorbing capacities at physiological pH of three poly(amido-amine) resins, and of poly(amido-amine)-surface-grafted glass microspheres, *Biomaterials*, 1983, **4**, 218-221.

P.Ferruti, *Macromol. Synth*, Poly(amido-amine)s, 1985, **9**, 25.

P.Ferruti, E.Ranucci, L.Sartore, F.Bignotti, M.A.Marchisio, P.Bianciardi and F.M.Veronese, Recent results on functional polymers and macromonomers of interest as biomaterials or for biomaterials modification, *Biomaterials*, 1994, **15**, 1235-1241.

P.Ferruti and J.C.Salamone (Eds), Ion-Chelating Polymers (Medical Applications), In *Polymeric Materials Encyclopedia*, CRC Press Inc., Boca Raton, Florida, 1996, **5**, 3334-3359.

P.Ferruti, S.Knobloch, E.Ranucci, R.Duncan and E.Gianasi, A novel modification of poly(L-lysine) leading to a soluble cationic polymer with reduced toxicity and with potential as a transfection agent, *Macromolecular Chemistry and Physics*, 1998, **199**, 2565-2575.

P.Ferruti, E.Ranucci, F.Trotta, E.Gianasi, E.G.Evagorou, M.Wasil, G.Wilson and R.Duncan, Synthesis characterization and antitumour activity of platinum (II) complexes of novel functionalised poly(amidoamine)s, *Macromolecular Chemistry and Physics*, 1999, **200**, 1644-1654.

P.Ferruti, S.Manzoni, S. C.W.Richardson, R.Duncan, N.G.Patrick, R.Mendichi and M.Casolaro, Amphoteric Linear Poly(amidoamine)s as endosomolytic polymers: Correlation between Physicochemical and Biological properties, *Macromolecules*, 2000, **33**, 7793-7800.

P.Ferruti, M.A.Marchisio and R.Duncan, Poly(amidoamine)s: Biomedical Application, *Macromolecular Rapid Communications*, 2002, **23**, 332-335.

- D.Fischer, T.Bieber, Y.Li, H.P.Elsasser and T.Kissel, A novel non-viral vector for DNA delivery based on low molecular weight, branched polyethylenimine: effect of molecular weight on transfection efficiency and cytotoxicity, *Pharmaceutical Research*, 1999, **16**, 1273-1279.
- E.Fiscaro, C.Compari, E.Duce, G.Donofrio, B.R-Roszak and E.Woëniak, Biologically active bisquaternary ammonium chlorides: physico-chemical properties of long chain amphiphiles and their evaluation as non-viral vectors for gene delivery, *Biochimica et Biophysica Acta (BBA) - General Subjects*, 2005, **1722**, 224-233.
- J.Franchini and P.Ferruti, Perspectives on: Recent Advances in Poly(amidoamine)s Chemistry, *Journal of Bioactive and Compatible Polymers*, 2004, **19**, 221-236.
- A.M.Funhoff, C.F.Van Nostrum, G.A.Koning, N.M.E.Schuurmans-Nieuwenbroek, D.J.A.Crommelin and W.E.Hennink, Endosomal escape of polymeric gene delivery complexes is not always enhanced by polymers buffering at low pH, *Biomacromolecules*, 2004, **5**, 32-39.
- A.M.Gallegosa, B.P.Atshavesa, S.Storeya, J.Schoera, A.B.Kierb and F.Schroeder, Molecular and fluorescent sterol approaches to probing lysosomal membrane lipid dynamics, *Chemistry and Physics of Lipids*, 2002, **116**, 19-38.
- D.R.Gauger, C.Selle, H.Fritzsche and W.Pohle, Chain-length dependence of the hydration properties of saturated phosphatidylcholines as revealed by FTIR spectroscopy, *Journal of Molecular Structure*, 2001, **565-566**, 25-29.
- E.Gazit, A.Boman, H.G.Boman and Y.Shai, Interaction of the mammalian antibacterial peptide cecropin P1 with phospholipid vesicles, *Biochemistry*, 1995, **34**, 11479-11488.
- J.Gehl, Electroporation: theory and methods, perspectives for drug delivery, gene therapy and research, *Acta Physiologica Scandinavica*, 2003, **177**, 437-447.
- W.T.Godbey, K.K.Wu and A.G.Mikos, Tracking the intracellular path of poly(ethylenimine) /DNA complexes for gene delivery, *Proceedings Of The National Academy Of Sciences Of The United States Of America*, 1999a, **96**, 5177-5181.
- W.T.Godbey, K.K.Wu and A.G.Mikos, Poly(ethylenimine) and its role in gene delivery, *Journal of Controlled Release*, 1999b, **60**, 149-160.
- W.T.Godbey, K.K.Wu and A.G.Mikos, Poly(ethylenimine)-mediated gene delivery affects endothelial cell function and viability, *Biomaterials*, 2001, **22**, 471-480.
- E.D.Goddard, Polymer/Surfactant Interaction: Interfacial Aspects, *Journal of Colloid and Interface Science*, 2002, **256**, 228-235.
- C-Gomez and R.Duncan, Everted rat intestinal sacs: a new model for the quantitation of P-glycoprotein mediated-efflux of anticancer agents, *Anticancer Research*, 2000, **20**, 3157-3161.
- L.G.Gregory, R.P.Harbottle, L.Lawrence, H.J.Knapton, M.Themis and C.Coutelle,

Enhancement of Adenovirus-Mediated Gene Transfer to the Airways by DEAE Dextran and Sodium Caprate *in Vivo*, *Molecular Therapy*, 2003, **7**, 19-26.

P.C.Griffiths and S.M.King, Small-Angle neutron scattering studies of absorbed polymer layers, In *Encyclopedia of Surface and Colloidal Science*, A.T.Hubbard (ed), 2002, **4**, 4700-4717.

P.C.Griffiths, A.Y.F.Cheung, G.J.Finney, C.Farley, A.R.Pitt, A. M.Howe, S.M.King, R.K. Heenan and B.L.Bales, Electron Paramagnetic Resonance and Small-Angle Neutron Scattering Studies of Mixed Sodium Dodecyl Sulfate and (Tetradecylmalono)bis(*N*-methylglucamide) Surfactant Micelles, *Langmuir*, 2002, **18**, 1065-1072.

P.C.Griffiths, A.Paul, Z.Khayat, K.W.Wan, S.M.King, I.Grillo, R.Schweins, P.Ferruti, J.Franchini and R.Duncan, Understanding the mechanism of action of poly(amidoamine)s as endosomolytic polymers: correlation of physicochemical and biological properties, *Biomacromolecules*, 2004, **5**, 1422-1427.

P.C.Griffiths, A.Paul, Z.Khayat, R.K.Heenan, R.Ranganathan and I.Grillo, A small-angle neutron scattering study of biologically relevant mixed surfactant micelles comprising 1,2-diheptanoyl-sn-phosphatidylcholine and sodium dodecyl sulfate or dodecyltrimethylammonium bromide, *Soft Matter*, 2005, **1**, 152-159.

J.Gruenberg, G.Griffiths and K.E.Howell, Characterisation of the early endosome and putative endocytic carrier vesicles *in vivo* and with an assay of vesicle fusion *in vitro*, *Journal of Cell Biology*, 1989, **108**, 1301-1316.

B.Gupta, T.S.Levchenko and V.P.Torchilin, Intracellular delivery of large molecules and small particles by cell-penetrating proteins and peptides, *Advanced Drug Delivery Reviews*, 2005, **57**, 637-651.

J.Haldar, V.K.Aswal, P.S.Goyal and S.Bhattacharya, Aggregation Properties of Novel Cationic Surfactants with Multiple Pyridinium Headgroups. Small-Angle Neutron Scattering and Conductivity Studies, *The Journal of Physical Chemistry B*, 2004, **108**, 11406-11411.

G.E.Ham, Polymeric Amines and Ammonium salt, E.J.Goethals (ed), Pergamon Press, 1980.

A.von Harpe, H.Petersen, Y.Li and T.Kissel, Characterization of commercially available and synthesized polyethylenimines for gene delivery, *Journal of Controlled Release*, 2000, **69**, 309-322.

J.M.Harris and R.B.Chess, Effect of pegylation on pharmaceuticals, *Nature Reviews Drug Discovery*, 2003, **2**, 214-221.

J.Hawiger, Noninvasive intracellular delivery of functional peptides and proteins, *Current Opinion in Chemical Biology*, 1999, **3**, 89-94.

R.C.Hedden and B.J.Bauer, Structure and Dimensions of PAMAM/PEG Dendrimer-

Star Polymers, *Macromolecules*, 2003, **36**, 1829-1835.

J.Heuser, Three-dimensional visualization of coated vesicle formation in fibroblasts, *Journal of Cell Biology*, 1980, **84**, 560-583.

I.R.C.Hill, M.C.Garnett, F.Bignotti and S.S.Davis, In vitro cytotoxicity of poly(amidoamine)s: relevance to DNA delivery, *Biochimica et Biophysica Acta*, 1999, **1427**, 161-174.

A.J.Hoff (Ed), Advanced EPR : applications in biology and biochemistry, Amsterdam ; Oxford : Elsevier, 1989.

M.J.Hope, M.B.Bally, G.Webb and P.R.Cullis, Production of large unilamellar vesicles by a rapid extrusion procedure: characterization of size distribution, trapped volume and ability to maintain a membrane potential, *Biochimica et Biophysica Acta*, 1985, **812**, 55-65.

K.Ibel (Ed), "Guide to Neutron Research Facilities at the ILL", Scientific Coordination Office, ILL, 1994.

ILL, diagram of the D11 instrument, <http://www.ill.fr/YellowBook/D11/>

ISIS, LOQ diffractometer, <http://www.isis.rl.ac.uk/largescale/loq/loq.htm>

L.Johannes and C.Lamaze, Clathrin-Dependent or Not: Is It Still the Question? *Traffic*, 2002, **3**, 443-451.

Joint United Nations Programme on HIV/AIDS (UNAIDS/WHO 2004 report on the global AIDS epidemic, <http://www.avert.org/worldstats.htm>.

A.T.Jones, M.Gumbleton and R.Duncan, Understanding endocytic pathways and intracellular trafficking: a prerequisite for effective design of advanced drug delivery systems, *Advanced Drug Delivery Reviews*, 2003, **55**, 1353-1357.

R.A.Jones, M.H.Poniris and M.R.Wilson, pDMAEMA is internalised by endocytosis but does not physically disrupt endosomes, *Journal of Controlled Release*, 2004, **96**, 379-391.

A.V.Kabanov, Taking polycation gene delivery systems from *in vitro* to *in vivo*, *Pharmaceutical Science & Technology Today*, 1999, **2**, 365-372.

N.Karoonuthaisiri, K.Titiyevskiy and J.L.Thomas, Destabilization of fatty acid-containing liposomes by polyamidoamine dendrimers, *Colloids and Surfaces B: Biointerfaces*, 2003, **27**, 365-375.

T.Kawano, T.Okuda, H.Aoyagi and T.Niidome, Long circulation of intravenously administered plasmid DNA delivered with dendritic poly(L-lysine) in the blood flow, *Journal of Controlled Release*, 2004, **99**, 329-337.

T.Kean, S.Roth and M.Thanou, Trimethylated chitosans as non-viral gene delivery

vectors: Cytotoxicity and transfection efficiency, *Journal of Controlled Release*, 2005, **103**, 643-653.

Z.Khayat, S.Tse, R.Duncan and P.C.Griffiths, Combining surface tension measurements, electron paramagnetic resonance (EPR) and small-angle neutron scattering (SANS) to better understand pH-responsive polymer-surfactant interaction, In *International Journal of Pharmacy Practice*, BPC, 2005, No.19.

Z.Khayat, P.C.Griffiths, I.Grillo, R.K.Heenan, S.M.King and R.Duncan, Characterising the size and shape of polyamidoamines in solution as a function of pH using neutron scattering and pulsed-gradient spin-echo NMR, *International Journal of Pharmaceutics*, 2006, **317**, 175-186.

A.Kichler, C.Leborgne, E.Coeytaux and O.Danos, Polyethylenimine-mediated gene delivery: A mechanistic study, *Journal of Gene Medicine*, 2001, **3**, 135-144.

E-M.Kim, H-J.Jeong, In-K.Park, C.S.Cho, H-S.Bom and C-G.Kim, Monitoring the effect of PEGylation on polyethylenimine *in vivo* using nuclear imaging technique, *Nuclear Medicine and Biology*, 2004, **31**, 781-784.

S.H.Kim, J.H.Jeong, K.C.Cho, S.W.Kim and T.G.Park, Target-specific gene silencing by siRNA plasmid DNA complexed with folate-modified poly(ethylenimine), *Journal of Controlled Release*, 2005, **104**, 223-232.

R.Kircheis, L.Wightman, ASchreiber, B.Robitza, V.Rossler, M.Kursa and E. Wagner, Polyethylenimine/DNA complexes shielded by transferrin target gene expression to tumors after systemic application, *Gene Therapy*, 2001, **8**, 28-40.

U.R.M.Kjellin, J.Reimer and P.Hansson, An investigation of dynamic surface tension, critical micelle concentration, and aggregation number of three nonionic surfactants using NMR, time-resolved fluorescence quenching, and maximum bubble pressure tensiometry, *Journal of Colloid and Interface Science*, 2003, **262**, 506-515.

T.M.Klein, E.D.Wolf, R.Wu and J.C.Sanford, High-velocity microprojectiles for delivering nucleic acids into living cells, *Nature*, 1987, **327**, 70-73.

L.Koester, H.Rauch, and E.Seymann, "Neutron Scattering Lengths: a Survey of Experimental Data and Methods", *Atomic Data and Nuclear Data*, Tables 49, 1991, 65.

A.R-Kristensen, J.P.Clamme, C.Vuilleumier, J.G.Kuhry and Y.Mely, Role of endocytosis in the transfection of L929 fibroblasts by polyethylenimine /DNA complexes, *Biochimica et Biophysica Acta*, 2001, **1514**, 21-32.

S.Kurata, M.Tsukakoshi, T.Kasuya and Y.Ikawa, The laser method for efficient introduction of foreign DNA into cultured cells, *Experimental Cell Research*, 1986, **162**, 372-378.

N.Lavignac, M. Lazenby, P.Foka, B.Malgesini, I.Verpilio, P.Ferruti and R.Duncan, Synthesis and Endosomolytic Properties of Poly(amidoamine) Block Copolymers, *Macromolecular Bioscience*, 2004, **4**, 922-929.

- N.Lavignac, M.Lazenby, J.Franchini, P.Ferruti and R.Duncan, Synthesis and preliminary evaluation of poly(amidoamine)–melittin conjugates as endosomolytic polymers and/or potential anticancer therapeutics, *International Journal of Pharmaceutics*, 2005, **300**, 102-112.
- D.Lechardeur, K.J.Sohn, M.Hardt, P.B.Joshi, M.Monck, R.W.Graham, B.Beatty, J.Squire, H.O'Broduvich and G.L.Lukacs, Metabolic instability of plasmid DNA in the cytosol: a potential barrier to gene transfer, *Gene Therapy*, 1999, **6**, 482-497.
- M.Lee, S.O.Han, K.S.Ko, J.J.Koh, J.S.Park, J.W.Yoon and S.W.Kim, Repression of GAD autoantigen expression in pancreas beta—cells by delivery of antisense plasmid/PEG-g-PLL complex, *Molecular Therapy*, 2001, **4**, 339-346.
- K.W.Leong, H.Q.Mao, V.L.Truong-Le, K.Roy, S.M.Welsh and J.T.August, DNA-polycation nanospheres as non-viral gene delivery vehicles, *Journal of Controlled Release*, 1998, **53**, 183-193.
- C.Loup, M-A.Zanta, A-M.Caminade, J-P.Majoral and B.Meunier, Preparation of Water-Soluble Cationic Phosphorus-Containing Dendrimers as DNA Transfecting Agents, *Chemistry - A European Journal*, 1999, **5**, 3644-3650.
- G.L.Lukacs, P.Haggie, O.Seksek, D.Lechardeur, N.Freedman and A.S.Verkman, Size-dependent DNA mobility in cytoplasm and nucleus, *Journal of Biological Chemistry*, 2000, **275**, 1625-1629.
- U.Lungwitz, M.Breunig, T.Blunk and A.Gopferich, Polyethylenimine-based non-viral gene delivery systems, *European Journal of Pharmaceutics and Biopharmaceutics*, 2005, **60**, 247-266.
- D.J.Lurie and K.Mäder, Monitoring drug delivery processes by EPR and related techniques—principles and applications, *Advanced Drug Delivery Reviews*, 2005, **57**, 1171-1190.
- K.D.Mack, R.Wei, A.Elbagarri, N.Abbey and M.S.McGrath, A novel method for DEAE-dextran mediated transfection of adherent primary cultured human macrophages, *Journal of Immunological Methods*, 1998, **211**, 79-86.
- S.Magazù, NMR, static and dynamic light and neutron scattering investigations on polymeric aqueous solutions, *Journal of Molecular Structure*, 2000, **523**, 47-59.
- N.Malik, R.Wiwattanapatapee, R.Klopsch, K.Lorenz, H.Frey, J.W.Weener, E.W.Meijer, W.Paulus and R.Duncan, Dendrimers: Relationship between structure and biocompatibility in vitro, and preliminary studies on the biodistribution of 125I-labelled polyamidoamine dendrimers in vivo, *Journal of Controlled Release*, 2000, **65**, 133-148.
- M.A.Marchisio, T.Longo and P.Ferruti, A selective de-heparinizer filter made of new cross-linked polymers of a poly-amido-amine structure, *Experientia*, 1973, **29**, 93-95.
- M.Marsh (Ed), Endocytosis, series editors: B.D.Hames and D.M.Glover, Oxford

university press, 2001, preface viii.

M.C.L.Martins, D.Wang, J.Ji, L.Feng and M.A.Barbosa, Albumin and fibrinogen adsorption on PU–PHEMA surfaces, *Biomaterials*, 2003, **24**, 2067-2076.

E.Mastrobattista, S.A.Bravo, M.van.der.Aa and D.J.A.Crommelin, Nonviral gene delivery systems: From simple transfection agents to artificial viruses, *Drug Discovery Today: Technologies- Drug delivery/formulation and nanotechnology*, 2005, **2**, 103-109.

C.D.Mathers, C.Boschi-Pinto, A.D.Lopez and C.J.L.Murray, Cancer incidence, mortality and survival by site for 14 regions of the World. Global Programme on Evidence for Health Policy Discussion Paper No.13. World Health Organisation, 2001.

L.D.Mayer, M.J.Hope and P.R.Cullis, Vesicles of variable sizes produced by a rapid extrusion procedure, *Biochimica et Biophysica Acta*, 1986, **858**, 161-168.

F.R.Maxfield and T.E.McGraw, Endocytic Recycling, *Molecular Cell Biology Nature Reviews*, 2004, **5**, 121-132.

D.L.McKenzie, K.Y.Kwok and K.G.Rice, A potent new class of reductively activated peptide gene delivery agents, *Journal of Biological Chemistry*, 2000, **275**, 9970-9977.

C.McIlwain, World leaders heap praise on human genome landmark, *Nature*, 2000, **405**, 983-984.

R.Mendichi, P.Ferruti and B.Malgesini, Evidence of aggregation in dilute solution of amphoteric poly(amido-amine)s by size exclusion chromatography, *Biomedical Chromatography*, 2005, **19**, 196-201.

T.Merdan, J.Kopecek and T.Kissel, Prospects for cationic polymers in gene and oligonucleotide therapy against cancer, *Advanced Drug Delivery Reviews*, 2002a, **54**, 715-758.

T.Merdan, K.Kunath, D.Fischer, J.Kopecek and T.Kissel, Intracellular processing of poly(ethylene imine)/ribozyme complexes can be observed in living cells by using confocal laser scanning microscopy and inhibitor experiments, *Pharmaceutical Research*, 2002b, **19**, 140-146.

T.Merdan, J.Callahan, H.Petersen, K.Kunath, U.Bakowsky, P.Kopeckova, T.Kissel and J. Kopecek, Pegylated polyethylenimine–FabV antibody fragment conjugates for targeted gene delivery to human ovarian carcinoma cells, *Bioconjugate Chemistry*, 2003, **14**, 989-996.

D.E.Meyer, G.A.Kong, M.W.Dewhirst, M.R.Zalutsky and A.Chilkoti, Targeting genetically engineered elastin-like polypeptide to solid tumors by local hyperthermia, *Cancer Research*, 2001, **61**, 1548-1554.

J.C.Moore, Gel permeation chromatography. I. A new method for molecular weight distribution of high polymers, *Journal of Polymer Science*, 1964, **2**, 835-843.

- S.A.Mousavi, L.Malerod, T.berg and R.Kjeken, Clathrin-dependent endocytosis, *Biochemical Journal*, 2004, **377**, 1-16.
- P.Mukerjee, C.Ramachandran and R.A.Pyter, Solvent effects on the visible spectra of nitroxides and relation to nitrogen hyperfine splitting constants. Nonempirical polarity for aprotic and hydroxilic solvents, *The Journal of Physical Chemistry*, 1982, **86**, 3189-3197.
- N.Murthy, J.R.Robichaud, D.A.Tirell, P.S.Stayton and A.S.Hoffman, The design and synthesis of polymers for eukaryotic membrane disruption, *Journal of Controlled Release*, 1999, **61**, 137-143.
- K.Mysels, The maximum bubble pressure method of measuring surface tension revisited, *Colloids and Surfaces*, 1990, **43**, 241-262.
- J.F.Nagle and M.C.Wiener, Structure of fully hydrated bilayer dispersions, *Biochimica et Biophysica Acta*, 1988, **942**, 1-10.
- D.R.Nelson, T.Piran and S.Weinberg (Eds), Statistical Mechanics of Membranes and Interfaces, World Scientific, Singapore, 1989.
- B.J.Nichols and J.L-Schwartz, Endocytosis without clathrin coats, *Trends in Cell Biology*, 2001, **11**, 406-412.
- T.Niidome and L.Huang, Gene therapy progress and prospects: nonviral vectors, *Gene Therapy*, 2002, **9**, 1647-1652.
- K.Nishida, K.Kaji, T.Kanaya, and T.Shibano, Added Salt Effect on the Intermolecular Correlation in Flexible Polyelectrolyte Solutions: Small-Angle Scattering Study, *Macromolecules*, 2002, **35**, 4084-4089.
- K.Nishikida, T.Housaki, M.Morimoto and T.Kinoshita, Gel permeation chromatography-Fourier transform infrared study of some synthetic polymers II. Instrumentation for the characterization of polyethylene", *Journal of Chromatography*, 1990, **517**, 209-217.
- C.T.Okamoto, Endocytosis and transcytosis, *Advanced Drug Delivery Reviews*, 1998, **29**, 215-228.
- M.Ogris, S.Brunner, S.Schuller, R.Kircheis and E.Wagner, PEGylated DNA/transferrin-PEI complexes: reduced interaction with blood components, extended circulation in blood and potential for systemic gene delivery, *Gene Therapy*, 1999, **6**, 595-605.
- M.Ogris and E.Wagner, Targeting tumours with non-viral gene delivery systems, *Drug Discovery Today*, 2002, **7**, 479-485.
- M.Ogris, G.Walker, T.Blessing, R.Kircheis, M.Wolschek and E.Wagner, Tumor-targeted gene therapy: strategies for the preparation of ligand-polyethylene glycol-polyethylenimine/DNA complexes, *Journal of Controlled Release*, 2003, **91**, 173-181.

P.Ohana, O.Gofrit, S.Ayesh, W.Al-Sharef, A.Mizrahi, T.Birman, T.Schneider, I.Matouk, N.de Groot, E.Tavdy, A.A.Sidi and A.Hochberg, Regulatory sequences of the H19 gene in DNA based therapy of bladder cancer, *Gene Therapy and Molecular Biology*, 2004, **8**, 181-192.

S.Opari, Management of the hypertensive patient with coronary artery disease, *American Journal of Hypertension*, 1999, **12**, 56S-62S.

D.Oupicky, M.Ogris and L.W.Seymour, Development of Long-circulating Polyelectrolyte Complexes for Systemic Delivery of Genes, *Journal of Drug Targeting*, 2002a, **10**, 93-98.

D.Oupicky, M.Ogris, K.A.Howard, P.R.Dash, K.Ulbrich and L.W.Seymour, Importance of lateral and steric stabilization of polyelectrolyte gene delivery vectors for extended systemic circulation, *Molecular Therapy*, 2002b, **5**, 463-472.

S-W.Pang, H-Y.Park, Y-S.Jang, W-S.Kim and J-H.Kim, Effect of charge and particle size of poly(styrene/(dimethylamino)ethyl methacrylate) nanoparticle for gene delivery in 293 cells, *Colloids and Surfaces B: Biointerface*, 2002, **26**, 213-222.

T.G.Park, J.H.Jeong and S.W.Kim, Current status of polymeric gene delivery systems, *Advanced Drug Delivery Reviews*, 2006, **58**, 467-486.

R.J.Parkes and S.L.Hart, Adhesion molecules and gene transfer, *Advanced Drug Delivery Reviews*, 2000, **44**, 135-152.

N.G.Patrick, S.C.W.Richardson, M.Casolaro, P.Ferruti, and R.Duncan, Poly(amidoamine)-mediated intracytoplasmic delivery of ricin A-chain and Gelonin , *Journal of Controlled Release*, 2001a, **77**, 225-232.

N.G.Patrick, P.Ferruti and R.Duncan, Demonstration of poly(amidoamine)-mediated lysosomal membrane perturbation after administration to rats in vivo, *Proc. Int. Symp. Control. Rel. Bioactive Mater*, 2001b, **28**, 864-865.

H.I.Petrache, S.T.Nagle, K.Gawrisch, D.Harries, V.A.Parsegian and J.F.Nagle, Structure and Fluctuations of Charged Phosphatidylserine Bilayers in the Absence of Salt, *Biophysical Journal*, 2004, **86**, 1574-1586.

G.Pitarresi, F.S.Palumbo, G.Giammona, M.A.Casadei and F.M.Moracci, Biodegradable hydrogels obtained by photocrosslinking of dextran and polyaspartamide derivatives, *Biomaterials*, 2003, **24**, 4301-4313.

C.Plank, B.Oberhauser, K.Mechtler, C.Koch and E.Wagner, The influence of endosome-disruptive peptides on gene transfer using synthetic virus-like gene transfer systems, *Journal of Biological Chemistry*, 1994, **269**, 12918-12924.

C.Plank, K.Mechtler, F.C.Szoka and E.Wagner, "Activation of the complement system by synthetic DNA complexes: a potential barrier for intravenous gene delivery", *Human Gene Therapy*, 1996, **7**, 1437-1446.

C.Plank, W.Zauner and E.Wagner, Application of membrane-active peptides for drug and gene delivery across cellular membranes, *Advanced Drug Reviews*, 1998, **34**, 21-35.

T.D.Pollard and W.C.Earnshaw (Eds), *Cell Biology*, 2002, 363-93.

C.W.Pouten, Nuclear import of polypeptides, polynucleotides and supramolecular complexes, *Advanced Drug Delivery Reviews*, 1998, **34**, 51-64.

C.W.Pouton and L.W.Seymour, Key issues in non-viral gene delivery, *Advanced Drug Delivery Reviews*, 1998, **34**, 3-19.

P.J.Quinn, *The Molecular Basis of Cell Membranes*, phospholipids composition of liver cell membranes, 1976, 33.

A.Ramzi, R.Scherrenberg, J.Joosten, P.Lemstra and K.Mortensen, Structure-Property Relations in Dendritic Polyelectrolyte Solutions at Different Ionic Strength, *Macromolecules*, 2002, **35**, 827-833.

S.Rangelov and W.Brown, Microgel formation in high molecular weight poly(ethyleneoxide), *Polymer*, 2000, **41**, 4825-4830.

E.Ranucci, P.Ferruti and M.G.Neri, Synthesis and preliminary evaluation as antimicrobial agents of new quaternary ammonium polymers, *Journal of Bioactive and Biocompatible Polymers*, 1989, **4**, 403.

E.Ranucci, G.Spagnoli, P.Ferruti, D.Sgouras and R.Duncan, Poly(amidoamines)s with potential as drug carriers: degradation and cellular toxicity, *Journal of Biomaterials Science. Polymer Edition*, 1991, **2**, 303-315.

S.C.W.Richardson, P.Ferruti and R.Duncan, Poly(amidoamine)s as potential endosomolytic polymers: evaluation in vitro and body distribution in normal and tumor-bearing animals, *Journal of Drug Targeting*, 1999, **6**, 391-404.

S.C.W.Richardson, N.G.Patrick, Y.K.Stella Man, P.Ferruti and R.Duncan, Poly(Amidoamine)s as a potential nonviral vectors: ability to form interpolyelectrolyte complexes and to mediate transfection in vitro, *Biomacromolecules*, 2001, **2**, 1023-1028.

S.Ristori, J.Oberdisse, I.Grillo, A.Donati and O.Spalla, Structural Characterization of Cationic Liposomes Loaded with Sugar-Based Carboranes, *Biophysical Journal*, 2005, **88**, 535-547

G.B.Robinson, The isolation and composition of membranes, In *Biological membranes*, D.S.Parsons (Ed), Oxford University press, 1975, 24.

J.Roe, The interaction of gelatin with anionic surfactants, PhD Thesis in Chemistry, Cardiff University, UK, 2000.

C.M.Roth and S.Sundaram, Engineering synthetic vectors for improved DNA delivery: insights from intracellular pathways, *Annual Review of Biomedical Engineering*, 2004,

6, 397-426.

T.Sato, T.Ishii, and Y.Okahata, In vitro gene delivery mediated by chitosan. Effect of pH, serum, and molecular mass of chitosan on transfection efficiency, *Biomaterials*, 2001, **22**, 2075-2080.

A.G.Schatzlein, Targeting of synthetic gene delivery systems, *Journal of Biomedicine Biotechnology*, 2003, **2003**, 149-158.

P.L.Schell, Uptake of polynucleotides by mammalian cells. XIV.Stimulation of the uptake of polynucleotides by poly(l-lysine), *Biochimica et Biophysica Acta*, 1974, **340**, 323-333.

C.Schnatwinkel, S.Christoforidis, M.R.Lindsay, S.U-Joseph, M.Wilm, R.G.Parton and M.Zerial, The Rab5 Effector Rabankyrin-5 Regulates and Coordinates Different Endocytic Mechanisms, *Plos Biology*, 2004, **2**, 1363-1380.

V.F.Sears (ed), "Neutron Scattering Lengths and Cross Sections", Neutron News 3, 1992, 26.

J.M.Seddon, G.Cevc, R.D.Kaye and D.Marsh, X-Ray diffraction study of the polymorphism of hydrated diacyl- and dialkylphosphatidylethanolamines, *Biochemistry*, 1984, **23**, 2634-2644.

J.M.Seddon, Structure of the inverted hexagonal (H_{II}) phase, and non-lamellar phase transitions of lipids, *Biochimica et Biophysica Acta (BAA)- Reviews on Biomembranes*, 1990, **1031**, 1-69.

M.Shibayama, H.Jinnia and T.Hashimoto, Neutron Scattering. In *Experimental methods in polymer science*, T.Tanaka (Ed), Academic Press, San Diego, 2000, 57-154.

E.V.Shumilina and Y.A.Shchipunov, Molecular shape of amphiphiles self-organised into bimolecular films, *Colloids and Surfaces A: Physicochemical and Engineering Aspects*, 1997, **121**, 23-26.

V.I.Slepnev and P.De.Camilli, Endocytosis: an overview, In *Self assembly Complexes for Gene Delivery: From Laboratory to Clinical Trail*, A.V.Kabanova, P.LFelgner and L.W.Seymour (Eds), 1998, 73-88.

S.C.De.Smedt, J.Demeester and W.E.Hennink, Cationic Polymer Based Gene Delivery Systems, *Pharmaceutical Research*, 2000, **17**, 113-126.

L.C.Smith, J.Duguid, M.S.Wadhwa, M.J.Logan, C-H.Tung, V.Edwards and J.T.Sparrow, Synthetic peptide-based DNA complexes for nonviral gene delivery, *Advanced Drug Delivery Reviews*, 1998, **30**, 115-131.

Smith and Wood (Eds), *Biological Membranes in Cell Biology*, 2nd edition, Published by Chapman & Hall, 1996, 144-149.

N.D.Sonawane, F.C.Szoka, and A.S.Verkmán, Chloride Accumulation and Swelling in

Endosomes Enhances DNA Transfer by Polyamine-DNA Polyplexes, *The Journal of Biological Chemistry*, 2003, **278**, 44826-44831.

J.A.Swanson and C.Watts, Macropinocytosis, *Trends in Cell Biology*, 1995, **5**, 424-428.
T.Takai and H.Ohmori, DNA transfection of mouse lymphoid cells by the combination of DEAE-dextran-mediated DNA uptake and osmotic shock procedure, *Biochimica et Biophysica Acta (BBA) - Gene Structure and Expression*, 1990, **1048**, 105-109.

M.C.Tanzi, G.Tieghi, P.Botto and C.Barozzi, Synthesis and characterization of poly(amido-amine)s belonging to two different homologous series, *Biomaterials*, 1984, **5**, 357-361.

M.Terakawa, M.Ogura, S.Sato, H.Wakisaka, H.Ashida, M.Uenoyama, Y.Masaki and M.Obara, Gene transfer into mammalian cells by use of a nanosecond pulsed laserinduced stress wave, *Optics Letters*, 2004, **29**, 1227-1229.

W.Tiyaboonchai, J.Woiszwilllo and C.R.Middaugh, Formulation and characterization of DNA-polyethylenimine-dextran sulfate nanoparticles, *European Journal of Pharmaceutical Sciences*, 2003, **19**, 191-202.

C.Trimble, C.T.Lin, C.F.Hung, S.Pai, J.Juang, L.He, M.Gillison, D.Pardoll, L.Wu and T.C.Wu, Comparison of the CD8+ T cell responses and antitumor effects generated by DNA vaccine administered through gene gun, biojector, and syringe, *Vaccine*, 2003, **21**, 4036-4042.

I.S.Trowbridge, J.F.Collawn and C.R.Hopkins, Signal-dependent membrane and protein trafficking in the endocytic pathways, *Annual Review of Cell Biology*, 1993, **9**, 129-161.

V.S.Trubetskoy, S.C.Wong, V.Subbotin, V.G.Budker, A.Loomis, J.E.Hagstrom and J.A.Wolff, Recharging cationic DNA complexes with highly charged polyanions for in vitro and in vivo gene delivery, *Gene Therapy*, 2003, **10**, 261-271.

W.C.Tseng and C.M.Jong, Improved stability of polycationic vector by dextran-grafted branched polyethylenimine, *Biomacromolecules*, 2003, **4**, 1277-1284.

R.Urade, Y.Hayashi and M.Kito, Endosomes differ from plasma membranes in the phospholipid molecular species composition, *Biochimica et Biophysica Acta (BBA) - Biomembranes*, 1988, **946**, 151-163.

A.Vaheri and J.S.Pagano, Infectious poliovirus RNA: a sensitive method of assay, *Virology*, 1965, **27**, 434-436.

S.Vansteenkiste, E.Schacht, E.Ranucci and P.Ferruti, Synthesis of a new family of poly(amido-amine)s carrying poly(oxyethylene) side chains, *Makromol Chem*, 1992, **193**, 937.

D.Voisin and B.Vincent, Flocculation in mixtures of cationic polyelectrolytes and anionic surfactants, *Advances in Colloid and Interface Science*, 2003, **106**, 1-22.

E.Wagner, Application of membrane- active peptides for nonviral gene delivery,

Advanced Drug Delivery Reviews, 1999, **38**, 279-289.

K-W.Wan, P.C.Griffiths, A.Paul, A.C.Hann, B.Malgesini, I.Verpilio, P.Ferruti and R.Duncan, Poly(amidoamine) salt form affects pH-dependent membrane activity and conformation in solution, *Biomacromolecules*, 2004, **5**, 1102-1109.

P.Watson, A.T.Jones and D.J.Stephens, Intracellular trafficking pathways and drug delivery: fluorescence imaging of living and fixed cells, *Advanced Drug Delivery Reviews*, 2005, **57**, 43-61.

P.V.deWetering, E.E.Moret, N.M.E.Schuurmans-Nieuwenbroek, M.J.van Streenbergen and W.E.Hennink, Structure-activity relationships of water-soluble cationic methylacrylate/ methacrylamide polymers for non-viral delivery, *Bioconjugate Chemistry*, 1999, **10**, 589-597.

P.V.deWetering, N.M.E.Schuurmans-Nieuwenbroek, M.J.van Steenbergen, D.J.A. Crommelin and W.E.Hennink, Copolymer of 2-(dimethylamino)ethyl methacrylate with ethoxytriethylene glycol methacrylate or N-vinyl-pyrrolidone as gene transfer agents, *Journal of Controlled Release*, 2000, **64**, 193-203.

S.H.White and G.I.King, Molecular packing and area compressibility of lipid bilayers, *Proceedings Of The National Academy Of Sciences Of The United States Of America*, 1985, **82**, 6532-6536.

C.M.Wiethoff and C.R.Middaugh, Barriers to nonviral gene delivery, *Journal of Pharmaceutical Sciences*, 2003, **92**, 203-217.

D.F.Williams (ed), Progress in Biomedical Engineering. 4. Definitions in Biomaterials, *Proceed. Of a Consensus Conference of European Society for Materials*, 1987.

R.S.Williams, S.A.Johnston, M.Riedy, M.J.DeVit, S.G.McElligott and J.C.Sanford, Introduction of foreign genes into tissues of living mice by DNA-coated microprojectiles, *Proceedings of the National Academy of Sciences of the United States of America*, 1991, **88**, 2726-2730.

R.Winter, Synchrotron X-ray and neutron small-angle scattering of lyotropic lipid mesophases, model biomembranes and proteins in solution at high pressure, *Biochimica et Biophysica Acta (BBA) - Protein Structure and Molecular Enzymology*, 2002, **1595**, 160-184.

G.D.S.-Wolf and I.G.H.S-Wolf, Non-viral and hybrid vectors in human gene therapy: an update, *Trends in Molecular Medicine*, 2003, **9**, 67-72.

M.A.Wolfert and L.W.Seymour, Atomic force microscopy analysis of the influence of the molecular weight of poly-(L)lysine on the size of polyelectrolyte complexes formed with DNA, *Gene Therapy*, 1996, **3**, 269-273.

G.Y.Wu and C.H.Wu, Receptor-mediated in vitro gene transformation by a soluble DNA carrier system, *Journal of Biological Chemistry*, 1987, **262**, 4429-4432.

M.-A.Yessine, M.Lafleur, H.-U.Petereit, C.Meier and J.-C.Leroux, Characterization of the membrane destabilizing properties of different pH-sensitive methacrylic acid copolymers, *Biochimica et Biophysica Acta*, 2003, **1613**, 28-38.

T.Yoshimori, A.Yamamoto, Y.Moriyama, M.Futai and Y.Tashiro, Bafilomycin A1, a specific inhibitor of vacuolar-type H(+)-ATPase, inhibits acidification and protein degradation in lysosomes of cultured cells, *Journal of Biological Chemistry*, 1991, **266**, 17707-17712.

Young and Lovell (Eds), Introduction to polymer, Published by Chapman & Hall, 1996, 1996, 2nd edition, 211-212.

Y.P.Zhang, B.Ceh and D.D.Lasic, Liposomes in Drug Delivery, In *Polymeric biomaterials*, S.Dumitriu (Ed), 2nd Edition, Publisher Marcel Dekker, 2002, 783-821.

J.A.Zhang and J.Pawelchak, Effect of pH, ionic strength and oxygen burden on the chemical stability of EPC/cholesterol liposomes under accelerated conditions: Part 1: Lipid hydrolysis, *European Journal of Pharmaceutics and Biopharmaceutics*, 2000, **50**, 357-364.

Z.Y.Zhang and B.D.Smith, High-generation polycationic dendrimers are unusually effective at disrupting anionic vesicles: membrane bending model, *Bioconjugate Chemistry*, 2000, **11**, 805-814.

R.I.Zhdanov, O.V.Podobed and V.V.Vlassov, Cationic lipid-DNA complexes-lipoplexes-for gene transfer and therapy, *Bioelectrochemistry*, 2002, **58**, 53-64.

H.Zhu, T.Yalcin, and L.Li, Analysis of the Accuracy of Determining Average Molecular Weights of Narrow Polydispersity Polymers by Matrix-Assisted Laser Desorption Ionization Time of-Flight Mass Spectrometry, *American Society for Mass Spectrometry*, 1998, **9**, 275-281.

B.H.Zinselmeyer, S.P.Mackay, A.G.Schatzlein and I.F.Uchegbu, The lower-generation polypropylenimine dendrimers are effective gene-transfer agents, *Pharmaceutical Research*, 2002, **19**, 960-967.

Appendix I

List of abstract and publication

Papers

P.C.Griffiths, A.Paul, Z.Khayat, K.W.Wan, S.M.King, I.Grillo, R.Schweins, P.Ferruti, J.Franchini and R.Duncan, Understanding the mechanism of action of poly(amidoamine)s as endosomolytic polymers: correlation of physicochemical and biological properties, *Biomacromolecules*, 2004, **5**, 1422-1427.

Z.Khayat, P.C.Griffiths, I.Grillo, R.K.Heenan, S.M.King and R.Duncan, Characterising the size and shape of polyamidoamines in solution as a function of pH using neutron scattering and pulsed-gradient spin-echo NMR, *International Journal of Pharmaceutics*, 2006, **317**, 175-186.

Abstracts

A.Paul, P.C.Griffiths, K.W.Wan, Z.Khayat, P.Ferruti and R.Duncan, Investigating the solution properties of poly(amidoamine)s by small-angle neutron scattering, In Proceedings of the 30th Annual Meeting of the Controlled Release Society, Glasgow, UK, 2003, No.461.

A.Paul, P.C.Griffiths, Z.Khayat, K.W.Wan, R.Duncan and P.Ferruti, Correlation of physicochemical and biological properties of poly(amidoamines)s, In 6th *International Symposium on Polymer Therapeutics: From Laboratory to Clinical Practice*, Cardiff, UK, 2004, 94.

J.Franchini, Z.Khayat, M.Lazenby, R.Duncan and P.Ferruti, Using controlled polyaddition to synthesise poly(amidoamine)s with specific chemical and biological characteristics, In 6th *International Symposium on Polymer Therapeutics: From Laboratory to Clinical Practice*, Cardiff, UK, 2004, 94.

Z.Khayat, R.Duncan, P.C.Griffiths and A.Paul, Investigation of mathematical models for interpretation of SANS of polyamidoamines in solution: Towards an accurate measure of shape and size, In 6th *International Symposium on Polymer Therapeutics: From Laboratory to Clinical Practice*, Cardiff, UK, 2004, 96.

Z.Khayat, R.Duncan, N.Lavignac, P.C.Griffiths and A.Paul, Use small-angle neutron scattering (SANS) and surface tension to better understand the mechanism of membrane and surfactant micelle interaction of endosomolytic polyamidoamines, In *International Journal of Pharmacy Practice*, BPC, 2004, No.36.

Z.Khayat, S.Tse, R.Duncan and P.C.Griffiths, Combining surface tension measurements, electron paramagnetic resonance (EPR) and small-angle neutron scattering (SANS) to better understand pH-responsive polymer-surfactant interaction, In *International Journal of Pharmacy Practice*, BPC, 2005, No.19.

Appendix II

Understanding the Mechanism of Action of Poly(amidoamine)s as Endosomolytic Polymers: Correlation of Physicochemical and Biological Properties

P. C. Griffiths,^{*,†} A. Paul,[†] Z. Khayat,^{†,‡} Ka-Wai Wan,[‡] S. M. King,[§] I. Grillo,^{||} R. Schweins,^{||} P. Ferruti,[⊥] J. Franchini,[⊥] and R. Duncan[†]

School of Chemistry, Cardiff University, PO Box 912, Cardiff CF10 3TB, United Kingdom, Centre for Polymer Therapeutics, Welsh School of Pharmacy, Redwood Building King Edward VII Avenue, Cardiff CF10 3XF, United Kingdom, ISIS Facility, Rutherford Appleton Laboratory, Chilton, Oxfordshire OX11 0QX, United Kingdom, Institut Laue-Langevin, 6 rue Jules Horowitz, Grenoble, France, and Dipartimento di Chimica Organica e Industriale, Università degli Studi di Milano, via Venezian 21, 20133, Milano, Italy

Received January 30, 2004; Revised Manuscript Received March 17, 2004

Bioresponsive poly(amidoamine)s (PAA)s are currently under development as endosomolytic polymers for intracellular delivery of proteins and genes. Here for the first time, small-angle neutron scattering (SANS) is used to systematically investigate the pH-dependent conformational change of an endosomolytic polymer, the PAA ISA 23. The radius of gyration of the ISA23 was determined as a function of pH and counterion, the aim being to correlate changes in polymer conformation with membrane activity assessed using a rat red blood cell haemolysis assay. With decreasing pH, the ISA23 radius of gyration increased to a maximum ($R_g \sim 80 \text{ \AA}$) around pH = 3, before subsequently decreasing once more. At high pH and therefore high ionic strengths, the polymer is negatively charged and adopts a rather compact structure ($R_g \sim 20 \text{ \AA}$), presumably with the dissociated carboxylic groups on the exterior of the polymer coil. At low pH, the coil again collapses ($R_g < 20 \text{ \AA}$), presumably due to the effects of the high ionic strength. It is concluded that the nature of the salt form has no direct bearing on the size of the polymer coil, but it does indirectly determine the prevailing pH and, hence, polymer conformation. Pulsed-gradient spin-echo NMR measurements were in good agreement with the SANS estimates of the radius of gyration, although ISA23 polydispersity does complicate the data interpretation/comparison. These results support the proposed mode of action of PAAs, namely a coil expansion on passing from a neutral pH (extracellular) to an acidic pH (endosomal and lysosomal) environments. The results do, however, suggest that the charge on the polymer shows a closer correlation with the haemolysis activity rather than the polymer conformation.

Introduction

Increased understanding of the genetic basis of disease has led to growing interest in the use of macromolecular drugs such as genes, proteins, and peptides. At the cellular level, inadequate cytosolic access is one major challenge that must be overcome if these macromolecules are to become effective therapies.¹ Consequently, there is a recognized need to design safe and efficient delivery vehicles. The viral vectors currently being used for gene delivery have clinical limitations including immunogenicity and transgene expression,^{2–4} so the search is on for endosomolytic polymers that can be used to design a synthetic viral mimetic. The construct must efficiently mediate membrane translocation from the endosomal compartment into the cytosol, delivering its payload there, thus avoiding lysosomal degradation.⁵

A number of bioresponsive, endosomolytic polymers (weak acids and weak bases) are under study as nonviral vectors. These include poly(ethylene imine) (PEI),⁶ poly-[(2-diethylaminoethyl)-methacrylate] (pDMAEMA),⁷ poly(ethyl acrylic acid) (PEAAc) and related polymers,^{5,8} poly-amidoamine (PAMAM) dendrimers,^{9,10} poly(2-methyl-acrylic acid 2-[(2-(dimethylamino)-ethyl)-methyl-amino]-ethyl ester) (pDAMA),¹¹ and linear polyamidoamines (PAAs).¹² The mechanism of this membrane destabilization is poorly understood but is triggered by a fall in pH following endocytic internalization of the polymer.

It has been suggested that PEI acts by the “proton sponge effect”.⁶ PEI entering the endosome absorbs protons, swells, and causes an influx of Cl^- which in turn creates an osmotic effect leading to water influx. These events are purported to cause membrane destabilization. The universal importance of the proton sponge effect is hotly debated. It has recently been shown that pDAMA-based polyplexes do not escape endosomes by this mechanism.¹¹

Over the past decade, we^{12,13} have designed PAAs as endosomolytic polymers for gene and nonpermeant toxin delivery.^{14,15,16,17} The preferred amphoteric PAA structures

* To whom correspondence should be addressed. Phone: +44-29 20875858. Fax: +44-29 20874030. E-mail: griffithspc@cardiff.ac.uk.

[†] School of Chemistry.

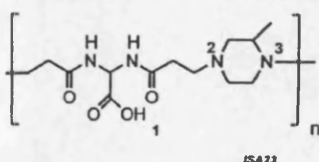
[‡] Welsh School of Pharmacy.

[§] Rutherford Appleton Laboratory.

^{||} Institut Laue-Langevin.

[⊥] Università degli Studi di Milano.

Table 1. Molecular Weight and Ionization Properties of ISA23



M_w (g/mol)	M_w/M_n	pK_{a1}	pK_{b2}	pK_{b3}
16 500	1.8	2.1	7.5	3.3

(including ISA 23; Table 1) are highly water-soluble, linear polymers and much less toxic than other polycations.¹⁵ Using both isolated rat red blood cells (RBCs) and isolated lysosomes,¹⁵ these PAAs have shown pH-dependent membrane perturbation that correlates with their ability to facilitate gene and toxin delivery in vitro. Furthermore, PAAs do not accumulate in the liver and intravenous injection and so can be used to target tumors by the EPR (enhanced permeability and retention) effect.¹⁸

Recent studies have shown the PAA counterion influences both membrane activity (in the RBC lysis model)¹⁹ and toxin delivery in vitro. Although PAA acetate, citrate, and lactate were nonhaemolytic at the starting pH of 5.5, the sulfate, hydrochloride, and phosphate forms ISA23 caused significant haemolysis (up to 80% Hb release at 1 h). The observation that systematic tailoring of the pK_a of monomers used to prepare PAAs did not enhance pH-dependent haemolysis compared to ISA23,¹³ PAA graft and block copolymers, ISA23-protein conjugates, and ISA23 of increased molecular weight (from ~15 kDa to 50 kDa) led to decreased membrane activity would suggest that PAA action is mediated predominantly by membrane interaction and not the proton sponge effect.

The aim of this study was to use small-angle neutron scattering (SANS) to systematically investigate the pH-dependent conformational change of ISA23 as a function of pH and counterion and to relate changes in polymer conformation with the membrane activity of ISA23. For comparative purposes, pulsed-gradient spin-echo NMR measurements were also used to obtain a complementary estimate of the solution conformation of ISA23 via the hydrodynamic radius (R_h).

Materials

ISA23 was synthesized as previously described¹⁵ by polyaddition of 2,2'-bis(*N*-acrylamido)acetic acid (BAC) and 2-methylpiperazine (2-MePip) (Table 1). ISA23 samples for SANS and NMR were prepared at a concentration of 50 mg/mL in D₂O. Subsequently, the pH was altered by the addition of concentration base (NaOD or NaOH) or acid (HCl or DCl). Given the strong buffering character of ISA23, this often resulted in significant changes in ionic strength.

Methods

Small-Angle Neutron Scattering. SANS measurements were performed on the LOQ diffractometer at the ISIS Spallation Neutron Source, Oxfordshire and on the D11 and D22 diffractometers at the ILL, Grenoble.

LOQ is a fixed-geometry, time-of-flight (TOF), instrument, whereas the ILL (D11 and D22) is a steady-state reactor source. Neutron wavelengths between 2 and 10 Å (LOQ) and 8 Å (D11) or 6 Å (D22) were employed to span Q-ranges of approximately 0.001 to 0.6 Å⁻¹. On D11 and D22, this required three separate instrument configurations (sample-detector distances and collimation).

On all of the instruments, the samples were contained in 2 mm path length, UV-spectrophotometer grade, quartz cuvettes (Hellma) and mounted in aluminum holders on top of an enclosed, computer-controlled, sample changer. Sample volumes were approximately 0.4 cm³. Temperature control was achieved through the use of a thermostated circulating bath pumping fluid through the base of the sample changer. Under these conditions, a temperature stability of ±0.5 °C can be achieved. All measurements were carried out at 25 °C. Experimental measuring times were approximately 40 min.

Dependent on which instrument was used, all scattering data were (a) normalized for the sample transmission and incident wavelength distribution, (b) background corrected using an empty quartz cell (this also removes the inherent instrumental background arising from vacuum windows, etc.), and (c) corrected for the linearity and efficiency of the detector response using the instrument-specific software package. The data were put onto an absolute scale by reference to the scattering from a well-characterized partially deuterated polystyrene-blend standard sample (LOQ) or flat scatterer such as water (D11, D22).

Pulsed-Gradient Spin-Echo NMR Studies. The self-diffusion measurements (¹H 360 MHz) were measured using a stimulated echo sequence. The attenuation of the spin-echo amplitude after Fourier transformation was recorded as a function of the duration, δ , of the applied gradient pulses for a fixed gradient intensity, G , and separation Δ . A typical diffusion time would be $\Delta = 500$ ms, and thus, the experiment is dominated by center-of-mass motion.

Many artifacts can be present in a PGSE-NMR experiment. Pulsed gradients often produce eddy currents in the metallic components of the probe and assembly that result in a mismatch between the pairs of gradient pulses used during the experiment. To eliminate these problems, a current regulated gradient driver delivers pairs of read and write gradients matched to better than 10 ppm, and three field gradient pre-pulses were applied to bring the effects of eddy currents to a first-order steady state. To minimize any physical disturbances associated with switching gradients, the gradient pulses are ramped up to their plateau value and back down to zero, typically over 250 μ s.

The self-diffusion coefficient, D_s , for isotropic, polydisperse polymer molecules is extracted by fitting to eq 1, the measured peak height, $A(\delta, G, \Delta)$, as a function of field gradient pulse duration, δ , intensity, G , and separation, Δ

$$A(\delta, G, \Delta) = A_0 \exp[-(kD_s)^\beta] \quad (1)$$

where $k = -\gamma^2 G^2 (30\Delta(\delta + \sigma)^2 - (10\delta^3 + 30\sigma\delta^2 + 35\sigma^2\delta + 14\sigma^3)/30)$.

γ is the magnetogyric ratio, and β is a phenomenological parameter which quantifies in a purely arbitrary manner, the

distribution of diffusion coefficients associated with polydisperse polymers.

Results and Discussion

The term "polymer therapeutic" has been coined to describe several new classes of polymer-based drugs and delivery systems.¹⁸ These include polymeric drugs,¹⁸ polymer-drug conjugates,²⁰ polymer-protein conjugates,^{21,22,23} polymer micelles which entrap drugs by covalent linkage,²⁴ and also those endosomolytic polymers used as nonviral vectors.^{6,16} These nanosized medicines are quite different to conventional drug delivery formulations that simply solubilize, entrap, or control drug release without resorting to chemical conjugation.¹⁸ Little is known of the solution properties of polymer therapeutics, and this study reports the first use of SANS to understand the conformation changes of an endosomolytic polymer being designed to assist protein and gene delivery. In parallel studies, we are applying the same methodology to gain increased understanding of the solution conformation of polymeric anticancer agents in early clinical development.^{25,26}

SANS experiments carried out at the ILL to determine the radius of gyration of ISA23 showed a pronounced upturn at low Q . The origin of this upturn is still under discussion. It could be due to an error in the transmission measurement because of fast neutrons going through the selector; however, the velocity selector lets through only neutrons with a selected wavelength $\pm 10\%$. Also, as neutron transmissions generally fall with increasing wavelength, fast neutron contamination would increase transmission with the result that the incorrect transmission would lower the scattering. It is more likely, although unfortunate, that this upturn at low Q is due to background scattering which arises from something in the instrument. The data obtained with the same samples at the LOQ (ISIS facility, U.K.) showed no evidence of this upturn although the Q range does not extend to quite the lowest values accessible on D22.

The low- Q scattering follows a power law $I(Q) \propto Q^{-n}$ with $n \approx 4.3 \pm 0.2$. Attempts to remove this scattering in the usual manner, i.e., subtract the scattering from an empty cell or a cell filled with D_2O , introduces further artifacts at low Q such as negative scattering. We therefore have adopted an approach where this anomalous scattering is fitted simultaneously to the polymer scattering. An example of this is shown in Figure 1.

A simple polydisperse Gaussian coil approach best describes the polymer scattering

$$I_{\text{polymer}}(Q) = \varphi V (\rho_{\text{polymer}} - \rho_{\text{solvent}})^2 \frac{\left(1 + \frac{u}{v}\right)^{(-1/v)} + u - 1}{(1 + v)u^2} \quad (2)$$

where φ is the polymer volume fraction and V is the sample volume. ρ is the scattering length density of the polymer and solvent (subscripts polymer and solvent respectively), with the bracket $(\rho_{\text{polymer}} - \rho_{\text{solvent}})^2$ being known as the "contrast"; this is an indication of how strongly (or not) a particular system scatters neutrons. v is a measure of the

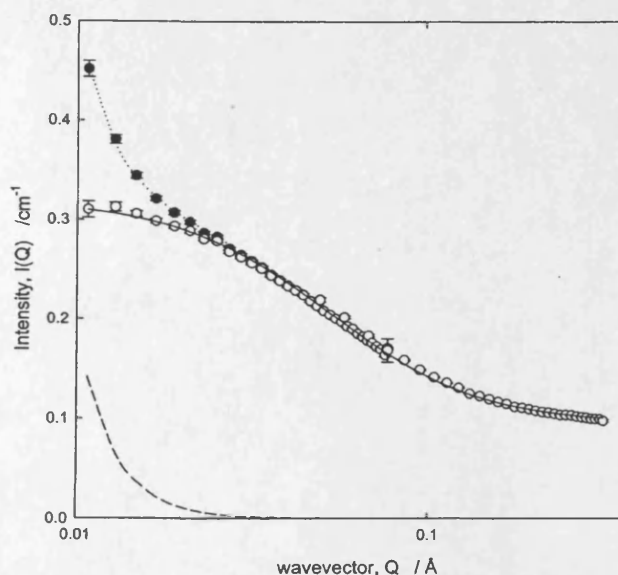


Figure 1. Typical raw SANS data for 5 wt % ISA23 polymer in D_2O (●), showing the separate "anomalous scattering" (long dashed line) and the polymer data (○). The fits to these data correspond to eq 3 (dotted line) and eq 2 (solid line).

polydispersity, $M_w/M_n - 1$ and $u = Q^2 R_g^2 / (1 + 2v)$ where R_g is the polymer radius of gyration.

Hence, the fit to the raw data in Figure 1 utilizes

$$I_{\text{polymer}}(Q) = I(Q)Q^{-n} + \varphi V (\rho_{\text{polymer}} - \rho_{\text{solvent}})^2 \frac{\left(1 + \frac{u}{v}\right)^{(-1/v)} + u - 1}{(1 + v)u^2} + B_{\text{inc}} \quad (3)$$

where the first term is the anomalous scattering, and the second term is that arising from the polymer. B_{inc} is the incoherent scattering, generally dominated by the protons present in the sample, which depends on the concentration of polymer, added base/acid etc. Having fitted the raw data to eq 3, the anomalous scattering can be easily subtracted leaving simply the polymer term as given by the open symbols in Figure 1. The fit to these data is shown as a solid line.

PAAAs are weak scatterers and in order to observe viable scattering, the experiments are performed at a polymer concentration that is significantly greater (> 50-fold) than that at which the physiological effects are observed in the RBC haemolysis assay. Figure 2 shows (a selection of) the data replotted in the form $I_{\text{polymer}}(Q) / \varphi V (\rho_{\text{polymer}} - \rho_{\text{solvent}})^2$ to remove the slight concentration and contrast variations within the pH series. Clearly, all of the data have a very similar form suggesting that there is no significant change in polymer morphology with pH, simply a change in radius of gyration. Some data extend to higher Q depending on the instrument configuration. A fit has been drawn through each dataset, and the thus obtained radii of gyration presented as a function of pH in Figure 3.

On decreasing the pH from pH = 14, the radius of gyration increases. The size attains a maximum value $R_g = 80 (\pm 3)$ Å at around pH = 3, roughly an order of magnitude greater than value at pH = 13. Subsequently, the radius further decreases with decreasing pH.

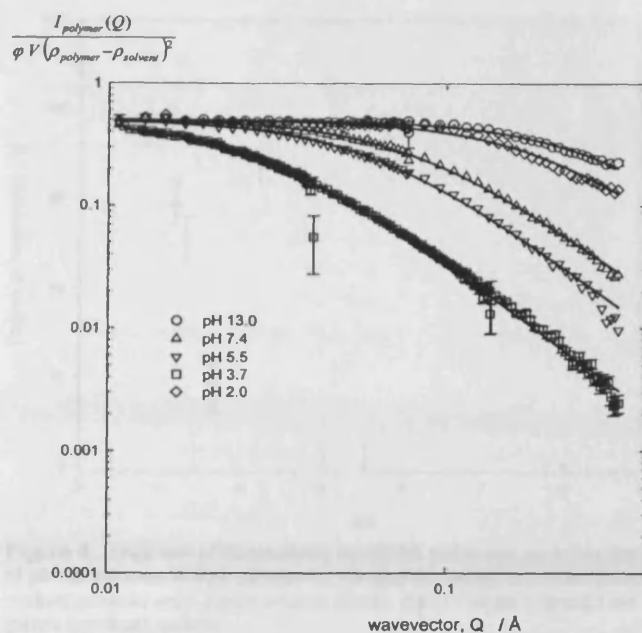


Figure 2. Normalized SANS data for $I_{\text{polymer}}(Q)/[\phi V(\rho_{\text{polymer}} - \rho_{\text{solvent}})^2]$ for 5 wt % ISA23 polymer in D_2O as a function of pH; diamonds pH = 2.0; squares pH = 3.7; inverted triangles pH = 5.5; triangles pH = 7.4; circles pH = 13.0.

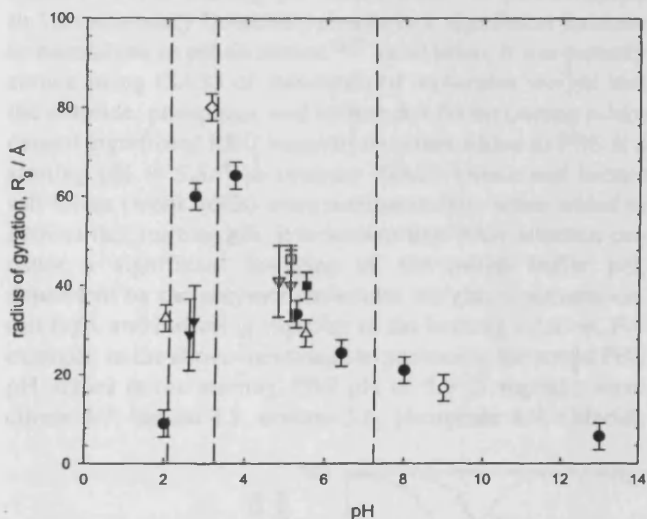


Figure 3. Radius of gyration of ISA23 polymers from the SANS data as a function of pH for various salt forms; (filled circles) hydrochloride (ILL data); citrate (empty squares); simple polymer, plus 0.1 M NaCl (empty circles); (filled triangles) hydrochloride (LOQ data); (filled squares) phosphate (LOQ data) and simple polymer (empty triangles). Also shown are the "weight average" PGSE-NMR estimates of the hydrodynamic radius for the citrate (inverted open triangles) and the hydrochloride (closed inverted triangles). The vertical lines correspond to the pK_a values presented in Table 1.

Table 1 presents the dissociation constants for the relevant functional groups. The carboxylic acid group has a pK_a of 2.1. It is generally accepted that at $pH = pK_a + 2$ there is 99% dissociation of the ionic species; therefore, at high pH (above $pH = 4.1$), 99% of the carboxylate groups are present in the deprotonated form (COO^-) and are hence negatively charged. In Table 1 the amine groups are considered in terms of their conjugate acids, the pK_a of which are 7.5 for N_1 and 3.3 for N_2 . Above their pK_a , these groups are present in the unprotonated (charge neutral) form. Hence, at high pH

($pH > 9.5$), the overall charge on the polymer is negative, arising from the deprotonated carboxylic acid groups. On decreasing the pH below pH 9, N_1 begins to become protonated, and hence, the overall charge on the polymer decreases (the polymer becomes less negatively charged), reaching the isoelectric point at $pH \sim 5.5$. Below this pH, protonation of the second amine group imparts an overall positive charge.

At $pH > 8$ the measured R_g was $\approx 20 \text{ \AA}$. This seems quite small for a polymer of this molecular weight. Poly(ethylene oxide) (PEO) of the same molecular weight in a theta solvent would have $R_g = 50 \text{ \AA}$, but interestingly, PEO with the same degree of polymerization as the ISA23 would have a similar R_g of 25 \AA . Thus, at this pH, we believe ISA23 adopts a rather compact structure; further, it is reasonable to assume that the fully deprotonated carboxylic anions are present at the exterior of the polymer coil. N_1 is only $\sim 20\%$ protonated (20% positively charged) at this point. With decreasing pH, the negative charges are compensated by the increasing protonation of N_1 ; that is, the polymer is ampholytic and adopts a less tightly coiled conformation and R_g increases.

Below the isoelectric point ($pH = 5.5$), the polymer coil expands significantly. This is slightly surprising as at this pH both the carboxylic groups and N_1 are fully charged. Clearly, the repulsion between the like-charged groups associated along the polymer backbone (both amine groups are present in the protonated form) must outweigh the intra group attraction between positive and negatively charged groups that would promote a collapse. With further decreases in pH, a coil collapse is observed, but this is likely to be due to the screening effect associated with the added ionic species.

Data obtained from the NMR experiment are shown in Figure 3. There is surprisingly good agreement between the NMR and SANS estimates of the radius, given the quite different nature of the two techniques and the polydispersity of the polymer. This result provides tacit confirmation that the anomalous scattering at low Q is not due to aggregation; to which the NMR experiment is highly sensitive.

A related study by Ferruti et al.¹³ used viscosity to study the effects of pH on the polymer conformation observed somewhat different behavior. They showed that, in 0.1 M NaCl, the reduced specific viscosity $(\eta - \eta_0)/\eta_0 c$ (where η is the polymer solution viscosity at a concentration c and η_0 is the solvent viscosity) of a related polymer decreased with a reduction in the pH showing two "steps" around the pK_a values associated with the two N atoms on that polymer. For ISA23, the same behavior was observed, but there was also additional viscosity increases at high pH due to the deprotonation of the carboxylic group. In the absence of the added salt, the viscosity of the related polymer increases with pH to a maximum around pK_{a1} before subsequently decreasing to a constant value around pK_{a2} . The interplay between pH, ionic strength, and polymer conformation is therefore somewhat complex.

PAAAs contain tertiary amino- and amido-groups regularly arranged along the macromolecular chain and thus behave as bases of moderate strength in aqueous solutions. Previ-

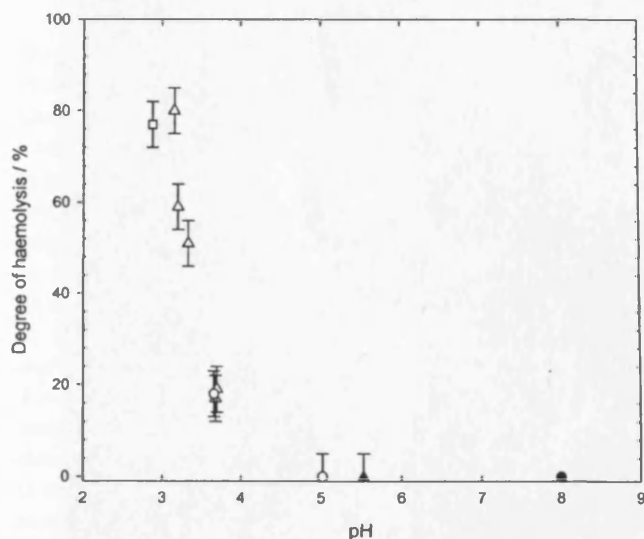


Figure 4. Degrees of haemolysis of ISA23 polymers as a function of pH for various IAS23 salt forms; (empty triangles) chloride; (filled circles) polymer only; (open circles) citrate; (filled triangles) phosphate; (open squares) sulfate.

ously reported haemolysis studies have shown that addition of PAAs (up to 1 mg/mL) to RBCs in phosphate buffered saline (PBS) at starting pH values from 7.4 (extracellular) to 5.5 (secondary lysosome) results in a significant increase in haemolysis as pH decreases.^{13,15} In addition, it was recently shown using ISA23 of standardized molecular weight that the chloride, phosphate, and sulfate salt forms (strong acids) caused significant RBC haemolysis when added to PBS at a starting pH = 5.5.¹⁹ In contrast ISA23 citrate and lactate salt forms (weak acids) were nonhaemolytic when added to PBS at this starting pH. It is known that PAA addition can cause a significant lowering of the initial buffer pH, dependent on the polymer molecular weight, concentration, salt type, and buffering capacity of the bathing solution. For example, in the above-mentioned experiments, the actual PBS pH values at the starting PBS pH of 5.5 (1 mg/mL) were citrate 4.7, lactate 4.9, acetate 5.6, phosphate 4.9, chloride

3.2, and sulfate 3.0. However, it is important to note that in the absence of the polymer such changes in pH per se in the range pH 3.0–9.0 do not cause RBC haemolysis.

As the actual pH of the ISA23 chloride solution drops to pH ~ 3 due to the presence of ISA3 chloride, and the prevailing pH of the citrate form is much higher, pH ~ 5, the resultant effect on PAA conformation could explain the apparent dependence of haemolysis on salt type. It has been hypothesised that during ISA23 protonation (Table 1) after internalization by the cells causes a change in polymer conformation thus allowing it to bind to the endosomal membrane, causing its disruption.¹⁵ Unravelling this mechanism in the biological environment is difficult as the intra-endosomal PAA concentration and the buffering capacity of the endosome are unknown. However, the observations presented here are consistent with changes in the conformation or ionic character of the polymer that may promote adsorption to- or interaction with (e.g., inducing curvature, pore formation) the membrane, causing it to disrupt.

The biological activity as manifested in terms of red blood cell (RBC) haemolysis (1 mg/mL) is shown as function of pH and salt type in Figure 4 for the same series of ISA23 polymers as studied with SANS (50 mg/mL). These results suggest that there is a critical pH below which haemolysis will occur, namely pH = 5.0 ± 0.25. Overlapping the haemolysis behavior and the corresponding radii (Figure 5) suggests that there is no obvious direct correlation with the Rg. A closer correlation of the biological activity may be seen if we consider the charge on the polymer. The haemolysis data in Figure 5 is overlaid with a plot of the pH-dependence of the charge on the polymer, considered in terms of the three functional groups and the overall charge. This suggests that a high degree of haemolysis is observed only once the second amine group begins to protonate and the overall charge on the polymer becomes positive. It may be that the polymer must attain a minimum degree of positive character before a membrane disrupting adsorption will occur.

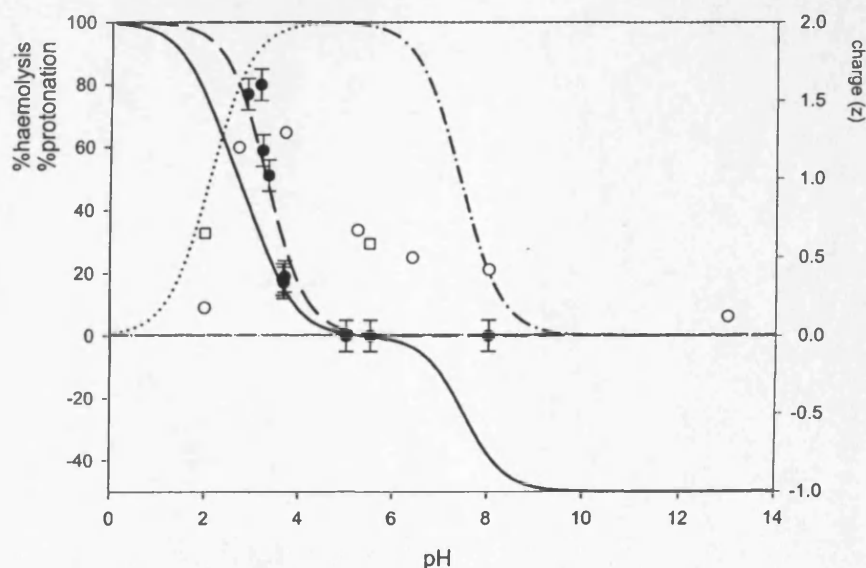


Figure 5. Haemolysis results (filled circles); radii from SANS (open circles), radii from PGSE-NMR (open squares). Solid line is the overall charge on the polymer, broken lines are percentage protonation of the functional groups; COOH (dotted), N₁ (dash-dot), N₂ (dashed).

Making the analogy with polymer adsorption to particulate surfaces,²⁷ the adsorption of PAA to the membrane may be rationalized based on the respective charges on the polymer and surface. On approach to a surface, the number of configurations a polymer can adopt, and hence its entropy, is greatly reduced. The polymer only adsorbs if the enthalpic interaction is greater than some critical value. In the case of polyelectrolytes, the strong electrostatic interactions result in a significant degree of binding and a flat conformation, at least for impenetrable substrates. The COO⁻ group, while in the deprotonated form, will hinder the adsorption, both due to the tightly coiled conformation and more significantly due to repulsion of like negative charges at the polymer/membrane interface. One could imagine, therefore, that for the case of PAA/membrane interactions a positive character is required before the polymer will adsorb to the negative membrane interface. Both of these characters are pH-dependent.

The different salt forms lead to a pH dependent haemolysis behavior that is difficult to rationalize based simply on the polymer conformation; the radius of gyration has already increased significantly at pH = 4, whereas the haemolysis has not. However, the salt form does have a secondary effect on the systems; the salts of weak acids are fully dissociated and hence determine the prevailing pH of the solution, which in turn affects the degree of protonation of the polymer.

Conclusions

The radius of gyration of ISA23 has been examined as a function of pH and salt type by SANS. A polydisperse Gaussian coil treatment describes the observed scattering, using a polydispersity value derived from gel permeation chromatography. The polymer size increases gradually over the range 6 < pH < 13, but increases sharply to a maximum around pH = 3. For pH values below this, the polymer coil collapses. PGSE-NMR measurements gave R_h estimates in agreement with the SANS data. These results broadly support the proposed mode of action of PAAs, namely, a pH driven coil expansion, and there is a clear correlation between the cationic character of the polymer and membrane activity.

Acknowledgment. We gratefully acknowledge support from the Leverhulme Trust, EPSRC and the ILL for provision of SANS beamtime.

References and Notes

- (1) Lackey, C. A.; Murthy, N.; Stayton, P. S.; Press, O. W.; Hoffman, A. S.; Tirrell, D. A. Enhancement of endosomal release and toxic activity of ricin A-chain by a pH-sensitive polymer. *Proceedings of the 26th International Symposium of Controlled Release and Bioactive Materials*, 1999 p 815–816.
- (2) Ferber, D. Gene therapy: Safer and virus-free? *Science* **2001**, *294*, 1638–1640.
- (3) Niidome, T.; Huang, L. Gene therapy progress and prospects: Nonviral vectors. *Gene Therapy* **2002**, *9*, 1647–1652.
- (4) Gore, M. E. Gene therapy can cause leukaemia: no shock, mild horror but a probe. *Gene Therapy* **2003**, *10*, 4.
- (5) Murthy, N.; Robichaud, J.; Tirrell, D.; Stayton, P.; Hoffman, A. The design and synthesis of polymers for eukaryotic membrane disruption. *J. Controlled Release* **1999**, *61*, 137–143.
- (6) Boussif, O.; Lezoualch, F.; Zanta, M. A.; Mergny, M. D.; Scherman, D.; Demeneix, B.; Behr, J.-P. A versatile vector for gene and oligonucleotide transfer into cells in culture and in vivo: polyethylenimine. *Proc. Natl. Acad. Sci. U.S.A.* **1995**, *92*, 7297–7301.
- (7) Cheng, J. Y.; van der Wetering, P.; Talsma, H.; Crommelin, D. J. A.; Hennink, W. E. *Int. J. Pharm.* **1999**, *183* (1), 25–28.
- (8) Kyriakides, T. R.; Cheung, C. Y.; Murthy, N.; Bornstein, P.; Stayton, P. S.; Hoffman, A. S. pH-sensitive polymers that enhance intracellular drug delivery in vivo. *J. Controlled Release* **2002**, *78*, 295–303.
- (9) Bielinska, A. U.; Kukowska Latallo, J. F.; Baker, J. R. The interaction of plasmid DNA with polyamidoamine dendrimers: mechanism of complex formation and analysis of alterations induced in nuclease sensitivity and transcriptional activity of the complexed DNA. *Biochim. Biophys. Acta* **1997**, *1353* (2), 180–190.
- (10) Tang, M. X.; Redemann, C. T.; Szoka, F. C. In vitro gene delivery by degraded polyamidoamine dendrimers. *Bioconjugate Chem.* **1996**, *7*, 703–714.
- (11) Funhoff, A. M.; van Nostrum, C. F.; Koning, G. A.; Schuurmans-Nieuwenbroek, N. M. E.; Crommelin, D. J. A.; Hennink, W. E. Endosomal Escape of Polymeric Gene Delivery Complexes Is Not Always Enhanced by Polymers Buffering at Low pH. *Biomacromolecules* **2004**, *5* (1), 32–39.
- (12) Ferruti, P.; Marchisio, M. A.; Duncan, R. Poly(amido-amine)s: Biomedical applications. *Macromol. Rapid Commun.* **2002**, *23*, 332–355.
- (13) Ferruti, P.; Manzoni, S.; Richardson, S. C. W.; Duncan, R.; Patrick, N. G.; Mendichi, R.; Casolaro, M. Amphoteric linear poly(amido-amine)s as endosomolytic polymers: correlation between physico-chemical and biological properties. *Macromolecules* **2000**, *33* (21), 7793–7800.
- (14) Duncan, R.; Ferruti, P.; Sgouras, D.; Tuboku-Metzger, A.; Ranucci, E.; Bignotti, F. A polymer-triton X-100 conjugate capable of pH-dependent red blood cell lysis: a model system illustrating the possibility of drug delivery within acidic intracellular compartments. *J. Drug Targeting* **1994**, *2*, 341–347.
- (15) Richardson, S.; Ferruti, P.; Duncan, R. Poly(amidoamine)s as potential endosomolytic polymers: Evaluation in vitro and body distribution in normal and tumour-bearing animals. *J. Drug Targeting* **1999**, *6* (6), 391–404.
- (16) Richardson, S. C. W.; Patrick, N. G.; Man, Y. K. S.; Ferruti, P.; Duncan, R. Poly(amidoamine)s as potential nonviral vectors: Ability to form interpolyelectrolyte complexes and to mediate transfection in vitro. *Biomacromolecules* **2001**, *2* (3), 1023–1028.
- (17) Patrick, N. G.; Richardson, S. C. W.; Casolaro, M.; Ferruti, P.; Duncan, R. Poly(amidoamine) mediated intracytoplasmic delivery of ricin A-chain and gelonin. *J. Controlled Release* **2001**, *77*, 225–232.
- (18) Duncan, R. The Dawning Era of Polymer Therapeutics. *Nat. Rev. Drug Discovery* **2003a**, *2* (5), 347–360.
- (19) Wan, K.-W.; Malgesini, B.; Verpillio, I.; Ferruti, P.; Griffiths, P. C.; Paul, A.; Hann, A. C.; Duncan, R. Poly(amidoamine) salt form affects pH-dependent membrane activity and polymer conformation in solution. *Biomacromolecules* **2004**, *5*, 1102–1109.
- (20) Duncan, R. Polymer-Drug Conjugates. In *Handbook of Anticancer Drug Development*; Budman, D., Calvert, H., Rowinsky, E., Eds.; Lippincott, Williams & Wilkins: Philadelphia, PA, 2003; pp 239–260.
- (21) Maeda, H.; Konno, T. In *Neocarzinostatin: The Past, Present, and Future of an Anticancer Drug*; Maeda, H., Edo, K., Ishida, N., Eds.; Springer-Verlag: Berlin, 1997; p 227–267.
- (22) Veronese, F. M.; Harris, J. M. Peptide and protein PEGylation. *Adv. Drug Delivery Syst.* **2002**, *54* (no. 4), whole issue.
- (23) Harris, J. M.; Chess, R. B. Effect of pegylation on pharmaceuticals. *Nature Rev. Drug Discovery* **2003**, *2*, 214–221.
- (24) Jones, M.-C.; Leroux, J.-C. Polymeric-micelles—a new generation of colloidal drug carriers. *Eur. J. Pharm. Biopharm.* **1999**, *48*, 101–111.
- (25) Vicent, M. J.; Paul, A.; Griffiths, P. C.; Duncan, R. Using small angle neutron scattering (SANS) to evaluate the conformation of PK1 and PK2: A potential explanation for their clinical behaviour. *Proceeding of the 6th Intl Symposium on Polymer Therapeutics: Laboratory to Clinic Practice*, 2004.
- (26) Paul et al. Correlation of physicochemical and biological properties of poly(amidoamines) Paul, A., Griffiths, P. C., Khayat, Z., Wan, K.-W., Duncan, R., Ferruti, P. *Proceeding of the 6th Intl Symposium on Polymer Therapeutics: Laboratory to Clinic Practice*, 2004.
- (27) See, for instance: Fleer, G. J.; Cohen Stuart, M. A.; Scheutjens, J. M. H. M.; Cosgrove, T.; Vincent, B. *Polymers at Interfaces*; Chapman and Hall: New York, 1993.

BM049936G



ELSEVIER

Available online at www.sciencedirect.com

SCIENCE @ DIRECT®

INTERNATIONAL JOURNAL OF
PHARMACEUTICS

International Journal of Pharmaceutics 317 (2006) 175–186

www.elsevier.com/locate/ijpharm

Characterising the size and shape of polyamidoamines in solution as a function of pH using neutron scattering and pulsed-gradient spin-echo NMR

Zeena Khayat^{a,b}, Peter C. Griffiths^{b,*}, Isabelle Grillo^c, Richard K. Heenan^d,
Stephen M. King^d, Ruth Duncan^a

^a Centre for Polymer Therapeutics, Welsh School of Pharmacy, King Edward's VII Avenue, Cardiff CF10 3XF, UK

^b School of Chemistry, Cardiff University, Main Building, Park Place, Cardiff CF10 3AT, UK

^c Institut Laue-Langevin, 6 rue Jules Horowitz, BP156-38042 Grenoble, Cedex 9, France

^d ISIS Facility, Rutherford Appleton Laboratory, Chilton, Oxfordshire OX11 0QX, UK

Received 20 July 2005; received in revised form 5 March 2006; accepted 7 March 2006

Available online 12 March 2006

Abstract

Bioresponsive polymers are being developed as synthetic viral mimetics to enhance the intracellular delivery of macromolecular therapeutic agents such as genes, proteins and peptides. In this context we have designed pH-responsive, amphoteric polyamidoamines (PAAs) which change conformation on passing from a neutral pH (extracellular) to an acidic pH (endosomal and lysosomal) environments. PAAs have already demonstrated cytosolic delivery of genes and non-permeant toxins (e.g. gelonin and ricin A chain). The aim of this study was to use small-angle neutron scattering (SANS) to investigate the most likely shape of the hydrochloride salt form of one particular PAA (ISA23) in solution, under pH conditions that mimic those the polymer would be expected to encounter during endocytic internalisation (pH 7.4–3). It was shown that models based on a Gaussian coil representation of the polymer conformation described the SANS data better over this pH range than models based on a rod-like conformation. The conformation of ISA23 at 37 °C was expanded (radius of gyration ~ 80 Å) at pH ~ 3 but collapsed with an increase in pH (radius of gyration ~ 20 Å at pH 7.4), a conclusion also reached in a *model-free* analysis of the neutron data. Outside this pH range – at the extremes of high and low pH – the polymer coil collapsed and interpretation of the scattering was slightly complicated by the presence of a very weak structure factor indicating that the polymer coils are highly charged. The PAA concentration did not significantly affect the polymer size over the concentration range 10–50 mg/ml. Characterisation of the dynamics of these polymer solutions – diffusion coefficients and viscosity – *ostensibly* suggest a very different conclusion with the polymer expanding as the pH is increased, but this arises due to weak aggregation of the amphoteric polymer coils.

© 2006 Elsevier B.V. All rights reserved.

Keywords: Polymer therapeutics; Endosomolytic polymers; Pulsed-gradient spin-echo NMR; Small-angle neutron scattering; Polyamidoamines

1. Introduction

Despite progress in genomics and proteomics research, it has proved much more difficult than originally envisaged to realise effective and practical therapies based on protein-, peptide- and gene-based therapeutics. The principal challenge remains identification of safe and effective delivery systems able to localise these macromolecular therapeutics to the diseased cells or tis-

sues where they are needed, and once there, promote their efficient delivery to the correct intracellular compartment, usually the cytosol (Wagner, 2004). Retroviral and adenoviral vectors are the favoured tools for gene therapy (Edelstein et al., 2004; Ilarduya and DuzgUnes, 2000). Undeniably, they promote highly efficient gene delivery, but they have also several disadvantages, particularly their mixed safety record. The death of an 18-year-old patient in 1999 due to an acute inflammatory reaction after gene therapy (Raper et al., 2003) and the more recent observation that 2 out of 10 children treated with gene therapy to correct severe combined immunodeficiency disease (SCID) developed a type of leukaemia that was clearly

* Corresponding author. Tel.: +44 29 20875858; fax: +44 29 20874030.

E-mail address: griffithspc@cardiff.ac.uk (P.C. Griffiths).

caused by the viral vector (Hacein-Bey-Abina et al., 2003) led many to question the risk/benefit of this approach (Check, 2003).

It is widely acknowledged that non-viral vectors offer potential advantages in terms of safety and ease of manufacture (Pack et al., 2005). Lipidic-DNA complexes (lipoplexes) and polymer-based DNA complexes (polyplexes) have been tested in clinical trials (Ohana et al., 2004). Their transfection efficiency is often extremely low and the most popular polymeric vectors used are very toxic (Fischer et al., 2003). Those most frequently used include poly cations, e.g. poly-L-lysine (PLL) (Wu and Wu, 1988) and poly(ethylene imine) (PEI) (Boussif et al., 1995), pH-responsive polyanions such as the poly(ethylacrylic acid) (PEAAc), and related polymers (Murthy et al., 1999), and the cationic poly(amidoamine) (PAMAM) dendrimers (Qin et al., 1998).

A large family of PAAs have now been synthesised. Various structures have been designed for different biomedical applications including heparin binding in blood perfusion filters, metal ion complexation, targetable anticancer PAA conjugates and particularly of importance here, as endosomolytic polymers for cytosolic delivery (reviewed in Ferruti et al., 2002). Our research has designed a family of linear poly(amidoamine)s (PAAs) (Duncan et al., 1994; Richardson et al., 1999; Ferruti et al., 2002) where polymer structure has been systematically optimised to give relatively non-toxic polymers (IC_{50} values > 1 mg/ml over 72 h) that are non-haemolytic at pH 7.4, but show pH-dependent breakage of model membranes (Richardson et al., 1999). Moreover, amphoteric structures can be synthesised, e.g. ISA23 (Ferruti et al., 2000), that do not accumulate in liver after intravenous injection, and that target tumours by the enhanced permeability and retention (EPR) effect (Richardson et al., 1999). ISA23 (Scheme 1) is able to deliver genes (Richardson et al., 2001) and promote cytosolic access of the non-permeant toxins ricin A chain and gelonin (Patrick et al., 2001a). Recent quantitative subcellular fractionation studies showed that PAA is transiently retained in the endosomal compartment (1 h) before transfer to the lysosomal compartment and that isolated vesicles containing PAAs show enhanced membrane permeability (Patrick et al., 2001b). The counterion of the PAA strongly affects the pH-dependent membrane interaction (Wan et al., 2004). Nevertheless, PAA toxin delivery is still very poorly efficient, requiring many polymer molecules to deliver a single toxin molecule. Hence there is an urgent need to better understand the physico-chemical properties of PAAs and their precise mechanism of membrane destabilisation so that more efficient second generation systems can be designed.

Relatively few studies have explored PAA physico-chemical properties. Early investigations used potentiometric titration, ^{13}C NMR, viscosity measurements and conformational analysis to examine the structure of a number of cationic PAAs, with different alkyl chain between amino groups. In this case they showed that the stiffness and the flexibility depended on various polymer features (Barbucci et al., 1981), such as degree of protonation.

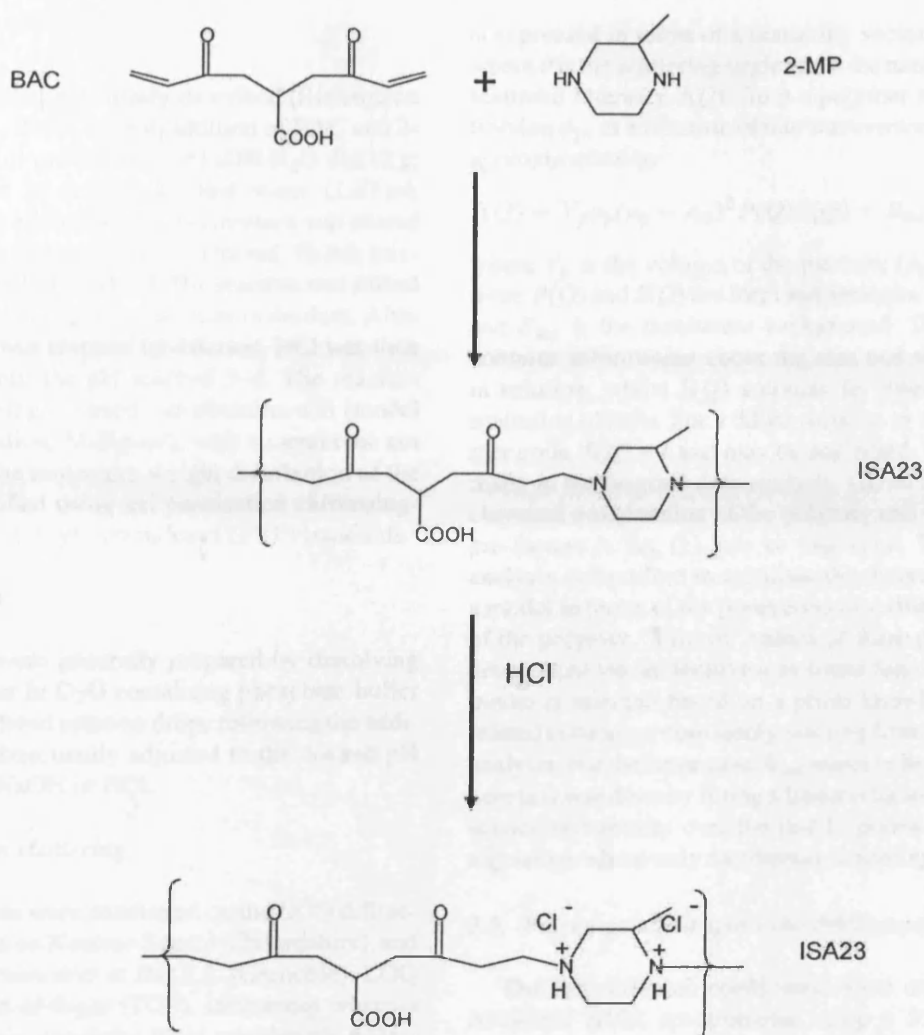
There is much debate as to the mechanism of endosomal permeabilisation of endosomolytic polymers. Behr and colleagues

(Boussif et al., 1995) advanced the polymer “proton-sponge effect” as a mechanism to explain PEI action, and others have suggested that this combines with polymer swelling in the acidic endosomal compartment to cause a local osmotic effect that then disrupts the endosomal membrane (Sonawane et al., 2003). Universal applicability of the proton-sponge hypothesis was recently questioned (Funhoff et al., 2004) when a novel polymer with two tertiary amine groups in each monomeric unit [poly(2-methyl-acrylic acid 2-[(2-(dimethylamino)-ethyl)-methyl-amino]-ethyl ester) (so-called pDAMA)] with pK_a values of ~ 9 , and ~ 5 was found to form polyplexes, but not to mediate endosomal escape. We believe that PAAs require direct membrane interaction to facilitate endosomal escape. It has also been shown that the counterion present is a vital component of this process (Wan et al., 2004). Observations that PAA-block copolymers (Lavignac et al., 2004), and PAA covalent conjugation via a terminal group leads to decreased membrane activity supports this hypothesis.

Of paramount importance here is the dependence of the polymer conformation on the effective charge of the polymer, the latter controlled via the solution pH and ionic strength. Such an understanding of the physico-chemical properties of endosomolytic PAAs is considered essential to allow further systematic structure optimisation. The conformation – or shape – of the polymer may be quantified using SANS.

Small-angle neutron scattering (SANS) is a particularly powerful tool that can bring a new perspective to the solution conformation of polymer therapeutics (as defined by Duncan in 2003), and also help to probe their mechanism of membrane interaction. SANS has however rarely been applied in this field yet it has been widely used to investigate the conformation of polymers in solution, polyelectrolytes (Nishida et al., 2002; Nakamura et al., 2005), copolymers (Pederson, 2002), at interfaces (Griffiths et al., 2004a; King et al., 2002) and in the presence of surfactant micelles (Aswal, 2003; Bergström et al., 2004; Griffiths et al., 2004a) and dendrimers (Ramzi et al., 2000; Hedden and Bauer, 2003).

A nominally identical ISA23 ($M_w = 42,700$ g mol $^{-1}$; $M_w/M_n = 1.7$) to that studied here has been previously examined by viscosity measurements in solutions at 35 °C buffered at pH 8 with a total ionic strength of 0.3 M (Ferruti et al., 2000). For a series of solutions satisfying the condition $[\eta]c = 0.1$, Ferruti et al. analysed their intrinsic viscosity data in terms of the Mark-Houwink model ($[\eta] = kM^\alpha$), concluding that amphoteric PAAs (in particular ISA23) possess rather stiff chains since the parameters $k = 9.53 \times 10^{-5}$ dl/g and $\alpha = 0.85$ were somewhat larger than expected for uncharged polymers of a comparable molecular weight. Further, the power law dependence of the radius of gyration on molecular weight had an exponent of 0.74 – $R \propto M^{0.74}$ – typical of an expanded (but random) coil structure. Ferruti's study also considered the viscosity of solutions of ISA23 as a function of pH with the viscosity decreasing from $\eta_{sp}/c = 0.6$ at pH 11 to a local minimum ($\eta_{sp}/c = 3.0$) at pH 5, before increasing once again below pH 3. Accordingly, this predicts a minimum in hydrodynamic volume coinciding with the isoelectric point of the polymer. A similar observation was made by Koetz et al. (1993) for the majority (but not all) of a



Scheme 1. Synthesis of ISA23.

number of polybetaine-based polyampholytes with differing chemical structure but all containing carboxylic acid groups and various basic nitrogen functions (Koetz et al., 1993). However, Feng and Huang (1997) have shown that polyampholytes of 2-acrylamido-2-methylpropane sulfonic acid (AMPS) and 2-dimethylaminoethyl methacrylate (DMAEMA) exhibit significantly enhanced intrinsic viscosity at the IEP of the polyampholyte.

In contrast to Ferruti's viscosity study, Griffiths et al. in their SANS study on ISA23 found that the PAA polymer coil *expands* as the pH decreases from pH 11 exhibiting a maximum at pH ~4—an apparent contradiction to the viscosity data (Griffiths et al., 2004a). The charge versus conformation behaviour of this polymer is rather important as recent experiments suggest that the degree of protonation determines whether an interaction occurs with model surfaces and membranes (surfactant micelles and liposomes). Therefore, the discrepancy between the scattering and viscosity insights needs addressing. The source of the inconsistency could be (i) the “form factor” – the mathematical model that embodies the shape and size of the

polymer coil – used in the analysis of the scattering data; (ii) the fact that a structure factor ($S(Q)$) was omitted in the data analysis; or (iii) that the polymer coils are aggregating in solution; the validity of these various approaches is addressed here.

2. Materials and methods

2.1. Materials

The monomer 2,2-bis(acrylamido)acetic acid (BAC) was synthesised as previously described (Ferruti et al., 1985). Hydrochloric acid (HCl) and sodium hydroxide (NaOH) were purchased from Fisher Scientific UK Ltd. Lithium hydroxide monohydrate ($\text{LiOH}\cdot\text{H}_2\text{O}$) and 2-methyl piperazine (2-MP), were purchased from Fluka. 2-MP was recrystallised from *n*-heptane and its purity was determined titrimetrically before use. Phosphate buffered saline tablets (PBS) (Oxoid Ltd., Basingstoke, UK) and deuterated water (D_2O) (Goss Scientific Instruments Ltd.) were used as supplied.

2.2. Synthesis of ISA23

ISA23 was synthesised as previously described (Richardson et al., 1999; Ferruti et al., 2000) by polyaddition of BAC and 2-MePip (Scheme 1). BAC (1 g; 5 mmol) and LiOH·H₂O (0.212 g; 5 mmol) were dissolved in double distilled water (1.67 ml, amount required to make 3 M of BAC), this mixture was stirred for 10 min or until all the chemicals have dissolved. To this mixture 2-MP (0.511 g; 5 mmol) was added. The reaction was stirred for 3 days at 25 °C under a nitrogen atmosphere in the dark. After this period, the reaction was stopped by dilution. HCl was then added to the mixture, until the pH reached 3–4. The reaction products were filtered using a stirred ultrafiltration cell (model 8200, Amicon Bioseparation, Millipore), with a membrane cut off of 10,000 g mol⁻¹. The molecular weight distribution of the polymer was then quantified using gel permeation chromatography (GPC) against poly(vinyl pyrrolidone) (PVP) standards.

2.3. Sample preparation

The ISA23 samples were generally prepared by dissolving a known mass of polymer in D₂O containing phosphate buffer (PBS). The pH of the buffered solution drops following the addition of ISA23, and is subsequently adjusted to the desired pH by adding concentrated NaOH or HCl.

2.4. Small-angle neutron scattering

The SANS experiments were conducted on the LOQ diffractometer at the ISIS Spallation Neutron Source (Oxfordshire), and the D11 and D22 diffractometers at the ILL (Grenoble). LOQ is a fixed-geometry, time-of-flight (TOF), instrument whereas D11 and D22 are variable-geometry fixed wavelength instruments. Neutron wavelengths between 2 and 10 Å (LOQ) or 8 Å (D11) or 6 Å (D22) were employed to span Q -ranges (see below) of approximately 0.001–0.6 Å⁻¹. In all cases the samples were placed in 2 mm pathlength, UV-spectrophotometer grade, quartz cuvettes (Hellma Ltd., UK) and mounted in aluminium holders on top of an enclosed, computer-controlled, sample changer. The sample volume was approximately 0.4 ml. Temperature control was achieved through the use of a thermostated circulating bath pumping fluid through the base of the sample changer. Under these conditions, a temperature stability of 0.5 °C could be achieved. Experimental measuring times were approximately 40 min per sample.

Dependent on which instrument was used, all scattering data were (a) normalised for the sample transmission and incident wavelength distribution, (b) background corrected using a solvent filled quartz cell (this also removes the inherent instrumental background arising from vacuum windows, etc.), and (c) corrected for the linearity and efficiency of the detector response using the instrument-specific software package. The data were put onto an absolute scale by reference to the scattering from a well-characterised partially deuterated polystyrene-blend standard (LOQ) or a 1 mm thick sample of water (D11, D22).

In a SANS measurement, the neutron beam is scattered by the nuclei of atoms in the sample through an angle (θ). The angle

is expressed in terms of a scattering vector, $Q = (4\pi/\lambda) \sin(\theta/2)$, where θ is the scattering angle and λ the neutron wavelength. The scattered intensity, $I(Q)$, from a polymer solution with volume fraction ϕ_p , as a function of this wavevector Q , is given to a good approximation by

$$I(Q) = V_p \phi_p (\rho_p - \rho_m)^2 P(Q) S(Q) + B_{\text{inc}} \quad (1)$$

where V_p is the volume of the particle; $(\rho_p - \rho_m)^2$ the contrast term; $P(Q)$ and $S(Q)$ the form and structure factors, respectively; and B_{inc} is the incoherent background. The form factor $P(Q)$ contains information about the size and shape of the polymer in solution, whilst $S(Q)$ accounts for interactions between the scattering objects. For a dilute solution or non-interacting polymer coils, $S(Q) = 1$ and may be neglected. This assumption was made in the original data analysis. Given the knowledge of the chemical composition of the polymer and its concentration, the pre-factors in Eq. (1) may be estimated. The approach to data analysis is therefore to calculate the theoretical scattering from a model in terms of the parameters describing the size and shape of the polymer. “Best fit” values of these parameters were then determined via an iterative non-linear least squares process. The model is selected based on a priori knowledge, comparison to related systems or commonly, starting from a model-free Guinier analysis. For the latter case, B_{inc} needs to be carefully subtracted; here this was done by fitting a linear relationship to the measured scattering intensity over the last 15 points of the data (i.e. over a Q range where only incoherent scattering is present).

2.5. Pulsed-gradient spin-echo NMR experiments

The self-diffusion coefficients were measured on a Bruker AMX360 NMR spectrometer using a 5 mm diffusion probe (Cryomagnet Systems, Indianapolis), a Bruker gradient spectroscopy accessory and a stimulated echo sequence.

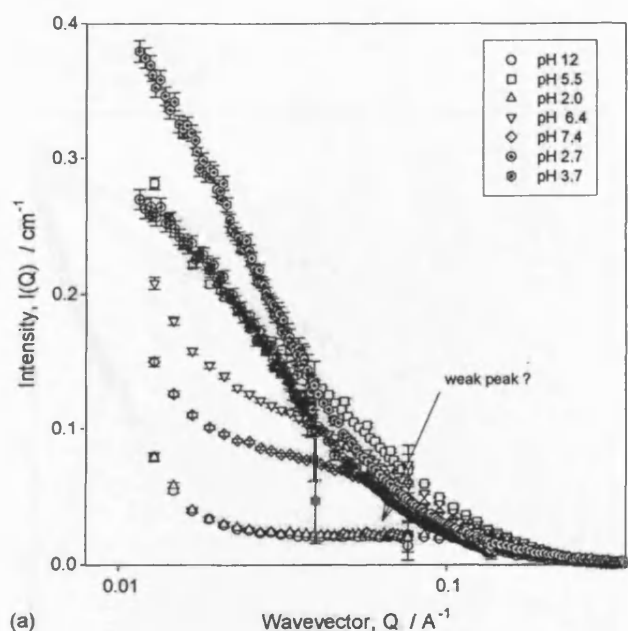
The self-diffusion coefficient D_s is extracted by fitting the integrals for a given peak to the following equation:

$$A(\delta, G, \Delta) = A_0 \exp[-(kD_s)] \quad (2)$$

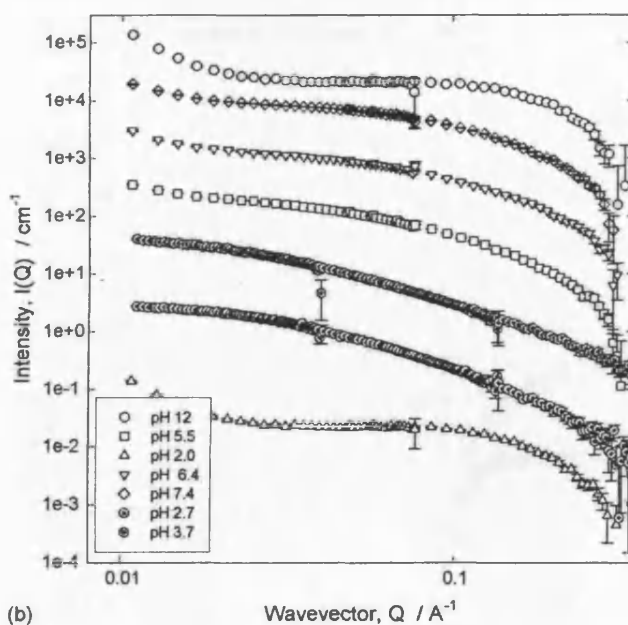
where $A(\delta, G, \Delta)$ is the signal integral in the presence and A_0 is the absence of the gradients. $k = -\gamma^2 G^2 ([30\Delta(\delta + \sigma)^2 - (10\delta^3 + 30\sigma^2\delta + 14\sigma^2)]/30)$ where γ is the magnetogyric ratio, Δ the diffusion time (0.24 s), σ the gradient ramp time (250 μ s), δ the gradient pulse length (400 μ s < δ < 2.8 ms) and G the field gradient strength (0.86 T m⁻¹) i.e. typically 3.8 A into a coil with $dG/dI = 0.227 \text{ T m}^{-1} \text{ A}^{-1}$.

3. Results and discussion

Consider the absolute intensity of the scattering, Fig. 1(a). For the data recorded at the ILL and for the particularly weak scattering systems, there is an upturn in scattering at low Q . This may be due to aggregation – an attractive interaction – although in our earlier treatment of related data, this was considered to be an artefact since (i) no such scattering was observed in similar samples recorded at ISIS and (ii) the Q dependence of this upturn is unphysical (i.e. greater than Q^{-4}). Accordingly initially at least,



(a)



(b)

Fig. 1. (a) Small-angle neutron scattering for ISA23 (5 wt.%) in D₂O as a function of pH; (b) small-angle neutron scattering for ISA23 (5 wt.%) in D₂O as a function of pH. Each dataset has been offset by a factor of 10.

ignore the first two or three datapoints in the following analysis. As Q tends to zero, the factors $P(Q)$ and $S(Q)$ in Eq. (1) also tend to unity, and thus one may write $I(Q \rightarrow 0) = V_p \phi_p (\rho_p - \rho_m)^2$ for a dilute system. From the composition of the polymer, the absolute intensity of the scattering of these solutions and noting that concentration is 50 mg ml⁻¹ in D₂O, the volume of the polymer coil (V_p) may be estimated; expressed in terms of a (spherical) radius this corresponds to $R \sim 50$ Å. Equally as important is the simple insight this approach provides into the change in volume due to the effects of pH—clearly, the data with pH 2.0 and

12.0 have least scattering (ignoring the weak upturn in the data) and are therefore, of smallest volume (collapsed). The scattering intensity for the solution at pH 3.7 is most intense, and therefore the polymer coil most expanded.

Overall, the intensity of the various datasets follow the pH order $3.7 > 5.5 \approx 2.7 > 6.4 > 7.4 > 12.0 \approx 2.0$. This apparently random order actually correlates well with a maximum in the volume of the polymer coil extracted from our previous analysis of such data, centred around pH 4.0 (± 0.5). The intensities over this pH range change by a factor of 5, corresponding to a change in the effective radius of a factor of ~ 2 . The data at pH 12.0 and 2.0 are different to those at the other pHs, with a very weak signature of a structure peak around $Q \sim 0.06$ Å. The data have been replotted in Fig. 1(b) with each dataset offset by a factor of 10 in an attempt to emphasise this feature. Such a peak arises due to a highly charged, collapsed structure such as a micelle, unfortunately rendering data interpretation less facile. However, since these polymers will not experience such extreme pHs during internalisation into cells, a rigorous analysis is not warranted.

When the shape of the scattering object is not known, is irregular or not describable in a simple manner, the low Q data from a SANS experiment may be analysed in a model-free fashion to yield an estimate of the size of the scatterer (Guinier and Fournet, 1955). The form factor, $P(Q)$, provided the system is dilute (non-interacting scatterers, $S(Q) = 1$), may be approximated at small Q as

$$P(Q \rightarrow 0) = \exp\left(-\frac{Q^2 R_g^2}{3}\right) \quad (3)$$

where R_g is the rms radius of gyration averaged over the volume of the polymer. A Guinier plot ($\ln I(Q)$ versus Q^2) will exhibit a linear portion over the region $QR_g < 1$.

However, to estimate the most likely overall shape of a scatterer, Eq. (3) may be generalised:

$$P(Q) = Q^{-D} \exp\left(\frac{-Q^2 R^2}{K}\right) \quad (4)$$

where R is the characteristic dimension—for a sphere, R corresponds to the radius, $D=0$ and $K=5$; for a long thin rigid cylinder, R is the cross-sectional radius, $D=1$ and $K=4$ and whilst for large rigid discs, R gives the thickness, $D=2$ and $K=12$. Thus, an appropriate form of Eq. (4) $\ln[I(Q)Q^D]$ versus Q^2 will display a linear region in an appropriate Q range if the scatterer conforms to that particular gross morphology, from which the characteristic dimension may be extracted.

To estimate the conformation of ISA23 under different environmental conditions, or to provide a coarse picture of the size at different pH values, the raw data obtained by SANS for ISA23 (37 °C at 50 mg/ml) were analysed in terms of a model-free Guinier analysis. Selected data are presented in Fig. 2(a)–(c) over the Q range for which the Guinier representation is valid ($QR_g < 1$). Clearly, the functional form of Fig. 2(a) exhibits the region of largest linearity, implying that the polymer has a more spherical shape, and one that does not change with pH. Derived radii are discussed later in this paper (Figs. 5 and 7).

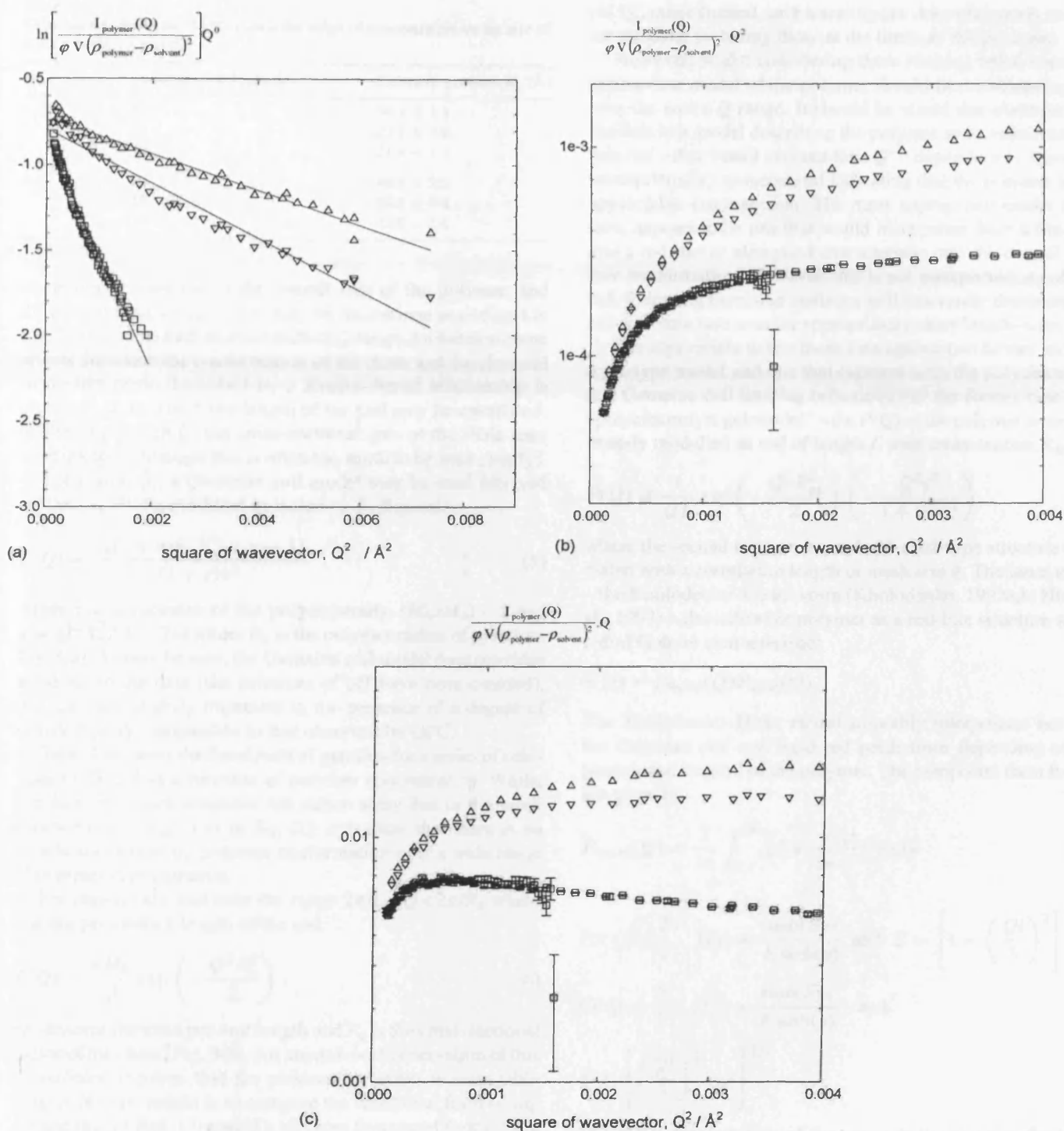


Fig. 2. (a) Spheres Guinier analysis $\ln[I_{\text{polymer}}(Q)/\phi V(\rho_{\text{polymer}} - \rho_{\text{solvent}})^2]Q^0$ for ISA23 (5 wt.%) D₂O as a function of pH: (□) pH 3.7; (▽) pH 5.5 and (△) pH 7.4. (b) Disk Guinier analysis for ISA23 (5 wt.%) polymer in D₂O as a function of pH: (□) pH 3.7; (▽) pH 5.5 and (△) pH 7.4. (c) Cylinder Guinier analysis for ISA23 (5 wt.%) polymer in D₂O as a function of pH; (□) pH 3.7; (▽) pH 5.5 and (△) pH 7.4.

Whilst such a model-free approach is helpful, a complete analysis of the data requires a somewhat more involved approach in order to fully characterise the polymer conformation. Criteria to assess the most likely shape include not only an appropriate fit to the data but also an assessment of the absolute scattering intensity. Given that upon protonation the polymer becomes

charged, and remembering the conclusions drawn from the viscosity data of Ferruti et al. (2000), an appropriate model to test is one that embodies an elongated or “rod-like” morphology.

For semi-flexible polymers in solution, the form factor can be “dissected” into three key parts, defined by an appropriate Q range: (i) at low Q – corresponding to large distances – the

Table 1
Gaussian coil fits to the SANS data—the effect of concentration on the size of ISA23, at pH 7.4 and 5.5

pH	Concentration (mg/ml)	Radius of gyration, R_g (Å)
7.4	10	24.7 ± 1.1
	25	23.5 ± 3.6
	50	21.4 ± 1.1
5.5	10	40.0 ± 2.3
	25	38.5 ± 8.6
	50	32.8 ± 1.1

scattering is sensitive to the overall size of the polymer, and the overall radius of gyration may be determined as outlined in Fig. 2(a)–(c); (ii) over an intermediate Q range, excluded volume effects dominate the conformation of the chain and the classical worm-like chain described by a Kratky–Porod relationship is observed, from which the length of the coil may be calculated; whilst (iii) at high Q , the cross-sectional area of the chain may be extracted (although this is often too small to be seen clearly).

For region (i), a Gaussian coil model may be used (derived by Debye, 1947), modified to include polydispersity:

$$P(Q) = \frac{2[(1 + uv)^{-1/v} + u - 1]}{(1 + v)u^2} \quad (5)$$

where v is a measure of the polydispersity, $(M_w/M_n) - 1$ and $u = Q^2 R_g^2 / (1 + 2v)$ where R_g is the polymer radius of gyration, Fig. 3(a). As may be seen, the Gaussian coil model does provide good fits to the data (the extremes of pH have been omitted), that are only slightly improved in the presence of a degree of polydispersity comparable to that observed by GPC.

Table 1 presents the fitted radii of gyration for a series of solutions of ISA23 as a function of polymer concentration. Whilst the data from such solutions are rather noisy due to the weak contrast $((\rho_p - \rho_m)^2)$ as in Eq. (1), it is clear that there is no significant change on polymer conformation over a wide range of polymer concentration.

For region (iii), and over the range $2\pi/L < Q < 2\pi/R_c$ where L is the persistence length of the rod:

$$P(Q) \approx \frac{\pi M_L}{Q} \exp\left(-\frac{Q^2 R_c^2}{2}\right) \quad (6)$$

M_L denotes the mass per unit length and R_c is the cross-sectional radius of the chain, Fig. 3(b). An unequivocal observation of this dependence requires that the persistence length is reasonably long. A further insight is to compare the functional form of Eq. (6) and that of Eqs. (3) and (5); all three functional forms scale as Q^{-2} .

Finally, for region (iii), the form factor may be considered as that of an infinitely thin needle of length L :

$$P(Q) = \frac{2}{QL} \left(\int_0^{QL} \frac{\sin(QL)}{QL} d(QL) - \frac{1 - \cos(QL)}{QL} \right) \quad (7)$$

which, at high Q , leads to the scaling Q^{-1} prediction of Eq. (6), $P(Q) \approx \pi/QL$. The prediction that $P(Q) \approx \pi/QL$ should be easily identifiable in the scattering. Fig. 3(c) shows that over the

pH QL range studied, such a scaling law does adequately account for the data, including those at the limits of the pH range.

However, whilst considering these limiting behaviours, any appropriate model of the polymer should fit the scattering data over the entire Q range. It should be stated that attempts to fit the data to a model describing the polymer as an infinitesimally thin rod – that would account for a Q^{-1} dependence – were (not unsurprisingly) unsuccessful indicating that the polymer has an appreciable cross-section. The most appropriate model therefore, appears to be one that would incorporate both a Gaussian and a rod-like or elongated characteristic into the overall polymer conformation. However, this is not unexpected; a polymer coil following Gaussian statistics will inherently demonstrate a rod-like structure over an appropriately short length-scale.

It is appropriate to test these data against two further models; a gel-type model and one that captures both the polyelectrolyte and Gaussian coil limiting behaviour. For the former case – the “polyelectrolyte gel model” – the $P(Q)$ of the polymer is approximately modelled as rod of length L with cross-section R_{ax} :

$$P(Q) \cong \frac{1}{QL} \exp\left(-\frac{Q^2 R_{ax}^2}{2}\right) \left(-\frac{Q^2 \xi^2}{1 + Q^2 \xi^2}\right) \quad (8)$$

where the second term accounts for the gel-type structure associated with a correlation length or mesh size ξ . The latter model – the Kholodenko–Dirac worm (Kholodenko, 1993a,b; Hickl et al., 1997) – describes the polymer as a rod-like structure with a radial Guinier characteristic:

$$I(Q) = P_{worm}(Q)P_{axial}(Q) \quad (9)$$

The Kholodenko–Dirac model smoothly interpolates between the Gaussian coil and rigid rod predictions depending on the persistence length l of the polymer. The composite form factors are given by

$$P_{worm}(Q) = \frac{2}{3n} \int_0^{3n} \left(1 - \frac{y}{3n}\right) f(y) dy \quad (10)$$

$$\text{For } Q \leq \frac{3}{l}, \quad f(y) = \frac{\sinh(Ey)}{E \sinh(y)} \quad \text{and } E = \left[1 - \left(\frac{Ql}{3}\right)^2\right]^{1/2},$$

$$\text{for } Q > \frac{3}{l}, \quad f(y) = \frac{\sinh(Fy)}{F \sinh(y)} \quad \text{and}$$

$$F = \left[\left(\frac{Ql}{3}\right)^2 - 1\right]^{1/2}$$

The radial cross-section of the worm is the same as the latter part of Eq. (6):

$$P_{axial}(Q) = N(\rho_p - \rho_m)^2 (AL)^2 \exp\left(-\frac{1}{2} Q^2 R_{ax}^2\right) \quad (11)$$

where A is the cross-sectional area of the polymer worm $A = 2\pi R_{ax}^2$ and L is the contour length, $L = nl$. Again note the similarity of the functional form of Eqs. (3), (6) and (11).

Taking the first of these two models (Eq. (8)), introducing a finite cross-section to the rod yields a better “fit” to the data compared with an infinitely thin model. A typical, illustrative

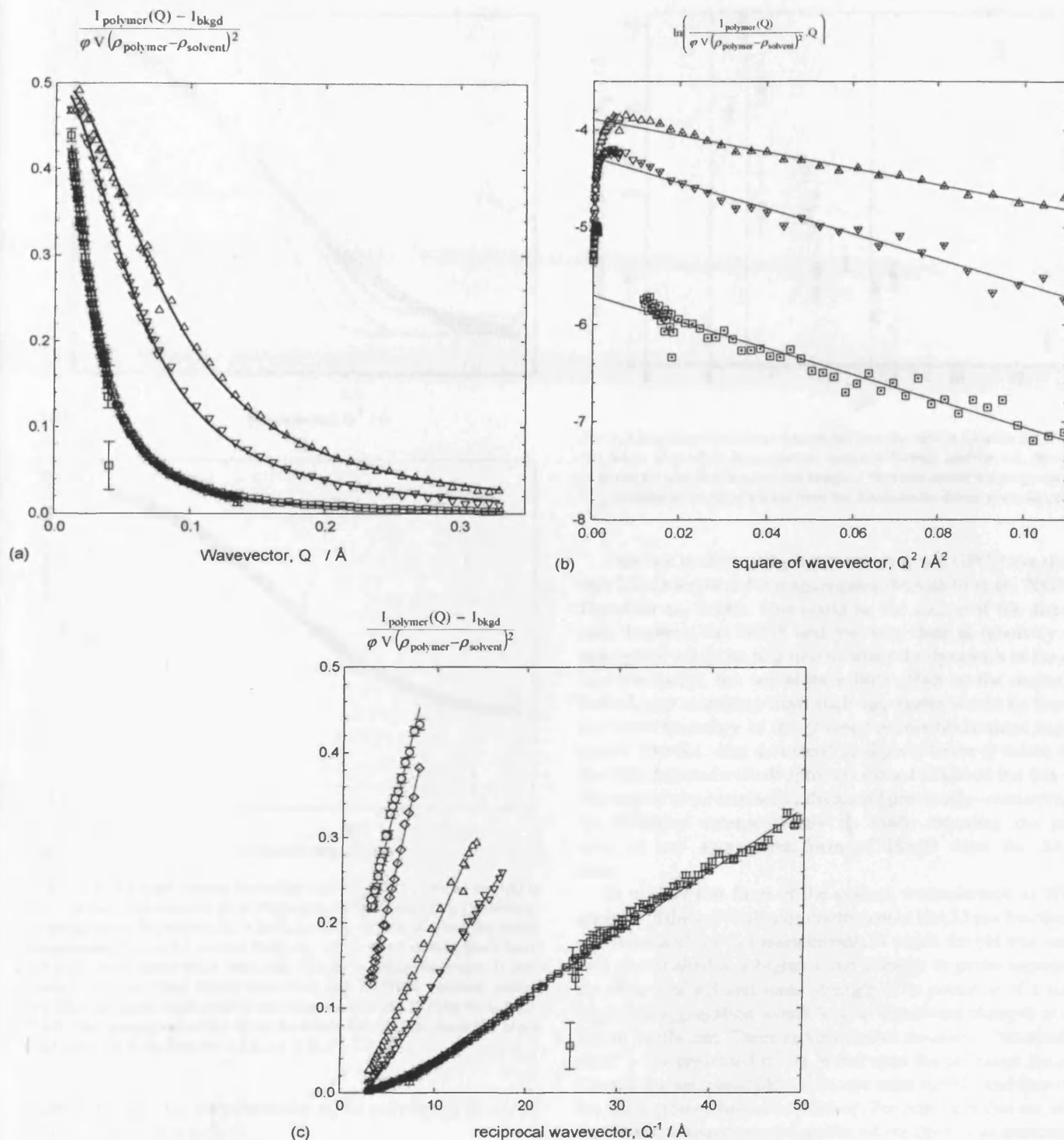


Fig. 3. (a) Normalised SANS data $I_{\text{polymer}}(Q) - I_{\text{bkgd}}/\varphi V(\rho_{\text{polymer}} - \rho_{\text{solvent}})^2$ for ISA23 (5 wt.%) polymer in D₂O as a function of pH: (□) pH 3.7; (▽) pH 5.5 and (△) pH 7.4. (b) Cross-sectional analysis for ISA23 (5 wt.%) polymer in D₂O as a function of pH: (□) pH 3.7; (▽) pH 5.5 and (△) pH 7.4. (c) Normalised SANS data $I_{\text{polymer}}(Q) - I_{\text{bkgd}}/\varphi V(\rho_{\text{polymer}} - \rho_{\text{solvent}})^2$ plotted as a function of reciprocal Q (Q^{-1}) for ISA23 (5 wt.%) polymer in D₂O as a function of pH: (◇) pH 2.0; (□) pH 3.7; (▽) pH 5.5; (△) pH 7.4; (○) pH 13.0.

dataset is presented in Fig. 4(a). The fit is best (but not good) when the cross-sectional radius is 21 Å, with (too) a short length (11 Å) i.e. more spherical than rod-like in shape. ξ is typically slightly longer than L for all cases. For the other pH data, the fits

were equally poor, suggesting that the dominant conformation of ISA23 in solution is not rod-like. The approach does invoke a rather distinct interface between the radial structure and the solvent, and in reality this interface will be rather more diffuse,

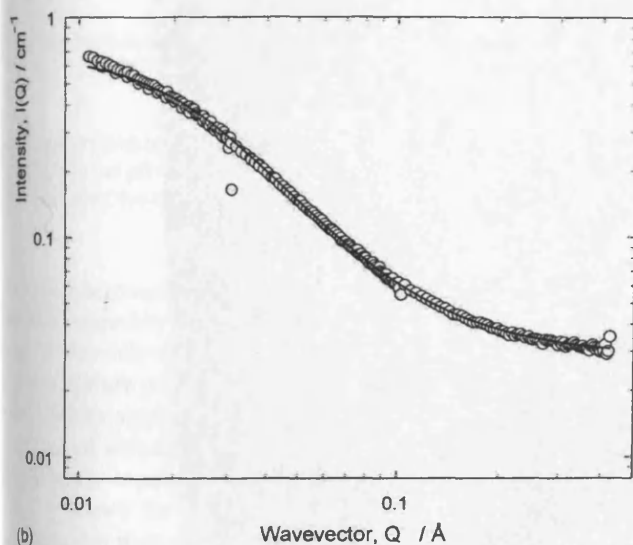
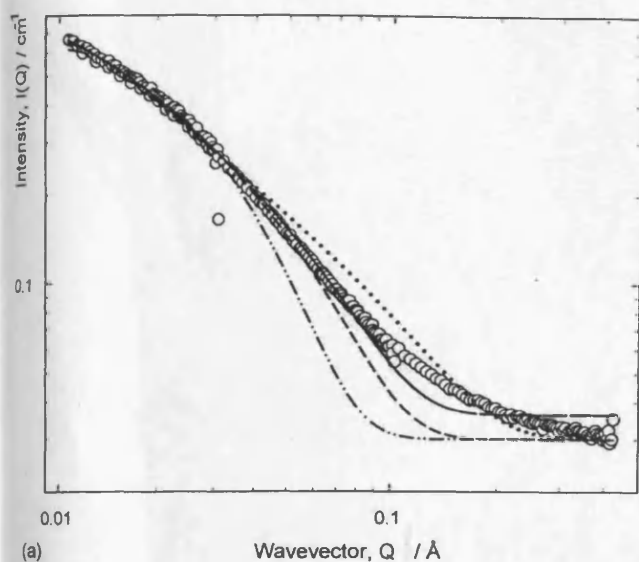


Fig. 4. (a) Small-angle neutron scattering data for ISA23 (5 wt.%) in D_2O at pH 4. The lines represent the fits to the polyelectrolyte model (Eq. (8)) with (i) an unconstrained fit yielding $R_{ax} = 21 \text{ \AA}$, $L = 11 \text{ \AA}$; (ii) fits in which the radius is constrained; $R_{ax} = 10 \text{ \AA}$ (dotted line), $R_{ax} = 20 \text{ \AA}$ (long dashed black line), $R_{ax} = 30 \text{ \AA}$ (dash dotted black line), and (iii) fits in which the length is constrained; $L = 100 \text{ \AA}$ (long dashed black line) and $L = 500 \text{ \AA}$ (medium dashed black line). (b) Small-angle neutron scattering data for ISA23 (5 wt.%) in D_2O , pH 4.0. The line represents the fits to the Kholodenko-Dirac wormlike chain model (Eqs. (9)–(11)) with $R = 2.2 \text{ \AA}$, $l = 12 \text{ \AA}$, $n = 125$.

which coupled to the polydispersity of the polymer, will render the fit less precise at high Q .

The second model – the Kholodenko-Dirac worm – (Eqs. (9) and (10)) represents a better treatment of the data, Fig. 4(b), and is as good as the Gaussian treatment (Eq. (5)) although it must be stressed that for a flexible chain, the Gaussian and Kholodenko-Dirac worm formulations (Eq. (9)) are equivalent.

Fig. 5 summarises the characteristic parameters extracted from the various analyses of the SANS data. Clearly, these all suggest that the polymer expands as the pH is reduced, reaching a maximum around pH 4.

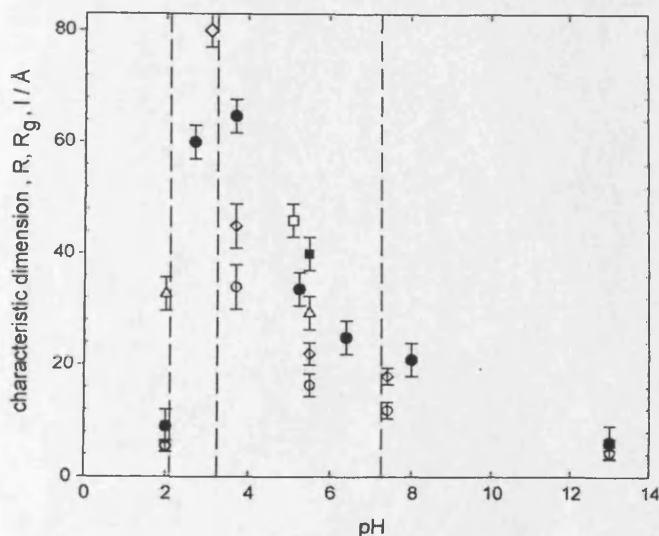


Fig. 5. Characteristic dimension extracted from the various fits to the SANS data: (\diamond) radius of gyration from a simple spherical Guinier analysis; (Δ , \bullet) radius of gyration from the Gaussian coil analysis (different counterion polymers) and (\circ) correlation length extracted from the Kholodenko-Dirac worm-like chain.

Previous studies, using light scattering and GPC, have shown that ISA23 tends to form aggregates (Mendichi et al., 2005a,b; Ferruti et al., 2000). This could be the source of the discrepancy between the SANS and viscosity data as relatively few aggregates would be required to affect the dynamics of the system (viscosity), but would have little effect on the scattering. Indeed, any scattering from such aggregates would lie beyond the lower boundary of the Q range accessible in these experiments. The ILL data do extend to slightly lower Q values than the ISIS data and a weak upturn is indeed observed but this was discounted as an artefact as discussed previously—accordingly, no definitive statement may be made regarding the presence of any aggregated form of ISA23 from the SANS data.

To explore this facet of the system, we undertook an NMR analysis of the self-diffusion coefficient of ISA23 as a function of pH. A parallel series measurements in which the pH was varied was also studied at a higher ionic strength to probe separately the effects of pH and ionic strength. The presence of a small degree of aggregation would lead to significant changes in diffusion coefficient. Three representative datasets – “attenuation plots” – are presented in Fig. 6 that span the pH range studied. Clearly, the sample at pH 4.5 decays most rapidly and therefore has the largest diffusion coefficient. For polymers that are identical in size (monodisperse) and/or where there is an association or aggregation process occurring on a timescale that is rapid compared with the timescale of the measurements (240 ms), a single exponential relationship should be observed (Eq. (2)) whose slope corresponds to the self-diffusion coefficient. Polydispersity gives rise to upward curvature in the attenuation plot, the degree of which increases with increasing polydispersity. Aggregation that is irreversible (or “slow” on the timescale of the experiment) would give rise to two characteristic slopes – the first corresponding to the diffusion of the aggregates, the sec-

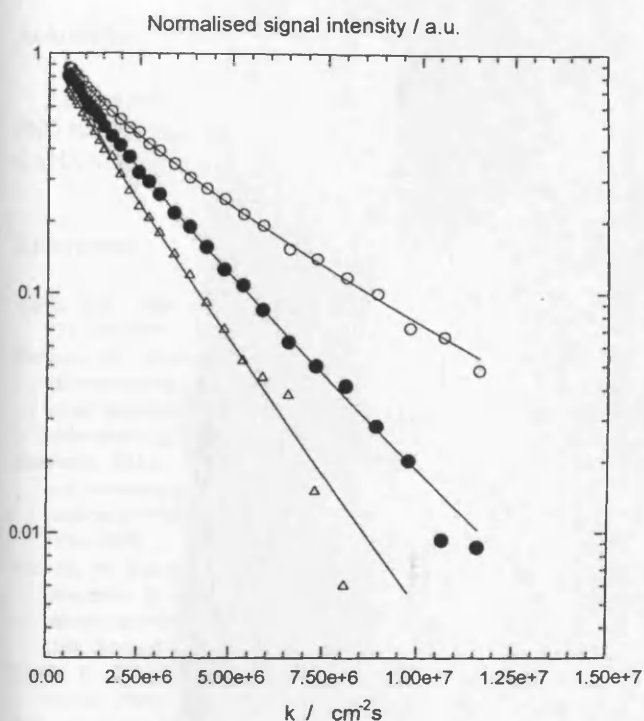


Fig. 6. Typical PGSE-NMR dataset for ISA23 (5 wt.%) in D₂O at 25 °C; pH 4.5 (Δ), pH 4 (\circ) and pH 9 (\bullet). The solid lines correspond to fits to a stretched exponential model that empirically accounts for small degrees of polydispersity.

and the non-aggregated polymers – with the balance of each term being determined by concentration of the polymers in each environment. The only slight departure from linearity indicates that the polymers are polydisperse but not significantly so, and that no irreversible aggregation is occurring. As might be expected, the effects of polydispersity are manifest more strongly when the polymer is expanded.

Fig. 7 shows the radii of hydration as a function of pH extracted from these NMR diffusion coefficients as a function of pH and the data are superimposed on the SANS results. As found in the viscosity data, the size clearly decreases with a decrease in pH attaining a minimum value around pH 43.5 i.e. close to the isoelectric point, before subsequently expanding at pH below 4.5. Interestingly, the agreement between the three approaches is reasonable for pH < 5. There appears to be no significant dependence on temperature or ionic strength.

Equally clear however, is the fact that the NMR and viscosity data display the opposite pH trend with respect to the SANS. Such a disagreement could occur if (i) the polymers are indeed adopting a more elongated structure such that the effective hydrodynamic radius scales as $R^2 = R_{ax}^2 + L^2$ but this would require L to be substantial; this is not observed in the SANS, or (ii) the polymers are indeed aggregating, but the effect would have to be small so as not to contribute significantly to the scattering. The self-association of ISA23 has been detected by SEC for a series of ISA23-based polymers, there being a small fraction of high molecular weight polymer present (Mendichi et al., 2005a,b). Such a component would be largely invisible in the SANS experiment, and provided it was

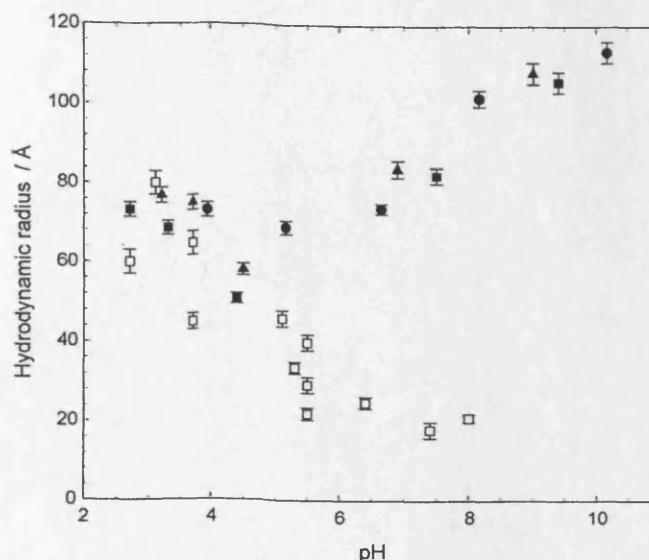


Fig. 7. Hydrodynamic radii superimposed on the "scattering dimension" (Q) (Fig. 5) as a function of pH calculated from the self-diffusion coefficients via the Stokes–Einstein equation; (\bullet) 1 wt.% ISA23 in D₂O at 25 °C; (\blacksquare) 1.5 wt.% ISA23 in 50 mM NaCl/D₂O at 37 °C and (\blacktriangle) 1.5 wt.% ISA23-HCl in D₂O at 37 °C.

dynamic, could lead to significant discrepancies between the two techniques.

Interestingly pH \approx 5.6–6.0 coincides with the switch from an overall positively charged polymer at low pH to a net negatively charged polymer above pH 5. Coincidentally, for pH > 5, the ability of these polymer to break the membrane of red blood cells – the degree of haemolysis – is minimal, indicating that either this aggregation reduces the ability of the polymers to interact with the membrane surface or the mechanism that drives aggregation is also involved in the membrane interaction (Griffiths et al., 2004b).

4. Conclusions

When interpreting neutron scattering data it is essential to choose an appropriate mathematical model to allow accurate estimation of the shape and size of the polymer coil in solution. This is not always as easy task as many models predict a particular Q dependence that may or may not be unequivocally demonstrated in the scattering depending in the size of the scatterer. The results presented here amply demonstrate this fact—a Gaussian coil model gives the best fit for ISA23 in solution (except at the limits of pH) but the "signature" of a rigid rod is also seen in the data due to a combination of the local flexibility of the polymer, its over size and the Q range. The Kholodenko–Dirac model captures both these facets and is also shown to provide an accurate treatment of the date. On balance, the polymers exhibit a Gaussian coil conformation – rather than a rod-like conformation – over a wide pH range and polymer concentrations examined (10–50 mg/ml). Irrespective of the precise model adopted however, these results support the proposed mode of action of PAAs; a pH driven coil expansion/rearrangement.

Acknowledgements

ZK would like to thank Cardiff University for supporting her PhD studentship, CCLRC and ILL are thanked for provision of SANS beam time.

References

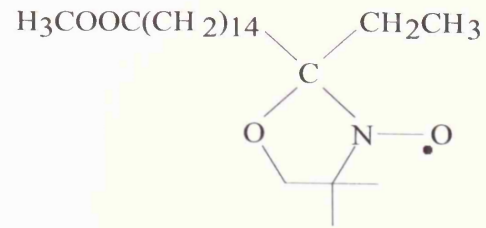
- Aswal, V.K., 2003. Salt effect in ionic mixed micelles. *Chem. Phys. Lett.* 371, 371–377.
- Barbucci, R., Casolar, M., Ferruti, P., Barone, V., Leij, F.L., Oliva, L., 1981. *Macroinorganics. 7. Property–structure relationships for polymeric bases whose monomeric units behave independently toward protonation. Macromolecules* 14, 1203–1209.
- Bergström, M.L.L., Kjellin, M.U.R., Claesson, P.M., 2004. Small-angle neutron scattering study of mixtures of cationic polyelectrolyte and anionic surfactant: effect of polyelectrolyte charge density. *J. Phys. Chem. B* 108, 1874–1881.
- Boussif, O., Lezoualch, F., Zanta, M.A., Mergny, M.D., Scherman, D., Demeneix, B., Behr, J.-P., 1995. A versatile vector for gene and oligonucleotide transfer into cells in culture and in vivo: polyethylenimine. *Proc. Natl. Acad. Sci. U.S.A.* 92, 7297–7301.
- Check, E., 2003. Harmful potential of viral vectors fuels doubts over gene therapy. *Nature* 423, 573–574.
- Debye, P., 1947. Molecular-weight determination by light scattering. *J. Phys. Colloid Chem.* 51, 18–32.
- Duncan, R., Ferruti, P., Sgouras, D., Tuboku-Metzger, A., Ranucci, E., Bignotti, F.A., 1994. Polymer–triton X-100 conjugate capable of pH-dependent red blood cell lysis: a model system illustrating the possibility of drug delivery within acidic intracellular compartments. *J. Drug Target.* 2, 341–347.
- Duncan, R., 2003. The dawning era of polymer therapeutics. *Nat. Rev. Drug Discov.* 2, 347–360.
- Edelstein, M.L., Abedi, M.R., Wixon, J., Edelstein, R.M., 2004. *J. Gene Med.* 6, 560–597.
- Feng, J., Huang, R., 1997. Studies on the aqueous solution properties of AMPS-DMAEMA polyampholytes. *Gaofenzi Cailiao Kexue Yu Gongcheng* 13, 109–113.
- Ferruti, P., Marchisio, M.A., Barbucci, R., 1985. Synthesis, physico-chemical properties and biomedical applications of poly(amido-amine)s. *Polymer* 26, 1336–1348.
- Ferruti, P., Manzoni, S., Richardson, S.C.W., Duncan, R., Patrick, N.G., Mendichi, R., Casolaro, M., 2000. Amphoteric linear poly(amidoamine)s as endosomolytic polymers: correlation between physicochemical and biological properties. *Macromolecules* 33, 7793–7800.
- Ferruti, P., Marchisio, M.A., Duncan, R., 2002. Poly(amido-amine)s: biomedical applications. *Macromol. Rapid Commun.* 23, 332–355.
- Fischer, D., Li, Y.X., Ahlemeyer, B., Krieglstein, J., Kissel, T., 2003. In vitro cytotoxicity testing of poly cations: influence of polymer structure on cell viability and hemolysis. *Biomaterials* 24, 1121–1131.
- Funhoff, A.M., van Nostrum, C.F., Koning, G.A., Schuurmans-Nieuwenbroek, N.M.E., Crommelin, D.J.A., Hennink, W.E., 2004. Endosomal escape of polymeric gene delivery complexes is not always enhanced by polymers buffering at low pH. *Biomacromolecules* 5, 32–39.
- Griffiths, P.C., Paul, A., Khayat, Z., Wan, K.W., King, S.M., Grillo, I., Schweins, R., Ferruti, P., Franchini, J., Duncan, R., 2004a. Understanding the mechanism of action of poly(amidoamine)s as endosomolytic polymers: correlation of physicochemical and biological properties. *Biomacromolecules* 5, 1422–1427.
- Griffiths, P.C., Paul, A., Heenan, R.K., Penfold, J., Ranganathan, R., Bales, B.L., 2004b. Role of counterion concentration in determining micelle aggregation: evaluation of the combination of constraints from small-angle neutron scattering, electron paramagnetic resonance, and time-resolved fluorescence quenching. *J. Phys. Chem. B* 108, 3810–3816.
- Guinier, A., Fournet, G., 1955. *Small Angle Scattering of X-rays*. Wiley, New York.
- Hacein-Bey-Abina, S., von Kalle, C., Schmidt, M., Le Deist, F., Wulffraat, N., McIntyre, E., Radford, I., Villeval, J.L., Fraser, C.C., Cavazzana-Calvo, M., Fischer, A., 2003. A serious adverse event after successful gene therapy for X-linked severe combined immunodeficiency. *New Engl. J. Med.* 348, 255–256.
- Hedden, R.C., Bauer, B.J., 2003. Structure and dimensions of PAMAM/PEG dendrimer-star polymers. *Macromolecules* 36, 1829–1835.
- Hickl, P., Ballauff, M., Scherf, U., Muellen, K., Lindner, P., 1997. Characterization of a ladder polymer by small-angle X-ray and neutron scattering. *Macromolecules* 30, 273–279.
- Ilarduya, C.T.D., Duzgunes, N., 2000. Efficient gene transfer by transferin lipoplexes in the presence of serum. *Biochim. Biophys. Acta* 1463, 333–342.
- Kholodenko, A.L., 1993a. Analytical calculation of the scattering function for polymers of arbitrary flexibility using the Dirac propagator. *Macromolecules* 26, 4179–4183.
- Kholodenko, A.L., 1993b. Scattering function for semiflexible polymers: Dirac versus Kratky-Porod. *Phys. Lett. A* 178, 1–2.
- King, S., Griffiths, P.C., Hone, J., Cosgrove, T., 2002. SANS from adsorbed polymer layers. *Macromol. Symp.* 190, 33–42.
- Koetz, J., Hahn, M., Philipp, B., Bekturov, E.A., Kudaibergenov, S.E., 1993. Inter- and intramolecular interactions in polyelectrolyte complex formation with polyampholytes. *Makromol. Chem.* 194, 397–410.
- Lavignac, N., Lazenby, M., Foka, P., Malgesini, B., Verpillio, I., Ferruti, P., Duncan, R., 2004. Synthesis and endosomolytic properties of poly(amidoamine) block copolymers. *Macromol. Biosci.* 20, 922–929.
- Mendichi, R., Ferruti, P., Malgesini, B., 2005a. Evidence of aggregation in dilute solution of amphoteric poly(amido-amine)s by size exclusion chromatography. *Biomed. Chromatogr.* 19, 96–201.
- Mendichi, R., Ferruti, P., Malgesini, B., 2005b. Evidence of aggregation in dilute solution of amphoteric poly(amido-amine)s by size exclusion chromatography. *Biomed. Chromatogr.* 19, 196–201.
- Murthy, N., Robichaud, J., Tirrel, D., Stayton, P., Hoffman, A., 1999. The design and synthesis of polymers for eukaryotic membrane disruption. *J. Contr. Release* 61, 137–143.
- Nakamura, K., Shikata, T., Takahashi, N., Kanaya, T., 2005. Highly extended conformation of polyelectrolytes incorporated into hybrid threadlike micelles studied by small angle neutron scattering. *J. Am. Chem. Soc.* 127, 4570–4571.
- Nishida, K., Kaji, K., Kanaya, T., Shibano, T., 2002. Added salt effect on the intermolecular correlation in flexible polyelectrolyte solutions: small-angle scattering study. *Macromolecules* 35, 4084–4089.
- Ohana, P., Gofrit, O., Ayes, S., Al-Sharef, W., Mizrahi, A., Birman, T., Schneider, T., Matouk, I., de Groot, N., Tavdy, E., Sidi, A.A., Hochberg, A., 2004. Regulatory sequences of the H19 gene in DNA based therapy of bladder. *Gene Ther. Mol. Biol.* 8, 181–192.
- Pack, D.W., Hoffman, A.S., Pun, S., Stayton, P., 2005. Design and development of polymers for gene delivery. *Nat. Rev. Drug Discov.* 4, 581–593.
- Patrick, N.G., Richardson, S.C.W., Casolaro, M., Ferruti, P., Duncan, R., 2001a. Poly(amidoamine) mediated intracytoplasmic delivery of ricin A-chain and gelonin. *J. Contr. Release* 77, 225–232.
- Patrick, N.G., Ferruti, P., Duncan, R., 2001b. Demonstration of poly(amidoamine)-mediated lysosomal membrane perturbation after administration to rats in vivo. *Proc. Int. Symp. Contr. Release Bioact. Mater.* 28, 864–865.
- Pederson, J.S., 2002. Modelling of small-angle scattering data from colloids and polymers systems. In: Lindner, P., Zemb, Th. (Eds.), *Neutrons, X-rays and Light: Scattering Methods Applied to Soft Condensed Matter*. North-Holland.
- Qin, L.H., Pahud, D.R., Ding, Y.Z., Beilinska, A.U., Kukowska-Latallo, J.F., Baker, J.R., Bromberg, J.S., 1998. Efficient transfer of genes into murine cardiac grafts by starburst polyamidoamine dendrimer. *Hum. Gene Ther.* 9, 553–560.
- Ramzi, A., Scherrenberg, R., Joosten, J., Lemstra, P., Mortensen, K., 2000. Structure–property relations in dendritic polyelectrolyte solutions at different ionic strength. *Macromolecules* 35, 827–833.

- Raper, S.E., Chirmule, N., Lee, F.S., Wivel, N.A., Bagg, A., Gao, G.P., Wilson, J.M., Batshaw, M.L., 2003. Fatal systemic inflammatory response syndrome in a ornithine transcarbamylase deficient patient following adenoviral gene transfer. *Mol. Genet. Metab.* 80, 148–158.
- Richardson, S.C.W., Ferruti, P., Duncan, R., 1999. Poly(amidoamine)s as potential endosomolytic polymers: evaluation in vitro and body distribution in normal and tumour-bearing animals. *J. Drug Target.* 6, 391–404.
- Richardson, S.C.W., Patrick, N.G., Man, Y.K.S., Ferruti, P., Duncan, R., 2001. Poly(amidoamine)s as potential nonviral vectors: ability to form interpoly electrolyte complexes and to mediate transfection in vitro. *Biomacromolecules* 2, 1023–1028.
- Sonawane, N.D., Szoka, F.C., Verkman, A.S., 2003. Chloride accumulation and swelling in endosomes enhances DNA transfer by polyamine–DNA polyplexes. *J. Biol. Chem.* 278, 44826–44831.
- Wagner, E., 2004. Strategies to improve DNA polyplexes for in vivo gene transfer: will artificial viruses be the answer? *Pharm. Res.* 21, 8–14.
- Wan, K.-W., Malgesini, B., Verpilio, I., Ferruti, P., Griffiths, P.C., Paul, A., Hann, A.C., Duncan, R., 2004. Poly(amidoamine) salt form affects pH-dependent membrane activity and polymer conformation in solution. *Biomacromolecules* 5, 1102–1109.
- Wu, G.Y., Wu, C.H., 1988. Receptor-mediated gene delivery and expression in vivo. *J. Biol. Chem.* 262, 14621–14624.

Appendix III

Appendix III

EPR



16 doxyl stearic acid methyl ester
16-DSE

- 249 -

